AUG 14 1958

Journal of Research

of the

National Bureau of Standards

UNIVERSITY
OF MICHIGAN

AUG 12 1958

PHYSICS
LIBRARY

JUNE 1958

VOLUME 60 NUMBER 6

U. S. DEPARTMENT OF COMMERCE
Sinclair Weeks, Secretary
NATIONAL BUREAU OF STANDARDS
A. V. Astin, Director

JUNE • 19
VOLUME •
NUMBER •

JOURNAL OF RESEARCH
of the
NATIONAL BUREAU OF STANDARDS

The National Bureau of Standards

Functions and Activities

The functions of the National Bureau of Standards are set forth in the Act of Congress, March 3, 1901, as amended by Congress in Public Law 619, 1950. These include the development and maintenance of the national standards of measurement and the provision of means and methods for making measurements consistent with these standards; the determination of physical constants and properties of materials; the development of methods and instruments for testing materials, devices, and structures; advisory services to Government Agencies on scientific and technical problems; invention and development of devices to serve special needs of the Government; and the development of standard practices, codes, and specifications. The work includes basic and applied research, development, engineering, instrumentation, testing, evaluation, calibration services, and various consultation and information services. Research projects are also performed for other Government agencies when the work relates to and supplements the basic program of the Bureau or when the Bureau's unique competence is required. The scope of activities is suggested by the listing of divisions and sections on the inside of the back cover.

Publications

The results of the Bureau's work take the form of either actual equipment and devices or published papers. These papers appear either in the Bureau's own series of publications or in the journals of professional and scientific societies. The Bureau itself publishes three monthly periodicals, available from the Government Printing Office: The Journal of Research, which presents complete papers reporting technical investigations; the Technical News Bulletin, which presents summary and preliminary reports on work in progress; and Basic Radio Propagation Predictions, which provides data for determining the best frequencies to use for radio communications throughout the world. There are also five series of nonperiodical publications: The Applied Mathematics Series, Circulars, Handbooks, Building Materials and Structures Reports, and Miscellaneous Publications.

Information on the Bureau's publications can be found in NBS Circular 460, Publications of the National Bureau of Standards ($1.25) and its Supplement ($0.75), available from the Superintendent of Documents, Government Printing Office, Washington 25, D. C.

Order all publications from the Superintendent of Documents
U. S. Government Printing Office, Washington 25, D. C.

Use of funds for printing this publication approved by the Director of the Bureau of the Budget (May 14, 1956)

Journal of Research of the National Bureau of Standards Vol. 60, No. 6, June 1958 Research Paper 2867

Measurement of Flame Speeds by a Nozzle Burner Method[1]

Carl Halpern

The literature records a great many measurements, using stationary flames on burners, of the speed with which flame moves through combustible mixtures of gases. Despite the fact that the method itself seems reasonably simple, the results obtained by various investigators often are not in good agreement. One of the phases of a program of research on combustion has been a study of some of the reasons for the differences among recorded values of flame speed measured by the burner method. The primary objective of this task has been to develop the precautions that should be observed in applying the method, rather than to evolve numerical values of flame speed. This paper describes progress that has been made since the apparatus was described originally in 1951, and presents values of flame speeds of methane-air mixtures obtained since then, together with comparisons of these values with those obtained by two flame theories.

1. Introduction

The capabilities and limitations of equipment designed for measuring flame speeds approaching the fundamental burning velocities have been described in previous publications [1, 2].[2] Briefly, this apparatus is designed for producing stable Bunsen-type flames above nozzles, from which the unburned mixture emerges at practically uniform velocity. Provision is made for varying and measuring initial mixture composition, temperature, and pressure, and for making direct and schlieren photographs of the inner flame cone. In the course of attempts to obtain values of burning velocity that are independent of the apparatus, a considerable number of the possible reasons for such dependence have been identified. Some of the disturbing factors have been eliminated and the effects of others have been reduced materially. It is hoped that this record of the precautions that have been found necessary in the measurement of burning velocities by a burner method may be useful to those who may choose to apply the method in the future.

2. Apparatus

The apparatus, patterned on that of Johnston [3], was described previously in reference [1], but since then numerous changes have been made to improve its performance. A brief description of the apparatus will be given and the major changes described fully. A schematic diagram is shown in figure 1. There are two separate systems for metering and controlling the rates of flow of fuel and air. The fuel is bottled methane, 99.65 percent pure; impurities are carbon dioxide, nitrogen, and ethane. Air is provided by the laboratory supply at 90 lb/in.^{2} gage. Each system comprises a pressure regulator, a drying unit, a thermocouple to measure gas temperature, a sharp-edged orifice, a manometer to measure the pressure drop across the orifice, a manometer to measure pressure in the system, a flow controller, and a control valve. A micromanometer, read to 0.001 in., can be connected to read the pressure drop across either orifice. Standard well-type manometers, read to 0.01 in., are used to measure other pressures. The burner assembly comprises a stainless-steel approach tube, 38 in. long and 1½-in. i. d., a chamber for heating the gas mixture to a constant temperature and for smoothing the flow of the gas, and a nozzle. Fuel and air are mixed and introduced at the base of the approach tube. The calming chamber and nozzle are enclosed in a steel box, having plate-glass windows, which may be pressurized or evacuated. The double-pass noncoincidence schlieren system comprises an air-cooled mercury-vapor lamp, a collimating lens, a 90° prism, a first knife edge, and 8-in. first-surface spherical mirror, a second knife edge, an image-forming lens, and a 35-mm camera body.

Drying systems: Originally it was planned to use the fuel and air saturated with water vapor. But as the amount of water vapor in a gas depends on its temperature and pressure, both of which are variable, and the calibration of the orifices involves the density of the gas, it was decided to dry the fuel and air to avoid uncertainties caused by fluctuating water content. The drying system for air, which is first passed through a filter to remove scale and oil, comprises a column of activated alumina followed by a cold trap immersed in a slush of dry ice in a mixture of carbon

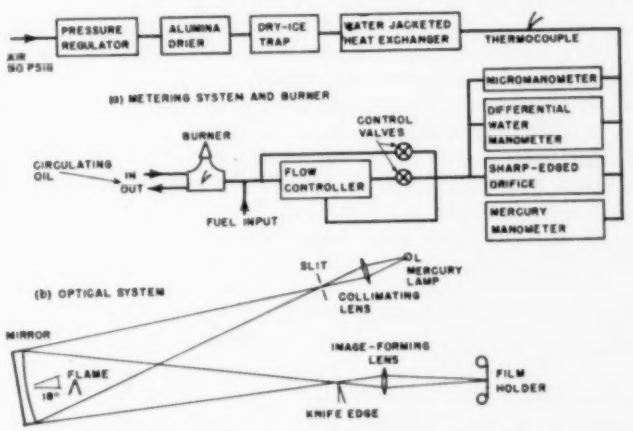

FIGURE 1. *Schematic diagram of metering, drying and schlieren equipment, and nozzle assembly.*

[1] The work described in this report was sponsored originally by the Bureau of Aeronautics, Department of the Navy.

[2] Figures in brackets indicate the literature references at the end of this paper.

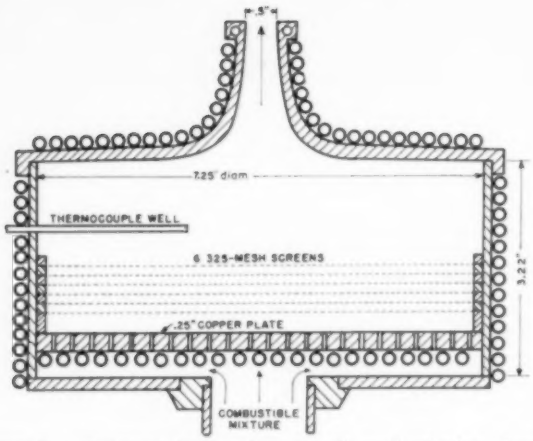

FIGURE 2. *Constant temperature nozzle and calming chamber.*

tetrachloride and chloroform at a temperature of about −112° F. The air is then warmed in a heat exchanger by tap water. The alumina column contains a built-in heating unit so the contents may be reactivated in place. The drying system for methane consists only of the cold trap and heat exchanger. Water content is thus kept at 0.03 percent by volume.

Orifices: The sharp-edged orifices were recalibrated several times because some discrepancies in calculated rate of gas flow were discovered. Calibrations obtained after correcting for or eliminating all known sources of error are felt to be accurate to about 0.5 percent. Orifices of extended range for use with larger nozzles, and new improved orifice holders have been built. Thermocouples made from specially calibrated wire are used to measure gas temperatures. Emf from these couples is measured by a precision electronic potentiometer to about 1 μv, or 0.04° F.

The constant-temperature calming chamber and nozzle are shown in figure 2. Three nozzles of ½-, ¾-, and 1$\frac{1}{16}$-in. port diameter were built. The combustible mixture enters the chamber from the burner tube, passes through the perforated plate, consisting of spirally wound coils of $\frac{3}{16}$-in. copper tubing, hard soldered to the under side of a copper disk, through copper gauze screens into the calming region above, and out through the nozzle. The nozzle and cylindrical sides of the chamber are wound with copper tubing, which is hard soldered to the surfaces. The lip of the nozzle contains a channel connected in series with the coils. The three coils that completely envelop the calming chamber and nozzle are manifolded and insure that the entire volume above the copper plate is practically isothermal. A thermocouple well made of 18–8 stainless steel tubing 0.090-in. o. d. and 0.010-in. wall thickness is mounted in the geometric shadow of the nozzle and is silver plated to decrease the effects of radiation. The hot thermostatically controlled fluid circulated through the coils is Plexol 201, a proprietary synthetic lubricant. The maximum temperature that can be used, about 350° F, is considerably below the boiling point of the liquid, which is about 500° F. Cavitation in the pump used to circulate the liquid appears to be the limiting factor. Temperature of the gas flowing through the calming chamber and nozzle can be controlled to ±0.5° F.

When the ½-in. nozzle and calming chamber were first put to use, turbulence induced by the gas issuing from the perforated copper plate resulted in a disturbed flame. A layer of glass wool on the copper plate retained by a 60-mesh copper screen was sufficient to smooth out inequalities in the gas flow through the ½-in. nozzle. These measures were inadequate for the ¾-in. nozzle, and it was necessary to use two 325-mesh screens above the plate and partly to stuff the approach tube with steel wool. The 1$\frac{1}{16}$-in. nozzle could not be placed in service because a flame of required quality could not be formed despite many attempts to smooth the gas flow. The measures taken to improve the gas flow through this large nozzle, however, greatly improved the performance of the smaller nozzles. The perforated copper plate in the calming chamber was redesigned and lowered. Six 325-mesh screens and spacers were installed, and the use of glass and steel wool was discontinued. It is felt that improperly smoothed gas flow rather than any inherent instability of large flames is the cause of the failure to obtain a satisfactory flame on the 1$\frac{1}{16}$-in. nozzle.

Schlieren system: A condenser discharge type of power supply to supplement the original power supply for the mercury-vapor lamp was built to provide a high-intensity flash to permit the study of disturbed flames. A 1-μf condenser is charged to 2,800 v and discharged through the lamp. An auxiliary series gap, ionized by an automobile spark coil, is used to insulate the capacitor until the flash is desired. A flash with a duration of about 30 μsec is obtained.

A 35-mm camera is used to photograph the flame, and all measurements are made from enlargements, which are printed on aerial mapping paper having a minimum of shrinkage. Only the body and the focal plane shutter of the camera are used. The camera lens is removed, and an achromatic lens of 60-cm focal length, placed a suitable distance behind the second knife edge, forms the image on the plane of the film in the camera. To record the visible and schlieren images simultaneously on the same film, the intensity of the light from the lamp is decreased by a variable-density filter until the two images are equal in intensity in the view finder of the camera. A section of a machinist's scale is positioned on the nozzle and photographed so the exact size of the photographed flames can be determined.

3. Measurement of Burning Velocity

The true burning velocity is the velocity of propagation of a flame, normal to the flame front, relative to the unburned mixture. It is thus a property of the mixture of fuel and oxidant, and of the physical condition of the mixture and is independent of the apparatus in which it is measured. Ideally, if the velocity of the unburned gas issuing from the port of a burner is uniform and the gas flow is parallel to the axis of the burner, the flame

FIGURE 3. *Typical methane-air flame above a nozzle burner.*

ront is a perfect right cone. The true burning elocity is then equal to the component of the elocity of the unburned gas, which is perpendicular o an element of the cone, and is given by

$$S_f = U_u \sin \alpha, \qquad (1)$$

here S_f is the true burning velocity; U_u, the velocity f the unburned gas; and α, one-half the angle of he apex of the flame cone.

Because the values reported in the literature as rue burning velocity differ so widely, obviously ctors other than properties of the combustible ixtures or their physical conditions have influenced he determinations. These cannot therefore be onsidered true burning velocities with any degree of accuracy, and until effects of these disturbing facors have been shown to be either eliminated or minimized, values presented here will be termed lame speeds.

As described in reference [1], flame speeds were rst calculated, using eq (1), from a group of obserations in which the image of the schlieren cone as projected on a ground-glass screeen, and its pex angle was measured directly by a goniometer. he results showed a variation of flame speed with as velocity of 30 percent over the range of gas elocities of 3 to 5 fps, and are inconsistent with the oncept of burning velocity as a property of the ixture and its state only.

At this point, a photographic study of flames was egun. Figure 3 is a photograph of a typical ethane-air flame atop a nozzle burner, showing oth the luminous and schlieren images taken simulaneously. The bases of both the schlieren and isible cones were found to be larger than the diameter of the port. The base of the schlieren cone, hich is defined by extending straight lines through he center of the schlieren trace to the top of the urner, was found to vary both with the velocity f the gas and with the fuel-air ratio.[3] The diameter

[3] Fuel-air ratio (F/A) is defined as the ratio of the weight of fuel to the weight of air in the combustible mixture.

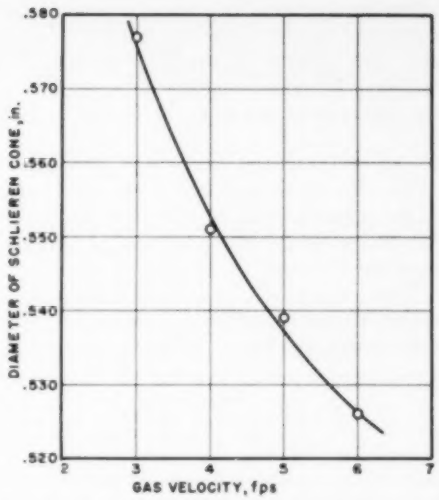

FIGURE 4. *Variation of diameter of base of schlieren cone with gas velocity, $F/A=0.058$, $T_u=75°$ F.*

of the base of the schlieren cone decreases as the gas velocity increases, and this effect is illustrated in figure 4. Using a nearly stoichiometric fuel-air mixture (F/A), at a constant nozzle temperature, (T_u), the diameter of the base of the schlieren cone, (D_c), was 0.573 in at a gas velocity of 3 fps but decreased to 0.521 in. at a gas velocity of 7 fps. The slight increase in diameter of the base of the schlieren cone with fuel-air ratio is illustrated in figure 5. At a constant gas velocity of 6 fps and a fuel-air ratio of 0.057, the diameter of the base of the cone was 0.526 in., whereas at fuel-air ratio of 0.067, the diameter was 0.531. Temperature of the combustible mixture was about 75° F. The diameter of the port of the nozzle is 0.504 in. at room temperature.

Previous tests had shown the flow of gas issuing from the nozzle in the absence of burning to be uniform and the velocity profile to be flat, so that this lateral expansion, which leads to an increase in the diameter of the base of the flame cone, must be caused by burning. Particle track studies [4] of burner flames show that the gas flow tends to diverge from parallel both at the rim of the burner and in the preheat region just ahead of the zone of combustion. It is widely considered that quenching of flame occurs at the rim of a burner, which acts as a sink for heat and active particles, and quenching may affect the flow of the gas. There exists a dark space just above the rim into which some of the combustible mixture may flow. It is also conceivable that air may infil-

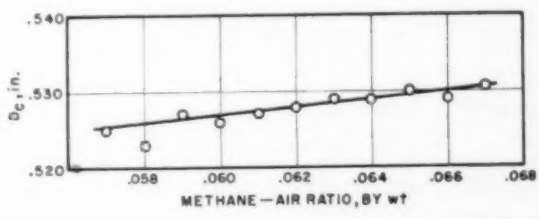

FIGURE 5. *Variation of diameter of base of schlieren cone with fuel-air ratio, $U_u=6$ fps, $T_u=75°$ F.*

trate into the dark space, cooling the gas and lowering the flame speed adjacent to the nozzle. The flow of gas through the nozzle, especially at low velocities, may be subject to the "teapot effect" [5], in which the effluent gas clings to and flows along the rim of the nozzle.

Because eq (1), which requires measurement of only gas velocity and the angle of the flame cone, does not yield reliable values of flame speeds, a means was sought to improve the reliability of the results. It was found that if eq (1) is modified by the empirical factor $(D_n/D_c)^2$, where D_n is the diameter of the port of the burner, and D_c is the diameter of the base of the schlieren cone, giving

$$S_f = U_n\left(\frac{D_n}{D_c}\right)^2 \sin\alpha, \tag{2}$$

the flame speed shows relatively little variation with gas velocity. Equation (2) is merely another way of expressing the well-known area method of calculating flame speeds:

$$S_f = V/A, \tag{3}$$

where V is the volumetric rate of flow of the unburned gas, and A is the surface area of the flame. For purposes of calculation, eq (3) may be written as

$$S_f = \frac{4V}{\pi D_c^2}\sin\alpha. \tag{4}$$

This requires a measurement of the angle of the apex of the schlieren cone and the diameter of the base of the schlieren cone. Use of eq (4) (termed the perfect cone technique) reduced the variation of flame speed with gas velocity from 30 percent over the range of gas velocities of 3 to 5 fps to about 4 percent over the increased range of 3 to 7 fps, at a gas temperature of about 75° F. Improvements to the burner and gas-measuring systems further decreased this variation.

Another method of determining the total area, called the "planimeter technique," is based on a method described by Albright, Heath, and Thena [6]. Here, the surface area of the flame cone is calculated by

$$A = \pi A_1 l/h, \tag{5}$$

where A_1 is the area, determined by a planimeter, of the vertical cross section of the schlieren cone as seen on a photograph of a flame; l, the slant height of the cone; and h, the height of the cone. Equation (5) can be transformed to

$$A = \frac{\pi}{4}(16A_1^2 + D_c^4)^{1/2}, \tag{6}$$

where only A_1, the area of a vertical cross section of the flame cone, and D_c, the diameter of the base of the schlieren cone, need be measured. The value of A so determined is substituted in eq (3) to determine S_f.

Equations (6) and (4) assume that the flame surface is a perfect right cone, and the closer the flame is to this ideal, the more nearly will these equations apply. The planimeter technique appears to be more accurate for determining surface areas of flames at low gas velocities than the perfect-cone technique. At low gas velocities the sides of the flame cone are somewhat curved, and it is difficult to select a straight line to represent the flame front; in fact, this is theoretically impossible. With only a slight curvature, however, the assumption of a perfect cone leads to a reasonably close approximation. Areas obtained with the planimeter are usually somewhat smaller than those calculated by the perfect-cone technique and lead to higher flame speeds. The most nearly theoretically exact method of measuring areas of flame surfaces that depart appreciably from conical is to divide the surface into a large number of segments and to sum those areas, is unfortunately laborious and difficult. Precision will decrease as measurements progress from the base to the tip because the image of the cone is somewhat diffuse. When such measurements have been made, the total area has been found to be smaller than that calculated by the perfect-cone method.

Results obtained with the planimeter technique still show a variation of flame speed with gas velocity, but the variation is linear, and the measured flame speed decreases with increasing gas velocity. A comparison of flame speeds obtained by the perfect-cone and planimeter techniques is presented in figure 6. The observed difference ranges from a minimum of about 0.4 percent at a gas velocity of

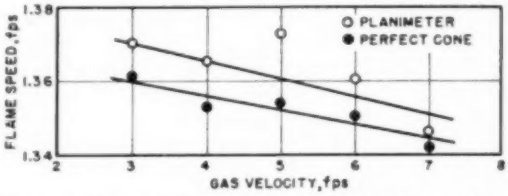

FIGURE 6. *Comparison of flame speeds obtained by the planimeter and perfect cone methods, $F/A = 0.062$, $T_n = 112°$ F, diameter of nozzle = ¾ in.*

7 fps to about 1.4 percent at 5 fps. If, however, we ignore the observation by the planimeter method at 5 fps, which appears to be out of line with the rest, the maximum difference remaining is less than 1 percent. Best results by either method indicate that the variation of flame speed with gas velocity has been reduced to about 1.5 percent in this range. Precision of measurement is the same in both techniques, about 0.25 percent. This small variation may be a result of averaging the flame speed over the entire flame surface. Near the tip of the flame cone, because of the strong curvature, the flame speed is probably highest; whereas at the base, due to the presence of the burner rim, it is lowest [7].

4. Some Factors Affecting Flame Speed

4.1. Gas Temperature

Some of the heat liberated by a flame is inevitably transferred to the burner and thence to the gas that

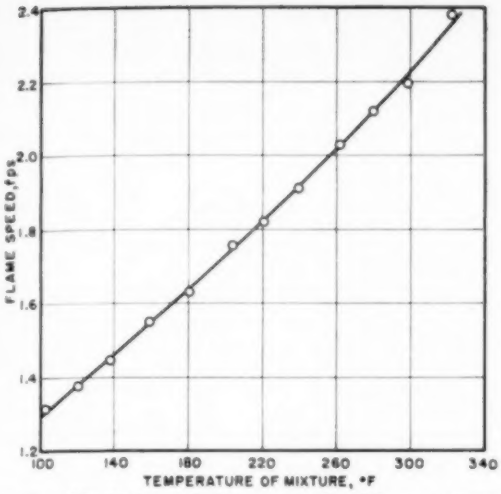

FIGURE 7. *Variation of flame speed with gas temperature, $F/A=0.062$, $U_u=6$ fps, diameter of nozzle=½ in.*

is flowing through it. Thus thermal gradients may be set up, with the gas nearest the wall being the hottest, and the over-all temperature of the combustible mixture at the burner will be higher than the temperatures of the fuel and air measured upstream. Any calculation of volume rate of flow that ignores this heating will be in error. The temperature gradient may lead to a distorted flame. Use of a constant-temperature nozzle and calming chamber is an attempt to insure that the temperature of the gas in the nozzle is known and that thermal gradients are at a minimum. As shown in figure 7, the flame speed is greatly affected by the initial temperature of the combustible mixture. (The flame speeds reported hereafter are averages of the values obtained by the perfect cone and planimeter techniques.) Over the range 100° to 325° F, the variation of flame speed with initial temperature is nearly linear and amounts to 0.0048 fps/° F. At 100° F, the flame speed is 1.305 fps, whereas at 320° F, it is 2.361 fps. The fuel-air ratio was 0.062, approximately the value for maximum flame speed, during this series of observations, and the unburned gas velocity was 6 fps. In view of this relationship between flame speed and initial temperature, the initial temperature of the combustible mixture must be controlled and specified if reported values of flame speeds are to have any significance.

4.2. Mixture Ratio

The variation of flame speed with mixture ratio at constant gas velocity was determined for three initial gas temperatures. The ¾-in. nozzle was used, and the gas velocity was 6 fps. The fuel-air ratio was varied from 0.054 to 0.072, and gas temperatures of 84.4°, 100°, and 120° F were used. A gas temperature of 84.4° F is the lowest that can be maintained at the nozzle by circulating oil, which is cooled in a heat exchanger by tap water. Results of these experiments are shown in figure 8. The maximum flame speed is found at a fuel-air ratio close to 0.062, and there seems to be no definite displacement with

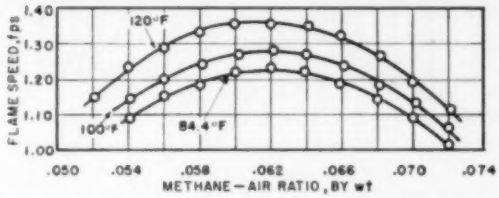

FIGURE 8. *Effect of fuel-air ratio on flame speed at three unburned gas temperatures, $U_u=6$ fps, diameter of nozzle= ¾ in.*

temperature over the limited range covered here.

Further measurements were made of flame speeds of methane-air mixtures at gas temperatures at the burner nozzle of 280° and 330° F, using the ½-in. nozzle. The velocity of the gas in the nozzle was varied from 4 to 7 fps at 280° F and from 5 to 10.2 fps at 330° F. The fuel-air ratio was varied from 0.054 to 0.072 except at a gas velocity of 10.2 fps and a temperature of 330° F, where the leanest mixture that would burn was at fuel-air ratio 0.056; below this, the flame blew off the nozzle. Variation of flame speed with fuel-air ratio at constant gas velocity and at 280° F is shown in figure 9, and at 330° F in figure 10. The maxima are seen to have shifted at the higher temperatures to slightly richer mixture ratios. The large effect of mixture ratio on flame speed is, of course, obvious, and emphasizes the fact that the fuel-air ratio must be specified in

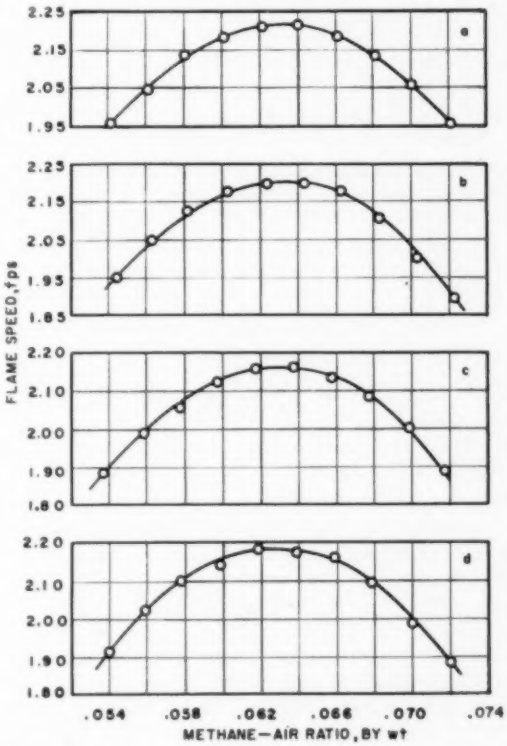

FIGURE 9. *Effect of fuel-air ratio on flame speed at constant gas velocity.*

T_u=280° F; U_u=(a) 4 fps; (b) 5 fps; (c) 6 fps; (d) 7 fps. Diameter of nozzle= ½ in.

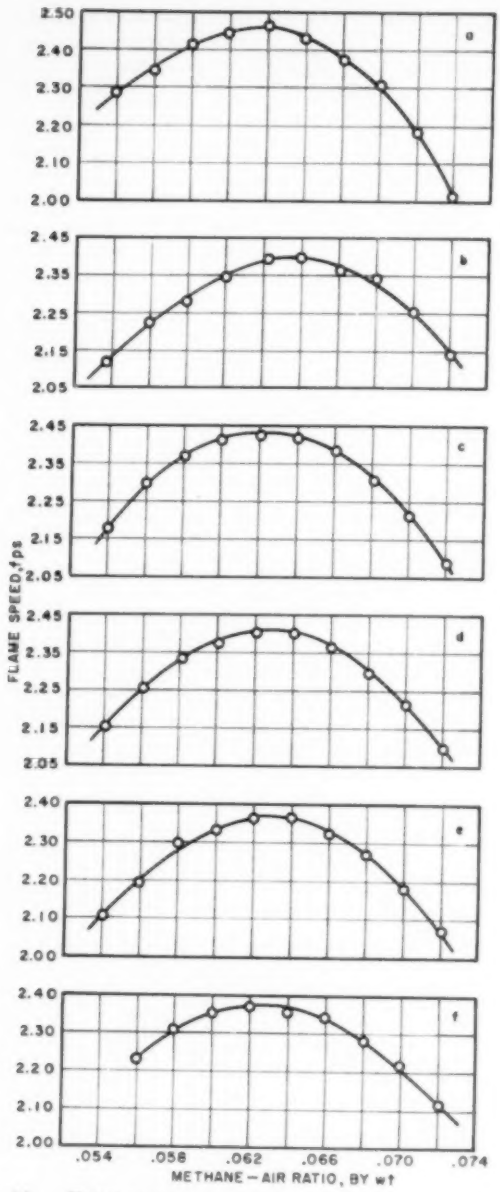

FIGURE 10. *Effect of fuel-air ratio on flame speed at constant gas velocity.*

T_u=330° F; U_u=(a) 5 fps; (b) 6 fps; (c) 7 fps; (d) 8 fps; (e) 9 fps; (f) 10.2 fps. Diameter of nozzle=½ in.

defining a value of flame speed. The maximum flame speeds and the fuel-air ratios at which these maxima occur, at various gas velocities, are shown in table 1.

4.3. Gas Velocity

If, as mentioned earlier, the measured flame speed or burning velocity is a property of the combustible mixture only, and is not influenced by the burner or associated equipment, the values obtained will be expected to be independent of the gas velocity, U_u. That the measured values are not independent of gas velocity is shown in figures 11 and 12, where flame speeds obtained at initial mixture tempera-

TABLE 1. *Maximum flame speeds at given fuel-air ratios*

Gas velocity	Fuel-air ratio for maximum flame speed	Gas temperature	Flame speed
fps		° *F*	*fps*
6	0.0619	84.4	1.233
6	.0621	100	1.283
6	.0618	120	1.364
4	.0634		2.212
5	.0636		2.201
6	.0627	280	2.164
7	.0628		2.180
5	.0623		2.457
6	.0632		2.400
7	.0627		2.426
8	.0630	336	2.406
9	.0632		2.372
10.2	.0628		2.360

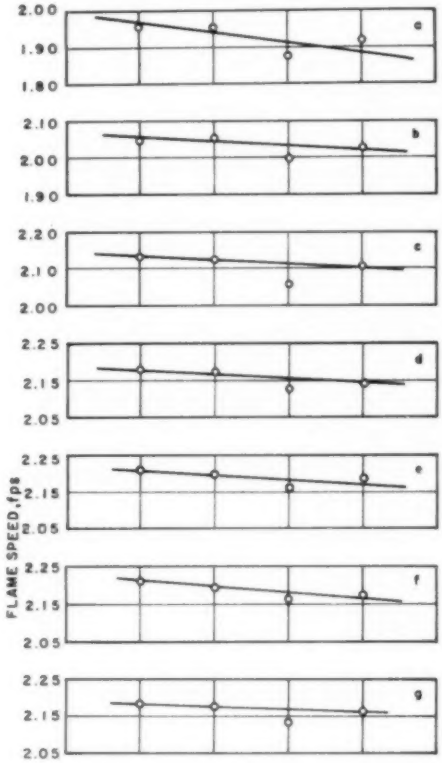

FIGURE 11. *Effect of gas velocity on flame speed at constant fuel-air ratio.*

T_u=280° F; F/A=(a) 0.054; (b) 0.056; (c) 0.058; (d) 0.060; (e) 0.062; (f) 0.064; (g) 0.066; (h) 0.068; (i) 0.070; (j) 0.072. Diameter of nozzle=½ in.

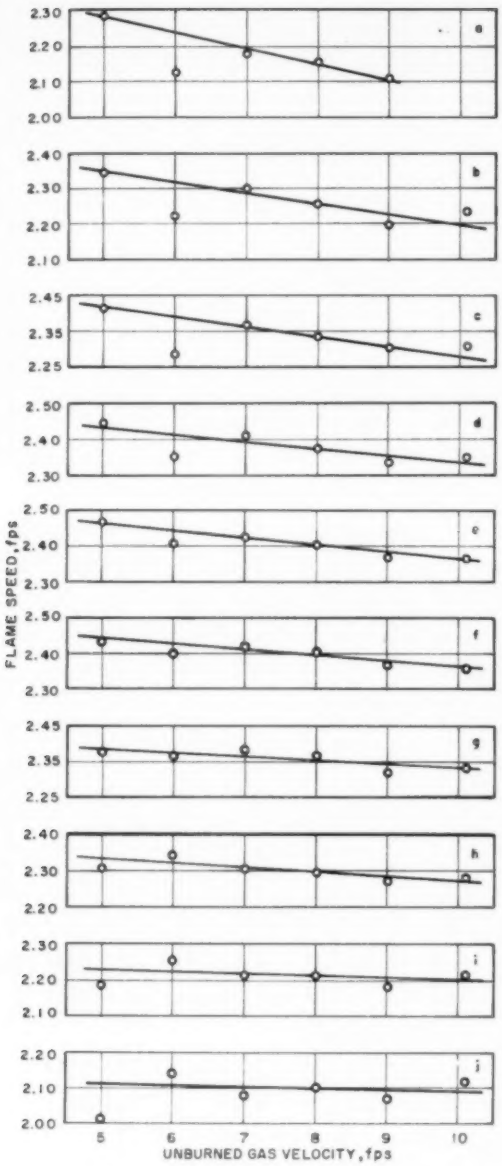

FIGURE 12. *Effect of gas velocity on flame speed at constant fuel-air ratio.*

T_u=330° F; F/A=(a) 0.054; (b) 0.056; (c) 0.058; (d) 0.060; (e) 0.062; (f) 0.064; (g) 0.066; (h) 0.068; (i) 0.070; (j) 0.072. Diameter of nozzle=½ in.

tures of 280° and 330° F, respectively, are seen to decrease in practically all cases as gas velocity increases. Reasons for this dependence on gas velocity are obscure, but changes in apparatus and analytical methods described above have reduced the variations from as much as 30 percent to those found here.

Variation of flame speed with gas velocity at the lower temperatures was about 1.5 percent on the average, increased to about 2 percent at a gas temperature of 280° F, and increased still further to an average of about 3.5 percent at a temperature of 330° F. This increase with temperature may be a result of increased convection in the air surrounding the flame induced by the temperature difference between the air and the nozzle. Stability of the flame may have been affected by this increased convection.

The greatest variation of flame speed with gas velocity at 330° F was about 7.5 percent over the range of gas velocities from 5 to 9 fps at a fuel-air ratio of 0.054. This decreased as the mixture became richer, to about 5 percent at 0.056, and to 1 percent at a ratio of 0.066. The mixture apparently is near the lean blow-off limit at a mixture ratio of 0.054 because this mixture would not burn at 10.2 fps, so the values at 0.054 may not be trustworthy. If these values are disregarded, the average variation at a gas temperature of 330° F of flame speed with gas velocity is about 2.8 percent.

4.4. Nozzle Size

Variation of flame speed with gas velocity may be due in part to quenching of the flame by the burner rim. If the size of the burner port is increased, it might be expected that this variation would be reduced because the ratio of burner rim to flame area decreases as the diameter of the port increases. Earlier workers [8] had reported that the size of the burner does affect the flame speed, although their burners were much smaller than the ones used in the present work. It has also been suggested that there exists a size above which the flame speed is no longer affected. The nozzle with the ¾-in. port was built to test this suggestion, and the results with it were compared with those obtained with the ½-in. nozzle. First results indicated that measured flame speeds were higher with the ¾-in. nozzle, and that the variation of flame speed with gas velocity was reduced over the range of gas flow from 3 to 7 fps. When, however, the gas flow was improved, oscillations were eliminated, and better control of gas temperature was established, the results showed no appreciable difference between the two nozzles. The variation of flame speed with gas velocity was about 1.5 percent in both over the range of gas velocities from 3 to 7 fps.

4.5. Oscillations

Oscillations were encountered in the flames during attempts to place the ¾-in. and 1 1/16-in. nozzles in operation. At times the tip of the flame cone fluctuated wildly, and a low-pitched buzzing was heard. To investigate this, a study of disturbed flames was made in which photographs, some of which are shown in figure 13, were taken at exposure times of 1/1000 sec and 5 sec at gas velocities of 3, 4, 5, 6, and 7 fps. Photographs taken at 1/1000 sec, which show only the schlieren image, are sharp, whereas those taken at 5 sec have the added visible image and are rather blurred; the taller flames are most disturbed. Because the camera has a focal plane shutter, what is seen in these pictures is a combination of the motion of the flame and the shutter.

High-speed motion pictures of these flames showed a series of pulsations beginning at the base and traveling up to the tip of the flame cone. Figure 14 shows the appearance of these pulsations in a picture

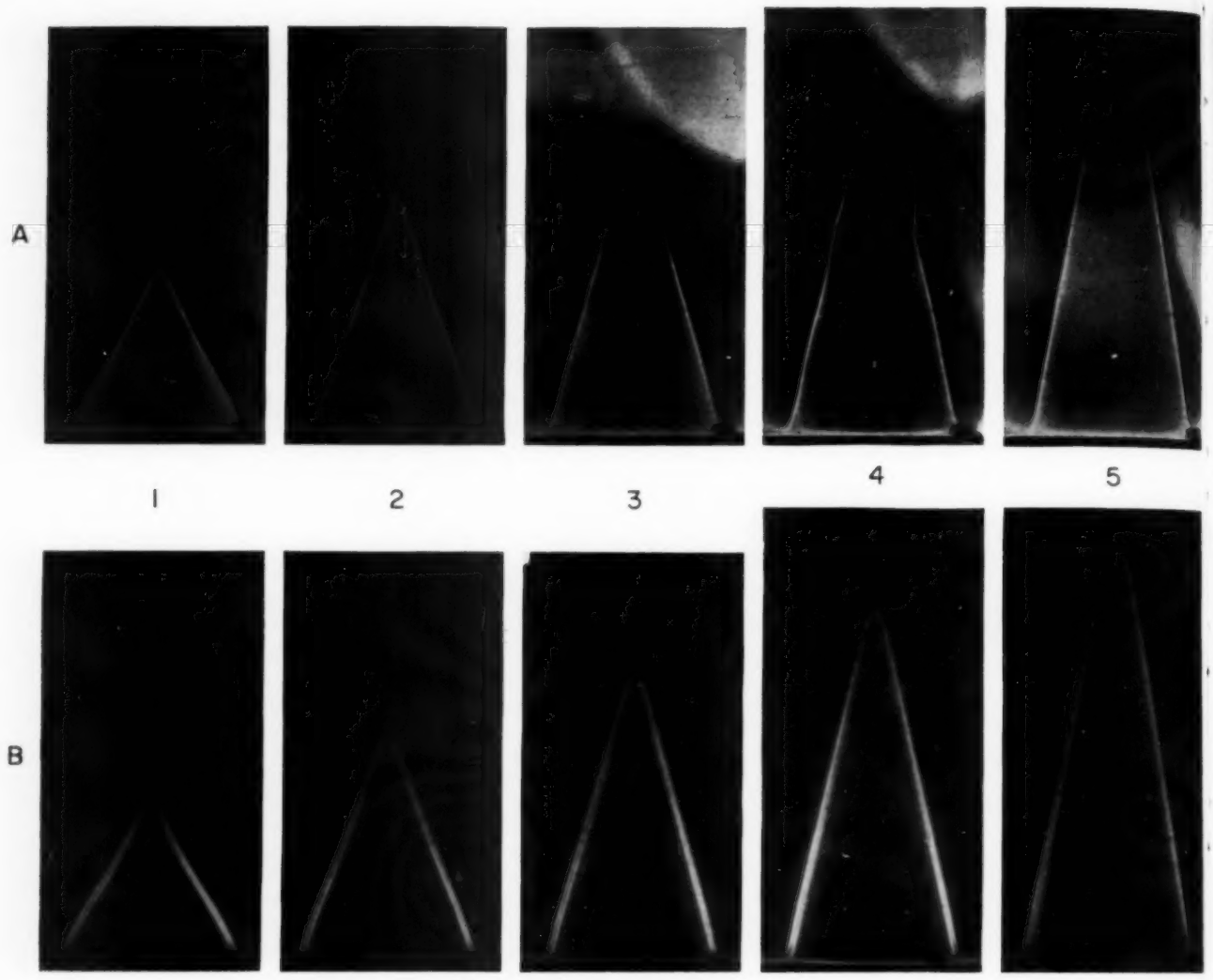

FIGURE 13. *Disturbed flames taken at (a) 0.001 and (b) 5-sec exposure time.*

Gas velocity = (1) 3 fps; (2) 4 fps; (3) 5 fps; (4) 6 fps; (5) 7 fps.

of a schlieren cone, taken by a high-intensity flash. The pulsations were removed completely from the flame by lining the burner enclosure with acoustic tile.

Comparison of oscillating and quiescent flames show that there is less scatter in measurements made on quiescent flames, but no significant difference is seen in the magnitudes of flame speeds derived from measurements of instantaneous photographs of the two types of flames. There is no difference in values obtained from instantaneous and time photographs of quiescent flames, but flame speeds obtained from time exposures of oscillating flames are excessively high. This latter effect may be caused by the increased intensity of the schlieren image, due to the horizontal knife edge, which results when the inclination of the side of the cone increases as a pulse travels up the cone. A time exposure of an oscillating flame thus would have greater intensity toward the inner edge of its blurred image and give the appearance of a smaller flame.

FIGURE 14. *Oscillating methane-air flame.*

5. Comparison of Experiment With Theories

The variation of flame speed with initial temperature had been determined for a methane-air mixture, $F/A=0.062$, at a gas velocity of 6 fps for the temperature range 312.5° to 434.9° K (102.7° to 323.1° F), and data were thus available for a comparison of the experimental results with those predicted by Semenov's thermal theory and Tanford and Pease's diffusion theory. Semenov's equation [9] for flame speed, assuming a bimolecular reaction, is

$$S_f=\left[\frac{2\lambda_f K a_o c_{p(f)}^2}{\bar{c}_p^3}\left(\frac{T_o}{T_f}\right)^2\left(\frac{\lambda}{c_p\rho D_f}\right)^2\left(\frac{n_1}{n_2}\right)^2\left(\frac{RT_f^2}{E}\right)^3\frac{e^{-E/RT_f}}{(T_f-T_o)^3}\right]^{1/2}, \quad (7)$$

where

T_0 = initial temperature, ° K
T_f = flame temperature, ° K
ρ = density of gas mixture, g/cm^3
λ_f = thermal conductivity at T_f, cal/cm sec °K
$c_{p(f)}$, $\bar{c}_p$ = specific heat at T_f, and mean specific heat, T_o to T_f, respectively, cal/°K g
$\frac{n_1}{n_2}$ = moles of reactants/moles of products
D_f = diffusion coefficient at T_f, cm/sec
R = gas constant, cal/g mole—° K
E = activation energy, cal/g mole
K = constant from the Arrhenius reaction rate equation
a_0 = number of molecules per unit volume of combustible in initial mixture.

Following Dugger's treatment [10], eq (7) reduces to

$$S_f\propto\left(T_0^2T_f^{1.9}\frac{e^{-E/RT_f}}{(T_f-T_o)^3}\right)^{1/2}. \quad (8)$$

The Tanford and Pease equation [11] for flame speed is

$$S_f=\left(\Sigma_i p_i D_i k_i L\frac{Q'}{QB_i}\right)^{1/2}, \quad (9)$$

where

p_i = mole fraction or partial pressure of a given active particle in the burnt gas
D_i = the diffusion coefficient of the active particle into the unburnt gas
k_i = a rate constant for reaction of an active particle with the unburnt gas
L = number of molecules per cubic centimeter of gas at some mean temperature
Q_i' = mole fraction of combustible in the unburnt gas
Q_i = mole fraction of potential combustion product in the burnt gas
B_i = term near unity, arising from radical recombination.

Again following Dugger, this is reduced to

$$S_f\propto[(\Sigma p_i D_{i,7})T_0^{1.67}T_{av}^{-1}]^{1/2} \quad (10)$$

where $D_{i,7}$ is the relative diffusion coefficient of the given radical with respect to the other radicals, T_0 is the initial temperature, and T_{av} is the average of initial and flame temperature.

Flame temperatures were calculated by the method of Hottel, Williams, and Satterfield [12]. Equilibrium partial pressures of hydrogen atoms, hydroxyl radicals, and oxygen atoms were calculated by the method of Huff and Calvert [13]. The activation energy, E, was taken as 26 kcal/g mole [14].

In figure 15, where temperatures are in degrees Kelvin and flame speeds are in centimeters per second, curve AB represents the experimental data; AC is calculated by Semenov's equation; AD is calculated from Tanford and Pease's equation, using $\Sigma p_i D_{i,7}=6.5\ p_H+p_{OH}+p_O$, and AE is calculated from Tanford and Pease's equation considering only p_H. Only the shape of the curves can be calculated; the calculation of absolute values of flame speeds depends on too many quantities that are uncertain or even unknown. The Semenov equation reproduces the shape of the experimental curve well, although it tends to diverge as the initial temperature increases. At 434.9° K, the divergence amounts to about 5 percent. Curves AD and AE from Tanford and Pease's equation are almost coincident, but the fit to the experimental data is not as good. At 434.9° K, there is a divergence of about 15 percent from the experimental curve.

The thermal theory thus appears to predict the effect of initial temperature on flame speed better than does the diffusion theory. However, as rather drastic assumptions were made in applying both

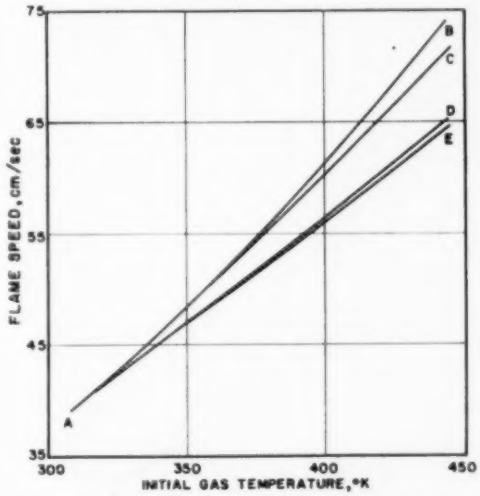

FIGURE 15. *Comparison of experimental values with those calculated from equations of Semenov and of Tanford and Pease.*

AB represents NBS; *AC*, Semenov; *AD*, Tanford and Pease, 6.5 $p_H+p_O+p_{OH}$; *AE*, Tanford and Pease, p_H only.

theories, it is possible that they were more favorable to Semenov's equation. Selection of the preferred theory from the data presented here therefore should be made with caution, if at all.

6. Experimental Observations

Observations of the effects of some variables on the flame are presented in detail in tables 2 to 7.

TABLE 2. *Variation of diameter of base of schlieren cone with gas velocity, at 75° F, fuel-air ratio=0.058*

Gas velocity	Diameter of base of schlieren cone	Gas velocity	Diameter of base of schlieren cone
fps	*in.*	*fps*	*in.*
3	0.577	5	0.539
4	.551	6	.526

TABLE 3. *Variation of diameter of base of schlieren cone with fuel-air ratio, at 75° F, gas velocity=6 fps*

Fuel-air ratio	Diameter of base of schlieren cone	Fuel-air ratio	Diameter of base of schlieren cone
	in.		*in.*
0.057	0.525	0.063	0.529
.058	.523	.064	.529
.059	.527	.065	.530
.060	.526	.066	.529
.061	.527	.067	.531
.062	.528		

TABLE 4. *Variation of flame speed with gas velocity at 112.3° F, fuel-air ratio=0.062*

Gas velocity	Flame speed	Gas velocity	Flame speed
(a) Perfect cone technique			
fps	*fps*	*fps*	*fps*
3	1.362	6	1.350
4	1.353	7	1.342
5	1.354		
(b) Planimeter technique			
3	1.370	6	1.360
4	1.366	7	1.347
5	1.373		

TABLE 5. *Variation of flame speed with temperature fuel-air ratio=0.062, gas velocity=6 fps*

Temperature	Flame speed	Temperature	Flame speed
° *F*	*fps*	° *F*	*fps*
102.7	1.316	220.7	1.819
120.6	1.376	240.3	1.910
138.3	1.443	262.4	2.028
159.7	1.550	280.4	2.121
181.1	1.632	298.7	2.196
203.6	1.754	323.1	2.379

TABLE 6. *Variation of flame speed with mixture ratio*

Fuel-air ratio	Flame speed	Fuel-air ratio	Flame speed
a. Gas temperature=84.4° F; gas velocity=6 fps			
	fps		*fps*
0.0541	1.094	0.0639	1.223
.0561	1.156	.0659	1.190
.0580	1.188	.0680	1.148
.0600	1.219	.0701	1.094
.0619	1.233	.0720	1.017
b. Gas temperature 100° F			
0.0542	1.145	0.0640	1.271
.0560	1.201	.0661	1.240
.0581	1.242	.0681	1.186
.0601	1.269	.0701	1.135
.0621	1.283	.0720	1.064
c. Gas temperature 120° F			
0.0521	1.150	0.0640	1.353
.0541	1.235	.0659	1.321
.0560	1.290	.0682	1.268
.0580	1.336	.0700	1.195
.0599	1.357	.0721	1.119
.0620	1.357		
d. Gas temperature 280° F			
(1) Gas velocity=4 fps			
0.0541	1.958	0.0641	2.211
.0561	2.044	.0661	2.183
.0580	2.134	.0681	2.131
.0601	2.180	.0703	2.054
.0622	2.208	.0721	1.957
(2) Gas velocity=5 fps			
0.0544	1.951	0.0643	2.197
.0564	2.051	.0663	2.176
.0582	2.122	.0683	2.104
.0603	2.176	.0703	2.008
.0624	2.198	.0724	1.890
(3) Gas velocity=6 fps			
0.0537	1.875	0.0636	2.161
.0558	1.997	.0658	2.135
.0577	2.059	.0677	2.084
.0597	2.128	.0698	2.001
.0618	2.161	.0718	1.887
(4) Gas velocity=7 fps			
0.0539	1.916	0.0639	2.176
.0559	2.026	.0659	2.162
.0579	2.101	.0679	2.091
.0599	2.141	.0700	1.990
.0619	2.186	.0720	1.870
e. Gas temperature 330° F			
(1) Gas velocity=5 fps			
0.0540	2.284	0.0640	2.431
.0560	2.347	.0661	2.378
.0580	2.414	.0680	2.308
.0600	2.447	.0700	2.186
.0620	2.468	.0720	2.013
(2) Gas velocity=6 fps			
0.0537	2.122	0.0640	2.397
.0560	2.223	.0660	2.364
.0580	2.286	.0680	2.343
.0600	2.350	.0700	2.259
.0620	2.407	.0720	2.140

TABLE 6. *Variation of flame speed with mixture ratio*—Con.

Fuel-air ratio	Flame speed	Fuel-air ratio	Flame speed
(3) Gas velocity = 7 fps			
0.0540	2.178	0.0640	2.419
.0560	2.299	.0661	2.383
.0581	2.367	.0681	2.306
.0600	2.410	.0701	2.212
.0620	2.425	.0721	2.079
(4) Gas velocity = 8 fps			
0.0541	2.153	0.0640	2.402
.0560	2.257	.0660	2.365
.0580	2.336	.0680	2.298
.0600	2.375	.0700	2.215
.0621	2.403	.0721	2.100
(5) Gas velocity = 9 fps			
0.0541	2.109	0.0640	2.369
.0560	2.197	.0660	2.329
.0580	2.303	.0680	2.270
.0600	2.336	.0701	2.181
.0620	2.367	.0721	2.072
(6) Gas velocity = 10.2 fps			
0.0562	2.236	0.0660	2.341
.0580	2.308	.0680	2.283
.0600	2.350	.0700	2.218
.0620	2.365	.0721	2.120
.0640	2.358		

TABLE 7. *Variation of flame speed with gas velocity*

Gas velocity	Flame speed	Fuel-air ratio	Gas velocity	Flame speed	Fuel-air ratio
a. Gas temperature 280° F					
fps	*fps*		*fps*	*fps*	
4	1.958	0.054	6	1.875	0.054
5	1.951		7	1.916	
4	2.044	.056	6	1.997	.056
5	2.051		7	2.026	
4	2.134	.058	6	2.059	.058
5	2.122		7	2.101	
4	2.180	.060	6	2.128	.060
5	2.176		7	2.141	
4	2.208	.062	6	2.161	.062
5	2.198		7	2.186	
4	2.211	.064	6	2.161	.064
5	2.197		7	2.176	
4	2.183	.066	6	2.135	.066
5	2.176		7	2.162	
4	2.131	.068	6	2.084	.068
5	2.104		7	2.091	
4	2.054	.070	6	2.001	.070
5	2.008		7	1.990	
4	1.957	.072	6	1.887	.072
5	1.890		7	1.870	

TABLE 7. *Variation of flame speed with gas velocity*—Con

Gas velocity	Flame speed	Fuel-air ratio	Gas velocity	Flame speed	Fuel-air ratio
b. Gas temperature 330° F					
fps	*fps*		*fps*	*fps*	
5	2.284	0.054	8	2.153	0.054
6	2.122		9	2.109	
7	2.178				
			8	2.257	
5	2.347	.056	9	2.197	.056
6	2.223		10.2	2.236	
7	2.299				
			8	2.336	
5	2.415	.058	9	2.303	.058
6	2.286		10.2	2.308	
7	2.367				
			8	2.375	
5	2.447	.060	9	2.336	.060
6	2.350		10.2	2.350	
7	2.410				
			8	2.403	
5	2.468	.062	9	2.367	.062
6	2.407		10.2	2.365	
7	2.425				
			8	2.402	
5	2.431	.064	9	2.369	.064
6	2.397		10.2	2.358	
7	2.419				
			8	2.365	
5	2.377	.066	9	2.329	.066
6	2.364		10.2	2.341	
7	2.383				
			8	2.298	
5	2.308	.068	9	2.270	.068
6	2.343		10.2	2.283	
7	2.306				
			8	2.215	
5	2.186	.070	9	2.181	.070
6	2.259		10.2	2.218	
7	2.212				
			8	2.100	
5	2.013	.072	9	2.072	.072
6	2.140		10.2	2.120	
7	2.079				

7. Conclusions

The apparatus for determining flame speeds has been improved so that stable flames, free from oscillations, can be maintained on ½- and ¾-in. nozzles at temperatures, measured in the throat of the nozzle, up to 330° F. The size of the nozzles is such that there are no gross effects of the burner on flame speeds. Temperature of gas in the nozzle can be controlled to ±0.5° F. Calibration of the sharp-edged orifices used to measure the flow of gases is now considered to be accurate to 0.5 percent.

Variation of flame speed with fuel-air ratio at constant gas velocity and constant inlet gas temperature has been determined for a range of temperatures up to 330° F.

Dependence of flame speed on initial gas temperature at constant gas speed was determined and the result compared with that predicted by two theories of flame propagation.

Variation of flame speed, at constant temperature, with gas velocity has been reduced, (a) by using the area technique of measuring flame speed instead of the angle technique, and (b) by improvements in the quality of the flame. Two different methods of

determining areas of the flame yield values of flame speeds that are in close agreement. From the study of photographs of flames, it was found that the diameter of the base of the schlieren cone increases as the fuel-air ratio increases, and decreases as the gas velocity increases. Conditions of flow in the nozzle during burning and quenching of flame by the nozzle undoubtedly are the cause of these effects. At an initial gas temperature of 112° F, the variation of flame speed with gas velocity over the range of gas velocities from 3 to 7 fps amounts to about 1.5 percent. This variation increases as the initial temperature increases.

Since there still remains some variation of flame speed with gas velocity, contrary to theoretical expectations, it is evident that the measurement of true burning velocity has not been achieved. However, in view of the relatively small variation remaining, it is reasonable to expect the values of flame speeds reported here approach closely the true burning velocity.

Gerry H. Morgan, now of the University of Connecticut, Storrs, Conn., did much of the early experimental work and contributed to the design of the apparatus. Many thanks are due Frank R. Caldwell for helpful discussions and encouragement.

8. References

[1] F. R. Caldwell, H. P. Broida, and J. J. Dover, Ind. Eng. Chem. **43,** 2731 (1951).
[2] G. H. Morgan and W. R. Kane, Fourth Symposium (International) on Combustion, p. 313 (Williams & Wilkins, Baltimore, Md., 1953).
[3] W. C. Johnston, Soc. Automotive Engrs. J. **55,** 62 (Dec. 1947).
[4] B. Lewis and G. von Elbe, J. Chem. Phys. **11,** 75 (1943).
[5] M. Reiner, Phys. Today **9,** 16 (Sept. 1956).
[6] R. E. Albright, D. P. Heath, and R. H. Thena, Ind. Eng. Chem. **44,** 2490 (1952).
[7] B. Lewis and G. von Elbe, Combustion, flames, and explosions of gases, p. 238 (Academic Press, N. Y., N. Y., 1951).
[8] F. A. Smith and S. F. Pickering, J. Research NBS **17,** 7 (1936) RP900.
[9] N. N. Semonov, Nat. Advisory Comm. Aeronaut. Tech. Mem. No. 1026 (1942).
[10] G. L. Dugger, J. Am. Chem. Soc. **72,** 5271 (1950).
[11] C. Tanford and R. N. Pease, J. Chem. Phys. **15,** 861 (1947).
[12] H. C. Hottel, G. C. Williams, and C. N. Satterfield, Thermodynamic charts for combustion processes (John Wiley & Sons, New York, N. Y., 1949).
[13] V. N. Huff and C. S. Calvert, Nat. Advisory Comm. Aeronaut. Tech. Note No. 1653 (1948).
[14] J. B. Fenn and H. F. Calcote, Fourth Symposium (International) on Combustion, p. 231 (Williams & Wilkins Co., Baltimore, Md., 1953).

Washington, December 5, 1957.

Journal of Research of the National Bureau of Standards Vol. 60, No. 6, June 1958 Research Paper 2858

Growth of Preferentially Oriented Aluminum Single Crystals

Theodore H. Orem

Monocrystalline aluminum specimens having both a preferential orientation and a specified cross-sectional shape are very difficult to produce. Such specimens must be grown in a vertical furnace, a condition which, while permitting the choice of cross-sectional shape in the specimen, makes it extremely difficult to obtain specimens of preferred orientation. It is fairly easy to grow preferentially oriented monocrystalline aluminum specimens when a horizontal furnace is used, but the use of such a furnace limits the choice of cross-sectional shapes in the finished crystal. Crystals of circular cross-sectional shape are practically impossible to grow in a horizontal furnace.

The method described herein can be used to grow monocrystalline aluminum crystals with any desired orientation or cross-sectional shape.

1. Introduction

Single crystals of metals are widely used in fundamental research on metals. They are grown by several different methods, one of the most popular being the Bridgman method of slow cooling from the melt.[1] The method consists essentially in causing a molten mass of metal to slowly enter a zone maintained at a temperature below the melting point of the metal. As this occurs, the small portion of the metal that enters the cool zone first, freezes. The remainder of the metal subsequently entering the cool zone will then solidify in accordance with the orientation of the initially solidified portion of the melt, if the rate of passage from the molten zone to the cool zone is properly controlled.

The most popular way of growing single crystals by this method is by the lowering of the molten metal from a hot zone in a vertical furnace into a zone whose temperature is below that of the melting point of the metal, or by raising a furnace over a stationary molten mass of metal so as to cause the metal to freeze first at its lowest point.

A variation of the Bridgman method makes use of a horizontal-type furnace in which the molten metal, in a boat-type container, is pulled slowly from the molten zone into a cool zone.[2]

It is often desirable that single crystals have their axes preferentially oriented. This is accomplished by a method generally known as "seeding." It consists in attaching a small crystal of the metal to the sample that is to be grown as a single crystal, in such a manner that the crystallographic orientation of the "seed" is parallel to the crystallographic orientation desired in the single crystal to be produced. One adjusts the heating conditions so that the entire charge, with the exception of a small portion of the seed crystal, is molten. By properly controlling the rate of withdrawal of the melt from the hot zone, it is possible to cause the molten metal to solidify as a single crystal whose crystallographic orientation is identical with that of the seed.

When grown by means of a vertical furnace it is possible to produce single crystals of any desired cross-sectional shape. It is, however, very difficult to grow single crystals of preferred orientation in a vertical furnace because of difficulty in attaching and partially melting the seed crystal. It is relatively more simple to attach and partially melt a seed crystal in order to grow preferentially oriented single crystals in a horizontal furnace. In such a furnace, however, it is impossible to grow single crystals of a desired cross-sectional shape.

Described herein is a method for growing single crystals of aluminum (mp 660° C) of any desired crystallographic orientation, using a vertical furnace, in order that crystals of any desired cross-sectional shape may be produced.

2. Materials and Description

The apparatus required for the production of aluminum single crystals of preferred axial orientation consists of a vertical tube furnace, a means of controlling and recording temperatures within the furnace, a means of conducting heat away from an area within the furnace, the usual crucibles used for melting metals, and a special crucible for melting the seed crystal. The crucibles are machined from graphite.

Figure 1 is a diagrammatic sketch of a furnace showing the equipment used for the seeding of aluminum single crystals grown by the Bridgman method of slow cooling from the melt. Figure 2 shows longitudinal sections of the main crucible, the seed-melting crucible and the device used for conducting heat away from the seed crucible. This latter device is the means by which it is possible to melt just a portion of the seed. Also shown is a second seed crucible whose function will be explained later.

In addition to the above, there is also required a quantity of seed crystals. These are aluminum single crystals, ¼ in. in diameter by 2½ in. long, which are grown in graphite crucibles by the Bridgman method. These are easy to grow and can be

[1] P. W. Bridgman, Proc. Am. Acad. Arts Sci. **60**, 305 (1935).
[2] B. Chalmers, Can. J. Phys. **31**, 132 (1953).

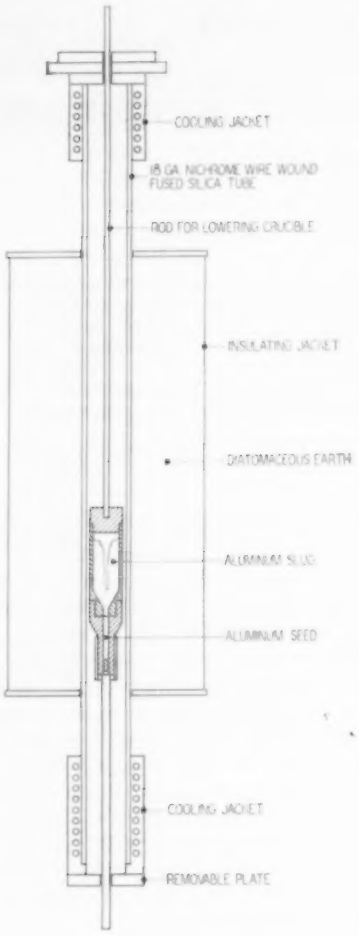

FIGURE 1. *Diagrammatic sketch of vertical crystal-growing furnace showing "seeding" device.*

Approximately one-tenth size.

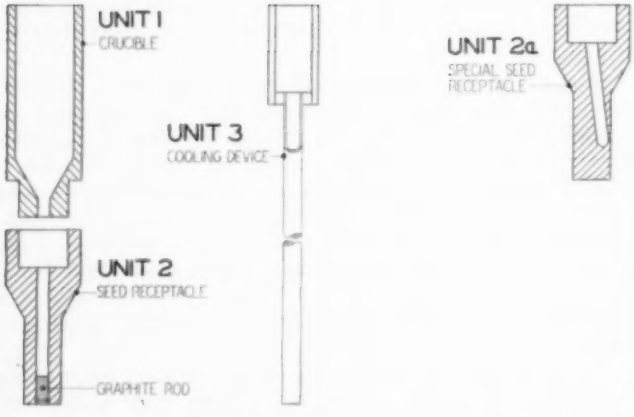

FIGURE 2. *Longitudinal sections of crystal crucible, "seed" crucibles, and cooling device.*

Approximately one-fifth size.

produced in multiple in a single crucible. The axia orientation of the seed crystals is obtained by X-ra diffraction methods.

The following procedure is used to assemble th apparatus prior to the growing of preferentiall oriented single crystals of aluminum.

(1) The charge is melted and allowed to solidif in the crucible shown in unit 1, figure 2, its botto having been fitted with a tightly fitting graphit cap in order to produce a flat surface on the botto of the ingot.

(2) The seed is put into unit 2, and units 1 and 2 are put together.

(3) By means of a tightly fitted graphite rod, th seed is pushed up until it is seated against the lowe surface of the ingot in unit 1. Units 1 and 2 are bot machined from graphite.

(4) The bottom of the seed receptacle is the placed in unit 3, the cooling device, the seed recep tacle bottom having been machined so that it wi fit snugly into unit 3. The receptacle of the coolin device is of copper, nickel-plated, and the long tub is of aluminum. The ring used to connect the nickel plated copper receptacle to the aluminum tube is o copper, tightly fitted into the receptacle, the alumi num tube in turn being tightly fitted into the con necting ring. The aluminum tube should be of suc length so that it extends out into the atmosphere, a shown in figure 1.

The object of the cooling device is to conduct jus enough heat away from the bottom of the seed re ceptacle so that only the upper portion of the see will melt. Then, upon slowly lowering the entir assembly in the furnace, the melted portion of th seed and the melt in unit 1 will freeze and assum the orientation of the unmelted portion of the seed

The correct furnace temperature to permit just par tial melting of the seed is obtained by trial, using thermocouple in the immediate vicinity of the re ceptacle of the cooling device to obtain the correc temperature for a specified location of the entir assembly in the furnace. It is suggested that seed of undesirable axial orientation be used in the de termination of the correct furnace temperature because, until this temperature is established for fixed position of the assembly in the furnace, ther is a possibility that the entire seed might be melted This temperature can usually be established after few trial runs. Once this temperature has bee fixed, the same percentage of seed can be melted o each subsequent run, provided the assembly is place in the same relative position in the furnace eac time. Seed crystals melted in this manner may b used over and over again.

It is possible that many seed crystals may b grown without obtaining any having the exac axial orientation desired. It is possible, however to obtain seeds having axial orientations within several degrees of being parallel to the desire orientation. Such seeds can be used for growin preferentially oriented single crystals by the prope placing of the seed in a seed receptacle that has it cavity at the same angle with the axis of the see receptacle as the axis of the seed makes with th

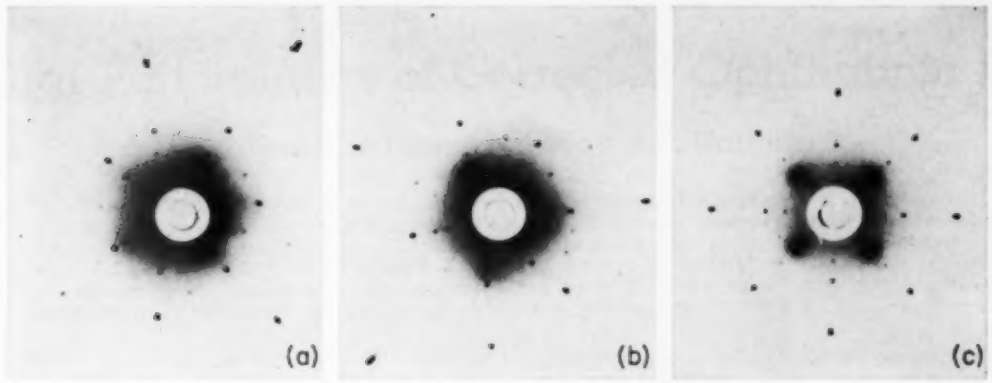

FIGURE 3.—*Laue back-reflection diffraction patterns showing axial orientations.*

(a) Aluminum seed crystal, (b) monocrystalline aluminum ingot grown under the condition where the axes of seed and ingot are parallel, and (c) monocrystalline aluminum ingot grown by tilting seed so that its cubic axis was parallel to the ingot axis.

orientation desired in the axis of the crystal to be grown. A sketch of such a seed receptacle is shown in unit 2a, figure 2. When a seed receptacle of this type is used, the top of the seed should be ground so that its surface is in the same plane as the bottom of the recess in the seed receptacle.

Figure 3 is a photograph of Laue back-reflection diffraction patterns obtained from an aluminum seed crystal and two monocrystalline aluminum ingots produced from the same seed crystal, the incident X-ray beam having been parallel to the axes of the seed and ingots. The patterns are typical of the accuracy attainable in the above-described method for growing preferentially oriented aluminum monocrystals.

The author expresses his appreciation to W. F. Gerhold for assistance in establishing the above-described method.

WASHINGTON, November 20, 1957.

Journal of Research of the National Bureau of Standards Vol. 60, No. 6, June 1958 Research Paper 2869

Marginal Performance of Corrected Ophthalmic Lenses

Francis E. Washer and Walter R. Darling

The measured values of the departures of the marginal meridional and cylindrical powers from the corresponding measured values of the axial powers for 311 corrected ophthalmic lenses are reported. The spherical refractive powers of the lenses studied range from +7.00 to −20.00 diopters with cylindrical powers of 0.00 to 4.00 diopters. The probable errors of measurement are discussed. A set of tolerance values is suggested, and the degree of compliance with these suggested tolerances is shown.

1. Introduction

In recent years, the performance of spectacle lenses has been receiving growing attention. In 1951, a study of the performance of spectacle lenses in the axial and extra-axial regions was initiated at the National Bureau of Standards at the request of the Veterans Administration. The objective of this investigation was the development of a set of tolerances to be used in purchase specifications. In order for these tolerances to be realistic, it was necessary to measure the refractive powers of a large number of spectacle lenses to determine what was currently feasible.

In a previous paper [1],[1] the results of measurement of the axial performance of 311 spectacle lenses were reported. At present, several organizations are working in unison and attempting to produce a generally accepted standard for spectacle lenses, with emphasis being placed primarily on axial performance. It is probable that a similar effort will be initiated at some future time to extend the coverage of such a standard to include tolerances for marginal power. It therefore seems worthwhile to report the measured values of the departures of the extra-axial powers from the axial powers for the same 311 lenses. A tentative set of tolerances has also been prepared, and the degree of compliance with these tolerances is shown.

2. Selection of Lenses for Measurement

The lenses selected for measurement are the same ones whose axial performance was reported in a previous paper [1]. The present study is therefore confined to single-vision lenses of the type called "corrected ophthalmic lenses" [2]. Lenses of this kind have the total spherical and cylindrical powers divided between the front and rear surfaces in such a manner that the difference in axial and marginal power is minimized as far as practicable. Lenses of this variety are commonly known as members of a "corrected curve" series.

The powers of the lenses studied ranged from +7.00 to −20.00 diopters of spherical power and 0.00 to +6.00 diopters of cylindrical power. The major emphasis was placed on lenses having spherical powers ranging from +7.00 to −6.00 diopters and cylindrical power ranging from 0.00 to +2.00. The few reported that are outside this range are perhaps sufficient to indicate the probable performance in the region of higher powers. In order to make measurements on more than one lens of the same power, lenses of identical powers were purchased from five different manufacturers. Some power combinations were not readily available from each of the five, but generally at least three makers were able to supply lenses of like power. The final total of lenses that were measured was 311, comprised of 3 to 5 lenses in each of 68 power combinations.

3. Theory

Spectacle lenses are normally specified in terms of spherical and cylindrical power as measured on the optical axis. The power of the lens, specified in this manner, is the best estimate of the correction required by the potential user. It is known, however, that the degree of correction afforded by a given lens varies as the eye rolls and looks successively through different areas of the lens. This cannot be avoided because the designer is constrained to work with but two surfaces and a single variety of glass at a time. If it were feasible to use two or more types of glass and a compound lens system in a spectacle lens, it might be possible to achieve a high degree of correction throughout the entire viewing area. This course of action is precluded by two principal factors, the first being excessive weight and the second being a substantial increase in the cost to the user. However, even for the simple lens type of construction, considerable improvement is effected by selection of the shape or form of the lens that yields best performance over the entire area.

To determine the difference in performance between the axial and marginal regions of a spectacle lens, it is customary to make all measurements with respect to the vertex sphere. The vertex sphere has its center at the center of rotation of the eye, and its surface is tangent to the rear surface of the spectacle lens at the point of intersection of the optical axis of the lens and its rear surface. The radius of the vertex sphere is usually accepted as being 27 mm. When all measurements of axial and marginal powers are made with reference to the vertex sphere, comparisons can be readily made between the power at any specified extra-axial region and that at the optical axis.

[1] Figures in brackets indicate the literature references at the end of this paper.

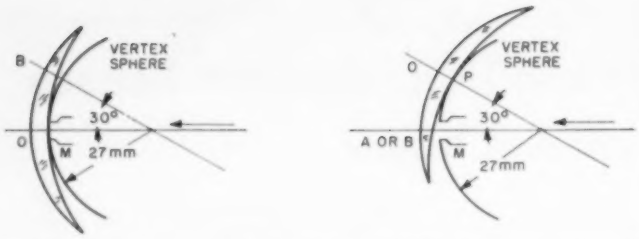

FIGURE 1. *Schematic diagram showing the positions assumed by a spectacle lens when tested on a modified vertometer.*

The left part of the figure shows arrangement for measurement of axial power. The fixed reference opening against which the lens is pressed is shown at M. The optical center O is made to coincide with the center of M. The trace of the vertex sphere is also shown. In the right part of the figure, point O is pressed against the vertex sphere as shown. Light from M passes through the lens under test at points A or B and the marginal power can thus be measured with respect to the vertex sphere.

Figure 1 is a schematic diagram showing a spectacle lens in position for measurement with respect to the vertex sphere. The left-hand portion of the sketch shows the lens in position for axial measurements; the right-hand portion shows the lens in position for the measurement of marginal power in the region at 30° from the axis. In attempting to compare the refractive powers in the marginal regions with that in the axial region, the use of the terms "spherical" and "cylindrical" power results in confusion. Consequently, in this paper, principal emphasis is placed on the "meridional power." The diagrammatic sketch, figure 2, shows the regions where the powers are measured. Measurements are made in the two principal meridians that yield the maximum and minimum meridional powers, respectively. In the figure, these meridians are designated by the symbols V and H, with the subscripts O, A, and B, indicating the axial and marginal regions of the lens.

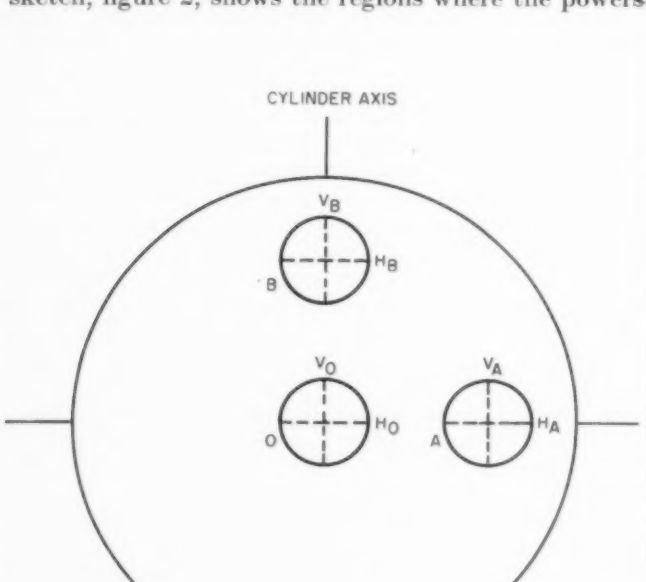

FIGURE 2. *Schematic diagram showing the actual regions where measurements are made.*

Each small area of the spectacle lens is treated as a separate lens and comparisons are made of the respective powers. The meridional axes of the various areas are as indicated.

3.1. Definitions

For convenience, the definitions of all symbols used in describing the various powers and their interrelations are collected into this section. This system specifying the powers in various areas is patterned to some extent after the system devised by Whitwell and referred to by Emsley and Swaine [3].

V_P=One of the principal meridional powers. It is given by the sum of the prescribed spherical and prescribed cylindrical power. It is the maximum meridional power when the prescribed powers are positive.

H_P=The second principal meridional power. It is usually the same as the spherical power. It is the minimum meridional power when the prescribed powers are positive.

C_P=Prescribed cylindrical power. It is the difference between the principal meridional powers and is given by the relation $C_P=V_P-H_P$.

V_O=Measured value of one of the meridional powers at the optical center of the lens. It is the measured power for vertical lines.

H_O=Measured value of the second meridional power at the optical center of the lens. It is the measured power for horizontal lines. (In the absence of cylindrical power, $V_O=H_O$.)

C_O=The measured cylindrical power at the optical center of the lens. It is obtained from the relation, $C_O=V_O-H_O$.

V_A, V_B=The measured marginal powers at points A and B in the same meridian as V_O or parallel to the meridian of V_O. These are the measured marginal powers for vertical lines.

H_A, H_B=The measured marginal powers at points A and B in the same meridian as H_O or parallel to the meridian of H_O. These are the measured marginal powers for horizontal lines.

C_A=The measured cylindrical power at point A, given by the relation $C_A=V_A-H_A$.

C_B=The measured cylindrical power at point B, given by the relation $C_B=V_B-H_B$.

3.2. Additional Relations

The following formulas are used in computing the departures of the measured values from the specified values for the axial region and the departures of the

measured marginal values from the corresponding measured axial values:

$$\Delta V_O = V_O - V_P \qquad \Delta V_A = V_A - V_O \qquad \Delta V_B = V_B - V_O$$

$$\Delta H_O = H_O - H_P \qquad \Delta H_A = H_A - H_O \qquad \Delta H_B = H_B - H_O$$

$$\Delta C_O = C_O - C_P \qquad \Delta C_A = C_A - C_O \qquad \Delta C_B = C_B - C_O$$

4. Method of Measurement

The axial and marginal powers of all lenses were measured on a standard vertex power-measuring instrument equipped with the modifying device described in a previous paper [2]. The axial powers were measured for the region shown at O in figure 2. It is evident from figure 2 that identical values of marginal power should be obtained for equivalent areas symmetrically located on either side of the axial point of the spectacle lens. Accordingly, in making the measurements of marginal power, it is customary to make and record five settings for both area A and its equivalent area and a similar series for both area B and its equivalent area. Some difference is found on opposite sides but it is usually sufficiently small that it can be neglected. The final accepted value for a given marginal power for a single observer represents an average for 10 settings. The measurements on each lens are made independently by each of three observers, and the final results are obtained by averaging the three sets. At the conclusion of the measurements, the values of the departures of the measured values from the specified values for the axial region and the departures of the measured marginal values from the corresponding measured axial values are determined with the aid of the equations given in section 3.2.

4.1. Variation in Measurements for Points 30° From the Axis for Three Observers

The determination of the refractive powers at 30° from the axis is subject to considerably more uncertainty than those measured on the axis. The quality of definition is generally somewhat lower than on the axis, which tends to reduce the precision of the power determinations. In addition, any error in properly establishing the angle separating the area under test and the axis may produce appreciable error in some instances. For example, the change in meridional power with angle of viewing is likely to be small in the vicinity of the axis but may be changing rapidly with changing angle at 30° from the axis. Consequently, a change of as little as ±0.5 degree in the region of 30° may produce changes in the measured values of marginal power of as much as ±0.10 diopters. The depth of focus, throughout which the change in quality of definition of the image of the target reticle is not too apparent, is appreciably greater than that for axial depth of focus.

Because of these additional possibilities for error, an investigation of the reliability of the measurements at 30° from the axis was also made for the three observers. Table 1 shows the values obtained by each of the three observers, identified as D, G, and B, for a representative group of six lenses. The fourth line in each case is the average value obtained and is the one accepted as correct. The symbols, ΔV_A, ΔV_B, ΔH_A, ΔH_B, ΔC_A, and ΔC_B, signify respectively the departure of the various powers at points A and B at 30° from the axis from the corresponding measured quantities on the axis. It may be noted that the departures from the average for each observer, although small, are appreciably greater than for measurements on the axis [1].

TABLE 1. *Values of the deviations, ΔV_A, ΔV_B, ΔH_A, ΔH_B, ΔC_A, and ΔC_B, for six lenses obtained by each of three observers (D, G, and B)*

The average values for the three observers are accepted as correct. All values are expressed in diopters.

Obs.	Sph.	Cyl.	ΔV_A	ΔV_B	ΔH_A	ΔH_B	ΔC_A	ΔC_B
D	7	2	0.05	−0.02	−0.29	−0.37	0.34	0.35
G			.14	−.12	−.43	−.33	.57	.21
B			.22	−.14	−.41	−.29	.63	.15
Avg			0.14	−0.09	−0.38	−0.33	0.51	0.24
D	4	2	−0.15	−0.31	−0.30	−0.40	0.15	0.09
G			−.13	−.25	−.28	−.36	.15	.11
B			−.18	−.40	−.34	−.51	.16	.11
Avg			−0.15	−0.32	−0.31	−0.42	0.15	0.10
D	1	2	+0.04	−0.13	−0.09	−0.26	0.13	0.13
G			.07	−.17	−.14	−.26	.21	.09
B			.13	−.13	−.06	−.20	.19	.07
Avg			0.08	−0.14	−0.10	−0.24	0.18	0.10
D	0	2	0.08	−.09	−0.02	−0.14	0.10	0.05
G			.17	−.13	−.04	−.11	.21	−.02
B			.16	−.08	−.03	−.15	.19	+.07
Avg			0.14	−0.10	−0.03	−0.13	0.17	0.03
D	−1	2	0.16	−0.16	−0.05	−0.21	0.21	0.05
G			.17	−.17	−.04	−.13	.21	−.04
B			.21	−.14	−.03	−.10	.24	−.04
Avg			0.18	−0.16	−0.04	−0.15	0.22	−0.01
D	−4	2	0.37	+0.17	+0.26	+0.10	0.11	+0.07
G			.30	.04	.22	.06	.08	−.02
B			.30	.13	.20	.02	.10	+.11
Avg			0.32	0.11	0.23	0.06	0.10	0.05
D	−6	2	0.49	0.27	0.41	0.12	0.08	0.15
G			.41	.32	.41	.20	.00	.12
B			.48	.29	.49	.15	−.01	.14
Avg			0.46	0.29	0.44	0.16	0.02	0.14

The results of measurements, made at 30° off-axis on 36 lenses of varied powers by 3 observers, were analysed to determine the magnitude of observer bias or systematic error. The results of this analysis are shown in table 2. The departures from the accepted average measured-power deviation were determined for each of the 3 observers for each of the 36 lenses.

The average departure was computed for each observer and is taken as a measure of the systematic error or bias for each observer. It is apparent that

TABLE 2. *Systematic differences in the values of ΔV_A, ΔV_B, ΔH_A, ΔH_B, ΔC_A, and ΔC_B for three observers, D, G, and B, based on measurements at 30° off-axis for 36 lenses*

The differences are given in diopters.

Observer	Average departure from the average of—					
	ΔV_A	ΔV_B	ΔH_A	ΔH_B	ΔC_A	ΔC_B
D	−0.013	+0.006	+0.007	−0.008	−0.016	+0.014
G	−.003	−.012	−.005	+.006	−.003	−.024
B	+.016	+.009	+.001	.000	+.019	+.001

so far as the determinations of ΔV and ΔH are concerned, the magnitudes of the systematic error are of the same order of magnitude as found for V and H on the axis [1]. The systematic errors in ΔC are greater at the margins than on the axis but are nevertheless small. It can therefore be assumed that the contribution of observer bias to measurements of ΔV_A, ΔV_B, ΔH_A, and ΔH_B, will not usually exceed ± 0.01 diopter. In addition, the contribution from the same source to measurements of ΔC_A and ΔC_B will not usually exceed ± 0.02 diopter. In view of the small magnitudes of observer bias and the probable error of a single determination for each observer, it can reasonably be claimed that the error of determinations of ΔV_A, ΔV_B, ΔH_A, ΔH_B, ΔC_A, and ΔC_B will generally be less than ± 0.03 diopter.

Table 3 shows a frequency distribution of the errors for the 3 observers in the determination of the marginal power of the 36 lenses. For example, in the determination of ΔV_A, the results of measurement by observer D are within ± 0.03 diopter of the accepted average value of ΔV_A for 53 percent of the lenses measured. It is also clear that for any of the observers, the likelihood of being in error by more than ± 0.06 diopter is quite small.

TABLE 3. *Frequency distribution of departures from the average value of ΔV_A, ΔV_B, ΔH_A, ΔH_B, ΔC_A, and ΔC_B for each of three observers*

The results are based on measurements of 36 lenses. All values are in diopters

A. Percentage of determinations that do not depart from average value of ΔV_A (or ΔV_B) by more than δV_A (or δV_B) for observer—

δV_A	ΔV_A			δV_B	ΔV_B		
	D	*G*	*B*		*D*	*G*	*B*
±0.03	53	84	61	±0.03	58	53	67
.06	92	97	89	.06	75	84	81
.09	100	100	100	.09	97	94	89
.12	----	----	----	.12	97	97	92
.15	----	----	----	.15	100	100	100

B. Percentage of determinations that do not depart from average value of ΔH_A (or ΔH_B) by more than δH_A (or δH_B) for observer—

ΔH_A	ΔH_A			δH_B	ΔH_B		
	D	*G*	*B*		*D*	*G*	*B*
±0.03	69	75	75	±0.03	56	72	47
.06	92	91	94	.06	86	97	81
.09	100	100	97	.09	94	97	94
.12	----	----	100	.12	94	100	100
.15	----	----	----	.15	100	----	----

C. Percentage of determinations that do not depart from average value of ΔC_A (or ΔC_B) by more than δC_A (or δC_B) for observer—

δC_A	ΔC_A			δC_B	ΔC_B		
	D	*G*	*B*		*D*	*G*	*B*
±0.03	42	69	44	±0.03	39	47	49
.06	83	97	72	.06	75	72	75
.09	97	100	94	.09	86	91	86
.12	97	----	97	.12	97	100	92
.18	100	----	100	.18	100	----	100

5. Results of Measurement on 311 Spectacle Lenses

The values of V_A, H_A, V_B, H_B, V_O, and H_O were measured for the entire group of 311 lenses. From these measured values the values of C_O, C_A, and C_B were determined. For the present purposes, the values of the departures of the measured values on axis from the prescribed axial values and the values of the measured marginal values from the measured axial values are of greater interest than the actual values of marginal and axial meridional power. The values of ΔV_O, ΔH_O, and ΔC_O are reported in an earlier paper [1]. In the present paper, the emphasis is given to the measured values of ΔV_A, ΔH_A, ΔC_A, ΔV_B, ΔH_B, and ΔC_B. The results of these determinations are given in tables 4 to 10. The order of the lenses in these tables is the same as that given in the earlier paper to facilitate comparison. It is evident from a cursory examination, that the values of ΔV_A, ΔH_A, ΔC_A, ΔV_B, ΔH_B, and ΔC_B are frequently quite large, particularly for the higher spherical and cylindrical powers.

6. Establishment of Tolerances

The establishment of tolerances for marginal power for spectacle lenses is somewhat more complex than is the case for axial power. The interrelation of the various powers in three areas instead of the single central area has to be kept constantly in mind. The performance in the peripheral regions of spectacle lenses made in accordance with recognized best practice is generally not equal to that commonly obtained in the axial regions. So for tolerances to serve a useful purpose, their magnitude must be made appreciably greater than those acceptable on axis, but at the same time, they should be held as small as feasible to insure optimum performance under the circumstances.

6.1. Proposed Tolerances for Marginal Powers

A careful analysis of the magnitudes of the deviations, ΔV_A, ΔV_B, ΔH_A, ΔH_B, ΔC_A, and ΔC_B, that are listed in tables 4 to 10, was made. On the basis of this analysis, tolerances were established for use in a purchase specification [4]. These tolerances are specified as follows:

(*a*) The marginal meridional powers referred to the vertex sphere at points A and B, located as shown in figure 2, shall not depart from the measured axial meridional powers by amounts in excess of those values of the tolerances for meridional power shown in tables 11 to 15.

(*b*) The cylindrical power, referred to the vertex sphere at points A and B shall not depart from the measured axial cylindrical powers by an amount in excess of those values of the tolerances shown in tables 11 to 15.

TABLE 4. *Measured values of the deviations in meridional power at the marginal points A and B from the measured axial power for 72 spectacle lenses having zero cylindrical power and with spherical power varying from +7.00 to −18.00 diopters*

The nominal prescribed spherical powers are listed under "Sph". The significance of the symbols at the heads of the columns is given in section 3.2 and figure 2. All values are expressed in diopters.

Sph.	ΔV_A	ΔH_A	ΔC_A	ΔV_B	ΔH_B	ΔC_B
7.00	−0.17	0.23	−0.40	0.23	−0.18	0.41
	−.25	−.05	−.20	−.04	−.24	.20
	−.22	+.02	−.24	+.02	−.21	.23
6.00	−0.04	−0.17	+0.13	−0.19	−0.04	−0.15
	−.20	−.24	.04	−.22	−.20	−.02
	−.01	−.19	.18	−.22	−.02	−.20
	−.09	−.18	.09	−.20	−.10	−.10
	−.06	−.25	.19	−.26	−.06	−.20
5.00	−0.21	−0.26	0.02	−0.21	−0.23	+0.02
	−.09	−.15	.06	−.19	−.15	−.04
	−.18	−.22	.04	−.18	−.15	−.03
	+.02	−.16	.18	−.18	+.03	−.21
	−.10	−.19	.09	−.22	−.10	−.12
4.00	−0.12	−0.14	0.02	−0.14	−0.13	−0.01
	+.03	−.08	.11	−.08	+.03	−.11
	.01	−.07	.08	−.02	.02	−.04
	−.20	−.27	.07	−.31	−.19	−.12
	−.13	−.13	.00	−.17	−.17	.00
3.00	−0.10	−0.13	0.03	−0.10	−0.13	+0.03
	+.02	−.08	.10	−.07	+.01	−.08
	.00	−.07	.07	−.08	.00	−.08
	−.24	−.20	−.04	−.20	−.21	+.01
	−.18	−.15	−.03	−.12	−.14	.02
2.00	−0.12	−0.09	−0.03	−0.10	−0.08	−0.02
	−.03	−.08	+.05	−.08	−.05	−.03
	−.07	−.08	.01	−.07	−.08	+.01
	−.05	−.07	.02	−.08	−.05	−.03
	−.04	−.03	−.01	−.03	−.02	−.01
1.00	−0.02	−0.01	−0.01	−0.01	−0.02	+0.01
	−.02	−.01	−.01	.00	−.01	.01
	−.03	−.02	−.01	−.03	−.02	−.01
	−.01	−.12	+.11	−.02	−.01	−.01
	−.04	−.05	+.01	−.03	−.05	+.02
0.00	+0.03	0.00	0.03	−0.05	+0.02	−0.07
	.00	.00	.00	+.01	.01	+.00
	−.01	.00	−.01	.00	−.01	.01
	−.02	+.02	−.04	.02	−.01	.03
	+.01	−.01	.02	−.01	+.01	−.02
−1.00	0.00	+0.06	−0.06	+0.08	0.02	+0.06
	−.03	.05	−.08	.01	−.06	.07
	−.01	.08	−.09	.06	−.01	.07
	.00	.04	−.04	.05	+.00	.05
	+.02	.05	−.03	.06	.01	.05
−2.00	0.02	0.09	−0.07	0.08	0.04	0.04
	−.09	.02	−.11	.02	−.08	.10
	+.09	.14	−.05	.11	+.11	.00
	.11	.13	−.02	.16	.12	.04
	.06	.19	−.13	.15	.06	.09
−3.00	0.09	0.15	−0.06	0.14	0.08	0.06
	.06	.08	−.02	.10	.03	.07
	.11	.17	−.06	.17	.16	.01
	.14	.16	−.02	.18	.13	.05
	.05	.15	−.10	.18	.02	.16
−4.00	0.14	0.19	−0.05	0.20	0.13	0.07
	.15	.26	−.11	.25	.15	.10
	.03	.17	−.14	.19	.01	.18
	−.07	.16	−.23	.15	−.06	.21
	+.17	.20	−.03	.20	+.17	.03
−6.00	0.31	0.32	−0.01	0.30	0.30	0.00
	.45	.33	+.12	.32	.39	−.07
	.35	.32	.03	.24	.30	−.06
	.25	.22	.03	.18	.24	−.06
	.22	.02	.20	.03	.20	−.17
−10.00	0.34	0.30	0.04	0.36	0.42	−0.06
	.16	.01	.15	.02	.15	−.13
	.21	.00	.21	.00	.20	−.20
−14.00	0.27	0.26	0.01	0.24	0.24	0.00
	−.04	.25	−.29	.24	−.02	+.26
	+.45	.57	−.12	.59	+.46	.13
−18.00	0.26	0.22	+0.04	.022	0.17	0.04
	−.24	−.02	−.22	−.02	−.23	.21
	+.18	+.30	−.12	+.30	+.22	.08

TABLE 5. *Measured values of the deviations in meridional power at the marginal points A and B from the measured axial power for 76 spectacle lenses having a cylindrical power of +1.00 diopter and with spherical power varying from +6.00 to −19.00 diopters*

The nominal prescribed spherical powers are listed under "Sph". The significance of the symbols at the heads of the columns is given in section 3.2 and figure 2. All values are expressed in diopters.

Sph.	ΔV_A	ΔH_A	ΔC_A	ΔV_B	ΔH_B	ΔC_B
7.00	0.06	−0.28	0.34	−0.20	0.08	−0.28
	.40	−.35	.75	−.18	.21	−.39
	−.13	−.35	.22	+.07	−.34	+.41
6.00	0.00	−0.35	0.35	−0.20	−0.11	−0.09
	+.22	−.27	.49	−.08	+.15	−.23
	.02	−.33	.35	−.14	−.19	+.05
	−.02	−.36	.34	−.20	−.11	−.09
	−.01	−.33	.32	−.19	−.06	−.13
5.00	−0.09	−0.37	0.28	−0.12	−0.15	+0.03
	−.06	−.28	.22	−.15	−.18	.03
	−.11	−.34	.23	−.18	−.19	.01
	−.10	−.30	.20	−.21	−.10	−.11
	+.05	−.28	.33	−.13	.00	−.13
4.00	−0.13	−.15	0.02	−0.19	−0.27	+0.08
	−.17	−.22	.05	−.05	−.09	.04
	−.05	−.01	−.04	−.01	−.21	.20
	.00	+.07	−.07	−.02	−.15	.13
	−.07	−.16	+.09	−.01	−.21	.20
3.00	−0.23	−0.28	0.05	−0.15	−0.20	0.05
	−.17	−.25	.08	−.07	−.13	.06
	+.06	−.17	.23	−.04	+.01	−.05
	.03	−.13	.16	+.01	.00	+.01
	.00	−.16	.16	−.04	.01	−.05
2.00	0.04	+0.01	0.03	0.03	−0.03	+0.06
	−.01	−.08	.07	−.09	−.18	.09
	−.01	−.13	.12	−.16	−.15	−.01
	−.13	−.13	.00	−.01	−.08	+.07
	−.02	.00	−.02	−.08	−.16	.08
1.00	−0.15	−0.13	−0.02	+0.01	−0.11	0.12
	+.04	−.15	+.19	.04	−.04	.08
	−.17	−.08	−.09	.05	−.03	.08
	+.02	−.03	+.05	−.02	−.10	.08
	.01	−.10	.11	−.09	−.11	.02
0.00	0.00	−0.07	0.07	−0.08	−0.09	0.01
	.05	−.05	.10	−.04	−.04	.00
	−.08	−.07	−.01	+.04	−.03	.07
	−.07	−.10	+.03	.07	−.05	.12
	−.09	−.05	−.04	.08	−.01	.09
−1.00	−0.04	−0.02	−0.02	0.08	−0.05	0.13
	−.01	−.01	.00	.11	−.01	.12
	+.08	−.02	+.10	−.07	−.03	−.04
	.09	+.02	.07	−.05	−.02	−.03
	−.03	−.03	.00	+.11	−.02	+.13
−2.00	+0.16	+0.07	0.09	0.02	0.06	−0.04
	−.08	.00	−.08	.17	−.02	+.19
	−.04	−.02	−.02	.11	−.04	.15
	+.03	+.01	+.02	.19	+.04	.15
	.15	.04	.11	.01	.00	.01
−3.00	0.11	0.02	0.09	0.19	0.05	0.14
	.10	.08	.02	.23	.10	.13
	.06	.00	.06	.22	.06	.16
	.15	.14	.01	.25	.19	.06
	.05	.09	−.04	.24	.12	.12
−4.00	0.30	0.19	+0.11	0.21	0.15	0.06
	.25	.22	.03	.16	.14	.02
	.24	.08	.16	.09	.13	−.04
	.07	.09	−.02	.18	.06	+.12
	.23	−.04	+.27	.00	.09	−.09
−6.00	0.23	−0.04	0.27	0.06	0.12	−0.06
	.34	+.25	.09	.34	.22	+.12
	.41	.41	.00	.39	.23	.16
	.33	.33	.00	.29	.26	.03
	−.05	.16	−.21	.23	.16	.07
−10.00	+0.79	0.37	+0.42	0.57	0.58	−0.01
	.72	.41	.31	.57	.56	+.01
	.22	.38	−.16	.43	.40	.03
	−.20	.05	−.25	.20	−.02	.22
−11.00	+0.20	0.17	0.03	0.16	+0.10	0.06
	.22	.67	−.45	.31	.39	−.08
	.33	.29	+.04	.10	.31	−.21
−15.00	−0.18	0.11	−.29	0.09	−0.41	0.50
	+.66	.61	+.05	.47	+.70	−.23
	.32	.43	−.11	.25	.24	+.01
−19.00	−0.22	0.10	−.32	0.04	−0.34	0.38
	+.48	.40	+.08	.26	+.48	−.22
	.17	.11	.06	.16	.12	+.04

TABLE 6. *Measured values of the deviations in meridional power at the marginal points A and B from the measured axial power for 71 spectacle lenses having a cylindrical power of +2.00 diopters and with spherical power varying from +7.00 to −20.00 diopters*

The nominal prescribed spherical powers are listed under "Sph". The significance of the symbols at the heads of the columns is given in section 3.2 and figure 2. All values are expressed in diopters.

Sph.	ΔV_A	ΔH_A	ΔC_A	ΔV_B	ΔH_B	ΔC_B
7.00	0.14	−0.38	0.52	−0.09	−0.33	0.24
	.32	−.43	.75	−.14	−.07	−.07
6.00	0.05	−0.51	0.56	−0.29	−0.20	−0.09
	.09	−.38	.47	−.17	−.10	−.07
	.35	−.33	.68	−.04	+.09	−.13
	.23	−.41	.64	−.10	−.50	+.40
5.00	0.04	−0.37	0.41	−0.10	−0.05	−0.05
	.06	−.50	.56	−.06	−.10	+.04
	.15	−.42	.57	−.09	−.66	.57
	−.09	−.45	.36	−.20	−.22	.02
4.00	−0.15	−0.31	0.16	−0.32	−0.42	0.10
	−.10	−.38	.28	−.06	−.18	.12
	+.08	−.27	.35	−.03	−.01	−.02
	.09	−.26	.35	+.02	+.01	+.01
3.00	−0.19	−0.33	0.14	−0.08	−0.23	0.15
	−.33	−.37	.04	−.08	−.20	.12
	−.15	−.35	.20	−.03	−.11	.08
	−.14	−.33	.19	−.05	−.15	.10
	+.03	−.28	.31	+.02	−.06	.08
2.00	−0.11	−0.23	0.12	0.02	−0.11	0.13
	−.05	−.18	.13	.05	−.04	.09
	−.02	−.09	.07	−.00	−.29	.20
	−.02	−.19	.17	−.27	−.30	.03
	−.19	−.36	.17	+.01	−.15	.16
1.00	0.02	−0.12	0.14	−0.19	−0.24	0.05
	−.23	−.22	−.01	+.09	−.10	.19
	+.01	−.18	+.18	.13	−.05	.18
	−.07	−.19	.12	.13	−.01	.14
	+.08	−.10	.18	−.14	−.24	.10
0.00	−0.11	−0.14	0.03	+0.16	−0.04	0.20
	+.14	−.03	.17	−.10	−.13	.03
	.13	−.05	.18	−.13	−.15	.02
	−.13	−.15	.02	+.13	−.05	.18
	−.14	−.16	.02	.09	−.08	.17
−1.00	−0.20	−0.12	−0.08	0.16	−0.03	0.19
	−.14	−.10	−.04	.16	−.05	.21
	−.10	−.09	−.01	.15	−.01	.16
	+.18	−.04	+.22	−.16	−.15	−.01
	.12	−.02	.14	−.05	−.11	+.06
−2.00	0.22	+0.01	0.21	−0.07	−0.04	−0.03
	−.04	−.07	.03	+.23	+.00	+.23
	+.22	+.03	.19	−.04	−.09	.05
	−.11	−.07	−.04	+.20	−.03	.23
	−.03	−.09	+.06	.21	+.03	.18
−3.00	−0.02	−0.01	−0.01	0.32	0.10	0.22
	−.05	−.04	−.01	.22	.00	.22
	+.02	−.01	+.03	.30	.10	.20
	.02	−.01	.03	.26	.20	.06
	.04	−.02	.06	.27	.13	.14
−4.00	0.02	+0.04	−0.02	0.29	−0.04	0.33
	.19	.09	+.10	.36	+.25	.11
	.32	.23	.09	.11	.06	.05
	.32	.07	.25	.02	.04	−.02
	.02	.04	−.02	.31	.20	+.11
−6.00	−0.26	0.00	−0.26	0.20	0.15	0.05
	+.25	.16	+.09	.41	.08	.33
	.33	.14	.19	.51	.31	.20
	.46	.44	.02	.29	.16	.15
−10.00	−0.32	0.12	−0.44	0.32	0.20	0.12
	+.64	.27	+.37	.65	.46	.19
	.91	.36	.55	.67	.45	.22
	−.06	.25	−.31	.42	.39	.03
−12.00	+0.40	0.89	−0.49	0.54	0.75	−0.21
	.44	.41	+.03	.11	.33	−.22
	.36	.36	.00	.26	.00	+.26
−16.00	0.98	0.66	0.32	0.68	0.96	−0.28
	.41	.32	−.11	.31	.34	−.03
	.08	.26	−.18	.26	−.11	+.37
−20.00	0.44	0.38	+0.06	0.62	+0.60	0.02
	.37	.60	−.23	.70	.39	.31
	−.17	.24	−.41	.02	−.18	.29

TABLE 7. *Measured values of the deviations in meridional power at the marginal points A and B from the measured axial power for 43 spectacle lenses having a cylindrical power of +3.00 diopters and with spherical power varying from +6.00 to −10.00 diopters*

The nominal prescribed spherical powers are listed under "Sph". The significance of the symbols at the heads of the columns is given in section 3.2 and figure 2. All values are expressed in diopters.

Sph.	ΔV_A	ΔH_A	ΔC_A	ΔV_B	ΔH_B	ΔC_B
6.00	0.32	−0.53	0.85	−0.05	0.07	−0.12
	.37	−.57	.94	−.18	−.12	−.06
	.30	−.47	.77	−.15	−.08	−.07
	.64	−.46	1.10	+.13	+.19	−.06
5.00	−0.03	−0.54	0.51	−0.21	−0.30	+0.09
	+.19	−.46	.65	−.07	−.13	.06
	.57	−.40	.97	+.10	+.12	−.02
	.18	−.53	.71	−.06	−.57	+.51
4.00	−0.09	−0.50	0.41	−0.11	−0.22	0.11
	+.12	−.30	.42	+.07	+.04	.03
	.30	−.47	.77	.00	−.13	.13
	−.17	−.53	.36	−.18	−.40	.22
3.00	−0.13	−0.37	0.24	+0.04	−0.05	0.09
	−.08	−.48	.40	−.03	−.14	.11
	−.33	−.47	.14	+.03	−.15	.18
	−.17	−.34	.17	−.02	−.09	.07
−1.00	−0.19	−0.17	−0.02	+0.22	+0.01	0.21
	−.29	−.19	−.10	.23	−.04	.27
	−.25	−.25	.00	.14	−.01	.15
	−.21	−.19	−.02	.24	−.10	.34
	−.24	−.20	−.04	.22	−.01	.23
−2.00	−0.24	−0.15	−0.09	0.27	+0.04	0.23
	−.20	−.16	−.04	.34	.03	.31
	−.09	−.17	+.08	.25	−.02	.27
	−.08	−.17	.09	.34	+.11	.23
	−.33	−.30	−.03	.18	−.15	.33
−3.00	−0.03	−0.06	+0.03	0.34	−0.04	0.38
	−.12	−.14	.02	.39	+.03	.36
	−.10	−.13	.03	.35	.07	.28
	−.11	−.12	.01	.38	.02	.36
	−.12	−.13	.01	.36	.11	.25
−4.00	0.00	−0.05	0.05	0.49	0.26	0.23
	−.03	−.05	.02	.40	−.01	.41
	−.07	−.08	.01	.41	+.10	.31
	−.05	−.05	.00	.40	.30	.10
−6.00	+0.46	+0.14	0.32	0.71	0.38	0.33
	.30	.11	.19	.59	.48	.11
	−.14	−.07	−.07	.36	.21	.15
	+.21	+.10	+.11	.55	.06	.49
−10.00	0.01	0.35	−0.34	0.57	0.64	−0.07
	−.22	.06	−.28	.33	.40	−.07
	+.71	.14	+.57	.78	.34	+.44
	.81	.23	.58	.85	.86	−.01

TABLE 8. *Measured values of the deviations in the meridional power at marginal points A and B from the measured axial power for 8 spectacle lenses having a cylindrical power of +5.00 diopters and with spherical powers of −1.00 and −2.00 diopters*

All powers are expressed in diopters

Sph.	ΔV_A	ΔH_A	ΔC_A	ΔV_B	ΔH_B	ΔC_B
−1.00	−0.21	−0.43	0.22	0.43	−0.04	0.47
	−.43	−.43	.00	.28	−.11	.39
	−.38	−.41	.03	.39	−.08	.47
	−.33	−.31	−.02	.34	−.04	.38
−2.00	−0.26	−0.34	+0.08	0.56	+0.01	0.55
	−.36	−.36	.00	.26	−.05	.31
	−.42	−.34	−.08	.48	+.04	.44
	−.27	−.29	+.02	.45	.10	.35

TABLE 9. *Measured values of the deviations in meridional power at the marginal points A and B from the measured axial power for 33 spectacle lenses having a cylindrical power of +4.00 diopters and with spherical power varying from +5.00 to −10.00 diopters*

The nominal prescribed spherical powers are listed under "Sph." The significance of the symbols at the heads of the columns is given in section 3.2 and figure 2. All values are expressed in diopters.

Sph.	ΔV_A	ΔH_A	ΔC_A	ΔV_B	ΔH_B	ΔC_B
5.00	0.24	−0.61	0.85	0.01	−0.30	0.31
	−.03	−.74	.71	−.19	−.27	.08
	+.32	−.56	.88	+.00	−.07	.07
	.25	−.75	1.00	−.01	−.05	.04
4.00	−0.09	−0.65	0.56	−0.11	−0.41	0.30
	−.09	−.57	.48	−.03	−.25	.22
	+.28	−.53	.81	+.18	+.04	.14
	.12	−.54	.66	.01	−.11	.12
−1.00	−0.33	−0.33	0.00	0.23	−0.02	0.25
	−.29	−.29	.00	.30	−.04	.34
	−.35	−.31	−.04	.23	−.10	.33
	−.16	−.29	+.13	.38	−.04	.42
−2.00	−0.24	−0.29	0.05	0.31	+0.07	0.24
	−.35	−.27	−.08	.35	.01	.34
	−.27	−.25	−.02	.32	.05	.27
	−.23	−.25	+.02	.32	.01	.31
−3.00	−0.23	−0.19	−0.04	0.42	0.02	0.40
	−.17	−.19	+.02	.43	.03	.40
	−.41	−.20	−.21	.43	.08	.35
	−.23	−.24	+.01	.39	.16	.23
−4.00	−0.10	−0.16	0.06	0.50	0.27	0.23
	−.04	−.07	.03	.48	−.02	.50
	−.09	−.13	.04	.57	+.14	.43
	−.08	−.10	.02	.47	−.01	.48
	−.08	−.15	.07	.51	+.22	.29
−6.00	+0.06	−0.03	0.09	0.60	0.00	0.60
	.18	+.02	.16	.75	.26	.49
	.06	−.03	.09	.57	.39	.18
	−.22	−.23	.01	.38	.42	−.04
−10.00	+0.84	+0.25	0.59	1.09	1.01	+0.08
	−.21	.24	−.45	.59	0.63	−.04
	−.32	.09	−.41	.42	.35	+.07
	+.65	.23	+.42	.95	.51	.44

TABLE 10. *Measured values of the deviations in the meridional power at marginal points A and B from the measured axial power for 8 spectacle lenses having a cylindrical power of +6.00 diopters and with spherical powers of −1.00 and −2.00 diopters*

All powers are expressed in diopters

Sph.	ΔV_A	ΔH_A	ΔC_A	ΔV_B	ΔH_B	ΔC_B
−1.00	−0.45	−0.49	0.04	0.32	−0.15	0.47
	−.29	−.20	−.09	.53	−.06	.59
	−.37	−.51	+.14	.31	−.08	.39
	−.33	−.34	.01	.47	+.02	.45
−2.00	−0.39	−0.36	−0.03	0.44	0.04	0.40
	−.32	−.35	+.03	.65	.01	.64
	−.47	−.48	.01	.40	−.02	.42
	−.46	−.47	.01	.51	+.02	.49

(c) The tolerances in marginal power contained in paragraphs (a) and (b) are only applicable to single vision lenses and to the distance portions of bifocal lenses. The range for which these tolerances apply is as shown in tables 11 to 15. The tolerances shown in tables 11 to 15 apply to lenses corrected for optimum marginal performance at large object distances. For lenses corrected for optimum marginal performance at near distances, the same tolerances shall apply, except that the measurements will be made with the test object at the specified near object distance, and the tolerances will be referred to the measured effective axial meridional and cylindrical powers.

TABLE 11. *Tolerances in meridional and cylindrical powers at 30° from the axis for lenses having spherical powers ranging from +7.00 to −20.00 diopters and zero cylindrical power*

V_O is the measured axial meridional power in one principal meridian and H_O is the measured axial meridional power in the second principal meridian ($H_O = V_O$ and corresponds to the prescribed spherical power.)

Meridional powers ($V_O = H_O$)	Meridional power		Cylindrical power	
	Point *A* and point *B*	Point *A* or point *B*	Point *A* and point *B*	Point *A* or point *B*
7.00	±0.38	±0.32	±0.38	±0.32
6.00	.38	.32	.32	.25
5.00	.32	.25	.32	.25
4.00	.32	.25	.25	.18
3.00	.25	.18	.18	.12
2.00	±0.18	±0.12	±0.18	±0.12
1.00	.18	.12	.18	.12
0.00	.18	.12	.18	.12
−1.00	.18	.12	.18	.12
−2.00	.25	.18	.18	.12
−3.00	±0.25	±0.18	±0.18	±0.12
−4.00	.32	.25	.25	.18
−5.00	.32	.25	.32	.25
−6.00	.38	.32	.32	.25
−7.00	.38	.32	.32	.25
−8.00	±0.38	±0.32	±0.32	±0.25
−9.00	.50	.38	.38	.32
−10.00	.50	.38	.38	.32
−14.00	.50	.38	.38	.32
−20.00	.50	.38	.38	.32

TABLE 12. *Tolerances in meridional and cylindrical powers for lenses having spherical powers ranging from +7.00 to −20.00 diopters and a cylindrical power of 1.00 diopter*

V_O is the measured axial meridional power in one principal meridian and H_O is the measured axial meridional power in the second principal meridian. (For positive cylindrical power, H_O corresponds to the prescribed spherical power; while for negative-cylindrical power, V_O corresponds to the prescribed spherical power.) All values are given in diopters.

Meridional powers		Meridional power		Cylindrical power	
V_O	H_O	Point *A* and point *B*	Point *A* or point *B*	Point *A* and point *B*	Point *A* or point *B*
8.00	7.00	±0.62	±0.50	±0.50	±0.38
7.00	6.00	.50	.38	.50	.38
6.00	5.00	.50	.38	.38	.25
5.00	4.00	.38	.25	.32	.25
4.00	3.00	.38	.25	.25	.18
3.00	2.00	±0.25	±0.18	±0.18	±0.12
2.00	1.00	.18	.12	.18	.12
1.00	0.00	.18	.12	.18	.12
0.00	−1.00	.18	.12	.18	.12
−1.00	−2.00	.25	.18	.18	.12
−2.00	−3.00	±0.38	±0.25	±0.25	±0.18
−3.00	−4.00	.38	.25	.32	.25
−4.00	−5.00	.50	.38	.38	.25
−5.00	−6.00	.50	.38	.38	.25
−6.00	−7.00	.50	.38	.38	.25
−7.00	−8.00	±0.50	±0.38	±0.38	±0.25
−8.00	−9.00	.62	.38	.50	.38
−9.00	−10.00	.62	.50	.50	.38
−14.00	−15.00	.62	.50	.50	.38
−19.00	−20.00	.62	.50	.50	.38

TABLE 13. *Tolerances in meridional and cylindrical powers for lenses having spherical powers ranging from +7.00 to −20.00 diopters and a cylindrical power of 2.00 diopters*

V_o is the measured axial meridional power in one principal meridian and H_o is the measured axial meridional power in the second principal meridian. (For positive cylindrical power, H_o corresponds to the prescribed spherical power, while for negative cylindrical power, V_o corresponds to the prescribed spherical power.) All values are given in diopters.

Meridional powers		Meridional power		Cylindrical power	
V_o	H_o	Point A and point B	Point A or point B	Point A and point B	Point A or point B
9.00	7.00	±0.62	±0.50	±0.62	±0.50
8.00	6.00	.62	.50	.62	.38
7.00	5.00	.50	.38	.50	.25
6.00	4.00	.38	.25	.38	.25
5.00	3.00	.38	.25	.32	.25
4.00	2.00	±0.38	±0.25	±0.25	±0.18
3.00	1.00	.38	.25	.25	.18
2.00	0.00	.38	.25	.25	.18
1.00	−1.00	.25	.25	.25	.18
0.00	−2.00	.25	.25	.25	.18
−1.00	−3.00	±0.38	±0.25	±0.32	±0.25
−2.00	−4.00	.38	.25	.38	.25
−3.00	−5.00	.50	.38	.38	.32
−4.00	−6.00	.62	.50	.50	.38
−5.00	−7.00	.62	.50	.62	.50
−6.00	−8.00	±0.62	±0.50	±0.62	±0.50
−7.00	−9.00	.62	.50	.62	.50
−8.00	−10.00	.62	.50	.62	.50
−13.00	−15.00	.62	.50	.62	.50
−18.00	−20.00	.62	.50	.62	.50

TABLE 14. *Tolerances in meridional and cylindrical powers for lenses having spherical powers ranging from +6.00 to −10.00 diopters and a cylindrical power of 3.00 diopters.*

V_o is the measured axial meridional power in one principal meridian and H_o is the measured axial meridional power in the second principal meridian. (For positive cylindrical power, H_o corresponds to the prescribed spherical power, while for negative cylindrical power, V_o corresponds to the prescribed spherical power.) All values are given in diopters.

Meridional powers		Meridional power		Cylindrical power	
V_o	H_o	Point A and point B	Point A or point B	Point A and point B	Point A or point B
9.00	6.00	±1.00	±0.50	±1.00	±0.50
8.00	5.00	0.87	.38	.87	.38
7.00	4.00	.75	.38	.75	.38
6.00	3.00	.62	.38	.62	.38
5.00	2.00	.50	.38	.50	.25
4.00	1.00	±0.50	±0.38	±0.50	±0.25
3.00	0.00	.50	.38	.50	.25
2.00	−1.00	.50	.38	.50	.25
1.00	−2.00	.50	.38	.50	.25
0.00	−3.00	.50	.38	.50	.25
−1.00	−4.00	±0.62	±0.38	±0.62	±0.38
−2.00	−5.00	.75	.38	.75	.38
−3.00	−6.00	.87	.50	.87	.38
−4.00	−7.00	1.00	.50	1.00	.50
−5.00	−8.00	1.00	.50	1.00	.50
−6.00	−9.00	±1.00	±0.50	±1.00	±0.50
−7.00	−10.00	1.25	.75	1.25	.75

Lenses, having cylindrical power, differ in meridional power in their two principal meridians. This introduces a duality that is reflected in the setting of tolerances. It is obvious that a tolerance that is entirely satisfactory for the lower of the two meridional powers may be too rigorous for the higher one. Likewise, a tolerance that is suitable for the higher of the two meridional powers may be less exacting than is desirable for the lower one. Consequently, in tables 11 to 15, one tolerance is listed that must be satisfied at both points A and B. Assuming that a given lens satisfies the large tolerance established for both points A and B, then for acceptance, it must also satisfy a lower value of the tolerance for either point A or point B. It is evident that the dual tolerances are necessary in tables 12 to 15, which list the tolerances for lenses having cylindrical power. In the case of lenses having no nominal cylindrical power, the presence of small amounts of tolerable axial cylindrical power necessitates a dual listing of tolerance in table 11.

TABLE 15. *Tolerances in meridional and cylindrical powers for lenses having spherical powers ranging from +6.00 to −10.00 diopters and a cylindrical power of 4.00 diopters.*

V_o is the measured axial meridional power in one principal meridian and H_o is the measured axial meridional power in the second principal meridian. (For positive cylindrical power, H_o corresponds to the prescribed spherical power, while for negative cylindrical power, V_o corresponds to the prescribed spherical power.) All values are given in diopters.

Meridional powers		Meridional power		Cylindrical power	
V_o	H_o	Point A and point B	Point A or point B	Point A and point B	Point A or point B
10.00	6.00	±1.00	±0.50	±1.00	±0.50
9.00	5.00	.87	.38	.87	.38
8.00	4.00	.75	.38	.75	.38
7.00	3.00	.62	.38	.62	.38
6.00	2.00	.50	.38	.50	.25
5.00	1.00	±0.50	±0.38	±0.50	±0.25
4.00	0.00	.50	.38	.50	.25
3.00	−1.00	.50	.38	.50	.25
2.00	−2.00	.50	.38	.50	.25
1.00	−3.00	.62	.38	.62	.38
0.00	−4.00	±0.75	±0.38	±0.75	±0.38
−1.00	−5.00	.87	.38	.87	.38
−2.00	−6.00	1.00	.50	1.00	.50
−3.00	−7.00	1.00	.50	1.00	.50
−4.00	−8.00	1.00	.50	1.00	.50
−5.00	−9.00	±1.00	±0.50	±1.00	±0.50
−6.00	−10.00	1.25	.75	1.25	.75

6.2. Degree of Compliance With Proposed Tolerances

The results of the measurements of marginal power made on the 311 lenses that are contained in tables 4 to 10 have been considered with respect to these tolerances to determine the degree of compliance. For the cases of lenses having axial cylindrical powers of 0.00, 1.00, and 2.00, the results of these considerations are shown graphically in figures 3 to 5. In the graphs, the abscissas show the values of axial meridional power, V_o, while the ordinates show the deviations in marginal meridional power and in cylindrical power at points A and B. The dotted lines bounding the horizontal zone in the central regions of the graph indicate the maximum tolerances for marginal performance for both A and B. The solid lines bound the zone of minimum tolerance for either A or B. To avoid plotting a multiplicity of points, only those are shown where one or both of the points fall outside tolerance. The uppermost frame of a given graph shows the nature of the lack of compliance with the meridional requirements for point A, the middle frame shows similar information

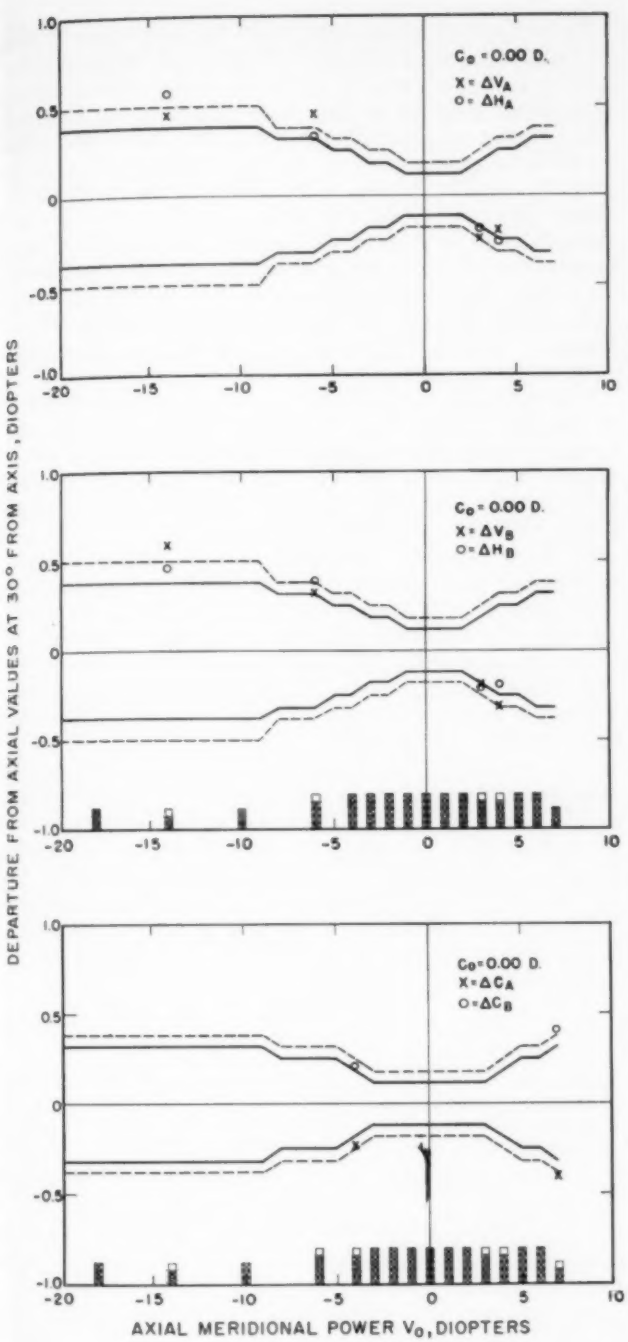
DEPARTURE FROM AXIAL VALUES AT 30° FROM AXIS, DIOPTERS
C_0 = 0.00 D.
X = ΔV_A
O = ΔH_A
C_0 = 0.00 D.
X = ΔV_B
O = ΔH_B
C_0 = 0.00 D.
X = ΔC_A
O = ΔC_B
AXIAL MERIDIONAL POWER V_0, DIOPTERS

FIGURE 3. *Degree of compliance with suggested tolerance for marginal power for 72 lenses having zero cylindrical power.*

Only those points are plotted for which noncompliance occurs for at least one member of a pair. The bar graphs at the bottoms of the center and lower frames show the number of lenses in the sample. Boxes containing an X in the center frame show compliance with the spherical tolerances; boxes containing an X in the lower frame indicate full compliance with spherical and cylindrical tolerances.

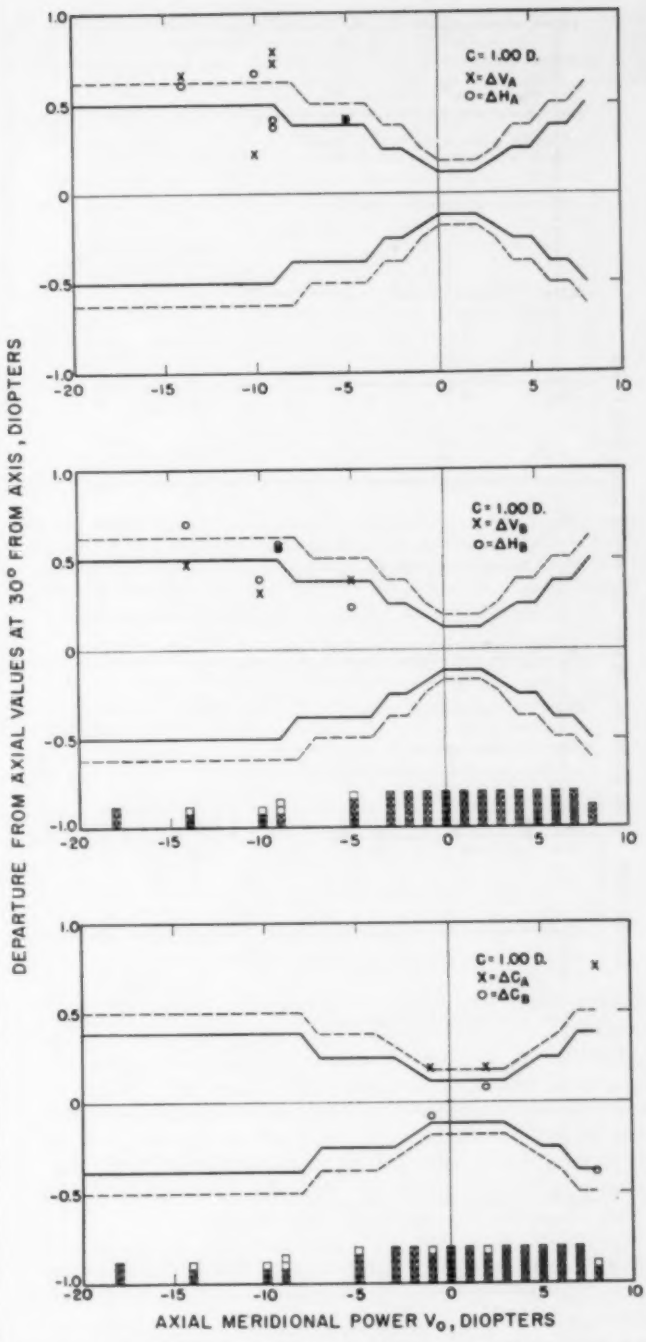
DEPARTURE FROM AXIAL VALUES AT 30° FROM AXIS, DIOPTERS
C = 1.00 D.
X = ΔV_A
O = ΔH_A
C = 1.00 D.
X = ΔV_B
O = ΔH_B
C = 1.00 D.
X = ΔC_A
O = ΔC_B
AXIAL MERIDIONAL POWER V_0, DIOPTERS

FIGURE 4. *Degree of compliance with suggested tolerance for marginal power for 76 lenses having cylindrical power of 1 diopter.*

Only those points are plotted for which noncompliance occurs for at least one member of a pair. The bar graphs at the bottoms of the center and lower frames show the number of lenses in the sample. Boxes containing an X in the center frame show compliance with the spherical tolerances; boxes containing an X in the lower frame indicate full compliance with spherical and cylindrical tolerances

for point B, and in addition the boxes in the bar graph in the lower portion shows the number of lenses in each sample. The number of boxes containing an X is the number of lenses of a given power that comply with the meridional requirements. The empty boxes indicate those lenses where at least one value of the meridional power at points A and B is in excess of tolerance. The lowest frame shows the degree of compliance with the requirements for cylindrical power. The bar graph at the bottom of this frame combines the results for all three frames.

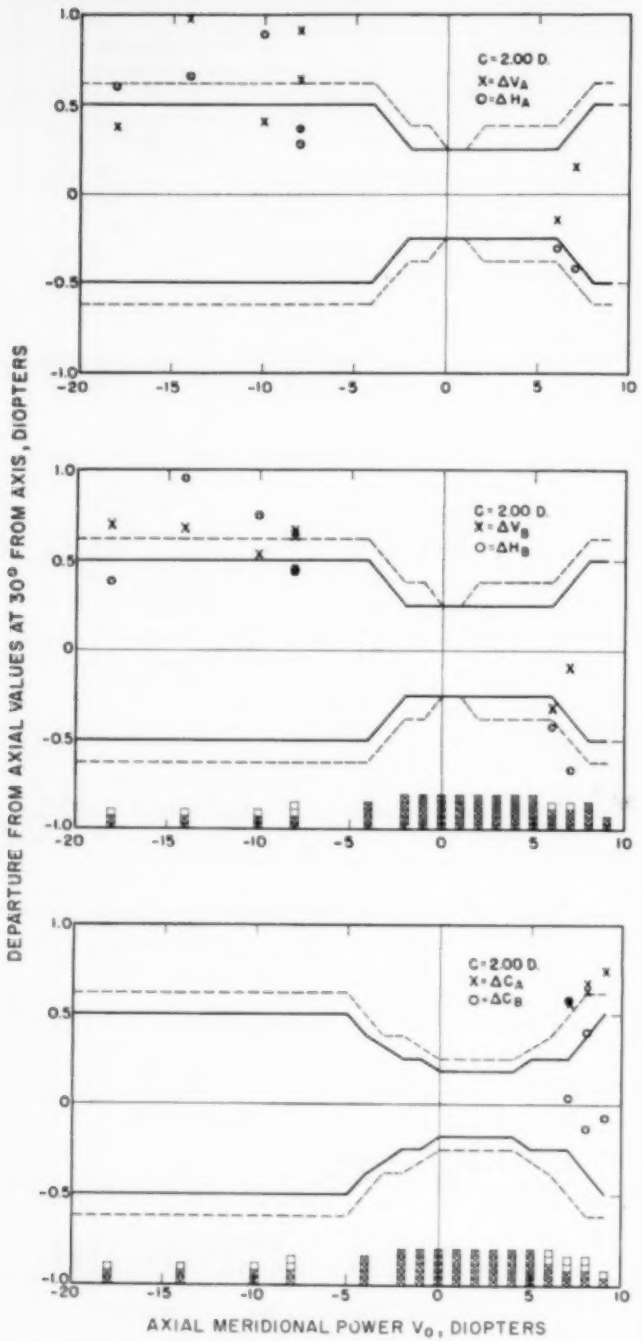

FIGURE 5. *Degree of compliance with suggested tolerance for marginal power for 71 lenses having cylindrical power of 2 diopters.*

Only those points are plotted for which noncompliance occurs for at least one member of a pair. The bar graphs at the bottoms of the center and lower frames show the number of lenses in the sample. Boxes containing an *X* in the center frame show compliance with the spherical tolerances; boxes containing an *X* in the lower frame indicate full compliance with spherical and cylindrical tolerances.

Consequently, a box containing an *X* in this graph indicates that a given lens complies in full with the tolerances for meridional and cylindrical power.

It is interesting to note, that for the cases shown, at least one and generally two or more lenses comply in full with the suggested tolerances which indicate that these tolerances can be and are being satisfied. The degree of compliance with the suggested tolerances is given in tabular form in tables 16 to 20 for 295 of the 311 lenses. In these tables is given the total number of lenses of a given power in each sample, together with information on the number of lenses complying with the minimum, the maximum, and the suggested tolerances for meridional and cylindrical power in the marginal regions of the lenses. At the bottom of each table, the percentage of lenses complying in each category is given.

At first glance, the tolerances set forth in tables 11 to 15 seem larger than need be. However, the study of the degree of compliance shown in tables 16 to 20 shows that this is not the case for presently existing lenses. For example, if these lenses were to comply fully with the minimum tolerance at both points *A* and *B*, it is clear that only a relatively small percentage of the lenses would satisfy the requirements; the percentages range from 83 percent for lenses having zero cylindrical power down to 15 percent for lenses having cylindrical power of 4.00 diopters. On the other hand, if these lenses were to comply fully with the maximum tolerance only at both points *A* and *B*, the percentages complying range from 96 to 85 percent. However, by using the minimum tolerance at either point *A* or point *B* and the maximum tolerance at both points *A* and *B* as suggested in paragraphs (a) and (b) of section 6.1, the total number complying is reduced only slightly, the percentages ranging from 92 to 84 percent, and somewhat better performance for the user is thus assured.

TABLE 16. *Degree of compliance with the minimum, maximum and suggested tolerances for marginal power for 72 lenses having axial meridional powers varying from +7.00 to −18.00 diopters and zero cylindrical power.*

Meridional power ($V_o = H_o$)	Number of lenses in sample	Number of lenses in sample complying with the following tolerances—		
		Minimum	Maximum	Suggested
7.00	3	2	2	2
6.00	5	5	5	5
5.00	5	4	5	5
4.00	5	4	5	4
3.00	5	4	5	4
2.00	5	5	5	5
1.00	5	5	5	5
0.00	5	5	5	5
−1.00	5	5	5	5
−2.00	5	4	5	5
−3.00	5	4	5	5
−4.00	5	3	5	4
−6.00	5	3	4	4
−10.00	3	2	3	3
−14.00	3	2	2	2
−18.00	3	3	3	3
Total	72	60	69	66
Percentage	.....	83	96	92

TABLE 17. *Degree of compliance with the minimum, maximum, and suggested tolerances for marginal power for 76 lenses having axial meridional powers varying from +8.00 to −18.00 diopters and cylindrical power of +1.00 diopter*

Meridional power (V_o=H_o+1.00)	Number of lenses in sample	Number of lenses in sample complying with the following tolerances—		
		Minimum	Maximum	Suggested
8.00	3	1	2	2
7.00	5	4	5	5
6.00	5	3	5	5
5.00	5	4	5	5
4.00	5	3	5	5
3.00	5	5	5	5
2.00	5	2	4	4
1.00	5	5	5	5
0.00	5	5	5	5
−1.00	5	2	4	4
−2.00	5	5	5	5
−3.00	5	3	5	5
−5.00	5	3	5	4
−9.00	4	2	2	2
−10.00	3	2	2	2
−14.00	3	1	2	2
−18.00	3	3	3	3
Total	76	53	69	68
Percentage	.....	70	91	90

TABLE 18. *Degree of compliance with the minimum, maximum, and suggested tolerances for marginal power for 71 lenses having axial meridional powers varying from +9.00 to −18.00 diopters and cylindrical power of +2.00 diopters*

Meridional power (V_o=H_o+2.00)	Number of lenses in sample	Number of lenses in sample complying with the following tolerances—		
		Minimum	Maximum	Suggested
9.00	2	0	1	1
8.00	4	0	2	2
7.00	4	0	2	2
6.00	4	0	3	3
5.00	5	0	5	5
4.00	5	2	5	5
3.00	5	4	5	5
2.00	5	5	5	5
1.00	5	2	5	5
0.00	5	1	5	5
−1.00	5	1	5	5
−2.00	5	0	5	5
−4.00	4	3	4	4
−8.00	4	2	2	2
−10.00	3	2	2	2
−14.00	3	1	2	2
−18.00	3	1	2	2
Total	71	24	60	60
Percentage	.....	34	85	85

6.3. Discussion of the Proposed Tolerances

In the preparation of tolerances for axial powers, it is possible to require that the deviation of measured from prescribed power be kept within a narrow enough range that normal depth of focus will still enable the unaccommodated eye to distinguish objects separated by 1 minute of arc. However, in the case of tolerances for marginal power, it is not readily possible to maintain such a high degree of performance because of limitations imposed by having only two surfaces available to the designer, conditions of use, and the cost. Although it is possible to design a lens for each power that will perform in excellent fashion for one viewing distance, it is not likely that it will perform equally well for all other viewing distances. In addition, it is impracticable because of cost to construct a special lens for each user, so it is usual to maintain a series of lenses whose base-curve changes in successive discrete steps to cover the entire range of use.

TABLE 19. *Degree of compliance with the minimum, maximum, and suggested tolerances for marginal power for 43 lenses having axial meridional powers varying from +9.00 to −7.00 diopters and cylindrical power of +3.00 diopters*

Meridional power (V_o=H_o+3.00)	Number of lenses in sample	Number of lenses in sample complying with the following tolerances—		
		Minimum	Maximum	Suggested
9.00	4	0	3	3
8.00	4	0	3	2
7.00	4	0	3	2
6.00	4	2	4	4
2.00	5	3	5	5
1.00	5	2	5	5
0.00	5	1	5	5
−1.00	4	0	4	4
−3.00	4	1	4	4
−7.00	4	1	4	2
Total	43	10	40	36
Percentage	.....	23	93	84

TABLE 20. *Degree of compliance with the minimum, maximum, and suggested tolerances for marginal power for 33 lenses having axial meridional powers varying from +9.00 to −6.00 diopters and cylindrical power of +4.00 diopters*

Meridional power (V_o=H_o+4.00)	Number of lenses in sample	Number of lenses in sample complying with the following tolerances—		
		Minimum	Maximum	Suggested
9.00	4	0	2	2
8.00	4	0	3	2
3.00	4	1	4	4
2.00	4	1	4	4
1.00	4	0	4	3
0.00	5	0	5	5
−2.00	4	1	4	4
−6.00	4	2	4	4
Total	33	5	30	28
Percentage	.....	15	91	85

The suggested tolerances for spherical power do not present any serious hardship for the wearer under middle age, as such a person is likely to have an amplitude of accommodation well above the maximum suggested tolerances. For a person having a small amplitude of accommodation, the marginal performance of a lens near the limits of the suggested tolerance will probably be noticeably lower than the axial performance. However, he will still usually be able to distinguish between objects separated by from 2 to 8 minutes of arc, depending upon the amount of departure of the marginal from the axial powers. This corresponds to a reduction in visual acuity down to 20/40 or 20/160, which is still adequate for the detection of large objects or movement.

In the case of astigmatism, the problem is more difficult. One cannot minimize astigmatism to an appreciable extent by the exercise of accommodative powers. Consequently, all users will suffer some reduction in visual acuity in the marginal regions,

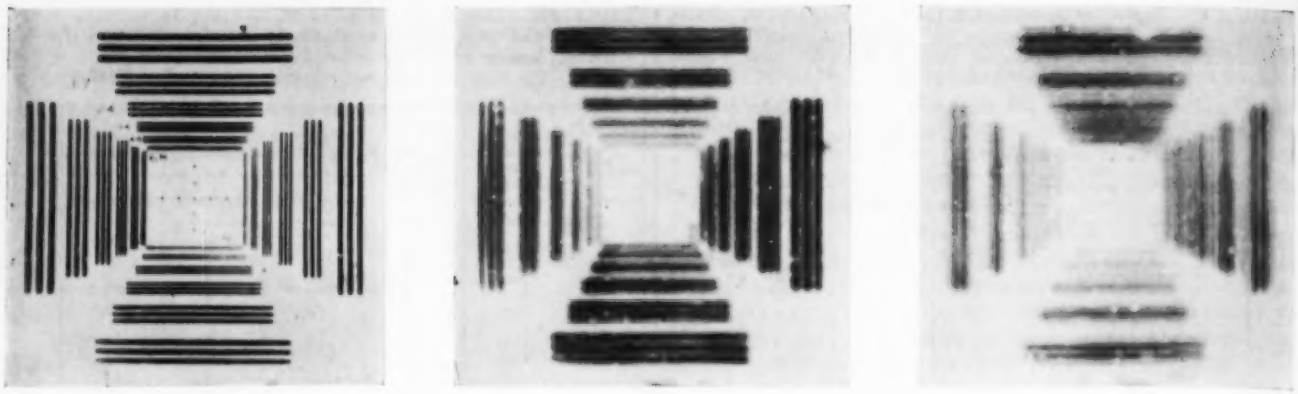

FIGURE 6. *Photographs showing change in imagery with departures from prescribed spherical power by definite amounts.*

A shows the imagery for the condition of best focus with $\Delta V_O = \Delta H_O = 0$; *B* shows the imagery for $\Delta V_O = H_O = +0.25$ diopters; and *C* shows the imagery for $\Delta V_O = \Delta H_O + 0.50$ diopters.

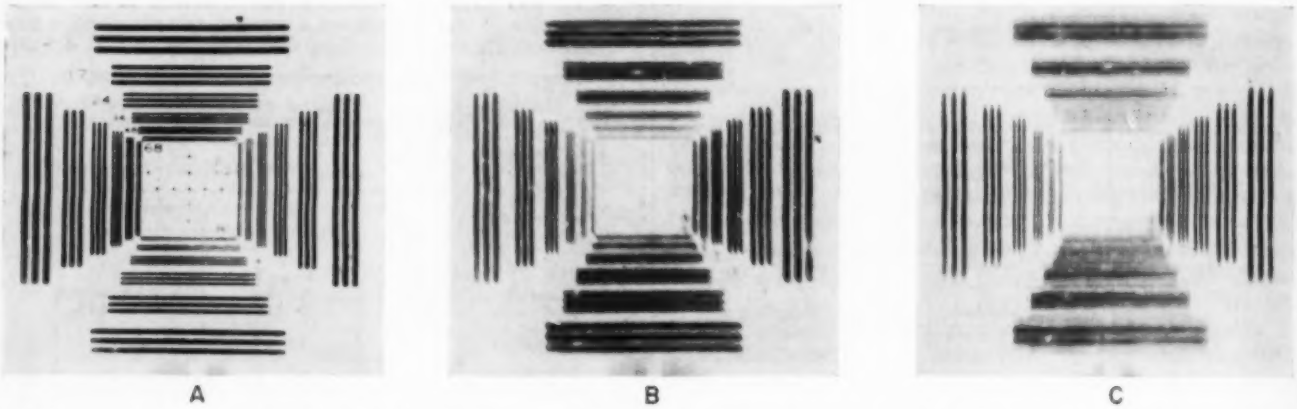

FIGURE 7. *Photographs showing change in imagery with departures from prescribed cylindrical power by definite amounts.*

A shows the imagery for the condition of best focus with $\Delta C_O = O$; *B* shows the imagery for $\Delta C_O = +0.25$ diopters; and *C* shows the imagery for $\Delta C_O = +0.50$ diopters.

except in those instances where the depth of focus is sufficient to provide adequate compensation. Of course, it is unlikely that anyone will be using the marginal portion of his spectacle lenses for an extended time, as it is more natural to turn the head so as to take advantage of central vision. Figures 6 and 7 show the quality of imagery that may be expected when looking through lenses whose powers vary from the prescribed by selected amounts [5].

In conclusion, it can be stated that there are now available a large number of lenses that are corrected to yield improved marginal performance, and that they do so. However, further efforts toward improvement should be made. If this is done, it may eventually be possible to reduce the tolerances suggested herein to values more nearly comparable to the depth of focus.

7. References

[1] F. E. Washer, Axial performance of spectacle lenses, J. Research NBS **57,** 355 (1956) RP2724.

[2] F. E. Washer, A simplified method of measuring the marginal power of spectacle lenses, J. Research NBS **55,** 79 (1955) RP2607.

[3] H. H. Emsley and William Swaine, Ophthalmic lenses, 6th ed., p. 237 (Hatton Press Ltd., London, 1951).

[4] Veterans Administration, specifications for optical lenses, frames and cases (April 23, 1956).

[5] F. E. Washer, Instrument for measuring the marginal power of spectacle lenses, J. Opt. Soc. Am. **45,** 719 (1955).

WASHINGTON, November 21, 1957

Journal of Research of the National Bureau of Standards Vol. 60, No. 6, June 1958 Research Paper 2870

Enthalpy and Heat Capacity from 0° to 900° C of Three Nickel-Chromium-Iron Alloys of Different Carbon Contents

Thomas B. Douglas and Ann W. Harman

The enthalpy relative to 0° C of three alloys was measured at nine temperatures from 100° to 900° C by a precise "drop" method. The alloys contained approximately 76 percent of nickel, 15 percent of chromium, and 8 percent of iron, with carbon contents of 0.02, 0.07, and 0.11 percent, respectively. The results are almost independent of the several variations in prior heat treatment investigated, and the heat-capacity–temperature curves of the three alloys are almost coincident, but there is a marked shift in each curve within the interval 500° to 600° C.

1. Introduction

The National Advisory Committee for Aeronautics has had underway a program of acquiring basic physical data important in the aerodynamic heating of the construction materials used in supersonic airplanes and guided missiles. As a part of the program, the Committee sponsored at the National Bureau of Standards measurements of the thermal conductivity, thermal expansion, total thermal emissivity, and heat capacity of nickel-chromium-iron alloys commercially produced as Inconel.

The investigation of these properties covered Inconel specimens whose carbon contents spanned more than the range normally encountered. The measurements of heat capacity are reported in this paper. The results of the measurements of heat capacity, thermal conductivity, thermal expansion, mechanical properties, electrical resistance, and emissivity of these Inconel alloys are summarized elsewhere [2].[1]

2. Alloys Investigated

The heat capacity was derived from enthalpy measurements on specimens that had been cut from hot-rolled, unannealed rods of ½-in. diameter furnished by the International Nickel Company, who supplied the chemical analyses of the three alloys given in table 1.[2] Before measurement of their enthalpy, the samples were subjected to the various annealing treatments specified in footnotes to the tables of enthalpy data (tables 3 to 5, section 4), and the average values of hardness found after annealing [2] are given in the last two columns of table 1. The enthalpy data of table 6 are preliminary values determined in an attempt to ascertain whether certain variations in prior annealing treatment affected the enthalpy appreciably. Although the hardness values were determined on various Rockwell superficial hardness scales, these results have been converted to approximate values on the Vickers scale, which also are given to afford ready comparison.

3. Calorimetric Method

The apparatus and method used in measuring the enthalpy were described in detail in a recent paper [3]. Briefly, the sample in a helium-filled container of the alloy 80 Ni-20 Cr was held inside a silver-core furnace in an atmosphere of helium until, as determined by preliminary "relaxation-time" tests [4], the sample had time to reach the furnace temperature within 0.01 deg C. The sample and container were

[1] Figures in brackets indicate the literature references at the end of this paper.

[2] Although these alloys were not reanalyzed at the Bureau to confirm these compositions, there are reasons for believing that in the temperature range investigated their enthalpies are insensitive to errors in composition. The heat capacities per unit mass of the three principal elements (nickel, chromium, and iron) are approximately the same, and there are no transitions in their ternary phase diagram near the compositions of the present alloys [1].

TABLE 1. *Chemical compositions of the alloys*

Sample number	Chemical composition (weight %)									Hardness	
	C	Ni	Cr	Fe	Mn	Si	Cu	S	Total	Rockwell, 15-T scale	Approximate equivalent value, Vickers scale
1	0.02	75.99	14.42	8.87	0.28	0.17	0.22	0.007	99.98	78	97
2	.07	76.45	14.96	7.89	.26	.19	.15	.007	99.98	80	106
3	.11	75.64	15.32	8.17	.33	.21	.19	.007	99.98	83	123

then dropped into a precision Bunsen ice calorimeter, the heat they delivered in cooling to 0° C being determined by the mass of mercury entering the calorimeter because of the reduction in volume caused by the melting of ice. Similar measurements were made on the empty container to account accurately for (a) the part of the heat due to the container when a sample was present, and (b) the heat lost elsewhere than to the calorimeter during the drop. The net heat contributed by the sample itself equals its difference in enthalpy between the furnace temperature and 0° C.

The furnace temperature, which was held constant to ±0.01 deg C during a heat measurement, was measured up to 600° C by a platinum thermometer and above 600° C by a platinum—platinum–10-percent rhodium thermocouple. Both measuring instruments, initially annealed and calibrated at the Bureau in terms of the International Temperature Scale of 1948, were recalibrated during the course of the present investigation; the thermometer had remained unchanged, and the temperature indications of the thermocouple had not changed by more than 0.1 deg C. The conversion factor of the ice calorimeter, 270.48 ±0.03 abs j/g of mercury, had been determined earlier in hundreds of electrical calibrations of the calorimeter [3]. Minor corrections were made for the very small, unavoidable variations in temperature and masses of container materials entering the calorimeter.

The major material constituting the sample container, the alloy 80 Ni-20 Cr, has been shown to exhibit an anomaly in heat capacity [5] similar in magnitude and temperature range to those of the alloys of the present investigation. However, this effect always canceled completely in subtracting the empty-container heat to obtain that of the alloy sample, for the empty-container heat values were determined on the same container and at the same temperatures as those used for the alloy samples.

4. Enthalpy Data

The principal series of individual heat measurements are recorded in table 2 for the empty container and in tables 3, 4, and 5 for the three alloys, which are numbered as in table 1. All individual-run values in each of tables 3, 4, and 5 are given in chronological order, and all intervening periods of time when the samples were in the furnace but no heat measurements were being made also are recorded. (In table 2 the values for any one furnace temperature are listed chronologically, but the temperatures themselves are not.) Each value in the fourth column of tables 3, 4, and 5 was obtained by subtracting from the corresponding value in the third column the mean heat for the empty container at that furnace temperature (from table 2) and then dividing by the sample mass.

Although enthalpy values at some temperature between 500° and 600° C were also desired, no significance is to be attached to the particular choice of 557.5° C.

An investigation was made of the effect of different prior heat treatments on the relative enthalpy of alloy 2. Measurements on three specimens of this alloy that had had different treatments are recorded in table 6, in chronological order for each specimen. A sequence of several measurements at each of the successive temperatures 600°, 900°, and 600° C was adopted, and the pertinent values from table 4 are included for comparison ("specimen C"). The mean empty-container value of enthalpy (table 2) was used at each temperature.

TABLE 2. *Enthalpy measurements—empty container*

Furnace temperature, t	Measured heat		Furnace temperature, t	Measured heat	
	Individual run	Mean		Individual run	Mean
°C	*abs j*	*abs j*	°C	*abs j*	*abs j*
100.00	510.2 509.5	509.8	500.00	2,790.8 2,791.1 2,790.7	2,790.9
200.00	1,050.2 1,049.9 1,049.6	1,049.9	557.50	3,146.5 3,146.2	3,146.3
300.00	1,611.8 1,614.9 1,612.1	1,612.9	600.00	3,410.6 3,412.6	3,411.6
400.00	2,192.1 2,196.2 2,197.6 2,193.7 2,200.2 2,192.1	2,195.3	700.0	4,083.7 4,078.8 4,076.7	4,079.7
			800.0	4,764.0 4,765.6	4,764.8
			900.0	5,460.0 5,464.4	5,462.2

TABLE 3. *Enthalpy measurements—alloy 1 (0.02% carbon)*[a]

(Sample mass=19.8559 g)

Furnace temperature, t	Time in furnace	Measured heat (sample plus container)	Net enthalpy of sample, $H_t-H_{0°C}$	
			Individual run	Mean
°C	*min*	*abs j*	*abs j g*$^{-1}$	*abs j g*$^{-1}$
100.00	32 34 54	1,404.7 1,407.8 1,410.4	45.07 45.23 45.36	45.22
200.00	34 34	2,896.9 2,895.8	93.02 92.96	92.99
300.00	40 44 50	4,435.6 4,439.6 4,441.8	142.16 142.36 142.47	142.33
400.00	44 44	6,032.7 6,035.5	193.26 193.40	193.33
500.00	49 44	7,678.1 7,675.9	246.14 246.02	246.08
600.00	44 44 54	9,396.7 9,406.9 9,406.2	301.43 301.94 301.91	301.76
700.0	44 44	11,242.0 11,237.3	360.71 360.47	360.59
800.0	44 44	13,116.1 13,117.0	420.60 420.64	420.62
900.0	79 44	15,048.6 15,050.6	482.80 482.90	482.85
557.50	45 45	8,657.8 8,657.1	277.58 277.54	277.56

[a] Prior treatment: Annealed at 1,010° C (1,850° F) and then quenched.

TABLE 4. *Enthalpy measurements—alloy 2 (0.07% carbon)*[a]

(Sample mass=19.9070 g)

Furnace temperature, t	Time in furnace	Measured heat (sample plus container)	Net enthalpy of sample, $H_t-H_{0°C}$	
			Individual run	Mean
°C	min	abs j	abs j g^{-1}	abs j g^{-1}
100.00	45	1,405.1	44.97	45.03
	45	1,407.4	45.09	
200.00	45	2,891.4	92.50	92.53
	45	2,892.4	92.55	
300.00	45	4,440.9	142.06	142.04
	45	4,439.9	142.01	
400.00	45	6,043.8	193.32	193.39
	45	6,046.6	193.46	
500.00	45	7,697.8	246.50	246.53
	45	7,699.3	246.57	
600.00	45	9,435.7	[b](302.61)	302.05
	45	9,424.9	302.07	
	45	9,425.1	302.08	
	45	9,423.3	301.99	
700.0	45	11,258.1	360.60	360.58
	45	11,257.7	360.57	
800.0	45	13,143.1	420.87	420.97
	45	13,146.9	421.06	
900.0	45	15,085.2	483.40	483.38
	45	15,084.3	483.35	
557.50	45	8,674.1	277.68	277.67
	45	8,673.8	277.67	
557.50	170	8,667.6	277.36	277.34
	183	8,666.9	277.32	
557.50	45	8,669.6	277.45	277.39
	50	8,667.1	277.33	
400.00	45	6,040.1	193.14	193.20
	50	6,042.5	193.26	
900.0	70	15,083.1	483.29	483.29
557.50	45	8,674.5	277.70	277.69
	50	8,674.3	277.69	

[a] Prior treatment: Annealed by heating at 1,120° C (2,050° F) for 7½ min and cooling in air, and then by heating at 1,010° C (1,850° F) for 20 min. In the latter case the method of cooling is not known.

[b] Omitted from the mean because of inferior precision.

TABLE 5. *Enthalpy measurements—alloy 3 (0.11% carbon)*[a]

(Sample mass=19.8347 g)

Furnace temperature, t	Time in furnace	Measured heat (sample plus container)	Net enthalpy of sample, $H_t-H_{0°C}$	
			Individual run	Mean
°C	min	abs j	abs j g^{-1}	abs j g^{-1}
100.00	45	1,406.1	45.19	45.18
	45	1,406.0	45.18	
200.00	45	2,890.8	92.81	92.83
	60	2,892.3	92.89	
	50	2,890.6	92.80	
300.00	45	4,437.7	142.41	142.39
	45	4,436.7	142.36	
400.00	45	6,039.7	193.82	193.75
	45	6,037.1	193.69	
500.00	45	7,690.9	247.04	247.02
	45	7,688.5	246.92	
	45	7,691.9	247.09	
557.50	45	8,676.0	278.78	278.57
	50	8,669.5	278.46	
	45	8,669.8	278.48	
600.00	45	9,412.9	302.57	302.50
	45	9,410.4	302.44	
700.0	45	11,256.2	361.81	361.70
	45	11,251.5	361.57	
	45	11,257.3	361.87	
	45	11,250.4	361.52	
800.0	45	13,139.1	422.20	422.17
	45	13,137.8	422.14	
900.0	45	15,070.6	484.42	484.24
	45	15,064.8	484.13	
	60	15,063.1	484.04	
	45	15,069.2	484.36	
200.00	45	2,892.1	92.88	92.84
	45	2,890.6	92.80	
500	180	[b]	--------	--------
200.00	45	2,890.1	92.78	92.78

[a] Prior treatment: Annealed by heating at 1,120° C (2,050° F) for 7½ min and cooling in air, and then by heating at 1,010° C (1,850° F) for 20 min. In the latter case the method of cooling is not known.

[b] No runs.

TABLE 6. *Variation of the relative enthalpy of alloy 2 with heat treatment and hardness*

Specimen	Prior treatment	Resulting hardness		Mean relative enthalpy, $H_t-H_{0°C}$[a]	
		Rockwell scales	Vickers scale (approx.)	t=600° C	t=900° C
				abs j g^{-1}	abs j g^{-1}
A	Hot-rolled, then machined to rod (diam, 0.5 in.).	31(Rc)	309	301.35 ±0.02(3) 301.07 ±0.00(2)	483.37 ±0.06(5)
B	Annealed at 1,000° C (1,830° F) for 1 hr and air-cooled. Then cold-rolled from 0.5- to 0.03-in. thickness in 3 steps, each followed by annealing at same temperature.	66(30T)	135	301.93 ±0.00(3) 301.30 ±0.11(3)	482.92 ±0.14(4)
C	Annealed at 1,120° C (2,050° F) for 7½ min, then at 1,010° C (1,850° F) for 20 min. Cooled in quiescent air.	80(15T)	106	302.05 ±0.02(3)	483.35 ±0.02(3)

[a] The number of individual measurements is given in parentheses, and the stated tolerance is the probable error of the mean. The second value at 600° C for each of specimens A and B was determined after the measurements on the specimen at 900° C. The results for specimen C have been repeated from table 4 for comparison.

5. Smoothed Values of Enthalpy and Heat Capacity

The mean observed values of relative enthalpy in the last columns of tables 3, 4, and 5 were smoothed by fitting to them empirical functions of temperature whose coefficients were determined by the method of least squares. The temperature derivatives of such functions give reliable smooth values of the instantaneous heat capacity in those temperature regions where there is evidence that inadequately represented irregularities, such as those often caused by transitions, do not occur.

The relative enthalpies of the three alloys per unit mass are obviously so nearly the same at the same temperature that a single equation to represent all three would be of some practical value. The best quadratic function of temperature giving in absolute joules per gram the enthalpy at $t°$ relative to 0° C was found to be

$$H_t - H_{0°C} = 0.43954t + 1.0832(10^{-4})t^2. \quad (1)$$

The corresponding heat capacity is

$$C_p = 0.4395 + 2.166(10^{-4})t. \quad (2)$$

The average deviation between the mean observed enthalpy for the three alloys and that calculated from eq (1) (without regard to sign) is 0.2 percent, and the maximum deviation is 0.8 percent. By dividing the difference between the mean observed enthalpies at two adjacent temperatures by the temperature difference, an "observed" value of heat capacity at the mean temperature is obtained for each alloy. These observed values are compared with eq (2) in figure 1.[3] The average deviation between mean and observed heat capacities is 0.75 percent, and the maximum deviation is 2 percent.

Equations (1) and (2) do not represent the data within their precision. In fact, it is evident from figure 1 that there are small but definite trends with temperature. A more refined representation of the enthalpy of each alloy was obtained by dividing the whole temperature range investigated into three contiguous intervals and then fitting the mean observed values in each interval to an empirical equation of suitable form. In the case of each alloy the two equations for each pair of adjacent temperature intervals were required to give the same value of enthalpy at the temperature common to the two intervals.[4]

The resulting equations, which give the enthalpy of the alloy relative to 0° C in absolute joules per gram at $t°$ C, are as follows:

Alloy 1 (0.02% carbon)—

0° to 500° C:

$$H_t - H_{0°C} = 0.49022t + 6.145(10^{-5})t^2 - 31.92 \log_{10}[(t+273.16)/273.16], \quad (3)$$

500° to 557.5° C:

$$H_t - H_{0°C} = -27.64 + 0.54737t, \quad (4)$$

557.5° to 900° C:

$$H_t - H_{0°C} = -12.65 + 0.47160t + 8.768(10^{-5})t^2. \quad (5)$$

Alloy 2 (0.07% carbon)—

0° to 500° C:

$$H_t - H_{0°C} = 0.48367t + 7.279(10^{-5})t^2 - 29.89 \log_{10}[(t+273.16)/273.16], \quad (6)$$

500° to 557.5° C:

$$H_t - H_{0°C} = -24.63 + 0.54231t, \quad (7)$$

557.5° to 900° C:

$$H_t - H_{0°C} = -9.55 + 0.46256t + 9.455(10^{-5})t^2. \quad (8)$$

Alloy 3 (0.11% carbon)—

0° to 500° C:

$$H_t - H_{0°C} = 0.47887t + 7.584(10^{-5})t^2 - 25.21 \log_{10}[(t+273.16)/273.16], \quad (9)$$

500° to 600° C:

$$H_t - H_{0°C} = 10.76 + 0.40369t + 1.3759(10^{-4})t^2, \quad (10)$$

600° to 900° C:

$$H_t - H_{0°C} = -22.06 + 0.49782t + 7.190(10^{-5})t^2. \quad (11)$$

The differences between the values of relative enthalpy given by the preceding equations and the corresponding mean observed values on which the equations are based are listed in table 7. No comparison is included based on eq (4), (7), and (10), as the agreement is automatically perfect in these short intermediate ranges of temperature because of the lack of data at additional temperatures in these ranges. Only the nonparenthesized entries in the table are significant with regard to the actually observed behavior of the alloys, as the parenthesized differences in a given column are based on extrapolated values of enthalpy calculated from the equation outside its temperature range of applicability.

Differentiation of eq (3) to (11) with respect to temperature gives the corresponding equations for instantaneous heat capacity, C_p. In the temperature ranges of their applicability the resulting equations provide the smoothed values of heat capacity given for round temperatures in table 9. A comparison between these equations and the corresponding mean "observed" heat capacities of the three alloys is afforded by figures 2, 3, and 4. It will be noted that these graphs do not include curves corresponding to eq (4), (7), and (10). These three equations give the best smoothed representation of the heat capaci-

[3] Two sets of the points in figure 1 have been displaced by small amounts in a direction parallel to the graph line to avoid confusion from overlapping.

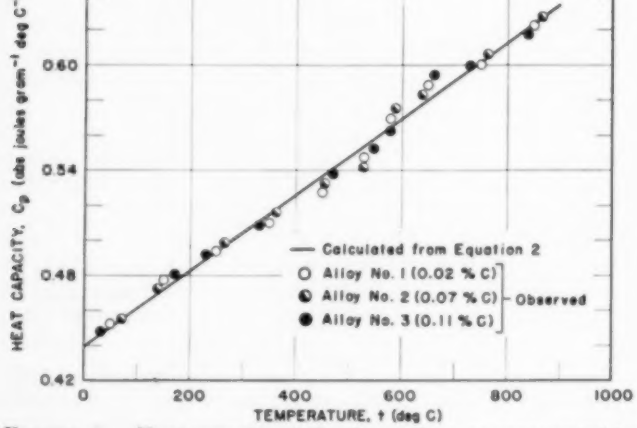

FIGURE 1. *Heat capacity of the three alloys as represented by a single equation.*

[4] None of the values of table 4 following the first two runs at 557.50° C was used in the derivation of the equations.

TABLE 7. *Differences between mean observed and calculated relative enthalpy of the three alloys*

Temperature, t	Mean observed minus calculated enthalpy H_t-H_0° C					
	Alloy 1 (0.02% C)		Alloy 2 (0.07% C)		Alloy 3 (0.11% C)	
	Eq (3)	Eq (5)	Eq (6)	Eq (8)	Eq (9)	Eq (11)
° C	*abs j g⁻¹*	*abs j g⁻¹*	*abs j g⁻¹*	*abs j g⁻¹*	*abs j g⁻¹*	*abs j g⁻¹*
0	0.00	(+12.65)	0.00	(+9.55)	0.00	(+22.06)
100	−.09	(+9.83)	−.01	(+7.38)	−.04	(+16.74)
200	+.11	(+7.81)	+.01	(+5.79)	+.04	(+12.46)
300	+.01	(+5.61)	.00	(+4.31)	+.02	(+8.63)
400	−.08	(+3.31)	−.01	(+2.80)	−.05	(+5.18)
500	+.04	(+1.01)	+.01	(+1.17)	+.02	(+2.19)
557.5	(+.59)	+0.04	(−.14)	−0.02	(+.22)	(+0.76)
600	(+1.62)	−.12	(+.73)	+.03	(+.61)	−.02
700	(+4.95)	+.16	(+2.84)	+.02	(+3.24)	+.05
800	(+8.09)	−.13	(+5.21)	−.04	(+5.52)	−.05
900	(+12.09)	+.04	(+8.00)	+.02	(+7.79)	+.02

TABLE 8. *Smoothed values of heat capacity of the three alloys*

Temperature	Heat capacity (C_p) of alloy—		
	No. 1 (0.02% C)	No. 2 (0.07% C)	No. 3 (0.11% C)
° C	*abs j g⁻¹ deg C⁻¹*	*abs j g⁻¹ deg C⁻¹*	*abs j g⁻¹ deg C⁻¹*
0	0.4395	0.4362	0.4388
50	.4534	.4508	.4526
100	.4654	.4635	.4648
150	.4758	.4748	.4758
200	.4855	.4854	.4861
250	.4944	.4953	.4959
300	.5029	.5048	.5053
350	.5110	.5139	.5144
400	.5188	.5226	.5233
450	.5263	.5313	.5321
500	[a] .5337	[b] .5397	[c] .5405
550	.547	.542	.555
600	.5768	.5761	[d] .5841
650	.5856	.5855	.5913
700	.5944	.5950	.5985
750	.6032	.6044	.6056
800	.6119	.6139	.6128
850	.6207	.6233	.6200
900	.6295	.6328	.6272

[a] Calculated from eq (3). [b] Calculated from eq (6).
[c] Calculated from eq (9). [d] Calculated from eq (11).

ties afforded by the data in the short transition range 500° to 557.5° or 500° to 600° C. The heat capacities change rather rapidly with temperature in this region, and data were not obtained at a sufficient number of temperatures to establish the heat capacity in this temperature range with high accuracy. However, the temperature interval is small, so that the resulting percentage uncertainty in the enthalpy change of the alloy is small for a large temperature interval and is negligible when the interval includes the entire region of enomaly.

6. Discussion

The heat capacities of the simplest crystalline materials are usually found to have reproducible values that increase in a regular manner with temperature. The alloys of the present investigation depart from this uncomplicated type of behavior in two apparently distinct respects. In the first place, as the temperature increases and passes through the region between approximately 500° and 600° C, the heat capacity rapidly increases to a magnitude between 3 and 5 percent greater than that which would be obtained by extrapolation from lower temperatures, and this change apparently takes place rapidly during either heating or cooling. Such an abnormally rapid rise of heat capacity with temperature was found to occur in the case of all three alloys investigated, the average temperature of rapid rise increasing slightly from alloy 1 to alloy 3. In the second place, much smaller and much slower changes in enthalpy (or mean heat capacity) appear to have occurred following changes in thermal history in the case of one of the alloys (No. 2).

The first anomaly is shown in a simple way by the heat-capacity–temperature graphs of the three alloys in figures 2, 3, and 4. Each continuous curve represents a single empirical equation, but only the solid portion of the curve fits the observed data, the dashed portion constituting an extrapolation where the deviations are large. When each of the alloys passes through the temperature region of anaomaly its heat capacity rather abruptly shifts onto the other curve, suggesting that in the process the alloy undergoes some type of transition accompanied by a change in its physical properties. Anomalies in the linear thermal expansion, the electrical resistivity, and the ultimate and yield strengths of the same alloys have been found to occur in approximately the same regions of temperature as the heat capacity [2, 6].

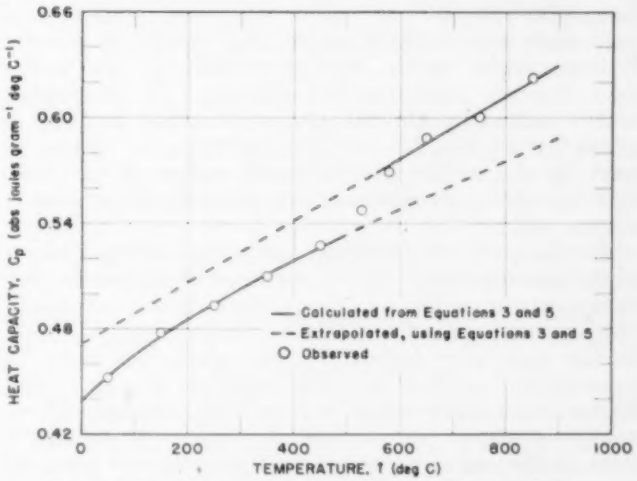

FIGURE 2. *Heat capacity of alloy 1 (0.02% carbon).*

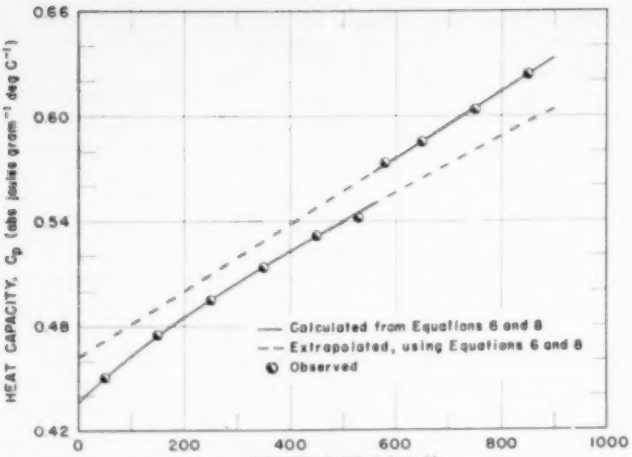

FIGURE 3. *Heat capacity of alloy 2 (0.07% carbon).*

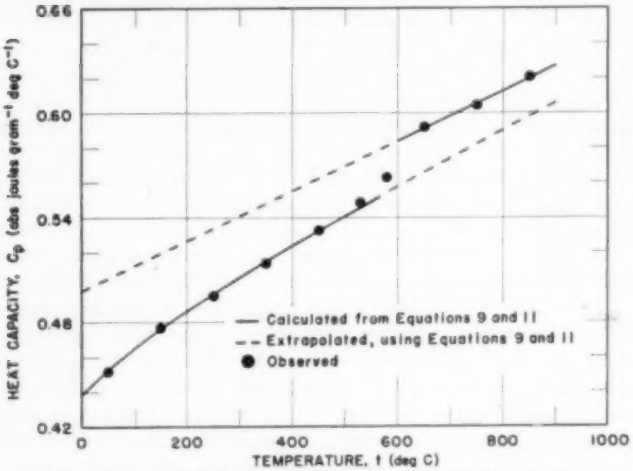

FIGURE 4. *Heat capacity of alloy 3 (0.11% carbon).*

The present enthalpy measurements provide an upper limit to the time required for this transition to occur in these alloys. Some experimental estimates of cooling rates in the calorimeter indicate that when the samples had been initially brought to temperatures above the anomalous region, they cooled from 600° to 500° C in less than half a minute, a rate that is thus fairly rapid, but would in general be comparable to the rate of quenching only in the case of much more massive samples. The total heat thus evolved by the sample as it cooled to 0° C is given by eq (5), (8), or (11), which corresponds in part to the area under a combination of the low- and high-temperature *solid* curves of figure 2, 3, or 4, respectively.

In this process of cooling one of the alloys from a high temperature, the heat-capacity curve in the temperature region of anomaly which will complete the accounting for the total observed enthalpy change is not uniquely defined by the data but may be reasonably assumed to join smoothly the low- and high-temperature solid curves. The observed enthalpy changes prove that this short intermediate part of the curve possesses no hump except possibly a small one. In fact, it may be that no hump at all exists, a situation approximating a zero heat of (first-order) transition. This situation is rather unusual, but has been reported in the cases of the similar alloy 80 Ni-20 Cr [5] and cobalt metal [7]. The sample of the former that was investigated had a composition analogous to that of the present alloys (77% Ni, 20% Cr, 0.4% Fe, 0.6% Mn, 1.4% Si, 0.04% C), and was found to have a very similar shift in its heat capacity-temperature curve.

Probably the most significant fact about the apparent *slow* changes of relative enthalpy observed with alloy No. 2 is their smallness. Strictly speaking, these small changes should be attributed not to the alloy specimen alone but to a combination of this alloy and the alloy 80 Ni-20 Cr constituting the container. All the heat measurements on the alloy specimen were carried out in this container, and the effect of prolonged times at elevated temperatures on the enthalpy of the empty container was not determined. For this reason there is no proof that the observed trends with time are not due, at least in part, to the container itself. However, as pointed out above, the chemical compositions of the two alloys involved are analogous. Hence if small changes were not actually exhibited by the alloy specimen, they must have been by a similar alloy.

The variation of the relative enthalpy of alloy 2 with hardness is shown in table 6. The first values at 600° C for the three specimens, determined immediately after the respective treatments indicated, show an increasing enthalpy with decreasing hardness, the total change of enthalpy amounting to 0.2 percent and lying well outside the limits of precision of the measurements. The subsequently determined enthalpies at 900° C show no systematic variation with hardness, but in the case of specimens A and B the enthalpy was then remeasured at 600° C and found somewhat lower than before. It will be noted from table 4 that holding specimen C for several hours at 557.5° C resulted in a decrease of relative enthalpy of 0.1 percent at this temperature but that the original higher value (at 557.5° C) was restored after renewed exposure of the specimen to 900° C. The causes of these small systematic variations in enthalpy were not determined.

7. References

[1] Metals Handbook, p. 1261, Am. Soc. Metals (Cleveland, Ohio, 1948).

[2] W. J. O'Sullivan, Jr., Some thermal and mechanical properties of Inconel to high temperatures for use in aerodynamic heating research, Am. Soc. Testing Materials Proc., **55,** 757 (1955).

[3] G. T. Furukawa, T. B. Douglas, R. E. McCoskey, and D. C. Ginnings, J. Research NBS **57,** 67 (1956) RP2694.

[4] D. C. Ginnings and R. J. Corruccini, J. Research NBS **38,** 593 (1947) RP1797.

[5] T. B. Douglas and J. L. Dever, Enthalpy and specific heat of four corrosion-resistant alloys at high temperatures, J. Research NBS **54,** 15 (1955) RP2560.

[6] P. Hidnert, Thermal expansion of some nickel alloys, J. Research NBS **58,** 89 (1957) RP2737.

[7] K. K. Kelley, Contributions to the data on theoretical metallurgy. X. High-temperature heat-content, heat-capacity, and entropy data for inorganic compounds, U. S. Bureau of Mines Bull. **476,** 59 (1949).

WASHINGTON, October 18, 1957.

Journal of Research of the National Bureau of Standards Vol. 60, No. 6, June 1958 Research Paper 2871

Relative Strengths of Forty Aromatic Carboxylic Acids in Benzene at 25° C.[1]

Marion Maclean Davis and Hannah B. Hetzer

The relative strengths of benzoic acid, 31 of its monosubstituted derivatives, 7 disubstituted derivatives, and one trisubstituted derivative have been measured in terms of the equilibrium constants (K'') for association with the reference base 1,3-diphenylguanidine in benzene at 25° C. The measurements were performed spectrophotometrically, using the indicator acid bromophthalein magenta E (tetrabromophenolphthalein ethyl ester) as the reference acid, the equilibrium constant K' for association of the indicator with diphenylguanidine being known from previous work. Equilibrium constants for *p*-orsellinic (2,6-dihydroxy-*p*-toluic) acid and 2,4,6-trinitrobenzoic acid could not be measured, as these acids appear to associate completely with diphenylguanidine under the conditions of the experiments.

Plotting log K'' values against the corresponding pK values for aqueous solutions of the acids gives an essentially linear relationship in the case of acids with *meta*- and *para*-substituents only, but the line for *para*-substituted acids has a slightly different slope from the line for *m*-substituted acids. Similar comparisons were made with published data on relative strengths in alcohols or dioxane-water mixtures. *ortho*-Substituted acids show marked solvent effects. Explanations of the solvent effects have been suggested, and various theoretical implications and possible applications of the results are discussed. The theoretical discussion includes evaluation of constants of the Hammett equation.

1. Introduction

Earlier reports from the Bureau [1][2] have dealt with qualitative and quantitative aspects of acid-base reactions in benzene at 25° C, placing particular emphasis on the behavior of different types of organic bases with the three indicator acids, bromophthalein magenta E (tetrabromophenolphthalein ethyl ester), picric acid, and trinitro-*m*-cresol. In this study information previously gained has been applied in measuring systematically the relative strengths of a group of related carboxylic acids—benzoic acid and various substituted benzoic acids—in benzene. The method consists of determining spectrophotometrically the equilibrium constant for the association of the carboxylic acid with the reference base, diphenylguanidine, in the presence of the indicator acid, bromophthalein magenta E, which competes for the base. Each acid is assumed to react with the base in conformance with the equation

$$\text{B (base)} + \text{A (acid)} \rightleftarrows \text{BA(salt)}.^{3} \qquad (1)$$

The equilibrium involving bromophthalein magenta E (yellow in benzene solution), diphenylguanidine (colorless), and the salt formed by their association (magenta) was previously studied [1 (a), (e)]. The data from this former study, together with absorbance data at 540 mμ obtained in the present study have been used to calculate the equilibrium constants K'' for the association of the various carboxylic acids with diphenylguanidine.

The acids studied included 31 acids having a single substituent atom or group in the *ortho*-, *meta*-, or *para*-position. In addition, 7 disubstituted benzoic acids and 3 trisubstituted acids were studied. Two of these acids—2,6-dihydroxy-4-methylbenzoic (*p*-orsellinic) and 2,4,6-trinitrobenzoic—combined so nearly completely with diphenylguanidine that their association constants could not be measured, and one of the acids (*o*-methoxybenzoic) was so unreactive that its K'' could be only approximately measured.

Benzoic acids have been investigated more extensively than any other group of acids with respect to their comparative strengths in aqueous and nonaqueous solvents (notably alcohols and dioxane-water mixtures). In the discussion to follow, the results of such previous studies are compared with the relative strengths in benzene found in this investigation.

2. Materials

2.1. Miscellaneous

The *benzene* used as solvent was of reagent grade, stated to meet ACS specifications. It was stored for at least a week over anhydrous calcium sulfate, then

[1] This research was supported in part by the United States Air Force, through the Air Force Office of Scientific Research of the Air Research and Development Command, under contract No. CSO-670-55-21.

[2] Figures in brackets indicate the literature references at the end of this paper.

[3] The salt BA is considered to consist of hydrogen-bonded ion-pairs. See [1(g)] and references cited therein.

distilled. A final boiling to remove moisture was performed shortly before use. *Bromophthalein magenta E* (*tetrabromophenolphthalein ethyl ester*) was a part of the product previously described [1 (a)]. A high grade *1,3-diphenyl-guanidine*, $C_6H_5NH{\cdot}C(=NH){\cdot}NHC_6H_5$, that had been crystallized from toluene was heated to about 67° in a vacuum oven to remove residual solvent. The melting point of the dried product was 149.4° to 149.9° C, and the purity as indicated by titrations in acetic acid and in aqueous ethanol was 99.8 percent.[4]

[4] Later experiments have shown that diphenylguanidine can be heated in an ordinary oven for as long as 24 hr at 80° C and for as long as 5 hr at 117° C without any noticeable effect on the melting point or the absorption spectrum in absolute ethanol.

2.2. Acids

Table 1 gives the list of acids used, with their melting points. The melting points agreed closely with accepted values in the literature.[5]

a. Acids of Commercial Origin

o-Acetoxybenzoic acid (*acetylsalicylic acid*, "*Aspirin*") in tablet form was recrystallized twice from benzene. Insoluble matter was removed in the first recrystallization. After a final washing with cyclohexane the crystals were heated to about 60° in a

[5] For example, see [2] and other references cited as sources of the pK values that are also listed in table 1. In regard to the measurements of the melting point, see footnote *b* of table 1. The log K''' values listed in table 1 are discussed in section 4.

TABLE 1. *List of aromatic carboxylic acids and pertinent physical constants*

Name of acid [a]	Melting point [b]	Purity [c]	Log K''' in benzene at 25° C [d]	pK in water at 25° C [e]
	°C	%		
Benzoic	121.8 to 122.5	100.0	5.26	4.20 [f]; 4.21 [g]
Monosubstituted benzoic acids				
o-Acetoxybenzoic (Acetylsalicylic, "Aspirin").	133.5 to 135		5.72	3.48 [h, i]
o-Aminobenzoic (Anthranilic).	146 to 147		4.94	4.95 [j]
m-Aminobenzoic	177 to 178		4.93	4.75 [j]
p-Aminobenzoic	186 to 186.5 d		4.45	4.89 [j]
**o*-Bromobenzoic	149 to 149.5		6.17	2.85 [f]
**m*-Bromobenzoic	154.5 to 155.5		6.06	3.81 [f, g]
**p*-Bromobenzoic	253.5 to 254.5		5.86	3.97 [f]; 4.00 [g]
**o*-Chlorobenzoic	141 to 142		6.08	2.94 [f]
**m*-Chlorobenzoic	155 to 156		6.06	3.83 [f, g]
**p*-Chlorobenzoic	239 to 240		5.82	3.98 [f]; 3.99 [g]
**m*-Cyanobenzoic	214.5 to 216		6.56	3.60 [g, k]
**p*-Cyanobenzoic	219.5 to 220		6.53	3.55 [g]; 3.54 [k]
m-Dimethylamino benzoic.	151 to 152		4.89	5.1 [l]
**o*-Fluorobenzoic	124 to 125		5.77	3.27 [f]
**m*-Fluorobenzoic	123 to 124		5.94	3.865 [f]
**p*-Fluorobenzoic	182 to 184 sb		5.61	4.14 [f]
o-Hydroxybenzoic (Salicylic).	158.5 to 159.5		7.45	3.00 [m]
m-Hydroxybenzoic	201.5 to 202.5		5.35	4.08 [g]
p-Hydroxybenzoic	214.5 to 215		4.94	4.58 [g]
**o*-Iodobenzoic	161 to 162.5		6.22	2.86 [f]; 2.84 [n]
**m*-Iodobenzoic	187 to 188		6.05	3.85 [f]; 3.86 [g]; 3.79 [n]
**p*-Iodobenzoic	270 to 271		5.85	3.98 [n]
o-Methoxybenzoic (*o*-Anisic).	101 to 102	100.0	3.7	4.09 [f]
m-Methoxybenzoic (*m*-Anisic).	105 to 106		5.38	4.09 [f]
p-Methoxybenzoic (*p*-Anisic).	183 to 184.5		4.92	4.47 [f]
Monosubstituted benzoic acids—Continued				
**o*-Methylbenzoic (*o*-Toluic).	104 to 104.5		4.94	3.91 [f]
**m*-Methylbenzoic (*m*-Toluic).	112 to 113		5.13	4.27 [f]; 4.24 [g]
**p*-Methylbenzoic (*p*-Toluic).	181 to 181.5		5.03	4.37 [f]; 4.34 [g]
**o*-Nitrobenzoic	147 to 148		7.44	2.17 [f]
**m*-Nitrobenzoic	141 to 142.5		6.82	3.49 [f]; 3.45 [g]
**p*-Nitrobenzoic	238 to 239		6.80	3.425 [f]; 3.44 [g]
Polysubstituted benzoic acids				
2,4-Dichlorobenzoic	163 to 164	99.9	6.55	[o] 2.76
*2,6-Dichlorobenzoic	143 to 144	99.9	7.34	[o] 1.82
3,4-Dichlorobenzoic	206 to 207	99.8	6.48	[o] 3.64
2,6-Dihydroxy-4-methylbenzoic (2,6-Dihydroxy-*p*-toluic, *p*-Orsellinic).	About 152.5 to 153.5 d.	99.9	Too great to measure	[b] 1.39; [p] 1.7
*2,6-Dimethoxybenzoic	187 to 188	99.1	4.92	[q] 3.44
*2,6-Dimethylbenzoic (2,6-Xylic).	114.5 to 115.5		5.24	[r] 3.25; [s] 3.23
3,5-Dimethylbenzoic (3,5-Xylic, Mesitylenic).	170 to 171		5.03	[r] 4.30; [b] 4.33
3,5-Dinitrobenzoic	204 to 205		8.23	[t] 2.82
*2,4,6-Trimethylbenzoic (*β*-Isodurylic, Mesitoic).	152.5 to 153.5		5.00	[r] 3.44; [b] 3.43
2,4,6-Trinitrobenzoic	216 to 223 d	99.3	Too great to measure	[t] 0.65

[a] Asterisks indicate the *meta-*, *para-*, *ortho-*, and *di-ortho*-substituted acids the log K''' and pK data for which were used in calculating the equations for the four lines shown in figures 1 and 2.

[b] Determined by the capillary-tube method, using an ASTM thermometer kept at 3-in. immersion. We are in agreement with a previous report (J. F. J. Dippy and R. H. Lewis, J. Chem. Soc. **1936**, 644) that slight softening a few degrees below the melting point seems to be a property of aromatic acids. In some cases partial sublimation was evident well below the melting point. A few cases in which sublimation (sb.) or decomposition (d.) seemed especially marked are noted in the table.

[c] The percent purity stated is based on potentiometric weight titrations. In other cases the purity probably ranged from 99.5 to 100.0 percent, but 100-percent purity was assumed in making computations.

[d] K''' is the equilibrium constant corresponding to the following equation: A (acid)+B (base)⇌S (salt), where A is the aromatic acid in question, B is 1,3-diphenylguanidine, and S is the salt formed by the addition of A to B. It is assumed that any other form of association (such as self-association of A or B) is negligible under the conditions of the experiments.

[e] When available, recent measurements giving "thermodynamic" pK values are cited.

[f] Measurements by Dippy and associates, cited by J. F. J. Dippy, Chem. Revs. **25**, 151 (1939); see Table I-(3)-(a), p. 206.

[g] G. Briegleb and A. Bieber, Z. Elektrochem. **55**, 250 (1951).

[h] Critical compilation of ionization constants by J. Kendall, Int. Crit. Tables VI, p. 259 f. (McGraw-Hill Book Co., New York, N. Y., 1929).

[i] At 17° the K-value 2.72×10^{-4} ($\diamond pK$ 3.565) was obtained by L. J. Edwards, Trans. Faraday Soc. **46**, 723 (1950).

[j] S. Kilpi and P. Harjanne, Suomen Kemistilehti [B] **21**, 14 (1948).

[k] S. Wideqvist, Arkiv Kemi **2**, 387 (1950).

[l] A. C. Cumming, Proc. Roy. Soc. (London), [A] **78**, 103 (1906).

[m] F. Bradley and W. C. M. Lewis, J. Phys. Chem. **29**, 782 (1925). See also S. Korman and V. K. LaMer, J. Am. Chem. Soc. **58**, 1396 (1936).

[n] J. M. Vandenbelt, C. Henrich, and S. G. VandenBerg, Anal. Chem. **25**, 726 (1954).

[o] M. M. Davis and H. B. Hetzer, J. Phys. Chem. **61**, 123 (1957).

[p] M. M. Davis and H. B. Hetzer, unpublished value, from potentiometric titrations.

[q] M. M. Davis and H. B. Hetzer, J. Phys. Chem. **61**, 125 (1957).

[r] J. F. J. Dippy, S. R. C. Hughes, and J. W. Laxton, J. Chem. Soc. **1954**, 1470.

[s] R. W. Hufferd and W. A. Noyes, J. Am. Chem. Soc. **43**, 925 (1921).

[t] J. F. J. Dippy, S. R. C. Hughes, and J. W. Laxton, J. Chem. Soc. **1951**, 2995. The value (2.38) for 2,4,6-trinitrobenzoic acid cited by G. F. Smith and D. H. Wilkins (Anal. Chim. Acta **8**, 209 (1953)) seems to have been derived by erroneous treatment of potentiometric titration data.

vacuum oven for several hours. *Benzoic acid* was NBS Standard Sample for calorimetry and acidimetry, and *p-methoxybenzoic* (*anisic*) *acid* was NBS Standard Sample for microanalytical determination of methoxyl. *2,4,6-Trinitrobenzoic acid* was used without treatment; the purity found by titration was 99.3 percent. All other acids of commercial origin were recrystallized at least once, using decolorizing carbon to remove any colored impurities. The solvents used for recrystallization were water, aqueous ethanol, benzene, cyclohexane, or benzene-cyclohexane. Samples were dried in a vacuum oven at temperatures high enough to ensure removal of solvent without incurring the danger of anhydride-formation or substantial loss of the acid through sublimation.

b. Other Acids

m-Cyanobenzoic acid. *m*-Aminobenzoic acid was converted to *m*-cyanobenzoic by the Sandmeyer reaction [3], following essentially the procedure of Valby and Lucas [4] for preparing *p*-cyanobenzoic acid. After three recrystallizations from water (using decolorizing carbon the first two times) and intermediate extractions with benzene (which removed a little brown, insoluble material), followed by heating in a vacuum oven to about 104° C, the product (needles) melted at 214.5° to 216° C. The final recrystallization did not alter the melting point. A trace of the related antidiazotate, which is formed as a byproduct in the Sandmeyer reaction, was probably present in the final product. Others, working with much larger amounts of material and after repeated recrystallizations, have obtained products with melting points ranging from 217° to about 221° [3,5,6].

p-Cyanobenzoic acid. The synthesis of *p*-cyanobenzoic acid closely paralleled that of the *m*-isomer. The crude product was recrystallized three times from water (using decolorizing carbon) and then from benzene. After washing with cyclohexane and air-drying, the product was heated to about 65° C in a vacuum oven. The melting point was 219.5° to 220° C. Others have reported the melting point as being 218.5° to 219.0° [4,6] or 219° [7]. Our product crystallized repeatedly in the form of needles, although previous workers who have mentioned the crystalline form referred to it as microscopic leaflets [7] or plates [4].

o-Fluorobenzoic acid and *m-fluorobenzoic acid* were prepared by oxidation of the corresponding fluorotoluenes, using the procedure and molecular proportions described for the preparation of *o*-chlorobenzoic acid [8]. *2,6-Dichlorobenzoic acid* and *2,6-dimethoxybenzoic acid* were prepared as previously described [9, 10].

2,6-Dihydroxy-4-methylbenzoic (*p-orsellinic*) *acid.* The carboxyl group was introduced into orcinol (1,3-dihydroxy-4-methylbenzene) by heating it with aqueous potassium bicarbonate [11]. The product crystallized in needles from benzene; titration gave a purity of 93.1 percent, indicating that about 71 percent was present as the monohydrate. The material was then heated to about 100° C in a vacuum oven, after which its purity by titration was 99.9 percent when the sample was dissolved at room temperature on the day of the titration.[6]

3,5-Dimethylbenzoic acid was a byproduct from the preparation of nitromesitylene. It was purified by recrystallizations from aqueous ethanol, using decolorizing carbon. To prepare *2,6-dimethylbenzoic acid*, 2,6-dimethylaniline was converted to the corresponding iodoxylene by the Sandmeyer reaction. The Grignard reagent was then prepared, and carbonation was effected with "dry ice", using conventional procedures. The product was recrystallized from water. *2,4,6-Trimethylbenzoic acid* was prepared in an analogous way, starting with bromomesitylene.

3. Experimental Procedures and Results

3.1. Procedure and Apparatus

In most experiments $5\times10^{-4}-M$ stock solutions of bromophthalein magenta E (A') and of diphenylguanidine (B) were prepared, and portions were transferred to 50-ml volumetric flasks in such quantities that upon dilution to the mark the stoichiometric concentration $C_{a'}$ of bromophthalein magenta was exactly 5×10^{-5} M and the stoichiometric concentration C_b of diphenylguanidine was nC', n being 0.5 or a whole number ranging from 1 to 4. Stock solutions of the carboxylic acid (A'') were *approximately* 5×10^{-4} M, and in the final mixtures the stoichiometric concentration $C_{a''}$ was $n''C_{a'}$, with n'' usually ranging from about 0.5 to about 6.[7] The K'' values reported were usually based on the results for ten different mixtures.

It seems very unlikely that for the solutions under study the presence of traces of moisture would noticeably affect the results, but all practicable measures were taken to minimize the moisture content. (1) The glassware used was thoroughly dried and thereafter stored in a desiccator or in a "dry box" maintained at about 10 to 30 percent relative humidity. (2) The benzene used for diluting solutions was boiled shortly before use and protected against moisture while cooling to room temperature. (3) Flasks containing the desired amounts of diphenylguanidine and bromophthalein magenta diluted to about one-half the final volume with benzene were heated until about 10 percent of the benzene had boiled off, and the contents were

---

[6] The sample could not be brought to constant weight by repeated heatings in the vacuum oven, probably because of slight decarboxylation and sublimation during heating. A lower titer was obtained when the solution had stood overnight or had been heated to hasten dissolving of the sample. The melting point cannot be used as a criterion of purity, because softening and evolution of gas (doubtless carbon dioxide) occurs gradually. The more gradual the heating, the lower the temperature at which pronounced evolution of gas begins and the more extended the temperature range over which decomposition occurs. The melting behavior before and after oven-drying appeared to be about the same. In one experiment, a specimen of the oven-dried product showed slight shrinking from about 149°, incipient liquefaction and bubble-formation at about 152.5°, and marked liquefaction and evolution of gas at 154° to 155° C. Compare [11].

[7] Solid samples were weighed on a high-precision assay-type balance when the amount taken was less than 0.1 g.

protected from moisture while cooling.[8] (4) The stock solutions of carboxylic acids were freshly prepared each day, using vacuum-dried samples and minimizing their exposure to moist air. Solution of the samples and subsequent operations of transfer, dilution to the mark, and filling of optical absorption cells were performed in the dry box. (5) In some cases desiccant was present in the cell box during absorbance measurements.

The changes in absorbance that accompany the conversion of bromophthalein magenta E to its diphenylguanidine salt have been described previously [1 (a), (e)]. The salt has an absorption band with a maximum near 540 mμ, and none of the other reacting species dealt with in these studies shows measurable absorption at this wavelength. The absorbance at 540 mμ decreases upon the addition of a carboxylic acid, owing to the competing tendency of this acid to combine with diphenylguanidine. Measurements at 540 mμ only were used in the investigations under discussion.[9] A Beckman Model DU quartz spectrophotometer was used for transmittance measurements, the temperature being maintained at 25.0°±0.1° in most of the experiments by the use of a thermostated air bath [1(f)]. The glass-stoppered absorption cells had quartz windows and were of four lengths (2.5 mm, 5.0 mm, 10 mm, and 20 mm) [1 (a)], the cell length being so selected that usually the transmittance values were within the range 20 to 70 percent. For calculations of K'' the transmittance values were converted in the usual way to absorbance (the negative logarithm of the transmittance) values.

3.2. Experimental Data and Calculation of Association Constants

The equilibrium constants K' and K'' corresponding to eq (1) are:

$$K' = \frac{[S']}{[A'][B]}, \tag{2}$$

$$K'' = \frac{[S'']}{[A''][B]}, \tag{3}$$

where the quantities in brackets signify molar concentrations of the different species in the equilibrium mixtures. B, A', and A'' were defined in section 3.1 S' and S'' refer to the diphenylguanidine salts of bromophthalein magenta E and the carboxylic acid respectively. Of necessity the activity coefficient are all assumed to be 1, but in such dilute solution this is a very reasonable assumption.

Applying these two equations the following expression was derived algebraically and used in calculating the K'' values:

$$K'' = \frac{x-y}{y[C_a'' - (x-y)]} \tag{4}$$

where $x = (C_a'/L)(nL-Z)$ and $y = (1/K')[Z/(L-Z)]$ Z is the absorbance of a given solution at 540 mμ per unit optical absorption cell length (here taken as 5 mm);[10] L (here taken as 1.017) is the limiting absorbance for the reaction of A' with B when C_a' is 5×10^{-5} M and the cell length is 5 mm; K' at 25° C is taken as $2.5_5\times10^5$;[11] and the remaining symbols are as already defined in this paper.

Experimental data and the calculated K'' values for 40 acids whose association with diphenylguanidine under the stated conditions was measurable are presented in table 2.[12] The values of K'' must be regarded as provisional until factors that may affect their accuracy have been more thoroughly studied. These factors include competitive associations,[13] traces of impurities, partial adsorption of reactants on the surface of vessels,[14] and the marked sensitivity of the equilibria to minute changes in the temperature.[15] In most experiments no values were excluded in computing the average K'', but in a few cases (indicated in table 2) widely divergent values were arbitrarily excluded. Obviously, some proportions of reactants are more favorable than others for obtaining accurate results, and the best results should be obtainable with acids that nearly match bromophthalein magenta E in strength.

It is worth noting that for most of the acids the log K'' value obtained upon measuring the mixture containing each of the three components (B, A', and A'') at the stoichiometric concentration 5×10^{-5} differed by no more than 0.02 unit from the logarithm of the *average* value of K''. This suggests a quick method for obtaining a good approximation of the association constant K''.

---

[8] It has been found that the absorbance measurements made after dilution to volume are unaffected by such heating, and that mixtures of these two compounds can be preserved for a long time without alteration if not too concentrated. (Crystallization of the salt occurs on standing if its concentration is as great as 5×10^{-4} M.) In later parts of the work the practice was adopted of preparing enough of these two stock solutions for several series of measurements and transferring samples to other flasks without delay (that is, before the concentrations of the stock solutions could be significantly increased by evaporation of the solvent), diluting the mixtures to about one-half of the final volume, and completing the experiments at convenience.

[9] This statement needs slight qualification. Each freshly prepared stock solution of bromophthalein magenta E was checked by dilution of a sample to 5×10^{-5} M and measurement of the transmittance at 405 mμ; for a 2.5-mm light path this was found to be 47.1 to 47.2 percent. An additional check was made at 540 mμ on a second solution in which C_a' and C_b were both 5×10^{-5} M; with this solution in a 2.5-mm optical absorption cell a transmittance reading of 41.3 or 41.4 percent was considered acceptable.

[10] In this paper the usual symbol (A) for absorbance is replaced by the symbol Z in order to avoid confusion with the use of A in referring to acids.

[11] For this work the measurement of K' (see [1 (a) (e)]) was repeated. In doing so an attempt was made to define the L-value (formerly taken as 1.02) more precisely as well as to introduce further improvements in technique. The value of K' is very sensitive to the temperature.

[12] An example of the method of calculating (as well as of correcting) K'' is given in section 4.1, table 4.

[13] See section 4.1.

[14] For examples of such adsorption see [1(a)], p. 243 and 246, and [1(e)], p. 49

[15] The temperature effect is being studied. The enthalpy change accompanying the reaction of bromophthalein magenta E with seven of the aromatic carboxylic acids appears to range from about 14 to about 19 kcal.

TABLE 2. *Experimental data and association constants for the reaction of aromatic carboxylic acids with 1,3-diphenylguanidine in benzene at 25° C*

C_a[a]	n[b]	Z[c]	K''[d]
Benzoic acid			
2.543×10^{-3}	0.5	0.3388	1.71×10^{5}
2.543	1.0	.6232	1.73
5.246	1.0	.4921	1.98
10.493	1.0	.3605	1.87
5.041	2.0	.8474	1.69
10.083	2.0	.6726	1.86
15.259	2.0	.5432	1.83
10.083	3.0	.8754	1.88
15.124	3.0	.7494	1.90
20.165	3.0	.6448	1.82
Average	---	---	1.83×10^{5}
***o*-Acetoxybenzoic acid**			
2.519×10^{-3}	0.5	0.2612	5.54×10^{5}
2.575	1.0	.5548	4.95
5.038	1.0	.3830	5.63
10.075	1.0	.2218	5.54
10.299	2.0	.5162	5.39
15.440	2.0	.3492	5.35
20.151	2.0	.2612	5.47
10.293	3.0	.8336	4.36
15.448	3.0	.5986	5.18
20.597	3.0	.4422	5.14
Average	---	---	5.26×10^{5}
***o*-Aminobenzoic acid**			
2.519×10^{-3}	0.5	0.3796	8.09×10^{4}
2.582	.5	.3782	8.09
5.039	.5	.3206	9.58
2.519	1.0	.6632	9.02
2.582	1.0	.6688	7.84
5.163	1.0	.5798	8.87
10.077	1.0	.4724	8.88
5.163	2.0	.8684	8.70
10.187	2.0	.7514	9.39
15.280	2.0	.6632	8.81
10.187	3.0	.8996	9.64
15.280	3.0	.8314	8.51
Average	---	---	8.78×10^{4}
***m*-Aminobenzoic acid**			
2.612×10^{-3}	0.5	0.3728	8.93×10^{4}
5.035	.5	.3206	9.59
2.612	1.0	.6596	9.04
5.224	1.0	.5832	8.41
10.070	1.0	.4672	9.24
5.224	2.0	.8730	7.40
10.187	2.0	.7620	8.49
15.280	2.0	.6737	8.21
20.140	2.0	.6055	8.16
15.674	3.0	.8314	8.00
20.374	3.0	.7773	7.44
Average	---	---	8.45×10^{4}
***p*-Aminobenzoic acid**			
2.589×10^{-3}	0.5	0.4222	2.15×10^{4}
5.090	.5	.3772	3.83
2.528	1.0	.7130	3.20
5.057	1.0	.6708	3.01
10.179	1.0	.6178	2.53
5.057	2.0	.9070	2.59
10.356	2.0	.8566	2.65
15.269	2.0	.8134	2.61
5.178	3.0	.9578	5.05[e]
10.114	3.0	.9344	3.05
15.269	3.0	.9144	2.43
Average	---	---	2.80×10^{4}

C_a[a]	n[b]	Z[c]	K''[d]
***o*-Bromobenzoic acid**			
2.528×10^{-3}	0.5	0.1910	1.53×10^{5}
5.056	.5	.0972	1.55
2.506	1.0	.5068	1.40
5.022	1.0	.2782	1.54
10.112	1.0	.1138	1.55
5.012	2.0	.7905	1.30
10.044	2.0	.3862	1.50
15.065	2.0	.2000	1.51
20.224	2.0	.1294	1.49
30.130	4.0	.2314	1.43
Average	---	---	1.48×10^{5}
***m*-Bromobenzoic acid**			
1.250×10^{-3}	1.0	0.6502	1.12×10^{5}
2.500	1.0	.5241	0.97
2.500	1.0	.5200	1.06
2.500	1.0	.5147	1.19
3.750	1.0	.3979	1.16
5.000	1.0	.3002	1.25
6.250	1.0	.2396	1.20
7.500	1.0	.1945	1.20
10.000	1.0	.1358	1.23
12.500	1.0	.1056	1.21
15.000	1.0	.0876	1.17
20.000	1.0	.0634	1.17
5.000	2.0	.7958	1.03
10.000	2.0	.4179	1.20
12.500	2.0	.3063	1.18
Average	---	---	1.16×10^{5}
***p*-Bromobenzoic acid**			
1.500×10^{-3}	0.5	0.3054	7.36×10^{5}
2.490	.5	.2381	7.88
5.042	.5	.1492	7.56
2.490	1.0	.5406	7.20
4.978	1.0	.3605	7.11
9.957	1.0	.1911	7.31
5.002	2.0	.7959	10.1[e]
10.004	2.0	.4908	7.09
15.126	2.0	.3072	7.20
20.008	4.0	.6289	6.85
Average	---	---	7.28×10^{5}
***o*-Chlorobenzoic acid**			
2.506×10^{-3}	0.5	0.2034	1.30×10^{5}
5.048	.5	.1102	1.28
2.506	1.0	.5143	1.18
5.078	1.0	.3002	1.19
10.097	1.0	.1334	1.25
5.078	2.0	.7905	1.04
10.023	2.0	.4214	1.16
15.034	2.0	.2299	1.22
20.194	2.0	.1505	1.23
30.046	3.0	.3080	1.16
Average	---	---	1.20×10^{5}
***m*-Chlorobenzoic acid**			
2.505×10^{-3}	0.5	0.2028	1.31×10^{5}
5.011	.5	.1157	1.19
2.505	1.0	.5186	1.08
5.011	1.0	.3063	1.17
10.022	1.0	.1428	1.14
10.168	2.0	.4134	1.16
15.253	2.0	.2343	1.14
20.043	2.0	.1626	1.12
15.253	3.0	.4895	1.11
20.337	3.0	.3054	1.13
Average	---	---	1.16×10^{5}

C_a[a]	n[b]	Z[c]	K''[d]
***p*-Chlorobenzoic acid**			
2.542×10^{-3}	0.5	0.2441	6.95×10^{5}
5.088	.5	.1562	6.81
2.542	1.0	.5421	6.43
5.021	1.0	.3635	6.78
10.176	1.0	.1984	6.62
5.088	2.0	.7905	10.1[e]
10.170	2.0	.4949	6.51
15.063	2.0	.3279	6.40
20.352	2.0	.2362	6.32
20.084	3.0	.4191	6.21
Average	---	---	6.56×10^{5}
***m*-Cyanobenzoic acid**			
2.527×10^{-3}	0.5	0.1367	3.82×10^{5}
5.014	.5	.0490	4.06
2.527	1.0	.4789	2.85
5.085	1.0	.1958	3.70
10.170	1.0	.0534	3.98
10.109	2.0	.2815	3.43
15.255	2.0	.0997	3.84
20.057	2.0	.0593	3.84
15.163	3.0	.3401	3.28
20.340	3.0	.1416	3.68
Average	---	---	3.65×10^{5}
***p*-Cyanobenzoic acid**			
5.031×10^{-3}	0.5	0.0498	3.96×10^{5}
2.537	1.0	.4789	2.74
5.044	1.0	.2078	3.30
5.048	1.0	.2062	3.36
10.061	1.0	.0556	3.87
15.179	1.0	.0305	3.86
20.239	1.0	.0214	3.77
5.075	2.0	.7747	2.86
10.088	2.0	.2934	3.13
10.095	2.0	.2916	3.16
15.092	2.0	.1059	3.66
20.122	2.0	.0604	3.74
25.299	2.0	.0420	3.73
15.133	3.0	.3538	3.00
15.224	3.0	.3507	2.94
25.299	3.0	.0872	3.67
20.299	4.0	.4012	2.75
Average	---	---	3.38×10^{5}
***m*-Dimethylaminobenzoic acid**			
2.509×10^{-3}	0.5	0.3836	7.43×10^{4}
2.509	1.0	.6688	8.21
5.139	1.0	.5916	7.89
10.270	1.0	.4882	7.70
5.135	2.0	.8706	8.31
10.277	2.0	.7680	7.88
15.405	2.0	.6820	7.67
10.277	3.0	.9070	7.61
15.405	3.0	.8404	7.53
20.073	3.0	.7766	7.71
Average	---	---	7.79×10^{4}
***o*-Fluorobenzoic acid**			
2.569×10^{-3}	0.5	0.2541	5.92×10^{5}
5.035	.5	.1603	6.57
5.211	.5	.1637	6.00
2.569	1.0	.5467	5.72
5.211	1.0	.3686	5.92
5.232	1.0	.3625	6.19
10.422	1.0	.2069	5.93
10.466	1.0	.2062	5.92
5.232	2.0	.7905	7.11[e]
10.422	2.0	.4989	5.84
10.466	2.0	.4976	5.81
15.105	2.0	.3410	5.90
15.634	2.0	.3298	5.85
15.413	3.0	.5850	5.71
20.551	3.0	.4248	5.67
30.826	3.0	.2636	5.73
Average	---	---	5.91×10^{5}

TABLE 2. *Experimental data and association constants for the reaction of aromatic carboxylic acids with 1,3-diphenylguanidin in benzene at 25° C*—Continued

C_a[a]	n[b]	Z[c]	K''[d]
m-Fluorobenzoic acid			
1.250×10^{-5}	1.0	0.6632	$5.56^{e}\times10^{5}$
1.250	1.0	.6517	10.2^{e}
2.500	1.0	.5352	7.83
2.500	1.0	.5302	8.02
3.750	1.0	.4236	8.47
5.000	1.0	.3372	8.74
5.000	1.0	.3335	9.04
6.250	1.0	.2708	9.10
7.500	1.0	.2269	8.98
10.000	1.0	.1688	8.88
10.000	1.0	.1658	9.13
12.500	1.0	.1337	8.78
15.000	1.0	.1062	9.17
20.000	1.0	.0815	8.66
10.000	2.0	.4572	9.04
25.000	5.0	.6326	8.76
50.000	10.0	.7570	8.13
Average	---	-------	8.76×10^{5}
p-Fluorobenzoic acid			
1.276×10^{-5}	0.5	0.3478	4.17×10^{5}
2.552	.5	.2827	3.99
5.104	.5	.1979	4.12
1.281	1.0	.6696	3.83
2.562	1.0	.5654	4.23
5.125	1.0	.4078	4.35
10.250	1.0	.2620	3.94
5.104	2.0	.8090	4.86
10.250	2.0	.5702	3.76
15.310	2.0	.4105	3.83
Average	---	-------	4.11×10^{5}
o-Hydroxybenzoic acid			
2.535×10^{-5}	0.5	0.0553	2.97×10^{7}
5.028	.5	.0086	2.86
5.046	1.0	.0793	2.94
10.056	1.0	.0088	2.83
10.093	2.0	.1095	2.93
15.085	2.0	.0171	2.85
20.113	2.0	.0090	2.78
15.139	3.0	.1391	2.59
20.185	3.0	.0253	2.79
Average	---	-------	2.84×10^{7}
m-Hydroxybenzoic acid			
2.504×10^{-5}	0.5	0.3224	2.27×10^{5}
5.072	.5	.2503	2.27
2.504	1.0	.6126	2.12
5.007	1.0	.4855	2.29
10.058	1.0	.3478	2.17
5.072	2.0	.8358	2.28
10.058	2.0	.6517	2.20
15.217	2.0	.5143	2.16
10.145	3.0	.8636	2.42
15.087	3.0	.7305	2.23
Average	---	-------	2.24×10^{5}
p-Hydroxybenzoic acid			
2.541×10^{-5}	0.5	0.3876	$6.68^{e}\times10^{6}$
2.035	1.0	.6840	8.58
2.551	1.0	.6614	9.11
5.087	1.0	.5882	8.30
5.103	1.0	.5814	8.87
7.122	1.0	.5400	8.20
7.652	1.0	.5320	7.97
5.103	2.0	.8660	9.65
7.652	2.0	.8134	8.80
10.203	2.0	.7598	8.65
15.308	2.0	.6726	8.25
5.103	3.0	.9526	13.3^{e}
12.753	3.0	.8636	9.20
17.789	3.0	.7916	8.77
Average	---	-------	8.70×10^{6}
o-Iodobenzoic acid			
2.520×10^{-5}	0.5	0.1853	1.69×10^{6}
5.144	.5	.0889	1.73
2.520	1.0	.4989	1.64
5.168	1.0	.2636	1.62
15.431	1.0	.0628	1.68
10.336	2.0	.3585	1.63
15.122	2.0	.1858	1.68
20.574	2.0	.1164	1.65
15.504	3.0	.4248	1.56
20.163	3.0	.2518	1.62
Average	---	-------	1.65×10^{6}
m-Iodobenzoic acid			
2.514×10^{-5}	0.5	0.2101	1.16×10^{6}
5.021	.5	.1160	1.18
5.031	1.0	.3063	1.15
10.042	1.0	.1428	1.14
15.086	1.0	.0909	1.11
10.061	2.0	.4260	1.11
15.086	2.0	.2388	1.13
20.084	2.0	.1640	1.10
15.092	3.0	.5045	1.06
20.123	3.0	.3170	1.09
Average	---	-------	1.12×10^{6}
p-Iodobenzoic acid			
2.512×10^{-5}	0.5	0.2411	7.42×10^{6}
5.044	.5	.1518	7.29
2.512	1.0	.5432	6.61
5.044	1.0	.3546	7.27
10.063	1.0	.1915	7.15
10.087	2.0	.4841	7.22
15.131	2.0	.3116	7.00
20.126	2.0	.2261	6.90
15.075	3.0	.5690	7.02
20.126	3.0	.3993	6.87
Average	---	-------	7.08×10^{6}
o-Methoxybenzoic acid			
2.514×10^{-5}	0.5	0.4316	$12.7^{e}\times10^{3}$
5.027	.5	.4285	7.67
10.054	.5	.4224	5.24
15.082	.5	.4076	6.00
5.022	1.0	.7352	7.60
10.044	1.0	.7212	5.46
15.067	1.0	.7122	4.39
2.508	1.5	.8972	2.20
5.016	1.5	.8850	4.40
7.524	1.5	.8826	3.28
10.032	1.5	.8754	3.44
5.006	2.0	.9320	6.69
10.012	2.0	.9268	4.08
15.018	2.0	.9194	3.65
15.022	3.0	.9656	3.23
20.030	4.0	.9790	3.37
25.037	5.0	.9842	4.29
30.044	6.0	.9870	5.30
Average	---	-------	4.72×10^{3}
m-Methoxybenzoic acid			
2.516×10^{-5}	1.0	0.6091	2.21×10^{5}
5.016	1.0	.4802	2.39
5.088	1.0	.4732	2.48
7.525	1.0	.3958	2.38
10.033	1.0	.3372	2.35
10.033	2.0	.6383	2.45
10.020	3.0	.8730	2.07
[e] 1.018	1.0	.0714	3.55^{e}
[f] 2.544	1.0	.2165	2.81
[g] 10.176	1.0	.9024	2.34
Average	---	-------	2.39×10^{5}
p-Methoxybenzoic acid			
1.276×10^{-5}	0.5	0.4034	9.87×10^{4}
2.552	.5	.3726	9.22
2.520	1.0	.6632	9.01
5.040	1.0	.5934	7.96
10.126	1.0	.4868	7.92
20.252	1.0	.3830	7.00
5.040	2.0	.8684	9.37
10.081	2.0	.7744	7.68
15.122	2.0	.6898	7.49
10.074	3.0	.9070	8.17
15.110	3.0	.8428	7.68
Average	---	-------	8.31×10^{4}
o-Methylbenzoic acid			
2.546×10^{-5}	0.5	0.3747	8.86×10^{4}
2.513	1.0	.6615	9.33
5.026	1.0	.5884	8.43
10.052	1.0	.4789	8.48
5.088	2.0	.8706	8.54
10.254	2.0	.7576	8.74
15.273	2.0	.6655	8.68
10.182	3.0	.9044	8.46
15.273	3.0	.8314	8.52
20.508	3.0	.7618	8.26
Average	---	-------	8.63×10^{4}
m-Methylbenzoic acid			
2.503×10^{-5}	0.5	0.3570	1.27×10^{5}
2.500	1.0	.6402	1.36
5.000	1.0	.5421	1.35
10.000	1.0	.4191	1.32
5.045	2.0	.8542	1.40
10.090	2.0	.7092	1.39
15.015	2.0	.5986	1.36
10.090	3.0	.8898	1.30
15.135	3.0	.7894	1.33
20.181	3.0	.6956	1.31
Average	---	-------	1.34×10^{5}
p-Methylbenzoic acid			
2.526×10^{-5}	0.5	0.3702	0.98×10^{5}
2.500	1.0	.6576	1.01
5.000	1.0	.5670	1.06
10.000	1.0	.4486	1.07
5.053	2.0	.8612	1.14
10.106	2.0	.7372	1.09
15.159	2.0	.6376	1.05
10.106	3.0	.8972	1.06
15.159	3.0	.8112	1.08
20.212	3.0	.7310	1.06
Average	---	-------	1.06×10^{5}
o-Nitrobenzoic acid			
2.544×10^{-5}	0.5	0.0550	2.92×10^{7}
5.011	.5	.0084	2.96
2.533	1.0	.4597	0.64^{e}
2.522	1.0	.4559	0.94^{e}
5.089	1.0	.0784	2.76
10.022	1.0	.0089	2.82
10.177	2.0	.1088	2.64
15.266	2.0	.0174	2.71
20.043	2.0	.0093	2.72
15.197	3.0	.1379	2.47
20.172	3.0	.0268	2.63
Average	---	-------	2.74×10^{7}

TABLE 2. *Experimental data and association constants for the reaction of aromatic carboxylic acids with 1,3-diphenylguanidine in benzene at 25° C*—Continued

C_a[a]	n[b]	Z[c]	K''[d]
m-Nitrobenzoic acid			
1.250×10^{-5}	0.25	0.0698	8.14×10^{6}
1.250	.5	.2468	10.4[e]
2.501	.5	.1095	6.90
1.251	1.0	.6345	8.88[e]
2.503	1.0	.4647	6.16
3.754	1.0	.2933	6.03
5.015	1.0	.1558	6.88
5.015	1.0	.1581	6.65
7.522	1.0	.0613	6.52
10.030	1.0	.0356	6.49
5.024	2.0	.7724	6.75
10.140	2.0	.2124	6.64
15.210	2.0	.0660	6.38
15.080	3.0	.2718	6.06
20.107	3.0	.0962	6.29
20.047	4.0	.3072	6.25
25.058	4.0	.1232	6.26
[f] 2.507	1.0	.0725	7.43
[g] 10.108	1.0	.3239	6.32
Average			6.60×10^{6}
p-Nitrobenzoic acid			
2.560×10^{-5}	0.25	0.0295	6.36×10^{6}
2.559	.5	.1084	6.42
5.121	.5	.0332	6.28
2.559	1.0	.4535	7.45[e]
5.118	1.0	.1527	6.43
10.242	1.0	.0358	6.19
10.237	2.0	.2107	6.29
15.353	2.0	.0666	6.14
15.356	3.0	.2522	6.11
Average			6.28×10^{6}
2,4-Dichlorobenzoic acid			
2.507×10^{-5}	0.5	0.1404	3.66×10^{6}
4.975	.5	.0531	3.72
5.009	1.0	.2028	3.62
9.950	1.0	.0601	3.60
15.041	1.0	.0332	3.56
10.018	2.0	.2827	3.59
12.534	2.0	.1616	3.62
14.925	2.0	.1091	3.63
20.036	2.0	.0639	3.54
19.900	3.0	.1580	3.41
25.045	3.0	.0939	3.45
Average			3.58×10^{6}
2,6-Dichlorobenzoic acid			
2.593×10^{-5}	0.5	0.0596	2.18×10^{7}
5.186	.5	.0099	2.32
2.593	1.0	.4397	1.59[e]
5.016	1.0	.0952	2.12
7.779	1.0	.0190	2.27
10.031	2.0	.1310	2.19
15.047	2.0	.0224	2.17
20.743	2.0	.0102	2.31
15.047	3.0	.1668	1.94
20.063	3.0	.0340	2.08
Average			2.18×10^{7}
3,4-Dichlorobenzoic acid			
2.513×10^{-5}	0.5	0.1479	3.17×10^{6}
5.025	.5	.0602	3.11
5.025	1.0	.2159	3.04
10.151	1.0	.0662	3.09
12.674	1.0	.0506	2.90
12.674	2.0	.1792	2.96
15.226	2.0	.1213	3.00
20.302	2.0	.0738	2.93
20.278	3.0	.1700	2.89
25.126	3.0	.1095	2.84
Average			2.99×10^{6}
2,6-Dimethoxybenzoic acid			
2.546×10^{-5}	0.5	0.3836	7.31×10^{6}
2.546	1.0	.6688	8.02
5.093	1.0	.5814	8.90
10.010	1.0	.4822	8.32
5.093	2.0	.8684	9.07
10.185	2.0	.7640	8.34
15.015	2.0	.6764	8.30
10.010	3.0	.9070	8.36
15.015	3.0	.8336	8.68
20.020	3.0	.7680	8.28
Average			8.36×10^{6}
2,6-Dimethylbenzoic acid			
2.509×10^{-5}	0.5	0.3316	1.96×10^{6}
2.509	1.0	.6214	1.83
5.049	1.0	.5130	1.75
10.037	1.0	.3696	1.87
5.049	2.0	.8474	1.68
10.097	2.0	.6802	1.75
15.056	2.0	.5530	1.77
20.075	2.0	.4584	1.82
10.097	3.0	.8850	1.47
15.146	3.0	.7660	1.64
Average			1.75×10^{6}
3,5-Dimethylbenzoic acid			
2.527×10^{-5}	0.5	0.3688	1.01×10^{6}
2.527	1.0	.6502	1.12
5.069	1.0	.5664	1.04
7.582	1.0	.4960	1.09
5.055	2.0	.8590	1.21
10.137	2.0	.7350	1.10
15.206	2.0	.6394	1.03
20.115	2.0	.5714	0.99
15.164	3.0	.8134	1.05
20.115	3.0	.7392	1.01
Average			1.06×10^{6}
3,5-Dinitrobenzoic acid			
2.594×10^{-5}	0.5	0.0188	1.67×10^{8}
5.189	1.0	.0236	1.67
6.347	1.0	.0054	1.71
7.507	1.0	.0028	1.86
7.616	2.0	.4414	0.29[e]
10.377	2.0	.0288	1.66
15.013	2.0	.0030	1.72
15.566	3.0	.0318	1.60
17.771	3.0	.0084	1.64
22.520	3.0	.0031	1.67
Average			1.69×10^{8}
2,4,6-Trimethylbenzoic acid			
2.528×10^{-5}	0.5	0.3688	1.01×10^{6}
2.528	1.0	.6632	0.90
5.060	1.0	.5664	1.05
10.113	1.0	.4524	1.02
5.060	2.0	.8612	1.14
10.119	2.0	.7474	0.99
15.170	2.0	.6412	1.03
10.113	3.0	.9044	0.87
15.179	3.0	.8134	1.05
20.239	3.0	.7372	1.01
Average			1.01×10^{6}

[a] Stoichiometric concentration of the aromatic carboxylic acid. All concentrations are expressed in moles per liter of solution.

[b] C_b (stoichiometric concentration of diphenylguanidine) $= n.C^{o\prime}$ (where $C^{o\prime}$ is the stoichiometric concentration of bromophthalein magenta E). $C^{o\prime}$ is $5\times10^{-5}M$ in all experiments except where otherwise indicated.

[c] Z (absorbance) $=-\log T$ (transmittance). In this paper the usual symbol (A) for absorbance is replaced by the symbol Z to avoid confusion with the use of A in referring to acids. The values given for Z are for the wavelength 540 mμ, per 5-mm cell length. Four decimal places were retained to avoid computational errors.

[d] K'' is the equilibrium constant for the reaction: B (diphenylguanidine)$+A''$ (aromatic carboxylic acid)$\rightleftarrows S''$ (diphenylguanidinium salt of the aromatic carboxylic acid) in benzene at 25° C. See section 3.2 for the mathematical expression used and the assumptions made in computing K''. Values marked with an asterisk were omitted in averaging. Note that the values of K'' given in this column were computed on the assumption that the aromatic carboxylic acid (A'') was entirely in the monomeric form. See section 4.1 for discussion and for "corrected" K'' values for some of the acids.

[e] $C^{o\prime}=10^{-3}\ M$.

[f] $C^{o\prime}=2.5\times10^{-3}\ M$.

[g] $C^{o\prime}=10^{-4}\ M$.

4. Discussion of Results

4.1. General Discussion of the Method

It is readily apparent that the relative strengths of different acids in a solvent as inert as benzene cannot be measured without the addition of a *reference base*. The choice of diphenylguanidine as the reference base was made after tests of numerous basic indicator dyes (in the form of the free base) showed that none possessed adequate solubility, stability, and reactivity.[16] In using diphenylguanidine, an indicator *acid* must be present. The acid selected was bromophthalein magenta E (tetrabromophenolphthalein ethyl ester), whose association in benzene solution with diphenylguanidine and with di-*o*-tolylguanidine has been studied in detail in this laboratory [1(a)(e), (f)]. The feasibility of assessing at least semiquantitatively the relative strengths of a large variety of organic acids in benzene, including acids as weak as acetic and benzoic acids, by measuring the ab-

[16] To be suitable for our purposes the base had to be fairly strong. This meant that it had to be sought among the strongest aliphatic amines or among the available guanidines, amidines, or their vinylogs. The indicator bases tested included members of the azo, azine, oxazine, and thiazine families of dyes, as well as anhydro-bases of the triphenylmethane group. A large proportion of the dyes were found to be too easily affected by light or too susceptible to attack by atmospheric moisture, oxygen, or acidic vapors. Others were of adequate stability, but reacted measurably only with acids of pK about 3 or less, and even in such cases a very large excess of the acid was usually required.

sorbance of very dilute solutions containing bromophthalein magenta E, the organic acid in question, and either diphenyl- or ditolylguanidine, all present at approximately the same stoichiometric concentration, was shown in exploratory studies made about twelve years ago.[17] Diphenylguanidine was selected in preference to di-*o*-tolylguanidine chiefly because its reactivity as a base in benzene (which is less than that of di-*o*-tolylguanidine [1 (a), (e), (f)]) was thought to be more suitable for the experiments contemplated.

The scheme adopted for this investigation has the disadvantage that any errors in the two constants L and K' (see section 3.2) will be reflected in the values obtained for K'', and still further study may result in slight modifications of these two values. However, this would cause little difference in the relative orders of strength.

The possibility of competitive associations must be kept in mind in planning and interpreting studies of acid-base equilibria in benzene as a solvent. Cryoscopic measurements have provided evidence that the base diphenylguanidine is intermolecularly associated to some extent, by hydrogen bonding, when dissolved in naphthalene [12] or benzene [13], but at room temperature and the low concentrations used in this work any error from this source may be presumed to be negligible. Intermolecular association of bromophthalein magenta E has not been observed, and is not to be expected [1 (a), p. 232].

On the other hand, the tendency for the molecules of carboxylic acids to associate in pairs, whether in the gaseous, liquid, or solid states or dissolved in a solvent like benzene, is a well-known manifestation of hydrogen bonding. At very high concentrations, still larger aggregates of molecules may exist. In dilute solutions, however, as shown by experimental studies (mostly of benzene solutions) reported within the last 15 years,[18] there appears to be an equilibrium between double and single molecules.

Information on the dimer $\rightleftarrows$ monomer equilibrium of benzoic acid and its derivatives is still very fragmentary, as is evident from an inspection of table 3. This table is a compilation of the available equilibrium constants K_{21} (corresponding to the equation $A_2 \rightleftarrows 2A$), converted where necessary to the same units of concentration (moles per liter) as those used in the work presented in this paper. Additional K_{21} values for 5.5°, 25°, and 30° C were computed in cases where K_{21} data for several temperatures were available, and are included in table 3. At 25° C most of the K_{21} values are in the range from about 1.4×10^{-3} to about 3.7×10^{-3}. *o*-Methoxybenzoic acid is a striking exception, showing only a slight tendency to become dimeric.[19] The K_{21} value reported for *p*-methoxybenzoic acid is about the same as K_{21} for benzoic acid, but the values that have been reported for *p*-fluorobenzoic and *p*-toluic acids indicate an appreciably greater tendency to dimerize.[20]

The experimental work involved in this survey was designed to yield comparative K'' values that would be reliable, at least as rough approximations, without taking the dimer-monomer equilibria of the carboxylic acids into account. It was thought that this objective could be achieved by keeping all of the concentrations low and using not greatly differing stoichiometric proportions of the three reacting components (see table 2). In one case—that of benzoic acid—an additional detailed study of the equilibria at 25° C was made in which stoichiometric concentrations of this acid ranging from one-half to as much as twenty times that of bromophthalein magenta E were used. The data of this experiment were used in calculating uncorrected values of K' and also in correcting K'' values by taking apparent dimer contents of solutions into consideration. The steps following in making the calculations are shown in detail in table 4. In the last column of this table are given the corrected K'' values obtained when K_{21} was assigned the value 1.9×10^{-3}. This is the K_{21} value considered to best fit the data after all of the values of $K_{21}(\times10^3)$ ranging from 1.1 to 3.0 by 0.1 increments had been tried and in each case the average deviation from the mean value of K'' had been computed. The value of K_{21} adopted is close to the values obtained by others from ebullioscopic, distribution, and isopiestic measurements (see table 3).[21] The mean value of K'' given in table 4 exceeds by about 14 percent the mean value given in table 2, but the difference would have been only 5 percent if three rather low values of K'' had been excluded in computing the average value given in table 2 and the remaining values had been corrected as in table 4.

In an analogous manner the K'' values of table 2 were corrected in the cases of *o*-chloro-, *m*-iodo-, and *p*-methoxybenzoic acids and the three toluic acids, using the K_{21} values given in table 3. This treatment brought about slightly increased precision of the results for *o*-toluic acid and *m*-iodo- and *p*-methoxybenzoic acids, but slightly reduced precision for the other three cases.[22] Increases of from 2.5 to 6.0 percent in the values of K'' also resulted.

In the discussion so far it has been assumed that the diphenylguanidine salts of bromophthalein magenta E and the various carboxylic acids all have the composition BA. Studies reported earlier [1(a),(e)] justify this assumption with respect to the diphenylguanidine salt of bromophthalein magenta E. However, the possibility of additional struc-

[17] Such experiments were referred to in [1 (a), p. 261].

[18] A recent comprehensive article on the association of carboxylic acids includes a summary and discussion of such studies [14].

[19] It should be pointed out that the data for this acid were derived from distribution measurements, so that the K_{21} value refers to water-saturated benzene solutions. In some cases it is very probable that the dimer-monomer equilibrium is affected by the presence of water. However, in the case of *o*-methoxybenzoic acid the conclusion of a low dimer content is substantiated by infrared data, which indicate that a relatively strong intramolecular hydrogen bond stabilizes the monomeric form of this acid [15, 16]. Intramolecular hydrogen bonding (that is, chelation) has also been suggested as explaining the comparatively high K_{21} value for *o*-fluorobenzoic acid (table 3, footnote j). The data of table 3 suggest that the other *o*-halogenated acids may also be chelated to a substantial degree in benzene. A different explanation—steric hindrance—was suggested to account for the relatively large value of K_{21} for *o*-toluic acid in comparison with the K_{21} values for benzoic and *m*-toluic acids (footnote g, table 3).

[20] Several investigators have pointed out that there seems to be a rough correlation between the tendency for carboxylic acids to exist in the monomeric state in benzene and their tendency to ionize in aqueous solution. The correlation is very imperfect, and there appear to be two separate relations for carboxylic acids—one covering acids in which there may be resonance between R— and —COOH (for instance, benzoic, cinnamic, and phenylpropiolic acids), and a second relation covering acids in which such resonance is not possible (for example, fatty acids) [14].

[21] According to A. A. Maryott, the electric polarization method, for reasons not understood, seems to give anomalous K_{21} results for benzoic acid (see table 3, footnote i).

[22] The measure of precision referred to here was the average deviation from the mean value of K''.

TABLE 3. *Dissociation constants (K_{21}) of dimeric benzoic acids in benzene*[a]

Temperature[b]	$(10^5)K_{21}$												
	Substituent												
	None	*o*-Br	*o*-Cl	*o*-F	*m*-F	*p*-F	*o*-OH	*m*-I	*o*-OCH_3	*p*-OCH_3	*o*-CH_3	*m*-CH_3	*p*-CH_3
°C													
5.5	[c] 0.572; [d] (.692); [e] .18; [f] .64; [g] (.596)	[c] 1.07	[d] (1.377)	.....	.....	.....	.....	[d] (0.974)	.....	[d] (0.648)	[g] (0.873)	[g] (0.445)	[d] (0.145)
25	[d] (1.76); [f] (2.0); [g] (1.61); [h] 1.9	.....	[d] (3.73)	.....	.....	.....	.....	[d] (2.43)	[f] (350)	[d] (1.80)	[g] (2.37)	[g] (1.37)	[d] (0.415)
30	[d] (2.18); [g] (2.04); [i] 5.3	.....	[d] (4.72)	[j] 5.2	[j] 0.56	[j] 0.78	.....	[d] (3.00)	[f] (370)	[d] (2.28)	[g] (2.99); [h] 2.44	[g] (1.78); [h] 2.00	[d] (0.531)
32	.....	.....	.....	.....	.....	.....	.....	.....	.....	.....	.....	[g] 1.97	.....
32.5	[g] 2.30	.....	.....	.....	.....	.....	.....	.....	.....	.....	[g] 3.38	.....	.....
35	[f] 2.7	.....	.....	.....	.....	.....	.....	.....	.....	.....	.....	.....	.....
40	[f] 3.2	.....	.....	.....	.....	.....	[f] 95	.....	[f] 436	[f] 4.67	.....	.....	.....
43.5	[g] 3.69	.....	.....	.....	.....	.....	.....	.....	.....	.....	[g] 5.43	[g] 3.45	.....
48	.....	.....	.....	.....	.....	.....	.....	.....	.....	[d] 6.40	.....	.....	.....
50	.....	.....	.....	.....	.....	.....	.....	.....	[f] 499	[f] 7.55	.....	.....	.....
54	[d] 5.59	.....	[d] 12.8	.....	.....	.....	.....	[d] 7.64	.....	.....	.....	.....	[d] 1.53
56.5	[g] 6.33	.....	.....	.....	.....	.....	.....	.....	.....	.....	[g] 9.27	[g] 6.31	.....
60	.....	.....	.....	.....	.....	.....	.....	.....	[f] 577	[f] 11.7	.....	.....	.....
61	.....	.....	.....	.....	.....	.....	.....	.....	.....	[d] 8.44	.....	.....	.....
65.5	[d] 8.54	.....	[d] 20.5	.....	.....	.....	.....	[d] 11.0	.....	.....	.....	.....	[d] 2.44
70	.....	.....	.....	.....	.....	.....	.....	.....	[f] 740	[f] 19.0	.....	.....	.....
80	[d] 13.6; [e] 9.7	.....	[d] 33.5; [e] 28	.....	.....	.....	[e] 56	[d] 18.4	.....	[d] 16.5	.....	.....	[d] 4.20

[a] K_{21} corresponds to the equation $A_2 \rightleftharpoons 2A$, and equals $(2\alpha^2 C_2)/(1-\alpha)$. All K_{21} values cited in this table are on the *molar* basis, conversion having been made where necessary by using the relations, K (*molar*) = K (*molal*) × d_4^t (benzene) = K (*mole fraction*) × $100_4^t/78.11$. Parentheses surrounding a K_{21} value signify that it was derived by interpolation or extrapolation. The experimental procedures used in measuring K_{21} are indicated in footnotes c to k.

[b] In some cases temperatures given in the original articles have been rounded off to the nearest degree or half-degree.

[c] B. C. Barton and C. A. Kraus, J. Am. Chem. Soc. **73,** 4561 (1951). (Cryoscopic.)

[d] G. Allen and E. F. Caldin, Trans. Faraday Soc. **49,** 895 (1953). (Ebullioscopic.)

[e] K. L. Wolf and G. Metzger, Ann. Chem. Liebigs **563,** 157 (1949). (Cryoscopic or ebullioscopic.)

[f] M. Davies and D. M. L. Griffiths, J. Chem. Soc. **1955,** 132. (Mostly distribution.)

[g] F. T. Wall and F. W. Banes, J. Am. Chem. Soc. **67,** 898 (1945). (Isopiestic.)

[h] M. M. Davis and M. Paabo. See section 4.1 of this paper. (Spectral absorption in the visible region.)

[i] H. A. Pohl, M. E. Hobbs, and P. M. Gross, J. Chem. Phys. **9,** 408 (1941). (Electric polarization.)

[j] A. A. Maryott, M. E. Hobbs, and P. M. Gross, J. Chem. Phys. **9,** 415 (1941). (Electric polarization.)

[k] A. A. Maryott, M. E. Hobbs, and P. M. Gross, J. Am. Chem. Soc. **71,** 1671 (1949). (Electric polarization.)

tures—in particular, the structure BA_2—for the carboxylic acid salts of diphenylguanidine must be considered. In fact, spectrophotometric evidence of such a structure was obtained in five experiments using indicator bases mentioned above (see footnote 16) mixed with different carboxylic acids.[23] But these were all cases in which the stoichiometric concentrations of acid had to be much greater than that of the indicator base (from a few hundred to several thousand times as great) for measurable changes in spectral absorption to occur; and in experiments with a very strong carboxylic acid in which only about five times as much acid as base was required, a salt of the structure BA appeared to be formed.

[23] Evidence of a similar nature has been obtained by others from conductance titrations of amines with carboxylic acids [17] and from cryoscopic measurements of amine-carboxylic acid mixtures [18] in benzene, as well as from infrared measurements of triethylamine-acetic acid mixtures in carbon tetrachloride [19]. In the last-mentioned case the authors concluded, for example, that 0.1-M acetic acid half-neutralized with triethylamine contains mainly a stable salt of the structure BA_2 which, upon further additions of triethylamine up to a concentration about twice that of the acetic acid, is gradually converted to the salt BA.

From the data of tables 2 and 4 and the above discussion, it seems justifiable to infer that dimerization of the carboxylic acid is the only competitive reaction of importance in the dilute solutions dealt with in this paper and that neglecting this source of error (as will be done in the subsequent discussion) does not invalidate the general conclusions reached. Still further justification is provided by a statistical analysis of the data for six of the acids, made by W. J. Youden of the Bureau. For these acids (which were the *o*-amino, *o*-fluoro, *o*-methoxy, *m*-bromo, *m*-nitro, and *p*-cyano derivatives of benzoic acid), there was no demonstrable connection between individual values derived for K'' and the concentrations employed.

In future work, however, it would be well to attempt to deduce K_{21} as well as K'', as illustrated in table 4, by working with somewhat larger con-

TABLE 4. *Calculation of K'', uncorrected and corrected, for the association of benzoic acid with diphenylguanidine in benzene at 25° C* [a]

n	C_a''	Z	[S'] [b] / [A']	[B] [c]	(5/L)(nL−Z)	[S''] [d]	[A''] [e]	[S'']/[A'']	$K''_{uncor.}$ [f]	α [g]	$K''_{cor.}$ [g]
0.5	2.500×10⁻³	0.3344	0.4899	0.1921×10⁻³	0.8559×10⁻³	0.6638×10⁻³	1.836×10⁻³	0.3615	1.88×10³	0.987	1.90×10³
.5	5.000	.2629	.3486	.1367	1.2074	1.071	3.929	.2726	1.99	.963	2.07
.5	9.993	.1900	.2297	.0901	1.5657	1.476	8.517	.1733	1.92	.925	2.08
.5	24.983	.1088	.1198	.0470	1.9649	1.918	23.06	.0832	1.77	.837	2.11
1.0	2.500	.6162	1.537	.6028	1.9703	1.368	1.132	1.208	2.00	.998	2.00
1.0	5.000	.5031	0.9790	.3840	2.5263	2.142	2.858	0.7495	1.95	.975	2.00
1.0	10.000	.3655	.5610	.2200	3.203	2.983	7.017	.4251	1.93	.935	2.06
2.0	10.000	.6676	1.911	.7495	6.715	5.966	4.034	1.479	1.97	.962	2.05
2.0	15.000	.5421	1.142	.4479	7.335	6.887	8.113	0.8489	1.90	.927	2.05
2.0	25.064	.3952	0.6356	.2493	8.057	7.808	17.26	.4524	1.81	.864	2.09
2.0	30.073	.3506	.5261	.2063	8.274	8.068	22.00	.3667	1.78	.832	2.12
2.0	40.028	.2884	.3958	.1552	8.583	8.428	31.60	.2667	1.72	.790	2.18
2.0	50.035	.2564	.3371	.1322	8.741	8.609	41.43	.2078	1.57	.755	2.08
2.0	60.101	.2261	.2859	.1121	8.888	8.776	51.32	.1710	1.53	.720	2.12
3.0	15.000	.7447	2.735	1.0725	11.336	10.263	4.737	2.167	2.02	.953	2.12
3.0	20.000	.6402	1.699	0.6663	11.852	11.186	8.814	1.269	1.90	.922	2.06
3.0	40.097	.4193	0.7015	.2751	12.939	12.66	27.44	0.4614	1.68	.809	2.08
3.0	50.035	.3629	.5548	.2176	13.214	13.00	37.04	.3510	1.61	.770	2.09
3.0	60.101	.3220	.4633	.1817	13.416	13.23	46.87	.2823	1.55	.735	2.11
3.0	80.134	.2688	.3593	.1409	13.676	13.54	66.59	.2033	1.44	.680	2.12
3.0	100.168	.2311	.2941	.1153	13.863	13.75	86.42	.1591	1.38	.635	2.17
Average											2.08×10³

[a] Provisional values obtained by M. M. Davis and M. Paabo. See the discussion in section 4.1, and also see section 3.2 for the meaning of the symbols, the value of L and of K', and the method of calculating $K''_{uncor.}$ All concentrations are in moles per liter.

[b] Z divided by L-Z gives [S']/[A']. Four decimal places were retained in the Z values to avoid computational errors.

[c] [S']/[A'] multiplied by $1/K'$ gives [B].

[d] Column 6 minus column 5.

[e] Column 2 minus column 7.

[f] See eq (3), section 3.2.

[g] The values of α were calculated from the eq $K_{21}=(2\alpha^2C_a)/(1-\alpha)$, assuming the value of K_{21} to be 1.9×10^{-3} (moles per liter) and substituting the various values in column 8 of this table for C_a. $K''_{cor.}$ (column 12) was then obtained by dividing $K''_{uncor.}$ by the corresponding value of α.

centrations of the carboxylic acids than those employed in most of this investigation.[24]

4.2. Comparative Strengths in Benzene and Water

Experimental work of recent years has shown clearly that the comparative reactivities of a series of acids in a nonionizing medium like benzene, as expressed by the *equilibrium constants for association* with a suitable reference base, should parallel the customary indexes of acidic reactivity in water, namely, the *ionic dissociation constants* [1]. This means, of course, that when ionic dissociation constants are expressed as pK (-log $K_{dissocn.}$) values, there should be an *inverse parallelism*. However, in water secondary phenomena (solvation, ionization) accompany the fundamental acid-base reaction eq(1), while in comparatively inert solvents like benzene various manifestations of hydrogen-bonding (for instance, chelation) become prominent. For such reasons, occasional deviations from a linear relationship between the two sets of equilibrium constants are to be expected.

a. Effects of Substituents on the Strength of Benzoic Acid

In considering the deviations observed in this investigation, it is necessary to have in mind current views as to how the nature and position of substituents account for the relative strengths of substituted benzoic acids. The following summary may be helpful to readers who are unfamiliar with recent developments in this area:[25]

(1) A substituent influences the strength of a carboxylic acid RCOOH according to its electron-attractive nature and its proximity to the —COOH group. Replacement of hydrogen atoms in the R-radical by atoms or groups that are more electron-attractive causes the electrons of the H—O linkage to be brought more under the control of the oxygen, thus facilitating the removal of the carboxylic proton. Some common substituents exhibit the following order of decreasing electron-attractive character:

$$NO_2>F>Cl>Br>I>OH>C_6H_5>H>CH_3$$

As the list indicates, most groups are more electron-attractive than hydrogen, and thus their substitution for hydrogen usually results in increased acidity, but the methyl group is less electron-attractive and can be expected to reduce the acidity.

(2) The electrical effect of the substituent is considered to be transmitted partly through space (or through the solvent) and partly through the molecule. The directly transmitted influence is known as the "field effect", and the influence transmitted through the molecule by relay from atom to atom is commonly referred to as the "inductive effect". Both effects operate in the same direction and fall off with increasing distance of the substituent from the —COOH group, the latter effect more rapidly than the former. They have often been treated as a single influence.[26]

[24] Lack of information about the dimer-monomer equilibria of the carboxylic acids concerned is likely to have been the principal reason for the failure of some earlier attempts to formulate quantitatively acid-base equilibria in benzene and in chloroform by spectrophotometric [20] and polarimetric [21] measurements. Those experiments employed stoichiometric concentrations of base and acid far larger than any used in this work. Other kinds of competitive associations may also have been involved.

[25] References [22] to [28], on which this summary is based, furnish more rigorous and detailed discussions of the effect of structural factors on acidic strengths, including the historical development of the ideas currently accepted, some recent experimental observations, and many additional references.

[26] Some recent efforts to disentangle the two effects are discussed in [28].

(3) In addition to the above effects, resonance (mesomeric) effects are important in benzoic acid and substituted benzoic acids. Several factors seem to be involved.

In benzoic acid itself, resonance is believed to have an acidity-reducing effect. This can be attributed to a reduction in the stability of the benzoate ion, as suggested in formulas I and II. That is, in resonance form II the carboxylate group is conjugated with

I II

the benzene ring. This increases the negative charge on the oxygens, thus making the —COOH proton less easily removed.

Resonance of the benzoate ion among forms like I and II can be either reinforced or opposed by substituting groups such as —OH, —OCH_3, —NH_2, —NO_2, and —CN in the *ortho* and *para* positions. These are all groups that can become conjugated with the ring—the first three by releasing electrons and the last two by acquiring electrons, as exemplified in formulas III and IV, respectively. As the

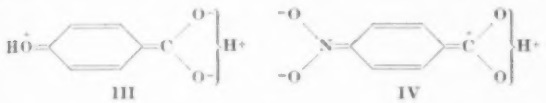

III IV

formulas indicate, e.g., —OH group in the *para* position reinforces, but a —NO_2 group opposes, the kind of acid-weakening resonance of the —COO— group with the ring which was illustrated in formula II. In III resonance opposes the acid-strengthening inductive and field effects of the substituent (—OH), but in IV it reinforces these effects. The —OCH_3 and —NH_2 groups resemble —OH, while —CN resembles —NO_2 in resonance behavior. Substituents do not become involved in such resonance when in the *meta* position, and their influence is then ascribed wholly (or almost wholly) to inductive and field effects.

A bulky substituent located close to the —COOH group, as in *o*-substituted benzoic acids, can prevent the nearly coplanar alinement of the phenyl and carboxyl groups thought to be essential for the kind of resonance indicated in formulas II to IV. This "steric inhibition of resonance" has been proposed as an explanation for such phenomena as the substantial increase in the ionization of *o*-toluic acid (pK=3.91) over that of benzoic acid (pK=4.20). Actually, as indicated above under 4.2.a(1), a —CH_3 group would be expected to *reduce* the strength of benzoic acid when in the *ortho* position—just as it does when in the *meta* or *para* position, but to an even greater degree.

(4) Finally, hydrogen bonding appears to affect the strengths of certain benzoic acids with *ortho* substituents, in some cases having an acid-strengthening effect and in others, a weakening effect. Thus, in accounting for the relatively great strength of salicylic acid (pK=3.00), it has been suggested that the anion is stabilized by the formation of a chelate ring in which the *phenolic hydrogen* is bonded to a *carboxylate oxygen* [29]. The still greater strengths of γ-resorcylic (2,6-dihydroxybenzoic) and *p*-orsellinic acids can be explained along similar lines [30].[27] On the other hand a tendency for bonding between the carboxylic hydrogen and an *ortho* substituent (see footnote 19) would reduce the tendency to ionize and react in other ways as an acid.

In large measure the ideas just summarized were founded on the ionic behavior of the acids in water, although other observations, such as the effects of substituents on the rates of various organic reactions, were also taken into account.

b. *meta*-Substituted Benzoic Acids

In applying these views to the equilibrium studies dealt with here, one will naturally expect to find that the *meta*-substituted benzoic acids, in which electrical influences of substituents seem to be transmitted to the —COOH group with little if any complication by resonance, steric hindrance, and hydrogen bonding, are the acids showing the most constancy in the order of relative strengths in the two solvents, benzene and water. Actually, as shown in figure 1, the relative

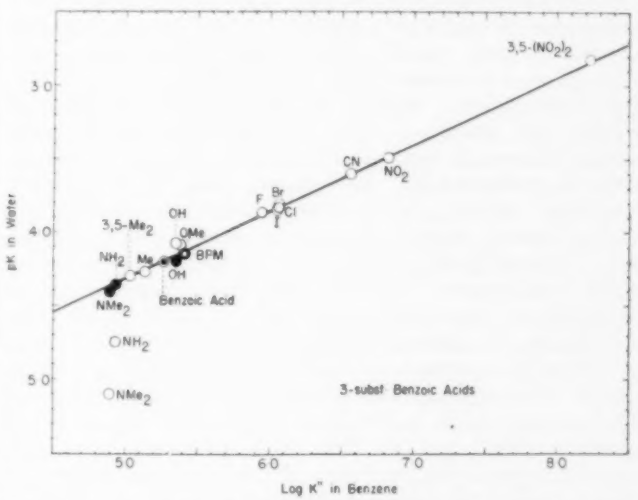

FIGURE 1. *Comparison of the strengths of 3-substituted benzoic acids in benzene and water, as measured by log K'' and pK, respectively; t=25° C.*

Open circles, *experimental pK* values plotted against log *K''* values. Solid circles, *pK* values *calculated* using Hammett σ values plotted against log *K''* values.

order of strength in the two solvents was found to be preserved very exactly for nine of the *meta*-substituted acids investigated.[28] Figure 1 was prepared by using the log K'' and pK values for *meta*-substituted acids compiled in table 1. The equation for the line, which was computed by the least squares method using the log K'' and pK values for the seven *meta*-substituted acids designated by asterisks, is

$$pK = -0.461 \log K'' + 6.623. \qquad (5)$$

[27] A similar explanation has been offered for the anomalously great ionization of *o*-toluic acid in water, but steric inhibition of resonance is now considered a more probable explanation.

[28] Note the open circles only.

Benzoic acid and bromophthalein magenta E may be added to this group of acids.[29]

It seems reasonable to consider the line as a standard or "norm" for the behavior of benzoic acids in comparisons employing log K'' and pK as the measures of acidity. Points falling above this line then refer to acids that appear to be too strong in water or too weak in benzene to conform to standard behavior, while the reverse is true for points located below the line. Four of the *meta*-substituted acids deviate significantly from standard behavior—for two of them (m-OH and m-OCH_3) the points are a little above the standard line, and for the other two (m-NH_2 and m-$N(CH_3)_2$) the points are substantially below the line. These cases are referred to again at the end of this section.

A very similar figure would have been obtained by plotting the Hammett *sigma* values against log K''. The σ values, as is well known, are obtained from the relationship known as "Hammett's equation":

$$\log k - \log k^\circ = \rho\sigma. \qquad (6)$$

Equation (6) was shown by Hammett to be applicable in a great many cases as an expression of the electrical effects of single *meta* or *para* substituents on rates as well as equilibrium constants of side-chain reactions of benzene derivatives [31,32]. Additional examples are continually being discovered. By definition, k is a reaction rate or equilibrium constant for a compound with a *meta* or *para* substituent, k° is the corresponding constant for the parent (unsubstituted) compound, ρ is a *reaction* constant that is constant for all substituents in any given reaction series under fixed reaction conditions (temperature, medium), and σ is a *substituent* constant determined only by the nature of the *meta* or *para* substituent. As the most convenient way of devising a numerical scale of σ values, ρ for the ionization of benzoic acids in water at 25° C was arbitrarily assigned the value 1 [31]. The σ values (with a few exceptions) are then obtained by making the appropriate substitutions in eq (6). It is evident from eq (6) that the substituents which most augment the acidity of benzoic acid have the most positive σ values. For other reaction series ρ can be obtained by plotting log k (customarily as the ordinate) against σ [31]. The slope of the best straight line through the points is the value of ρ. Applying this procedure to the reaction of diphenylguanidine with the "standard" *meta*-substituted benzoic acids in benzene yields 2.17 as the value for ρ.[30]

In terms of electron theory, the quantity ρ measures the susceptibility of a given reaction to a change in electron density at the reaction site. Positive and negative values of ρ indicate reactions facilitated by low and high electron density, respectively. As indicated above, the values of σ for various substituents measure their capacities to cause changes in electron density at the reaction site [31,32].

Hammett did not derive the σ values for m- and p-NH_2 from the aqueous ionization constants of the aminobenzoic acids, but rather from published data on the alkaline hydrolysis of the ethyl benzoates in 87.83 percent ethanol at 30° ([31 (d)], table I). Using the σ value so obtained (−0.161) and eq (6) to *calculate* the pK for m-aminobenzoic acid gives the value 4.36. The point located by plotting this pK value against our log K'' value is indicated by a solid circle in figure 1. An alternative method of calculating—substituting our log K'' value in eq (5)—gives the almost identical value 4.35.

The σ value for the group m-$N(CH_3)_2$, derived from published data for the reaction of phenolate ions with propylene oxide in 98 percent ethanol at 70.4°, is −0.211 [31 (d)], and the pK value calculated using this is 4.41. This pK value was used as described in the preceding paragraph for locating a solid circle. Once more, the solid circle falls close to our standard line. The pK value calculated by substituting our log K'' value in eq (5) is 4.37.

One can easily see why it is unsatisfactory to use aqueous ionization constants in assessing the effect of an amino or substituted amino group on the dissociation of the —COOH proton. For one thing, the aminobenzoic acids have *two* ionization constants, and these constants are not very widely separated.[31] Also, the inductive and field effects of the amino group and its resonance with the benzene ring are undoubtedly affected by coordination with water molecules. Furthermore, it has been concluded on the basis of several types of physical evidence that m-aminobenzoic acid exists primarily as the zwitterion in water [34].[32]

An attempt has been made to deduce the effect of the m-NH_2 group on the aqueous ionization of benzoic acid by employing the relationship [34]:

$$pK_D = pK_1 + pK_2 - pK_E. \qquad (8)$$

In eq (8) pK_1 and pK_2 are the experimentally obtained values for the ionization of $H_3\overset{+}{N}$— and —COOH, respectively, pK_E is an experimental value for the ionization of $H_3\overset{+}{N}C_6H_4COOCH_3$ or $H_3\overset{+}{N}C_6H_4COOC_2H_5$ (taken as 3.56 for the m-amino substituted ester), and the value of pK_D is considered to indicate the effect of an *uncharged* m-amino group on the ionic dissociation of the —COOH group. It is assumed that —COOH and —COOR have identical effects on the dissociation of $H_3\overset{+}{N}$—.[33] Using the data of footnote 31 (a) to calculate pK_D gives the value 4.26. This is fairly close to the value

[29] Bromophthalein magenta E is too insoluble in water for an exact measurement of its pK value, but a rough measurement has indicated this to be, as expected, practically the same as the pK value for bromophenol blue (4.15).

[30] Equation (5) is equivalent to:

$$\log K'' = -2.17\,pK + 14.37; \qquad (7)$$

ρ is the negative coefficient of pK in eq (7).

[31] The following values were obtained in recent attempts to evaluate the thermodynamic pK_1 and pK_2 values for three aminobenzoic acids: (a) For o-, m-, and p-aminobenzoic acids, respectively, pK_1 values obtained by potentiometric procedure are 2.05, 3.07, and 2.38; the corresponding pK_2 values are 4.95, 4.75, and 4.89. (See table 1, footnote ‖.) (b) For o- and p-aminobenzoic acids, the respective pK_1 values obtained employing spectrophotometry are 2.14 and 2.29, and the pK_2 values, 4.80 and 4.86 [33].

[32] In contrast, the isomeric o and p-substituted acids are thought to exist largely, though not exclusively, as uncharged molecules in water [34].

[33] See [34 (a), ch. 4] for further discussion of this calculation.

(4.35) calculated from our eq (5) and log K'' data. The latter value is probably the more accurate index of the effect of m-NH_2 on the ionization of benzoic acid.

Previously, in the study of reactions in ethanol-water mixtures of varying ethanol content, the substituent constant σ for m-OH has been observed to be very sensitive to the composition of the solvent.[34] An average value, -0.002 [32], was substituted in Hammett's equation in computing the pK value used to locate the solid circle in figure 1. A σ value of about $+0.05$ for m-OH and m-OCH_3 (actually, $+0.04$ and $+0.06$, respectively) is deduced with the use of our eq (5) and log K'' values. Modification of the electrical influences of the two groups resulting from coordination with solvent molecules offers a reasonable explanation of the variation of σ with solvent composition. As with m-NH_2 and m-$N(CH_3)_2$, one may presume the results obtained for benzene solutions to furnish a more reliable index of electrical effects of these substituent groups on the —COOH group than those obtained for aqueous or alcoholic solutions.

In short, it seems correct to conclude that among the *meta*-substituted benzoic acids departures from a linear relation of strengths in water and benzene will be rare, and that explanations for such departures should usually be sought in phenomena characteristic of aqueous systems.

c. *para*-Substituted Benzoic Acids

In analyzing the relative acidic behavior of *para*- and *ortho*-substituted benzoic acids in the solvents benzene and water it is immediately evident that most of the ones studied fail to conform to the "norm" defined in 4.2.b and indicated by the heavy line in figure 2.

For the *para*-substituted acids the departures from the norm are in general rather small.[35] However, it seems apparent that while the acids containing —Cl, —Br, or —I deviate only very slightly from the norm, the acids containing substituents commonly regarded as being decidedly electron-releasing (—F, —OH, —OCH_3, —NH_2) are relatively stronger in benzene than in water whereas the two acids with electron-attracting substituents (—CN, —NO_2) are relatively weaker in benzene than in water. Using data for the seven *para*-substituted acids marked with asterisks in table 1 gives the equation

$$pK = -0.557 \log K'' + 7.218 \qquad (9)$$

as an expression of the relation of the strengths of this group of acids in benzene and water. The straight line corresponding to this equation is indicated by the faint line intersecting the norm in figure 2.

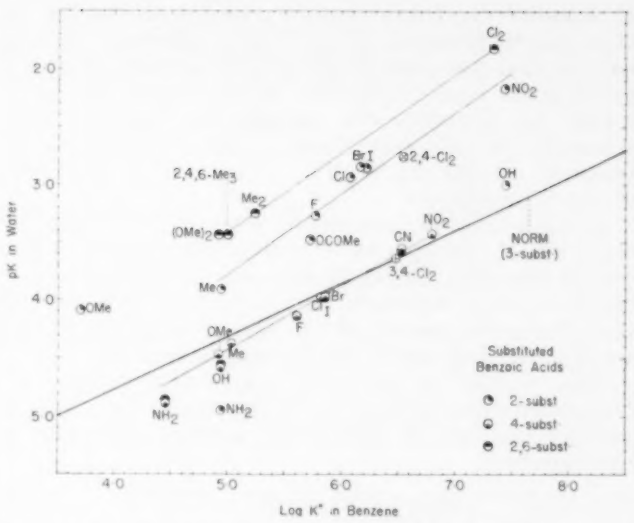

FIGURE 2. *Comparison of the strengths of some 2-, 4-, and 2,6-substituted benzoic acids in benzene and water, as measured by log K'' and pK, respectively; $t = 25°$ C.*

The solid circles apply to cases where pK values were calculated using Hammett σ values. In all other cases the values plotted were obtained experimentally.

No attempt will be made here to account in detail for the deviations from linearity, but it is easily seen that bonding of water to a *para* —CN or —NO_2 group (see formula IV) might accentuate the acid-strengthening resonance of either group with the ring. Hydration of —F, —OH, —OCH_3, or —NH_2 could reduce their acid-weakening resonance with the ring (compare formula III); however, the acid-strengthening field effect would also be reduced. As a matter of fact, several investigators have called attention to the existence of a solvent influence on the σ values of *para* substituents like —OH, —$N(CH_3)_2$, —CN, and —NO_2 [32]. The electrical effect of p-CH_3, also, appears to vary somewhat with the medium [35]. For example, values of σ for p—CH_3 ranging from -0.17 (in water) to -0.08 (in hexane) have been calculated from studies of reactions of p-toluidine [35]. It is worth noting that the pK value (4.28) calculated by substituting -0.08 in eq (6) is practically the same as the pK value (4.30) calculated using eq (5) and the log K'' value for p-toluic acid.

It seems evident that the aqueous pK values of *para*-substituted benzoic acids are not infallible indexes of intrinsic acidic strengths or sources of universally valid σ values. In spite of experimental uncertainties in this work, the log K'' values obtained with the benzene solutions are probably, on the whole, more accurate indexes of the relative intrinsic acidities than are the aqueous pK values.

d. Mono-*ortho* and Di-*ortho* Substituted Benzoic Acids

It is well known that the influence of substituents in close proximity to a reacting group, such as the —COOH group of benzoic acid, is generally unpredictable. Reference to some of the recognized anomalies in the strengths of *ortho*-substituted benzoic acids in water, and to some of the attempts

[34] See p. 232-3 of [32]. In the ionization of m-hydroxybenzoic acid, for example, the value of σ changed from $+0.124$ in water to -0.134 in 100-percent ethanol.

[35] The three solid circles (for p-NH_2, p-OH, and p-CN) that are partly visible in figure 2 have the same significance as in figure 1. That is, they mark the points obtained on plotting against log K'' the pK values *calculated* by using eq (6) with the Hammett σ values given in table 7 of [32]. All three solid circles are slightly closer to our norm than are the corresponding open circles.

to account for the anomalies, was made earlier in this paper (section 4.2.a.). An analysis of the nature and the extent of the deviations of *ortho*-substituted acids from the norm, which has been found to describe the parallelism between the strengths of *meta*-substituted acids in water and in benzene, should be helpful in accounting for part of the anomalies.

On only a casual inspection of figure 2 it is evident that all of the points for *ortho*-substituted acids except one (that for *o*-aminobenzoic acid) are located above the line representing the norm. This means that the acids are either too strong in water or too weak in benzene (or both) for conformance.

The points in question are rather scattered. Using the data for the six acids containing a single halogen, methyl, or nitro group in the *ortho* position the equation

$$pK = -0.70 \log K'' + 7.26 \qquad (10)$$

was calculated by the least squares method. The corresponding line is indicated faintly in figure 2. This line is helpful in guiding the eye to the vicinity of most of the points for mono-*ortho*-substituted acids, but we believe it to represent no more than a crude approximation of a norm for this class of acids.

o-Methoxybenzoic acid is by far the weakest in benzene of all the acids studied. In fact, this acid is so much weaker than bromophthalein magenta E in benzene that the precision of the measurements was very poor (see table 2) and the log K'' value reported is considered only a rough approximation. It can scarcely be doubted that the comparatively feeble tendency for this acid to combine with diphenylguanidine in benzene results from the stability of a chelate structure in which the —COOH proton is attracted toward the oxygen of $—OCH_3$. Infrared data have already been interpreted as indicating the existence of this structure in another inert solvent, carbon tetrachloride (see footnote 19). In water, hydrogen bonding of the solvent to $—OCH_3$ would oppose formation of the chelate structure and would also undoubtedly modify the inductive and field effects of $—OCH_3$ on —COOH and alter its resonance with the benzene ring. Hydration could also increase the bulk of $—OCH_3$ to such a degree as to cause steric inhibition of resonance of —COOH with the ring.

The point for salicylic (*o*-hydroxybenzoic) acid is so close to the norm as to suggest that in benzene the anion exists largely in the same chelated structure that accounts well for the relatively great acidity of the compound in water—a structure in which the phenolic hydrogen is bonded to a carboxylate oxygen (see section 4.2.a (4)). Possibly the slightly reduced acidity in benzene indicates part of the molecules to be in a chelated form analogous to that which has been suggested for *o*-methoxybenzoic acid. The aqueous pK value at 25° for aspirin (*o*-acetylsalicylic acid) has not been measured with the same degree of care as that of many of the other benzoic acids. The value cited, if assumed to be substantially correct, suggests some tendency in inert solvents for chelation of the same type as that of *o*-methoxybenzoic acid.

The case of anthranilic (*o*-aminobenzoic) acid seems too complex for analysis at this time of its differing acidic behavior in benzene and water. Gordy concluded from infrared data [36] that in carbon tetrachloride solutions the amino hydrogen of methyl anthranilate—like the hydroxyl hydrogen of methyl salicylate—is bonded to the carbonyl oxygen. The hypothesis of a chelated *o*-aminobenzoate ion, analogous in structure to the generally accepted salicylate ion structure, appears reasonable. A zwitterionic structure seems less probable (see footnote 32). Perhaps the unpublished studies of hydrogen bonding referred to in [37] will make the acidic behavior of anthranilic acid more comprehensible.

The acidic behavior observed for *o*-toluic acid in benzene is of exceptional interest. Hitherto, on the basis of aqueous pK values, *ortho* substitutions have been believed to increase the strength of benzoic acid—*without exception*—even though the methyl group, being less electron-attractive than hydrogen (see section 4.2.a(1)), would be expected to reduce the acidity of benzoic acid when in the *o*-position as well as when in the *m*- and *p*-positions. Table 1 and figure 2 show that this expectation is fulfilled for benzene solutions. That is, a single *o*-CH_3 substituent does not appear to cause steric inhibition of resonance of the —COOH with the aromatic ring *when in benzene solution*. This suggests that in aqueous solutions the clustering of water molecules about —COOH[36] leads to steric inhibition of resonance of the aromatic ring with —COOH in the case of *o*-toluic acid. If this supposition is correct, then hydration of —COOH must contribute generally to steric inhibition of resonance in *ortho*-substituted benzoic acids when in aqueous solutions, resulting in enhancement of their intrinsic acidities.

It would not be justifiable to conclude merely from the preceding discussion that the behavior of *o*-toluic acid in benzene is completely normal. However, a study of figure 3 indicates that this conclusion is warranted. In this figure, the aqueous pK values at 25° reported in the literature for a number of *phenols* substituted by methyl or halogen in various positions of the ring (see table 5) have been plotted against the log K'' values for the *benzoic acids* with the corresponding substitutions.[37] There is good evidence that the aqueous pK values for methyl-substituted phenols and also those of methyl-substituted pyridinium cations provide valid evidence as to the electrical influence of the methyl group on the acidity of the parent substance, regardless of the position of substitution.[38] Figure 3 reveals a close linear relationship of the strengths of the phenols in water and the strengths of the correspondingly substituted benzoic acids in benzene not only in all cases of substitution in the *m*- or *p*-positions with halogen or methyl, but also in cases of substitution in the *o*-position with a single methyl group. An analogous linear relation-

[36] The discussion starting on p. 428 of [38] is of interest in this connection.
[37] The log K'' value (4.74) used for 2,4-dimethylbenzoic acid in figure 3 is from incomplete studies of M. M. Davis and M. Paabo.
[38] For example, see the discussion in [27].

ship of the aqueous pK values for pyridinium ions and the log K'' values for benzoic acids can be demonstrated.[39]

Within the experimental uncertainty of the pK and log K'' values, the influence of two methyl groups in the 2,4- or 3,5-positions of phenol or of benzoic acid is additive, and this is also true for 2,6-dimethylphenol (see tables 1 and 5). On the other hand, it is clear from a study of figure 3 and also of tables 1 and 6 that substitution of $-CH_3$ in both *ortho* positions of benzoic acid produces anomalously great acidities in both benzene and water. In the case of 2,6-dimethylbenzoic acid, for example, the log K'' value for benzene solutions should be about 4.62—that is, 5.26 minus 2(0.32)—if the polar influences of the two *o*-CH_3 groups were additive. Instead, the introduction of a second *o*-CH_3 restores the log K'' value (5.24) almost to that of benzoic acid. In water, as already noted, a single *o*-CH_3 substitution enhances the acidity of benzoic acid (by 0.29 pK unit). The total increment in acidity (0.95 pK unit) produced by two *o*-CH_3 substitutions in benzoic acid shows that the second *o*-CH_3 has more than twice the acidity-augmenting effect of the first *o*-CH_3.

Jenkins, in considering the ionic dissociation constants for aqueous solutions of the isomeric halo- and nitrobenzoic acids, reached the conclusion [40] [40] that the inductive effect of the substituent is the predominant factor, and that anomalies in the ionizing behavior of the *ortho*-substituted acids are nonexistent. However, this opinion has not been universally shared,[41] and the conclusions reached in this paper about the anomalously great strength of *o*-toluic acid in water seem likely to apply to other cases of *ortho*-substitution, at least to cases in which the substituent is comparable in bulk to $-CH_3$.[42] Nevertheless, it seems probable that an additional factor—a pronounced tendency toward internal hydrogen bonding when in benzene solution—is partly responsible for the displacements from the norm of the points for the four *o*-halobenzoic acids, shown in figure 2 [43] (see also footnote 19).

Figure 3 provides further indirect evidence on this point. In examining this figure no doubt the reader has already noticed the displaced positions of the points for acids substituted in the 2-position with —Br or —Cl. The displacements indicate two possibilities—either there is some factor causing excessively great acidity of the *o*-halophenols in water, or there is a factor reducing the acidity of the *o*-halobenzoic acids in benzene. There is no reason to consider that *o*-halophenols are anomalously strong

[39] Other evidence bearing on this discussion was obtained by Norris and Strain [39], who compared the rates of reaction of different acids with di-*p*-tolyldiazomethane in toluene at 25° C with the corresponding aqueous ionization constants. They remarked that —Cl, —Br, and $-NO_2$ in the *o*-position of benzoic acid greatly increase both reactivity and ionization, while $-CH_3$ and $-OCH_3$ in the *o*-position increase ionization but decrease reactivity.

[40] See also the discussion in sections IV–G and V of [24 (a)].

[41] For example, see [27, p. 605].

[42] Pauling gives the following tabulation of van der Waals radii (in A) for substituents of interest in this discussion: H, 1.2; F, 1.35; Cl, 1.80; Br, 1.95; I, 2.15; CH_3, 2.0 [41].

[43] An important study of the OH-vibration frequencies of carboxylic acids and phenols, including many *m*- and *p*-substituted benzoic acids, in dilute carbon tetrachloride solutions at 25° C deliberately excluded the compounds *expected* to have internal H-bonds, such as *o*-substituted phenols and benzoic acids [42], but no experimental evidence of hydrogen-bonding in *o*-halobenzoic acids was located in the literature.

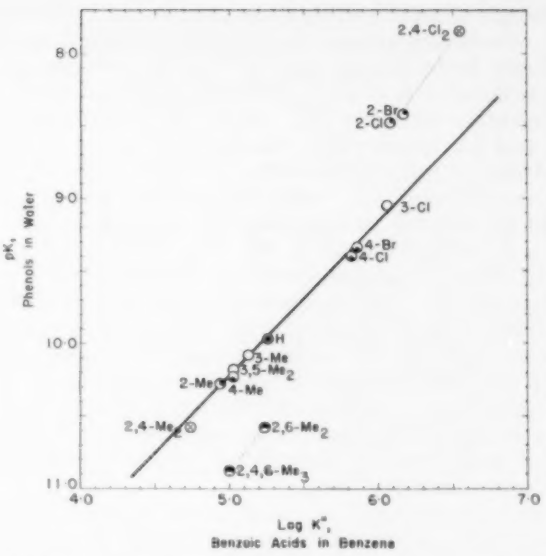

FIGURE 3. *Comparison of the effects of different substitutions on the acidity of phenol in water (as measured by pK) and the acidity of benzoic acid in benzene (as measured by log K''); $t = 25°$ C.*

TABLE 5. *Ionic dissociation constants of phenols in water at 25° C*

Substituent [a]	pK	Avg. pK
None*	[b] 10.00 [c] 9.98 [d] 9.95 [f] 9.94 [g] 9.99	9.97
2-Methyl*	[b] 10.29 [f] 10.28	10.28
3-Methyl*	[b] 10.09 [c] 10.08	10.08
4-Methyl*	[b] 10.26 [c] 10.25 [f] 10.19	10.23
2,4-Dimethyl	[f] 10.58	10.58
2,6-Dimethyl	[g] 10.58	10.58
3,5-Dimethyl*	[c] 10.17 [g] 10.18	10.18
2,4,6-Trimethyl	[f] 10.88	10.88
2-Bromo	[d] 8.42	8.42
4-Bromo*	[c] 9.34	9.34
2-Chloro	[d] 8.48	8.48
3-Chloro*	[c] 9.08 [d] 9.02	9.05
4-Chloro*	[c] 9.42 [d] 9.38	9.40
2,4-Dichloro	[d] 7.85	7.85

[a] Asterisks indicate the acids whose pK and log K'' data were used in calculating the equation for the line in figure 3.
[b] A. I. Biggs, Trans. Faraday Soc. **52,** 35 (1956).
[c] F. G. Bordwell and G. D. Cooper, J. Am. Chem. Soc. **74,** 1058 (1952).
[d] C. M. Judson and M. Kilpatrick, J. Am. Chem. Soc. **71,** 3110 (1949).
[f] H. Kloosterziel and H. J. Backer, Rec. trav. chim. **72,** 185 (1953).
[g] G. R. Sprengling and C. W. Lewis, J. Am. Chem. Soc. **73,** 5709 (1953).
[g] G. W. Wheland, R. M. Brownell, and E. C. Mayo, J. Am. Chem. Soc. **70,** 2492 (1948).

TABLE 6. *Calculated and observed increments in the strength of benzoic acid produced by 2, 6-disubstitutions* [a]

2- and 6-substituents	Δ log K'' (benzene)		$-\Delta$ pK (water)	
	Calculated	Observed	Calculated	Observed
CH_3	−0.64	−0.02	+0.58	+0.95
Cl	+1.64	+2.08	+2.52	+2.38
OCH_3	−3.2	−0.34	+0.22	+0.76

[a] Data all refer to 25° C, and were computed from the pK and log K'' data given in table 1 for the corresponding mono-*ortho*-substituted acids. Positive and negative increments indicate, respectively, increases and decreases in acidic strength.

in water. Indeed, while Jenkins has concluded that *ortho* effects are absent [43], slightly reduced acidity resulting from persistence of the chelate structure [44] in water has been tentatively deduced from the comparative aqueous pK_a values of substituted phenols and pyridines [45]. Knowledge as to whether the electrical influences of two *o*-halogen substitutions on the aqueous pK value of phenol are additive would be helpful in deciding this question, but the only pK values found in the literature for phenols substituted by halogen in the 2- and 6-positions are untrustworthy. Regardless of which view is correct, the displacement of the points in figure 3 suggests a marked tendency for intramolecular hydrogen bonding of the *o*-halobenzoic acids when in benzene.

o-Nitrobenzoic acid is considered to exhibit only a slight tendency toward chelation, and this is not regarded as surprising, because the chelate ring would be seven-membered [46].

Figure 2 discloses an exact inverse parallelism of the aqueous pK and the log K'' values for the only 2,6-disubstituted acids of suitable strength that were available for inclusion in this study—namely, 2,6-dimethoxy-, 2,6-dimethyl-, 2,6-dichloro-, and 2,4,6-trimethylbenzoic acids.[44] The closely linear relation of the two sets of values may be accidental, and it is clearly desirable to extend pK and log K'' measurements to benzoic acids with other substitutions in the 2- and 6-positions. With two substitutions in the *ortho* position, steric inhibition of resonance appears to result both in water and benzene, whatever the nature of the substituent. But, as table 6 shows, the observed acidities in the two solvents are in marked disagreement with predictions based on the assumption that substitution in both *ortho* positions will produce twice the effect of a single *ortho* substitution.

4.3. Comparative Strengths in Benzene and Other Nonaqueous Solvents

Numerous investigators have studied the effects of different nonaqueous solvents (most commonly, lower alcohols or alcohol-water mixtures) on the relative strengths of acids, employing a variety of experimental procedures—colorimetric, conductometric, kinetic, and potentiometric. A series of systematic studies by Kilpatrick and co-workers is of particular interest for comparison with the results presented in this paper. Some of their results were obtained colorimetrically, but in the most complete set of measurements the strengths of some 20 monosubstituted benzoic acids relative to benzoic acid itself were compared by an emf method in 8 different solvents, 5 of which were anhydrous alcohols and the remaining 3, dioxane-water mixtures of varying dielectric constant [47 and 6]. The method adopted (compare [48]) employed concentration cells of the type:

Au	HB...0.005 M LiB...0.005 M LiCl..0.045 M Quinhydrone	||	LiCl 1.00 M	||	HX..0.005 M LiX..0.005 M LiCl..0.045 M Quinhydrone	Au

HB signifies benzoic acid and LiB, its lithium salt; HX signifies the substituted benzoic acid and LiX, its lithium salt. The presence of a high concentration of lithium chloride ensured negligible junction potentials. The equilibrium being measured can be expressed as

$$A_x + B_o^- \rightleftarrows A_o + B_x^- \qquad (12)$$

Here, following Brönsted symbolism, A_o and A_x represent benzoic acid and the substituted benzoic acid, respectively, while B_o^- and B_x^- represent the corresponding anions ("conjugate bases"). Using the concentration cell described above, the equilibrium constant at 25° C—referred to as $K_{A_xB_o}$ [47]—can be obtained from the relationship:

$$E(\text{emf}) = 0.05915 \log K_{A_xB_o}. \qquad (13)$$

In cases in which tests were made, the values of $K_{A_xB_o}$ seemed to be independent of the ionic strength [47]. It is evident that log $K_{A_xB_o}$ is equivalent in meaning to such other notations as log K_r [49], log (K_{HB}/K_{HX}), Δ log K, or $-\Delta pK$.[45]

In table 7 the Δ log K values for some 20 *o*-, *m*-, and *p*-substituted benzoic acids in water, in the eight nonaqueous solvents just referred to, and in benzene have been compiled. The values given in table 7 were used in preparing figures 4 to 6, in which the increments $-\Delta pK$ (for aqueous solutions) or the increments log $K_{A_xB_o}$ have been plotted against the increments Δ log K'' obtained in this investigation for benzene solutions.

The symbols used in figures 4 to 6 have the same significance as in figure 2.[46] Also, just as in the preceding figures, each solid line indicates a "norm"—that is, a linear relationship of the strengths of *meta*-substituted benzoic acids in benzene and in the second medium, having the form

$$-\Delta pK (\text{or } \log K_{A_xB_o}) = m(\Delta \log K'') + b. \qquad (14)$$

The constants m and b of eq (14) for the different media, computed by the least-squares method with the data indicated in table 7, are compiled in table 8. The compilation includes the results for *o*- as well as for *m*-substituted acids.

a. *meta*-Substituted Acids

Taking a "bird's-eye view" of figures 4 to 6 and also referring to the values listed in table 8, it is quickly apparent that for the *meta*-substituted acids the slope increases sharply upon changing from water

[44] The line connecting the points corresponds to the equation

$$pK = -0.680 \log K'' + 6.814. \qquad (11)$$

The constants of this equation were calculated by the least-squares procedure, using all of the available data.

[45] For our purposes Δlog K values and absolute values of ionic dissociation constants in the various media are equally good. To obtain the latter, a reliable value of the dissociation constant of any one of the series—say, benzoic acid itself—is necessary (see the discussion in [47].

[46] To avoid confusion, only points meriting special attention have been labeled in figures 4 to 6. The remaining points can be identified by the aid of table 7.

TABLE 7. *Effect of the solvent on the comparative strengths of benzoic acid and various of its monosubstituted derivatives at 25° C*

Substituent	$-\Delta pK$[a]	Log $K_{A_2B_0}$ (μ=0.05)[b]								$\Delta\log K''$[c]
	Solvent[d]									
	Water	MeOH	EtOH	*n*-PrOH	*n*-BuOH	Ethylene glycol	Dioxane-water, Wt % dioxane			Benzene
							26.5	43.5	73.5	
	(78.5)	(31.5)	(24.2)	(20.1)	(17.4)	(37.6)	(55)	(40)	(15)	(2.28)
Ortho-substituted benzoic acids										
Br[e]	1.35	1.27	1.16	1.16	1.09	1.20	1.13	1.00	0.88	0.91
Cl[e]	1.26	1.21	1.12	1.09	1.08	1.14	1.08	0.97	.84	.82
F	0.93	1.00	1.02	0.96	0.93	0.69	.....	.....	.....	.51
OH	1.20	1.49	1.63	1.57	1.50	1.50	1.49	1.60	1.78	2.19
I[e]	1.34	1.19	1.08	1.10	1.04	1.10	1.00	0.87	0.75	0.96
OCH_3	0.11	0.17	0.24	0.26	0.28	0.18	−0.06	−.10	−.07	−1.6
CH_3[e]	.29	.09	.02	.04	.00	.05	.04	−.08	−.21	−0.32
NO_2[e]	2.03	1.83	1.77	1.80	1.78	1.74	1.78	1.66	1.58	2.18
Meta-substituted benzoic acids										
Br[f]	0.39	0.60	0.65	0.63	0.58	0.54	0.43	0.47	0.53	0.80
Cl[f]	.37	.59	.63	.61	.58	.52	.44	.48	.53	.80
F[f]	.34	.51	.53	.52	.42	.45	.41	.41	.49	.68
OH	.12	−.11	−.16	−.16	−.16	−.03	.01	.00	−.02	.09
I[f]	.35	.55	.62	.62	.57	.49	.37	.40	.46	.79
CH_3[f]	−.07	−.09	−.06	−.10	−.10	−.09	−.12	−.14	−.14	−.13
NO_2[f]	.71	1.05	1.17	1.15	1.10	.93	.89	.97	1.06	1.56
CN	.52	0.83	0.97	.....	.....	.73	.....	.....	.....	1.30
Para-substituted benzoic acids										
Br	0.23	0.42	0.47	0.43	0.42	0.37	.....	0.38	0.43	0.60
Cl	.22	.34	.42	.39	.39	.30	.....	.38	.39	.56
F	.06	.18	.23	.21	.22	.17	0.15	.22	.25	.35
OH	−.38	−.53	−.55	−.57	−.57	−.45	−.42	−.47	−.53	−.32
I	.22	.39	.45	.45	.40	.36	.....	.38	.38	.59
OCH_3	−.27	−.36	−.32	−.36	−.36	−.32	−.33	−.32	−.36	−.34
CH_3	−.17	−.18	−.18	−.21	−.19	−.17	−.23	−.22	−.21	−.23
NO_2	.78	1.02	1.17	1.14	1.14	.96	.97	1.10	1.18	1.54
CN	.65	0.91	1.00	.....	.....	.82	.....	.....	.....	1.27

[a] pK, as usual, equals $-\log K_{\text{dissocn.}}$ $\Delta pK = pK'' - pK_0''$, where K_0'' is the ionization constant of benzoic acid and K'' is the ionization constant of the monosubstituted benzoic acid under consideration. The data given in table 1 were used in computing ΔpK.

[b] Log $K_{A_2B_0}$ is the same as log K''−log K_0''. These values are from the work of Kilpatrick and co-workers [47,6], and were obtained by an emf method. The ionic strength, μ, was mostly due to added lithium chloride. The original results have been rounded off to two decimal places.

[c] $\Delta\log K''$=log K''−log K_0''; this work, computed from data presented in table 1. As previously emphasized, here K'' and K_0'' are *association* constants.

[d] The dielectric constants of solvents, as stated in the original articles, are given in parentheses below the names.

[e] Indicates the acids the data for which were used in calculating equations pertaining to *ortho*-substituted acids (see table 8).

[f] Indicates the acids the data for which were used in calculating least-squares equations for the solid lines shown in figures 4 to 6. See table 8.

TABLE 8. *Slopes and intercepts of equation (14)*[a]

Solvent	Dielectric Constant	*meta*-Substituent		*ortho*-Substituent	
		Slope	Intercept	Slope	Intercept
Water	78.5	0.461	0	0.742	0.561
Methanol	31.5	.676	0.028	.690	.490
Ethanol	24.2	.730	.043	.694	.399
n-Propanol	20.1	.742	.015	.708	.394
n-Butanol	17.4	.715	−.011	.706	.355
Ethylene glycol	37.6	.606	.019	.670	.436
Dioxane-water	55	.594	−.042	.690	.378
Dioxane-water	40	.654	−.059	.690	.256
Dioxane-water	15	.707	−.042	.710	.122

[a] Equation 14 is $-\Delta pK$ (or log $K_{A_2B_0}$)=m(Δlog K'')+b. See further discussion in the text.

to methanol as a solvent. Moreover, further increases in slope occur on shifting successively to ethanol and *n*-propanol. Such results are to be expected, for as others have pointed out [48,50],[47] an equation of the form

$$\Delta W = e\mu\cos\theta/\epsilon r^2 \qquad (15)$$

expresses the increase in the work of ionic dissociation of an acid like benzoic acid upon the introduction of a polar substituent having only an electrostatic effect on the ionizing group. In eq (15) e is the charge on the ion; r is the distance from the substituent to the —COOH group; $\mu\cos\theta$ is the component of the electric moment of the substituent along r; and ϵ is the dielectric constant of the medium. ΔW is negative or positive in sign according as the substituent facilitates or makes more difficult the removal of the proton. The equation, as applied to *meta*-substituted benzoic acids, predicts that changing the solvent to one of lower dielectric constant should cause an increase in the strength relative to benzoic acid when the substituent is one that promotes ionization (for example, —Cl or —NO_2), but a decrease in strength relative to benzoic acid when a substituent such as —CH_3 is present in the ring.

[c] Also see [47,51].

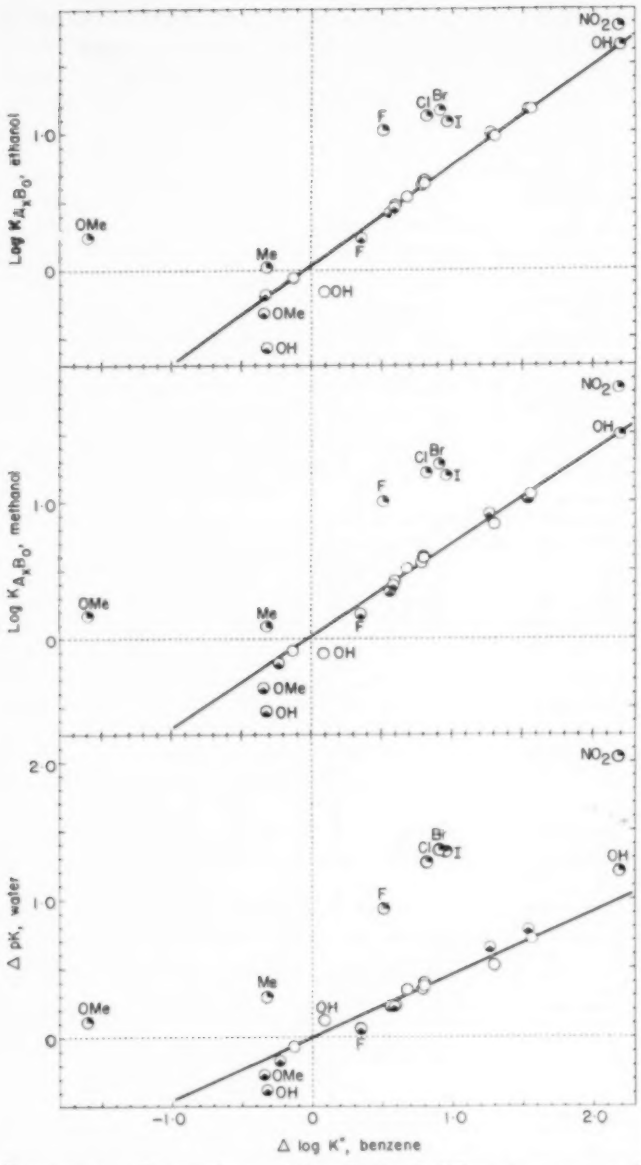

FIGURE 4. *Comparison of the effects of different o-, m-, and p-substitutions on the strength of benzoic acid in benzene, water, methanol, and ethanol at 25° C.*

See table 7 for data used. The symbols have the same significance as in figures 1 and 2.

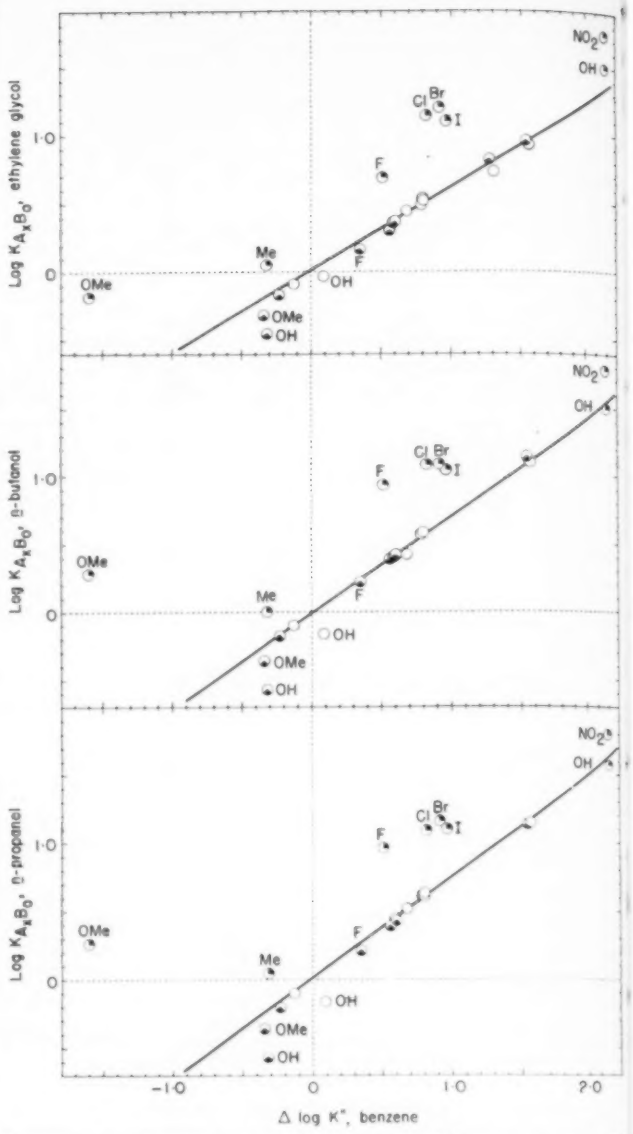

FIGURE 5. *Comparison of the effects of different o-, m-, and p-substitutions on the strength of benzoic acid in benzene, n-propanol, n-butanol, and ethylene glycol at 25° C.*

See table 7 for data used. The symbols have the same significance as in figures 1 and 2.

With the exception of *m*-hydroxybenzoic acid, figures 4 to 6 show close linearity of the strengths of *meta*-substituted acids in benzene and in the other solvents considered here. The existence of solvent effects on the acidic behavior of *m*-hydroxybenzoic acid was previously referred to (see footnote 34). Such effects are also noticeable in table 7 and figures 4 to 6. Thus, while *m*-hydroxybenzoic acid is stronger than benzoic acid in water, as well as in benzene, it appears to be decidedly weaker in all of the monohydric alcohols. On the other hand, the results for ethylene glycol or dioxane-water solutions indicate a strength differing very little from that of benzoic acid. A difference in the manner of hydrogen-bonding of the solvent to the substituent —OH group is possibly a factor in the differing solvent effects on the acidity. Such possibilities would include bonding of the two types:

(1) $HOOC{\cdot}C_6H_4{\cdot}OH \ldots OH_2$ and
(2) $HOOC{\cdot}C_6H_4{\cdot}O(\ldots HOH)H$

The former way, which seems likely to be favored because of the acidic character of a phenolic —OH, should increase the negative charge on the phenolic oxygen. Under such conditions, an enhancement of the acid-strengthening influence of *m*-OH could be expected. With hydrogen-bonding of type (2), however, a reduction of the acid-strengthening influence of *m*-OH could be looked for. In dioxane-water mixtures, perhaps extensive hydrogen-bond-

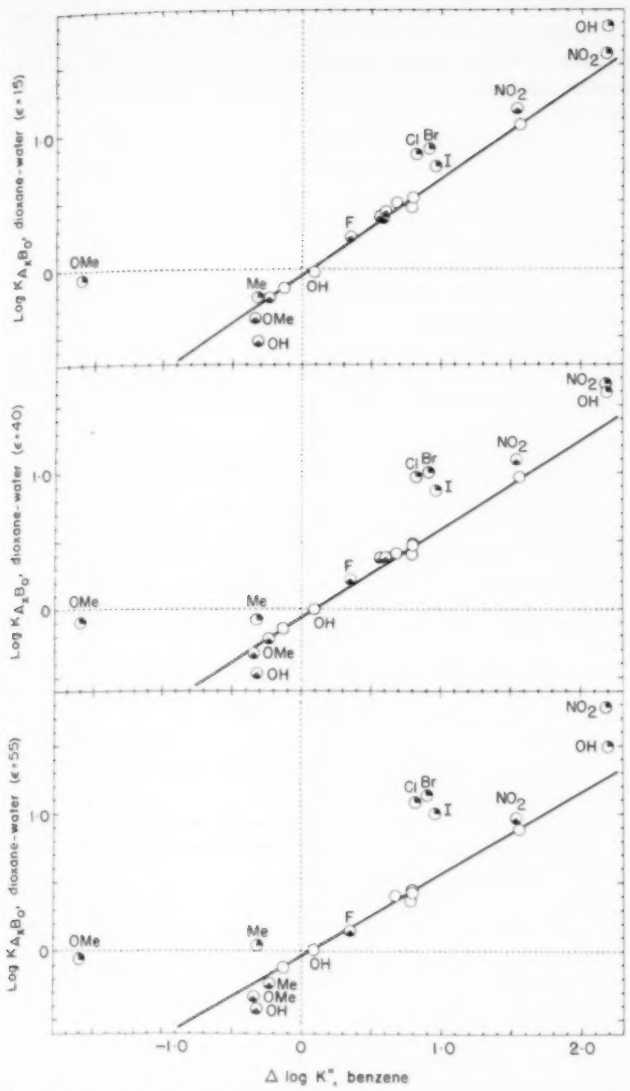

FIGURE 6. *Comparison of the effects of different o-, m-, and p-substitutions on the strength of benzoic acid in benzene and in three dioxane-water mixtures having the dielectric constants 55, 40, and 15, respectively; t=25° C.*

See table 7 for data used. The symbols have the same significance as in figures 1 and 2.

ing of dioxane with water [52] appreciably reduces solvation of the *m*-OH group.

b. *para*-Substituted Acids

Most of the *para*-substituted acids conform well to the norms indicated in figures 4 to 6. However, *p*-hydroxybenzoic acid is seen to be decidedly weaker in all of the alcohols and dioxane-water mixtures than in benzene. *p*-Methoxybenzoic acid shows the same weakening, but to a smaller degree. Hydrogen-bonding of solvent to the —OH or —OCH_3 group (compare 4.2.b and 4.3.a) offers a reasonable explanation for the reduced strength. A similar tendency for hydrogen-bonding to *p*-F seems indicated for water and all of the alcohols except *n*-butanol (figs. 4 and 5), although it is not evident for dioxane-water mixtures (fig. 6).

The points for *p*-nitrobenzoic acid suggest that its strength is anomalously great in water and in partly aqueous solvents, although not so in the alcohols. This conclusion, if correct, is understandable, as the six-membered ring formed by bonding of both hydrogens of water to the oxygens of the —NO_2 group should have greater stability than structures formed by hydrogen-bonding of alcohol molecules to the —NO_2 group. As mentioned above (section 4.2.c), the expected effect of solvation of the nitro group is enhancement of the acidity.

c. *ortho*-Substituted Acids

A glance at table 8 reveals that the slopes of eq (14), as calculated from data for *ortho*-substituted acids (see table 7), range from 0.69 to 0.71 except in one case—that in which *water* was the solvent being compared with benzene. The approximate constancy in slope contrasts sharply with the variation in slopes (from 0.46 to 0.71), previously noted for *meta*-substituted acids. This variation was shown (4.2.b) to be consistent with the thesis that the influence of *m*-substituents on the acidity of benzoic acid is principally electrostatic in nature. The near constancy of slope for *o*-substituted acids, irrespective of the dielectric constant of the solvent, indicates that the influence of *o*-substituents on —COOH is not solely an electrostatic effect. Instead, we must conclude—as so many others have done in studying effects of *ortho*-substitutions on various benzene side-chain reactions—that local effects such as steric hindrance and hydrogen-bonding are very important.

Figures 4 and 5 show that deviations of *o*-substituted acids from the norm are smaller in the case of alcohols than in the case of water. Furthermore, the general picture is much the same for all of the alcohols. However, increasing the dioxane content of dioxane-water mixtures (see fig. 6) has the effect of bringing the points for most of the *o*-substituted acids closer to the norm until in the dioxane-water solvent of lowest dielectric constant (15), the only major remaining deviation is in the case of *o*-methoxybenzoic acid. The chelation of *o*-methoxybenzoic acid obviously does not persist in solvents which, like the alcohols or dioxane-water, can become hydrogen-bonded to the —OCH_3 group.

Previously, in comparing relative strengths in benzene and water (see 4.2.d and fig. 2), the small displacement from the norm of the point for salicylic acid was assumed to indicate a reduced strength in benzene, and it was suggested that in benzene part of the acid may have a chelated structure analogous to that of *o*-methoxybenzoic acid. However, the points for salicylic acid are not displaced from the norms in the plots for the four monohydric alcohols (figs. 4 and 5). Therefore, an alternative explanation—hydrogen-bonding of solvent molecules to the *o*-OH group—should not be excluded in accounting for the departures from the norms observed for solutions in water, dioxane-water, and ethylene glycol.[48]

[48] This alternative explanation is in harmony with the suggestion (see p. 480 of [47(a)]) that the acid-strengthening type of chelation becomes favored as the number of hydroxyl groups in the solvent available for solvation of —COOH decreases (which occurs in alcohols as the dielectric constant decreases).

It seems desirable to reemphasize what we consider an especially important result of this investigation: the discovery that *o*-toluic acid shows normal acidity in benzene, instead of the anomalously high acidity exhibited when in aqueous solutions (4.2.d). This must mean that steric inhibition of resonance when in water—which seems the most reasonable of the explanations that have been offered for the enhanced acidity of this acid—results because solvent molecules become attached to the —COOH group. From figures 4 to 6 one would judge that solvation is most marked in water solutions. Evidently it falls off as increasing amounts of the water are replaced by dioxane, as shown by the progressive approach of the points for *o*-toluic acid to the lines representing norms. For the solvent that contained 73.5 weight-percent of dioxane ($\epsilon=15$) the point is very close to the norm.[49] In the alcohols the acidity of *o*-toluic acid appears to be much less enhanced by solvation of the —COOH group.[50]

To reiterate what was said above (4.2.d), the findings about *o*-toluic acid make it seem probable that hydration of the —COOH contributes rather generally to enhancement of the strengths of *ortho*-substituted benzoic acids when in water-containing solvents, because the added bulk promotes steric inhibition of resonance. In alcoholic solutions, also, solvation probably produces some steric inhibition of resonance, with consequent enhancement of acidity, but solvation by alcohols seems less prone to occur than solvation by water.

Our previous conclusion (4.2.d) that the reactivities of *o*-halobenzoic acids in benzene are reduced by internal hydrogen-bonding is further supported by the displacements to be noted in figures 4 to 6. Earlier it was suggested [53] that chelation of *o*-halobenzoic acids [51] occurs to an increasing extent with decreasing dielectric constant of the solvent, as in passing successively from water to methanol, then to ethanol. This would imply still greater chelation in benzene. However, a relationship of chelation to the hydrogen-bonding capacity of the solvent seems more probable than a relationship to the dielectric constant. To sum up the discussion of *o*-halobenzoic acids:

(1) Internal hydrogen-bonding (chelation) appears to be an important factor in the reductions in apparent acidity observed on changing from water to nonaqueous solvents such as those dealt with here. This conclusion seems to apply to *o*-fluoro- as well as to the other *o*-halobenzoic acids.

(2) For at least some of the group (those having an *o*-substituent comparable in bulk to $-CH_3$) steric inhibition of resonance consequent to solvation of the —COOH group may tend to augment the acidity in solvents of good solvating power—water in particular.

As to *o*-nitrobenzoic acid, solvation of the $-NO_2$ group by the solvent when in water may be of importance (compare 4.3.b), as well as the two factors suggested in accounting for solvent effects on *o*-halobenzoic acid. Here there seems to be somewhat less basis, however, for attributing an important role to chelation.

The literature on the acidic strengths of benzoic acids having the same group substituted in *both ortho*-positions is meager, even for aqueous solutions (compare footnotes o and q of table 1). In reviewing the work of other investigators we have noted only one case of such an acid—that of 2,4,6-trimethylbenzoic acid—in which the effect of a change of solvent (from water to *n*-butanol) on the acidity was measured [48]. Further studies of the sort should be valuable in judging how steric inhibition of resonance, and likewise hydrogen-bonding, affect the strengths of benzoic acids.

This section may be concluded by citing a few important pioneering studies [48, 49, 54] by authors who clearly recognized that changes of solvent may markedly alter relations in the strengths of acids, notably such acids as *o*-substituted benzoic acids. Their observations and conclusions, though more fragmentary, were in general harmony with those which have been presented above.

4.4. Correlations With Other Spectral Data

a. Ultraviolet Data

Of late years there has been a marked growth of interest in the study of steric effects on the electronic spectra of conjugated systems. Included in these studies have been some attempts to correlate ultraviolet absorption spectra of substituted benzoic acids with the nature and position of substituent groups. In one such study, with dioxane as the solvent, it was concluded that steric inhibition of resonance occurs in 2,6-dichlorobenzoic acid, but not appreciably in 2,4-dichlorobenzoic acid [55]. Later, in a more comprehensive study, ultraviolet absorption curves were obtained for benzoic acid itself and the derivatives *o*-, *m*-, and *p*-monosubstituted and 2,6-disubstituted with $-CH_3$, —Cl, —Br, $-OCH_3$, or —OH, all in 95-percent ethanol [56]. Still more recently, data have been obtained for absolute ethanol solutions of the benzoic acids substituted in the *o*-, *m*-, and *p*-positions with —F, —I, and $-NO_2$ [57(a)]. In most cases these acids were found to exhibit three absorption bands in the ultraviolet region, which have been designated as the A, B, and C bands [56]. Of these bands, the B-band (located in the vicinity of 230 mμ) seems most sensitive to steric effects of substituents. The C-band seems to be comparatively insensitive to small steric effects, but sensitive to hydrogen-bonding [56, 57].

The ultraviolet absorption spectra of *meta*-substituted acids show a general resemblance to the spectrum of benzoic acid, but with slightly decreased absorption intensity attributed to inductive effects. The B-band of *para*-substituted acids shows a considerable bathochromic shift from its position in benzoic acid, the extent of the shift paralleling approximately the mesomeric (resonance) effect of the substituent, and the intensity of the B-band

[49] The marked reduction in the strength of *o*-toluic acid in the two dioxane-water solvents of lowest dielectric constant was noted earlier [47 (d)] (also see [53]). However, no explanation could be offered at that period.

[50] Enhancement of acidity resulting from solvation of the $-CH_3$ group seems improbable.

[51] And also of *o*-nitrobenzoic acid. Chelation of *o*-fluorobenzoic acid was considered unlikely, however.

also shows marked enhancement; here, the inductive effect seems to be of secondary importance [56, 57].[52]

In the most recent analyses of the effects of steric hindrance on B-bands the following assumptions have been made [57]:

(1) *o*-Disubstituted derivatives (when in neutral solutions) would have approximately the same absorption as that of their *p*-isomers were it not for steric interference with resonance.

(2) Three types of steric effects can be distinguished—(a) Reduced intensity of absorption, produced when steric interference is slight; (b) a shift in the wavelength of absorption, accompanied by reduced intensity, caused by a somewhat greater degree of steric interference; (c) more or less complete disappearance of the B-band,[53] when steric effects are large.

In line with these assumptions, the benzoic acids with a single *ortho*-substituent generally exhibit steric interference of type (b), whereas the effect of di-*ortho*-substitution is of type (c) [55 to 57]. For details the reader is referred to the papers cited.

However, one point merits special attention here: the puzzling spectral behavior of *o*-toluic acid [57 (a)].[54] *o*-Methylacetophenone, where the —OH of *o*-toluic acid is replaced by $-CH_3$, shows little evidence of steric hindrance to resonance, and it therefore seemed surprising that the alcoholic absorption spectrum of *o*-toluic acid, when compared with that of *p*-toluic acid, exhibits a pronounced hypsochromic shift of the B-band together with marked reduction in the intensity of absorption. To account for this discrepancy the usual explanation of the steric effect due to an *o*-substituent had to be modified [57 (a)]. Now the evidence obtained in this investigation (4.3.c) that steric inhibition of resonance in *o*-toluic acid is evident only when the solvent (water, alcohols) is one which would tend to solvate the —COOH group appears applicable to the problem of interpreting the ultraviolet absorption spectrum of *o*-toluic acid when in alcoholic solution. It seems likely that solvent effects on ultraviolet absorption—which are evident even for benzoic acid [59]—will prove to be still more noticeable for *o*-toluic and other *o*-substituted acids, and that further progress in the correlation of ultraviolet spectra and steric interferences can be accelerated by accumulation of data for solutions in hydrocarbon solvents.

b. Infrared Data

Goulden measured OH-vibration frequencies of 67 carboxylic acids and phenols in dilute carbon tetrachloride solutions at 25° C, to determine whether the frequencies could be correlated with the aqueous *pK* values [42] (see footnote 43). Four correlations of OH-frequencies with *p*H values were discovered—one for the phenols and three for carboxylic acids.

[52] The spectra of *m*- and *p*-nitro- and iodobenzoic acids are irregular, showing dominating effects of the $-NO_2$ and —I groups [57(a)].

[53] The absorption bands characteristic of separate chromophoric groups in a molecule disappear when the chromophores become conjugated, being replaced by a "conjugation" band [58], here referred to as the B-band. When the B-band disappears because of steric inhibition of resonance the separate bands are observed.

[54] Also see p. 807 of [56].

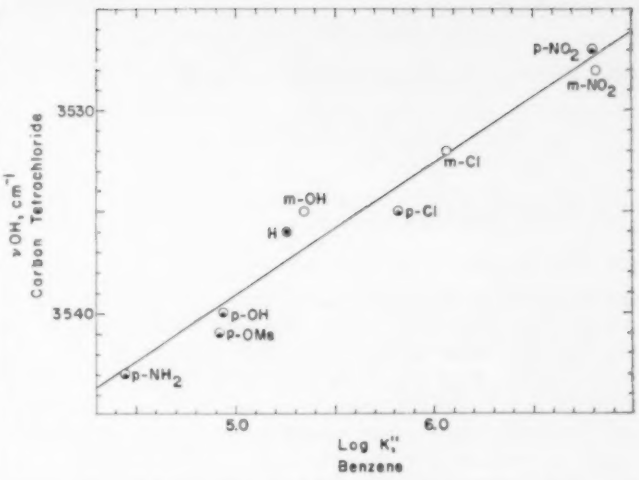

FIGURE 7. *Relationship of* OH-*vibration frequencies of m- and p-substituted benzoic acids when dissolved in carbon tetrachloride and the log K'' values for combination with diphenylguanidine in benzene. t=25° C.*

The carboxylic acids were divided into the following types: (1) Those containing $-C{=}C-COOH$. This included unsaturated aliphatic, naphthoic, cinnamic, and substituted benzoic acids. (2) The $R_3C-COOH$ type, where R=alkyl, halogen, phenoxy, or methoxy. (3) The type $-C{=}C-CH_2-COOH$.

Nine of the benzoic acids (all *m*- or *p*-substituted) included in Goulden's study were the same as ones included in this study. Figure 7 shows the correlation of the OH-vibration frequencies [55] with the log K'' values obtained in this work. The degree of linearity is excellent considering the experimental uncertainties in both sets of measurements.

Although measurement of the OH-vibration frequencies of *o*-substituted benzoic acids in carbon tetrachloride was not undertaken, because a good correlation with the aqueous *pK* values was not to be expected, it is to be hoped that such infrared data will become available. They should be valuable in accounting for solvent effects on the acidic behavior of *o*-substituted benzoic acids.

Thompson and Steel [60] computed the logarithms of the intensities of the fundamental vibration bands of the —CN group in various *m*- and *p*-substituted benzonitriles, and found good linearity of the values with the Hammett σ values. They suggested that it may be "legitimate" to read off from their plots the σ values corresponding to the band intensities observed for five *ortho*-substituted benzonitriles. In a similar way the Δ log *K''* values and the value for ρ (2.17) (see footnote 30), obtained in this investigation can be used to deduce σ values for *ortho* substituents. Table 9 compares the five values deduced by Thompson and Steel with the corresponding values derived from data given in this paper. Both methods of estimating σ give almost the same results for o-CH_3, o-Cl, and o-NO_2. Good agreement in the two sets of values for o-NH_2 and

[55] These were thought to be accurate to ± 1 cm^{-1} for most acids, and ± 2 cm^{-1} for the more difficultly soluble ones [42].

TABLE 9. *Hammett sigma values deduced for ortho substituents*

ortho substituent	σ value, ref. 60	σ value, this work
NH_2	−0.35	−0.15
OH	−.2	+1.01
CH_3	−.1	−0.15
Cl	+.4	+.38
NO_2	+.95	+1.00

o-OH is not to be expected in view of the evidence of hydrogen bonding with the —COOH group in anthranilic and salicylic acids. However, on the assumption that the influence of $-NH_2$ or —OH is largely governed by resonance and is about the same in the *ortho* and *para* positions [61], one may estimate σ values for *o*-NH_2 and *o*-OH from the log *K''* values for *p*-amino- and *p*-hydroxybenzoic acids. These values (respectively, −0.37 and −0.15) are strikingly similar to the values deduced by Thompson and Steel.

4.5. Summary and Concluding Remarks

Hitherto no method has existed for measuring the relative strengths in benzene of acids comparable in strength to benzoic acid. This paper has described a spectrophotometric method, using 1,3-diphenylguanidine and bromophthalein magenta E as special reagents, for securing such information. The results, which were obtained at 25° C, are expressed as equilibrium constants for association with diphenylguanidine. The acids for which measurements were made were benzoic acid itself, 31 of its monosubstituted derivatives (including all of the acids substituted in the *o*, *m*-, or *p*- positions with $-NH_2$, —Br, —Cl, —F, —OH, —I, $-OCH_3$, $-CH_3$, or $-NO_2$) and eight di- or tri-substituted benzoic acids (including acids with —Cl, $-OCH_3$, or $-CH_3$ in both *ortho*-positions).

The relative strengths of the benzoic acids in benzene have been compared with previously published data (obtained by electrochemical methods) on the relative strengths in water, methanol, ethanol, *n*-propanol, *n*-butanol, ethylene glycol, and three dioxane-water mixtures. In the case of the *meta*-substituted acids, except for *m*-hydroxybenzoic acid, an exact order of relative strengths is preserved in all of the solvents mentioned, supporting previous evidence that the electrostatic effect of the substituent is the dominating influence on the acidity. Irregularities in the behavior of *m*-hydroxybenzoic acid are attributed to hydrogen-bonding with solvent molecules. For *para*-substituted acids, also, a constant relation of strengths is generally preserved in the solvents in question, but here there is evidence that solvation of the substituent sometimes increases and sometimes decreases its influence on the acidity. The relative acidities measured in benzene for these two groups of acids are thought to reflect the intrinsic acidities more accurately than the acidities measured in the other solvents mentioned.

Previous investigators have recognized that a group of acids that includes *ortho*-substituted benzoic acids is likely to show inversions in the order of strengths when the solvent is changed—even when the change is to a solvent of closely similar type (as, for example, in changing from water to a lower alcohol). Comparisons made in this paper of relative strengths in the various solvents have led to several conclusions, prominent among which are the following:

(1) Hydration of the —COOH group appears to enhance the acidic behavior of *ortho*-substituted acids in water. Thus, *o*-toluic acid, which is recognized as being anomalously strong in water, shows normal acidic behavior in benzene. This conclusion has a bearing on attempts to relate apparent acidities with structure or with spectral absorption in the ultraviolet region.

(2) Internal hydrogen-bonding (chelation) markedly depresses the reactivity of *o*-methoxybenzoic acid as an acid when in benzene. The chelated structure has little or no tendency to persist in solvents with hydrogen-bonding capacity.

(3) *o*-Halobenzoic acids appear relatively weaker in benzene than in the other solvents, although the effect is much less marked than with *o*-methoxybenzoic acid. This weakening is probably partly caused by a tendency toward chelation in benzene. Infrared evidence on this question is needed. An enhancement of acidity in water by hydration of the —COOH group also appears probable.

(4) A still smaller tendency toward chelation seems evident for *o*-nitrobenzoic acid. There also appears to be enhancement of the acidity in aqueous solvents. Here, hydration of the $-NO_2$ group seems a probable factor.

(5) The effect of a second *ortho*-substitution on the acidity, as indicated by the available data—which exist only for a few acids, in the solvents water and benzene—is far from additive. Further study of such acids is needed for improved understanding of steric effects on acidity (as well as on spectral absorption).

It seems desirable to underline the conclusion that the acidities measured in water do not provide a completely accurate scale of relative intrinsic strengths. The proton, to be sure, is very minute in size, but one should bear in mind that it does not exist in solutions as an independent entity. Water, because of its great hydrogen-bonding capacity, can not only solvate the proton (with four water molecules per proton, according to the most recent estimate) but also can solvate substituents in the benzoic acid molecule, as well as the —COOH group, with consequent modifications of electrostatic, resonance, and steric effects. The most complete understanding of the relation of structure and acidity can be gained by systematic measurements in solvents of varied types.

Another point to be noted is that information on interactions of colorless acids and bases can be ob-

tained spectrophotometrically by measurements in the visible region, as well as by measurements in the infrared or ultraviolet. The possibility of measurements in the visible region greatly extends the range of solvents that can be used. An indicator dye of suitable characteristics is needed, of course, and a suitable reference base must also be available. Further studies in all of the spectral regions are very desirable.

No reader should be left with the impression that benzoic acids are exceptional in showing inversions in the order of strength on changes of solvent. There is much additional evidence in the literature of solvent effects on relative acidities. For example, the effect of changes of solvent may be different for groups such as cation acids (with some divisions into subgroups), phenols, aliphatic acids, and aromatic acids. One of the most comprehensive reviews on effects of solvents on the strengths of acids was published in a Russian periodical [62]. The existence of such varied solvent effects indicates that no exact, universally valid scale of relative strengths can be constructed. However, in various areas of limited scope acidity scales of practical usefulness should be obtainable. Studies of relative acidities in various solvent media should be helpful in defining such areas.

Finally, the studies reported here, although they represent only the beginning of an effort to gain needed information about acid-base interactions in solvents like benzene, point to a few applications of immediate practical interest. Thus, the solvent effects on acidity which create problems in the construction of practical acidity scales may be turned to advantage in effecting separations and in selecting conditions for obtaining more distinct end-points in titrations of mixtures. A possible application of the method described here is in getting a quick estimate of the acidity of an acid, especially of an acid almost insoluble in water (see 3.2). Such measurements consume only a minute quantity of acid—usually less than a centigram. One more suggested application is in estimating the dimer-monomer equilibrium constants of carboxylic acids in benzene, as illustrated in 4.1. Table 3 illustrates the serious need for such data.

Special thanks are due to the Heyden Chemical Corp. for the 3,4-dichlorobenzoic acid and to the National Aniline Division of Allied Chemical and Dye Corp. for the *m*-dimethylaminobenzoic acid used in this work; to Priscilla J. Schuhmann for assistance in some of the purifications and in the exploratory experiments that preceded this investigation; to Maya Paabo for assistance in the study of the dimer-monomer equilibrium of benzoic acid (see 4.1); to A. A. Maryott for helpful information about measurements of the dimer-monomer equilibria of carboxylic acids by the electric polarization method; and to W. J. Youden for statistical analyses of data.

5. References

[1] (a) M. M. Davis and P. J. Schuhmann, J. Research NBS **39,** 221 (1947) RP1825.
(b) M. M. Davis, P. J. Schuhmann, and M. E. Lovelace, J. Research NBS **41,** 27 (1948) RP1900.
(c) M. M. Davis and E. A. McDonald, J. Research NBS **42,** 595 (1949) RP1997.
(d) M. M. Davis, J. Am. Chem. Soc. **71,** 3544 (1949).
(e) M. M. Davis and H. B. Hetzer, J. Research NBS **46,** 496 (1951) RP2219.
(f) M. M. Davis and H. B. Hetzer, J. Research NBS **48,** 381 (1952) RP2326.
(g) M. M. Davis and H. B. Hetzer, J. Am. Chem. Soc. **76,** 4247 (1954).
(h) M. M. Davis and H. B. Hetzer, J. Research NBS **54,** 309 (1955) RP2593, sec. 4.5.
[2] J. F. J. Dippy and R. H. Lewis, J. Chem. Soc. **1936,** 644.
[3] T. Sandmeyer, Ber. deut. chem. Ges. **18,** 1496 (1885).
[4] E. P. Valby and H. J. Lucas, J. Am. Chem. Soc. **51,** 2718 (1929).
[5] S. Wideqvist, Arkiv Kemi **2,** 383 (1950).
[6] M. Kilpatrick and R. D. Eanes, J. Am. Chem. Soc. **65,** 589 (1943).
[7] P. Kattwinkel and R. Wolffenstein, Ber. deut. chem. Ges. **34,** 2423 (1901).
[8] H. T. Clarke and E. R. Taylor, Organic syntheses, collective volume II, p. 135 (A. H. Blatt, ed.; John Wiley & Sons, Inc., New York, N. Y., 1943).
[9] M. M. Davis and H. B. Hetzer, J. Phys. Chem. **61,** 123 (1957).
[10] M. M. Davis and H. B. Hetzer, J. Phys. Chem. **61,** 125 (1957).
[11] (a) A. Bistrzycki and S. von Kostanecki, Ber. deut. chem. Ges. **18,** 1983 (1885).
(b) J. Herzig and F. Wenzel, Monatsh. Chem. **27,** 781 (1906).
[12] L. Hunter and J. A. Marriott, J. Chem. Soc. **1941,** 777.
[13] N. E. White and M. Kilpatrick, J. Phys. Chem. **59,** 1044 (1955).
[14] G. Allen and E. F. Caldin, Quart. Revs. (London) **7,** 255 (1953).
[15] (a) J. J. Fox and A. E. Martin, Nature **143,** 199 (1939).
(b) J. J. Fox and A. E. Martin, Trans. Faraday Soc. **36,** 897 (1940).
[16] M. Davies and D. M. L. Griffiths, J. Chem. Soc. **1955,** 132. See also M. Davies, Chem. & Ind. (London) **1953,** 614.
[17] A. A. Maryott, J. Research NBS **38,** 527 (1947) RP1794.
[18] S. Kaufman and C. R. Singleterry, J. Phys. Chem. **56,** 604 (1952).
[19] G. M. Barrow and E. A. Yerger, J. Am. Chem. Soc. **76,** 5211 (1954).
[20] A. Weissberger and K. Fasold, Z. physik. Chem. (Leipzig) [A] **157,** 65 (1931).
[21] S. Bodforss, Kgl. Fysiograf. Sällskap. Lund, Förh. **19,** 55 (1949).
[22] W. A. Waters, Physical aspects of organic chemistry (D. Van Nostrand Co., New York, N. Y., 5th ed., 1954).
[23] H. B. Watson, Modern theories of organic chemistry (Oxford University Press, London, England, 2d ed., 1941).
[24] (a) J. F. J. Dippy, Chem. Revs. **25,** 151 (1939).
(b) J. F. J. Dippy, S. R. C. Hughes, and J. W. Laxton, J. Chem. Soc. **1954,** 1470.
[25] G. E. K. Branch and M. Calvin, The theory of organic chemistry (Prentice-Hall, Inc., New York, N. Y., 1941).
[26] C. K. Ingold, Structure and mechanism in organic chemistry (Cornell University Press, Ithaca, N. Y., 1953).
[27] H. C. Brown, D. H. McDaniel, and O. Häfliger, Dissociation constants, chapter 14 in Determination of organic structures by physical methods, edited by F. C. Nachod and E. A. Braude (Academic Press, Inc., New York, N. Y., 1955).

[28] (a) J. D. Roberts and W. T. Moreland, Jr., J. Am. Chem. Soc. **75,** 2167 (1953).
(b) J. D. Roberts and R. A. Carboni, J. Am. Chem. Soc. **77,** 5554 (1955).
[29] G. E. K. Branch and D. L. Yabroff, J. Am. Chem. Soc. **56,** 2568 (1934).
[30] W. Baker, Nature **137,** 236 (1936).
[31] (a) L. P. Hammett, Chem. Revs. **17,** 125 (1935).
(b) L. P. Hammett, J. Am. Chem. Soc. **59,** 96 (1937).
(c) L. P. Hammett, Trans. Faraday Soc. **34,** 156 (1938).
(d) L. P. Hammett, Physical organic chemistry, chapter 7 (McGraw-Hill Book Co., New York, N. Y., 1940).
[32] H. H. Jaffé, Chem. Revs. **53,** 191 (1953).
[33] A. M. Liquori and A. Ripamonti, Gazz. chim. ital. **85,** 578 (1955).
[34] (a) E. J. Cohn, T. L. McMeekin, J. T. Edsall, and M. H. Blanchard, J. Am. Chem. Soc. **56,** 784 (1934).
(b) E. J. Cohn and J. T. Edsall, Proteins, amino acids, and peptides as ions and dipolar ions (Reinhold Publishing Co., New York, N. Y., 1943).
[35] H. Kloosterziel and H. J. Backer, J. Am. Chem. Soc. **74,** 5806 (1952).
[36] (a) W. Gordy and S. C. Stanford, J. Am. Chem. Soc. **62,** 497 (1940).
(b) W. Gordy, J. Chem. Phys. **8,** 516 (1940).
[37] A. E. Kellie, D. G. O'Sullivan, and P. W. Sadler, J. Org. Chem. **22,** 29 (1957).
[38] M. L. Huggins, J. Org. Chem. **1,** 407 (1936).
[39] J. F. Norris and W. H. Strain, J. Am. Chem. Soc. **57,** 187 (1935).
[40] H. O. Jenkins, J. Chem. Soc. **1939,** 640.
[41] L. Pauling, The nature of the chemical bond (Cornell University Press, Ithaca, N. Y., 1st ed., 1939; 2d ed., 1940).
[42] J. D. S. Goulden, Spectrochim. Acta **6,** 129 (1954).
[43] H. O. Jenkins, J. Chem. Soc. **1939,** 1137.
[44] (a) O. R. Wulf and U. Liddel, J. Am. Chem. Soc. **57,** 1464 (1935).
(b) L. Pauling, J. Am. Chem. Soc. **58,** 94 (1936).
(c) O. R. Wulf, U. Liddel, and S. B. Hendricks, J. Am. Chem. Soc. **58,** 2287 (1936).
(d) W. F. Anzilotti and B. C. Curran, J. Am. Chem. Soc. **65,** 607 (1943).
(e) G. Rossmy, W. Lüttke, and R. Mecke, J. Chem. Phys. **21,** 1606 (1953).
[45] D. H. McDaniel and H. C. Brown, J. Am. Chem. Soc. **77,** 3756 (1955).
[46] E. N. Lassettre, Chem. Revs. **20,** 259 (1937).
[47] (a) J. H. Elliott and M. Kilpatrick, J. Phys. Chem. **45,** 454, 466, 472, 485 (1941).
(b) J. H. Elliott, J. Phys. Chem. **46,** 221 (1942).
(c) M. Kilpatrick, Chem. Revs. **30,** 159 (1942).
[48] L. A. Wooten and L. P. Hammett, J. Am. Chem. Soc. **57,** 2289 (1935).
[49] W. F. K. Wynne-Jones, Proc. Roy. Soc. (London) [A] **140,** 440 (1933).
[50] A. Eucken, Angew. Chem. **45,** 203 (1932).
[51] G. Schwarzenbach and H. Egli, Helv. Chim. Acta **17,** 1183 (1934).
[52] W. Gordy, J. Chem. Phys. **4,** 769 (1936).
[53] M. Kilpatrick and W. H. Mears, J. Am. Chem. Soc. **62,** 3051 (1940).
[54] W. L. Bright and H. T. Briscoe, J. Phys. Chem. **37,** 787 (1933).
[55] S. D. Ross, J. Am. Chem. Soc. **70,** 4039 (1948).
[56] C. M. Moser and A. I. Kohlenberg, J. Chem. Soc. **1951,** 804.
[57] (a) W. F. Forbes and M. B. Sheratte, Can. J. Chem. **33,** 1829 (1955).
(b) W. F. Forbes and W. A. Mueller, Can. J. Chem. **34,** 1340 (1956).
(c) W. F. Forbes and A. S. Ralph, Can. J. Chem. **34,** 1447 (1956).
[58] A. Burawoy, J. Chem. Soc. **1939,** 1177.
[59] H. E. Ungnade and R. W. Lamb, J. Am. Chem. Soc. **74,** 3789 (1952).
[60] H. W. Thompson and G. Steel, Trans. Faraday Soc. **52,** 1451 (1956).
[61] R. W. Taft, Jr., J. Am. Chem. Soc. **74,** 3120 (1952).
[62] N. A. Izmaĭlov, Zhur. Fiz. Khim. **24,** 321 (1950). See also Chem. Abst. **44,** 6706 (1950).

WASHINGTON, September 10, 1957.

Journal of Research of the National Bureau of Standards Vol. 60, No. 6, June 1958 Research Paper 2872

Shape of the Liquidus Surface as a Criterion of Stable Glass Formation

Edgar H. Hamilton and Given W. Cleek

The slope of the liquidus curve or surface at a point in a phase diagram representing a specific chemical composition has been found to be a reliable indication of the glass-forming tendency of that composition. The observed effect is interpreted in terms of the structure of the glass.

1. Introduction

The structure of glass has been the subject of much discussion, but no theory has been propounded that will explain all the known facts about glass. Much of the present theory is based on the assumption of a continuous and completely random network as developed by Zachariasen [1][1] and considered to be confirmed by Warren and his associates [2]. Supporters of the network theory associate discontinuities and anomalies in properties with the "silicon to oxygen ratio", number of "single-bonded" oxygen ions, polarizability of ions, deformability of the large O^{2-} ions and changes in coordination number, particularly of the boron ion. While discontinuities in physical properties may be explained in terms of these concepts, some evidence has been presented indicating a structural arrangement in glass other than a random three-dimensional network.

A number of investigators, including Faick and Finn [3], Glaze, Young, and Finn [4], and Preston and Turner [5] have found evidence suggesting the existence of compounds in Na_2OSiO_2 glasses. Huggins [6] has presented his "structon" theory and Tilton [7] his "vitron" theory, both based on data on silicate glasses.

In the present paper some observations on the stability of glasses as indicated by the shape of the liquidus surface or curve will be discussed. Throughout the paper, glass stability means resistance to crystallization.

Grauer and Hamilton [8] have pointed out that in any study of glass stability one must take into account (1) the liquidus temperature or maximum temperature at which equilibrium exists between the glass and the primary crystalline phase and (2) the rates of crystal growth at various temperatures. The rate of crystal growth at the liquidus temperature is zero, it reaches a maximum at some lower temperature, and then approaches zero as the temperature is further reduced. Because the melt must be cooled through these temperatures during fabrication and annealing, the rate of crystal growth is of practical as well as theoretical importance.

2. Experimental Procedure

In the course of the development of new optical glasses for various purposes, data have been collected on a large number of systematically arranged series of glasses. Most of the series are in the following systems: BaO-B_2O_3-SiO_2 [9], BaO-BeO-B_2O_3-SiO_2 [10], Na_2O-TiO_2-SiO_2 [11], BaO-TiO_2-SiO_2 [12], ZnO-B_2O_3-SiO_2 [11], BaO-La_2O_3-SiO_2 [11], BaO-Ta_2O_5-SiO_2 [11], and multicomponent glasses, including rare-earth oxide glasses based on the above systems. Data were also collected on a number of series of multicomponent glasses that had base compositions in the CaO-MgO-Al_2O_3-SiO_2 system. The latter series of glasses contained from 0 to 12 mole percent of SiO_2. The glasses were developed by the partial substitution of one oxide for another in a base composition on a mole for mole basis, i. e. one La_2O_3 for one BaO.

The change in liquidus temperature as a function of SiO_2 content when SiO_2 is substituted for B_2O_3 in the BaO-B_2O_3-SiO_2 glasses is plotted in figure 1. The letters under each curve indicate the primary phase, which crystallizes at the liquidus. Similar curves for the change in liquidus temperature as a function of BaO content when BaO is substituted for TiO_2 in the BaO-TiO_2–SiO_2 glasses are given in figure 2. The primary phases have not been identified in this system, and consequently the curves as drawn may be subject to revision when the primary phases are known.

The details of the procedure of melting and annealing the glasses have been published elsewhere [12]. Briefly, the procedure is as follows: The glasses were made in 500- to 600-g melts in platinum crucibles. The melts were stirred with platinum–10-percent-rhodium propeller-type stirrers to obtain homogeneity. Compositions that could not be cooled as homogeneous glasses in blocks 3 by 3 by ½ to ⅝ in. in size are not here considered to be glass forming. The size of the block will affect the cooling rate of the glass in the interior, which in turn will affect the range of glass formation. Many compositions that can be melted in small melts and then cooled in thin pieces as homogeneous glasses would consist of a mass of crystals and glass under the conditions for glass formation discussed above.

3. Discussion

Hamilton, Cleek, and Grauer [9] observed that for a given system, the composition ranges of most stable glass formation are found in the primary fields that have relatively flat liquidus surfaces. These authors suggest that the glasses may contain

[1] Figures in brackets indicate the literature references at the end of this paper.

units of the same compositions as the compounds indicated by the vertices of the composition triangles of the phase diagram of the system. The relation between relatively flat liquidus fields and stable glasses has been observed for the $3BaO{\cdot}3B_2O_3{\cdot}2SiO_2$ primary field in the BaO-B_2O_3-SiO_2 system [9], $BaO{\cdot}TiO_2{\cdot}2SiO_2$ in the BaO-TiO_2-SiO_2 system [12], and $ZnO{\cdot}B_2O_3$ in the ZnO-B_2O_3-SiO_2 system [11]. Similar observations have been made on the rare-earth–barium-crown [10] and Na_2O-TiO_2-SiO_2 glasses [11] for which phase diagrams are not available. In the development at the Bureau of new optical glasses, such as the rare-earth–barium-crown glasses and barium-titanium silicate infrared-transmitting glasses, the liquidus curves have been very valuable guides.

Compounds which have flat liquidus fields possess a high degree of dissociation at the liquidus [13]. The flatter the liquidus field, the more highly dissociated will be the primary phase. Then, if the other factors that affect the rate of crystallization are equal, the less will be the tendency for crystal formation during the cooling of the melt to glass, because it is necessary for the primary compound to reassociate before crystals can form. Of course other factors, such as viscosity, polarizability, etc., would affect the rate at which the molecules reassociate and then orient themselves and continue to associate to form crystals.

Another factor that affects the stability of the glasses is the presence of, and also the amount of, phases other than the primary phase in the melt. In composition ranges where part of the liquidus surface is steep and two curves intersect to form a minimum, the most stable glasses are found near the minimum and on the side of the minimum with the lesser slope (see figs. 1 and 2). In the vicinity of the minimum, the percentage of the primary phase is approaching a minimum and the percentage of the other compounds present, a maximum. This does not mean that the percentage of the primary compound is approaching zero, for after the minimum is passed the amount of this compound will continue to decrease, but it will no longer be the primary phase because on passing the minimum, a new primary field is entered.

As the compositions change along a steep slope, the difficulties encountered in cooling the melts as glasses increase until homogeneous glasses can be obtained, if at all, only by drastic quenching of the melt. The liquidus curves are also solubility curves and indicate the change in solubility of the primary phase in the melt with change in temperature. As the melt is cooled below the liquidus, it will become supersaturated with respect to the primary phase, and crystallization can take place. The steeper the curve and the higher the composition is located on the curve, the greater the amount of supersaturation and the greater the probability of crystallization. The ease and greatly increased rates of crystallization of melts of compositions on steep curves over melts with compositions on flat curves or flat liquidus fields suggest the presence in the former of molten species of the same chemical compositions as the crystals that form so rapidly.

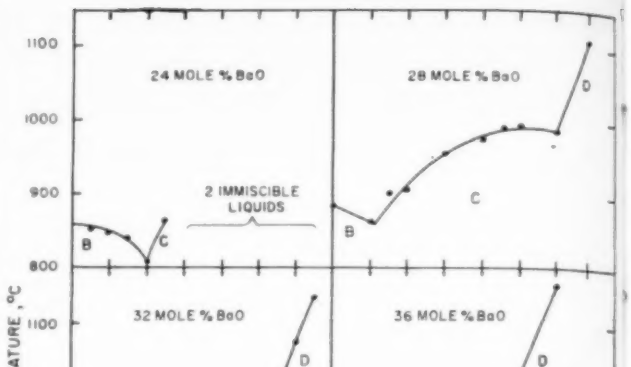

FIGURE 1. *Changes in liquidus temperature as a function of* SiO_2 *content of glasses in the* BaO-B_2O_3-SiO_2 *system; change in composition obtained by the substitution of* SiO_2 *for* B_2O_3 *on a mole for mole basis.*

Primary phases are indicated by the following symbols: A, $BaO{\cdot}B_2O_3$; B, $BaO{\cdot}2B_2O_3$; C, $3BaO{\cdot}3B_2O_3{\cdot}2SiO_2$; D, $BaO{\cdot}2SiO_2$. Solid solution is between $2BaO{\cdot}3SiO_2$ and $BaO{\cdot}2SiO_2$.

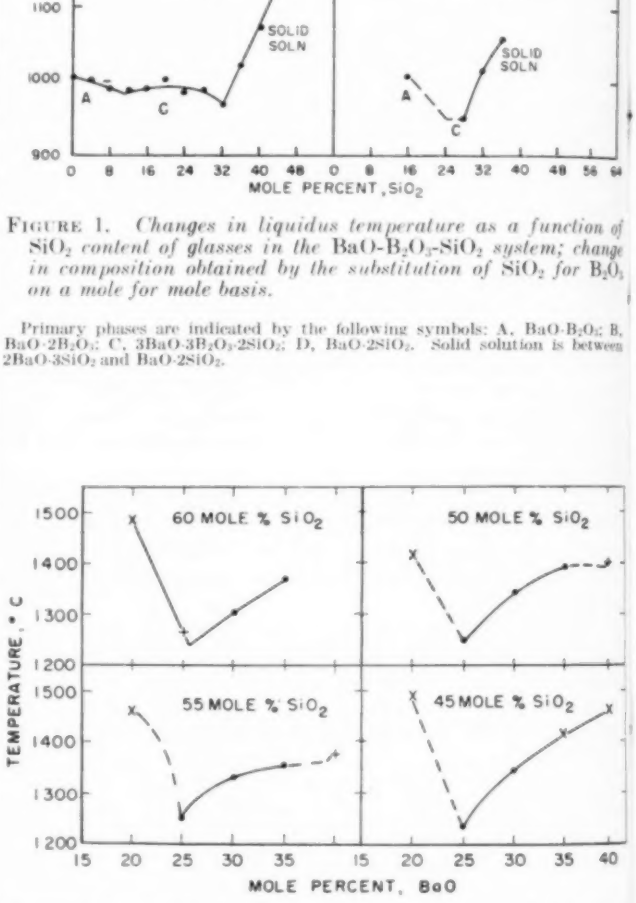

FIGURE 2. *Change in liquidus temperature as a function of* BaO *content for some glasses in the* BaO-TiO_2-SiO_2 *system; change in composition obtained by the substitution of* BaO *for* TiO_2 *on a mole for mole basis.*

●, All glass; +, small amount of crystals present; ×, devitrified, opaque.

The foregoing observations apply equally well to all the glass systems that have been studied by the authors. Because of the unusual shape of part of the glass-forming area in the BaO-TiO_2-SiO_2 system, it has been chosen to illustrate the relation between glass formation and the chemical compositions of structural entities or units. The properties of the glasses in this system were reported by Cleek and Hamilton [12], and the glass-forming compositions are indicated in figure 3. SiO_2 is the only oxide in the system that can form a glass and therefore can be rightfully called a glass-former. If SiO_2 alone is responsible for glass formation in this system, it is to be expected that the glass-forming area would be continuous along the $BaO{\cdot}TiO_2$-SiO_2 join to the SiO_2 vertex. However, such is not the case. Hence it is necessary to explain why, along the $BaO{\cdot}TiO_2$-SiO_2 join, glasses are formed only in the narrow composition range of 40 to 50 mole percent of SiO_2, and in particular, why, as SiO_2 is increased slightly to 52.5 mole percent or more, a mixture of glass and crystals is obtained. The phase diagram of the $BaO{\cdot}TiO_2$-SiO_2 system [14] suggests a simple explanation. The portion of the liquidus curve for the SiO_2-rich region of the system is extremely steep; therefore, it is difficult to keep the primary phase, SiO_2, in solution as the melt is cooled. This phenomenon is not confined to the system under discussion. Na_2O-SiO_2 melts with high SiO_2 contents become opaque when cooled to glasses in blocks of the dimensions specified under experimental procedure, and the crystallization continues during the annealing of the glasses. Although there is no doubt that SiO_2 can form glass in a limited-composition region, it appears to lose this ability in the region between the glass-forming area of the BaO-TiO_2-SiO_2 system and the SiO_2 vertex. Hence it is necessary to look for a structural unit other than SiO_2 that is responsible for glass formation in that system. For a limited high-silica range, Dietzel and Wickert [15] attribute similar lowered glass-forming ability of SiO_2 to the severe loosening of the silica network produced by small amounts of Na_2O. In other composition ranges, richer in Na_2O, they find a definite correlation between the degree of glass-forming ability of compositions in the Na_2O-SiO_2 system and the primary phases present at the liquidus.

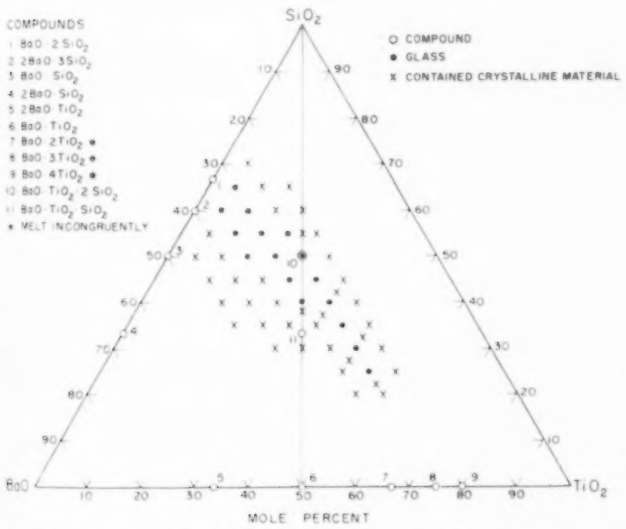

FIGURE 3. *Glass-forming area of the* BaO-TiO_2-SiO_2 *system.*

Of course, the BaO-TiO_2-SiO_2 system is not the only system with SiO_2 as a component in which SiO_2 itself does not seem to be responsible for glass formation. The most stable glasses on the high-Al_2O_3 side of the CaO-MgO-Al_2O_3-SiO_2 system contained 8 mole percent of SiO_2. Glasses have been made in the BaO-Ta_2O_5-SiO_2 system containing 42 mole percent of SiO_2. In these glasses the Si/O ratio is less than 0.25, which is the conventional ratio for isolated silicon-oxygen tetrahedra, and a silicon-oxygen network would require an even higher ratio.

Glass formation in the BaO-TiO_2-SiO_2 system appears to be associated with the compound, $BaO{\cdot}TiO_2{\cdot}2SiO_2$, which has a narrow primary field with a very flat liquidus surface. $BaO{\cdot}TiO_2{\cdot}2SiO_2$ is the only compound that occurs in the glass-forming area, and this area extends from it in all directions except toward the SiO_2-TiO_2 side of the system.

In the half of the system to the left of the $BaO{\cdot}TiO_2$-SiO_2 join, glass formation extends practically to the compound compositions, $2BaO{\cdot}3SiO_2$ and $BaO{\cdot}2SiO_2$, which can be cooled as glasses when cast as thin plates. The compound composition, $BaO{\cdot}SiO_2$, cannot be cooled as a glass and glass formation ceases midway between this composition and $BaO{\cdot}TiO_2{\cdot}2SiO_2$.

On the $BaO{\cdot}TiO_2$-SiO_2 join, the compound composition, $BaO{\cdot}TiO_2{\cdot}SiO_2$, is not glass forming. Glass formation extends slightly over halfway from $BaO{\cdot}TiO_2{\cdot}2SiO_2$ toward this compound.

To the right of the $BaO{\cdot}TiO_2$-SiO_2 join there is only one series of glasses. This glass-forming area extends from the $BaO{\cdot}TiO_2{\cdot}2SiO_2$ composition halfway toward the compound, $BaO{\cdot}3TiO_2$, which melts incongruently at 1,357° C. For the glasses in this series a change in composition of plus or minus 2½ mole percent of BaO produces a mixture of glass and crystals. Hence the glass-forming area in this region is extremely narrow, less than 5 mole percent wide, and approaches a straight line. Such an extremely narrow field may indicate that the glasses are composed of two chemical entities whose compositions lie on the line or the extension of the line. If there were a third entity, the area should have appreciable width. The relative amounts of each entity in a glass would be a function of the composition.

The shape of the liquidus curve for the glasses containing 25 mole percent of BaO, figure 4, indicates that the composition of the second chemical entity is beyond the glass-forming region. It could be $BaO{\cdot}3TiO_2$ or a three-component entity with a composition intermediate between $BaO{\cdot}3TiO_2$ and $BaO{\cdot}TiO_2{\cdot}2SiO_2$ and containing less than 20 mole percent of SiO_2. Because glass formation extends over half the composition range between $BaO{\cdot}TiO_2{\cdot}2SiO_2$ and $BaO{\cdot}3TiO_2$, as it did between $BaO{\cdot}TiO_2{\cdot}2SiO_2$ and the other two contiguous nonglass-

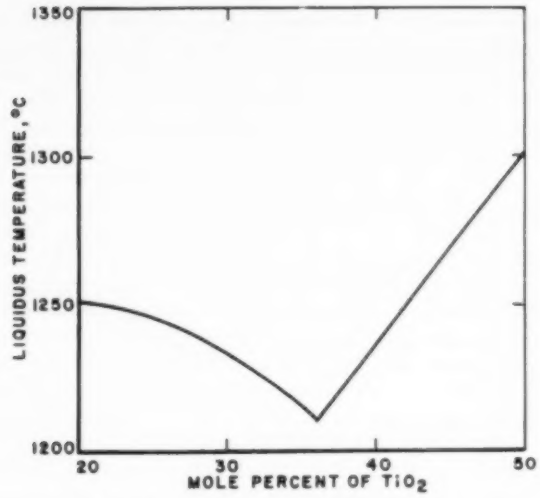

FIGURE 4. *Liquidus curve for* BaO-TiO_2-SiO_2 *glasses containing 25 mole percent of* BaO.

forming compounds, and, as the liquidus temperatures of all the glasses in the series are 50 to 140 deg C below the temperature at which $BaO{\cdot}3TiO_2$ melts incongruently, the second chemical entity could have the same composition as the compound, $BaO{\cdot}3TiO_2$. Then the shape and size of the glass-forming area of the BaO-TiO_2-SiO_2 system would be a function of the solubilities at glass-forming temperatures of the contiguous compounds in $BaO{\cdot}TiO_2{\cdot}2SiO_2$.

4. Summary

Some of the criteria that have been adopted as guides in the development of new glasses are discussed in the light of the phase diagrams. After comparing the shapes of the liquidus curves and surfaces with rates of crystallization, it is postulated (1) that certain chemical entities or structures are in the glasses and, with the possible exception of single-component glasses, (2) that the presence of a compound with a high degree of dissociation in the glass-forming temperature range is essential to permit glass formation.

Thus, it seems probable that multicomponent glasses are essentially solutions of one or more chemical entities or structures in highly dissociated chemical entities that have developed such high viscosities as a result of cooling that they possess many of the properties normally associated with solids. In the case of three-component glasses these chemical entities probably have the same compositions as the compounds indicated by the vertices of the composition triangles and are present in the proportions indicated by the position of the glass composition in the composition triangle.

5. References

[1] W. H. Zachariasen, The atomic arrangement in glass, J. Am. Chem. Soc. **54,** 3841 (1932).
[2] B. E. Warren, Summary of work on atomic arrangement in glass, J. Am. Ceram. Soc. **24,** 256 (1941); J. Biscoe and B. E. Warren, X-ray diffraction study of soda-boric oxide glass, J. Am. Ceram. Soc. **21,** 287 (1938).
[3] C. A. Faick and A. N. Finn, The index of refraction of some soda-lime-silica glasses as a function of the composition, BS J. Research **6,** 993 (1931) RP320.
[4] F. W. Glaze, J. C. Young, and A. N. Finn, The density of some soda-lime silica glasses as a function of the composition, BS J. Research **9,** 799 (1932) RP507.
[5] E. Preston and W. E. S. Turner, Methods of determining the constitution of glasses, J. Am. Ceram. Soc. **17,** 26 (1934); Recent investigations into the question of the presence of compounds in molten glass, J. Soc. Glass Technol. **20,** 144 (1936).
[6] M. L. Huggins, Structure of amorphous materials, J. Phys. Chem. **58,** 1141 (1954); Maurice L. Huggins, The structure of glass, J. Am. Ceram. Soc. **38,** 172 (1955).
[7] L. W. Tilton, Noncrystal ionic model for silica glass, J. Research NBS **59,** 139 (1957) RP2782.
[8] O. H. Grauer and Edgar H. Hamilton, An improved apparatus for the determination of liquidus temperatures and rates of crystal growth in glasses, J. Research NBS **44,** 495 (1950) RP2096.
[9] Edgar H. Hamilton, G. W. Cleek, and O. H. Grauer, Some properties of glasses in the BaO-B_2O_3-SiO_2 system, J. Am. Ceram. Soc. **41,** 209 (1958).
[10] Edgar H. Hamilton, Oscar H. Grauer, Zeno Zabawksy and C. H. Hahner, Changes in the indices of refraction and liquidus of a barium crown glass produced by the partial substitution of some oxides, J. Research NBS **40,** 361 (1948) RP1881.
[11] Unpublished data.
[12] Given W. Cleek and Edgar H. Hamilton, Properties of barium titanium silicate glasses, J. Research NBS **57,** 317 (1956) RP2720.
[13] John E. Ricci, The phase rule and heterogeneous equilibrium, p. 123 (D. Van Nostrand Co., Inc., New York, N. Y., 1951).
[14] D. E. Rase and Rustum Roy, Phase equilibria in the system-$BaTiO_3$-SiO_2, J. Am. Ceram. Soc. **38,** 389 (1955).
[15] A. Dietzel and H. Wickert, The degree of glass formation in the system Na_2O-SiO_2, Glastech. Ber. **29,** 1 (1956).

WASHINGTON, November 19, 1957.

Journal of Research of the National Bureau of Standards Vol. 60, No. 6, June 1958 Research Paper 2873

Twinned Epitaxy of Copper on Copper

Theodore H. Orem

A study of the X-ray diffraction patterns of copper electrodeposited on copper monocrystals having surfaces parallel to the cubic, dodecahedral, and octahedral planes shows an interesting relationship between electrodeposit and base crystal. At the current density used for electrodeposition, the electrodeposit on the surface parallel to the dodecahedral plane was a monocrystalline continuation of the orientation of the base crystal in every respect. The electrodeposit on the surface parallel to the octahedral plane was a highly preferentially oriented polycrystalline electrodeposit made of microcrystals, some of which continued the orientation of the base crystal, whereas others were twinned with respect to the surface plane of the base crystal. In the case of electrodeposition on the surface parallel to the cubic plane, the electrodeposit was also a highly preferentially oriented polycrystalline electrodeposit made up of microcrystals, some of which continued the orientation of the base crystal, whereas others bore a twin relationship to the close-packed planes of the base crystal.

1. Introduction

A considerable number of investigators working in the field of electrodeposition have established that there exists a propensity for the crystallographic orientation of the electrodeposit to be the same as that of the basis metal, if favorable conditions of electrodeposition are maintained [1,2,3,4,5].[1] A discussion based on these references is contained in Barrett's "Structure of Metals" [6]. This continuity of orientation (epitaxy) has been shown to be possible even though the substrate and electrodeposit are two different metals, provided the atomic radii of the two metals do not vary from each other by more than a certain critical percentage [7,8,9]. Takahashi [10] found an orientation relationship when a face-centered cubic metal, copper, was electrodeposited on beta brass, which is body-centered cubic.

In the course of an investigation designed to study the fundamental manner in which metals corrode, several specimens of monocrystalline copper were plated with copper in an effort to determine the orientation of the facets of etch pits that develop during the attack by a certain corrodent, in the hope that the plated facets, continuing the original orientation, would be more readily distinguishable than the original. X-ray diffraction patterns of the electrodeposited specimens showed slight but distinct differences compared to the diffraction patterns of similarly oriented unplated copper single crystals. The differences were considered significant enough to justify further investigation. Some of the results are described herein.

2. Materials and Procedures

A monocrystalline copper ingot, grown by the Bridgman method of slow cooling from the melt, was sectioned to produce specimens having surfaces approximately parallel to the cubic, dodecahedral, and octahedral planes. The specimens were mounted in Lucite, ground and polished, and then electropolished to remove cold work imparted during the mechanical grinding and polishing operations. Laue back-reflection diffraction patterns were obtained from each specimen, using unfiltered radiation from a cobalt target, in order to determine the degree in which the surface was parallel to the desired crystallographic plane. The specimens were then reground and repolished, when necessary, until the surfaces were within one-half degree of being parallel to the cubic, dodecahedral, or octahedral planes. Electrodeposition was carried out in an acid sulfate bath at a current density of approximately 30 ma/cm^2. Electrolytic copper was used as the anode. Periods of plating ranged from a few minutes up to 18 hr. Back-reflection diffraction patterns at normal incidence and using the same radiation as above were then obtained from the electrodeposited copper specimens. After analysis of the various diffraction patterns, the electrodeposits were electropolished, electroetched, and examined microscopically.

3. Results and Discussion

Figure 1 is a series of three photomicrographs showing the microstructures of the electrodeposits on the monocrystalline copper specimens having surfaces parallel to the cubic, dodecahedral, and octahedral planes. Two of the photomicrographs in figure 1 appear to be of polycrystalline metal, but figure 1,b is definitely monocrystalline in character. Figures 1,a and 1,c exhibit strong evidences of twinning in their microstructures, but figure 1,b shows no twinning.

3.1. Deposition on Surface Parallel to an Octahedral Plane

A photograph of a normal incidence Laue back-reflection diffraction pattern obtained from a copper monocrystal whose surface is parallel to an octahedral plane is shown in figure 2,a. Figure 2,b is the same type of pattern from the same specimen after it had received an electrodeposit of copper. It is obvious that X-rays were reflected from more planes in the electrodeposited copper than were reflected from planes in the base crystal.

[1] Figures in brackets indicate the literature references at the end of this paper.

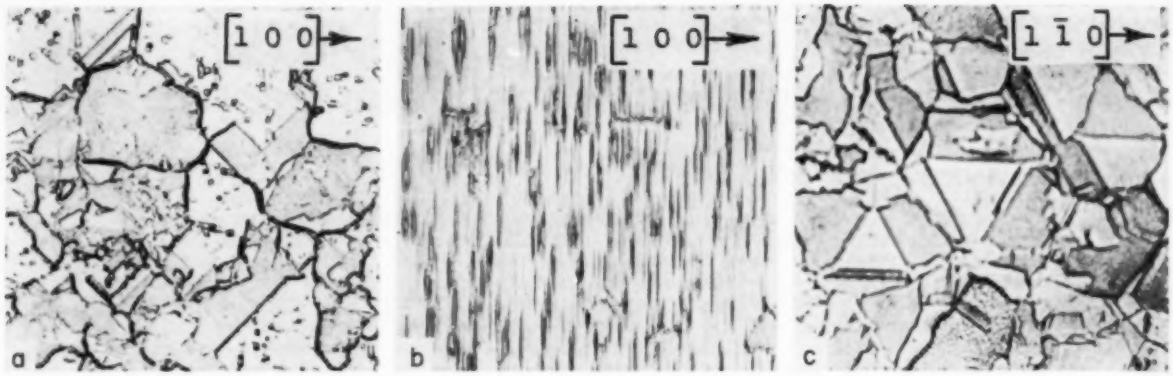

FIGURE 1. *Photomicrographs of electropolished and electroetched copper electrodeposits on monocrystalline copper surfaces.*

(a) Surface parallel to (0 0 1), (b) surface parallel to (0 1 1), and (c) surface parallel to (1 1 1). A principal direction in the surface of the base crystal is indicated on each photomicrograph. X 250.

The normals of the reflecting planes represented by Laue spots in figure 2,a were plotted in a stereographic triangle, as shown in figure 3,a. The normals of the reflecting planes represented by Laue spots in figure 2,b are shown in the stereographic triangle shown in figure 3,b. The solid circles represent normals of reflecting planes from which spots were obtained on both the unplated and plated specimens, and the open circles in figure 3,b are the normals to the reflecting planes represented by Laue spots obtained only from the plated specimen. The sizes of the circles are roughly proportional to the intensities of the pertinent Laue spots. Due to difficulty in photographically reproducing many of the less intense Laue spots present on the diffraction patterns used to obtain figure 2, there is a seeming discrepancy between the number of Laue spots on these photographs and the number of corresponding poles indicated in figure 3. The latter, however, are the factual representation of the poles of the planes from which reflections were obtained, as determined from the diffraction patterns. This same apparent discrepancy between spots on photographs of diffraction patterns and poles shown in corresponding stereographic triangles will be noted in the discussion of electrodeposition on surfaces parallel to the dodecahedral and cubic planes. In each instance the poles shown in the stereographic triangles represent the Laue spots actually observed. The circles containing a cross will be explained later in a discussion of the means of indexing the various spots shown in figure 3.

The stereographic triangles shown in figure 3 are oriented so that the poles of the projection correspond to the spots in a segment of the diffraction patterns in figure 2. The segment is outlined only on the diffraction pattern from the base crystal, figure 2,a. The segment for the pattern in figure 2,b, is in the same relative position as that in figure 2,a because the azimuthal orientations of both patterns are the same. This same manner of presentation of

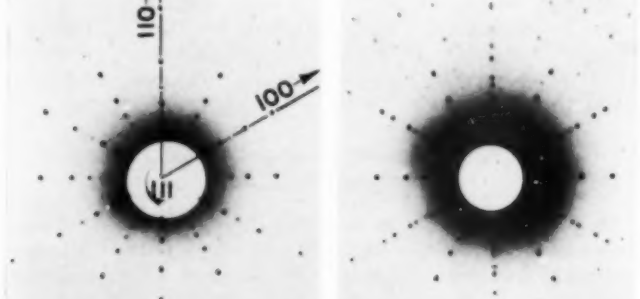

FIGURE 2. *Laue back-reflection diffraction patterns.*

(a) Before, and (b) after electrodeposition of copper in a copper monocrystal. The surface was parallel to an octahedral plane and the X-ray beam normal to the surface.

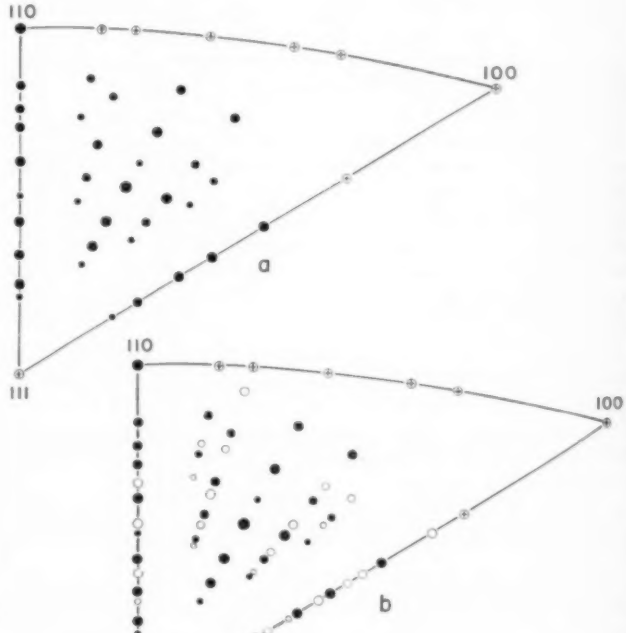

FIGURE 3. *Unit stereographic triangles showing orientation of poles that correspond to the reflection spots in figure 2.*

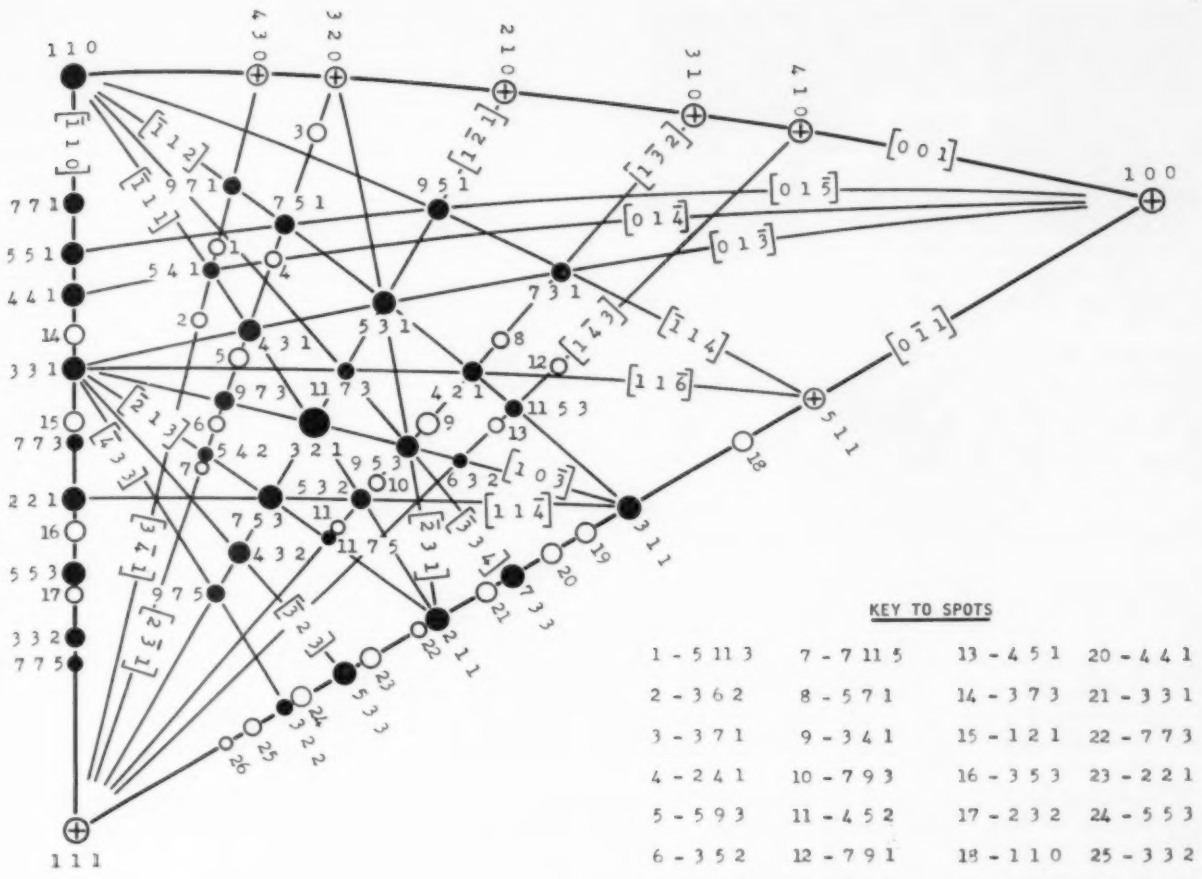

FIGURE 4. *Stereographic triangle identifying spots and zones shown in figure 3.*

stereographic triangles is followed throughout this paper.

Figure 4 is a stereographic triangle showing the spots shown in figure 3,b. In this triangle it is necessary to know the location of certain poles, which could not be located from the pertinent diffraction pattern spots because of size limitations of the camera, in order to index certain zones that contain poles corresponding to Laue spots found in the diffraction pattern. These poles, not present as Laue spots on the diffraction pattern, have been located by means of circles containing crosses in order to distinguish them from all other poles in the triangle, which were actually located from Laue spots present in the diffraction pattern.

It will be noted that each of the solid circles in figure 4 is at the intersection of two or more zones and that the formulation of the indices of the spots represented by the solid circles is in accordance with the conventional crystallographic method for indexing such spots. The open-circle spots in figure 3,b, indexed in figure 4, are the location of poles corresponding to the Laue spots from the twin of the surface plane of the base crystal caused by a 60° clockwise rotation about the octahedral axis parallel to the surface normal. An explanation of the method of indexing the open-circle spots is given in the appendix. An interpretation of figure 2,b, from which the position of the poles with respect to the octahedral pole in the stereographic triangle shown in figure 4 were determined, indicates that the twinning plane in the electrodeposit is parallel only to the octahedral plane parallel to the surface of the base crystal. At the current density used for this work, twinning occurred only on the surface plane. At other current densities it is conceivable that twinning might also occur on close-packed planes other than the surface plane.

A careful investigation of the spots from the twin orientation showed that, as electrodeposition progressed, they gradually increased in intensity to a value equal to that of the intensity of a corresponding spot in the base crystal. This would appear to indicate that a constant ratio between the twinned and untwinned orientations was built up in the electrodeposit.

The method of packing spheres to illustrate the regular and the twin position of an atom with respect to the uppermost two layers in the octahedral plane of the base crystal is shown in figure 5. Figure 5,a shows the atoms as they would be packed in the uppermost two layers of a monocrystalline specimen whose surface is parallel to an octahedral plane. Figure 5,b shows an atom (dark sphere) as it would be located in the first layer of the electrodeposit if

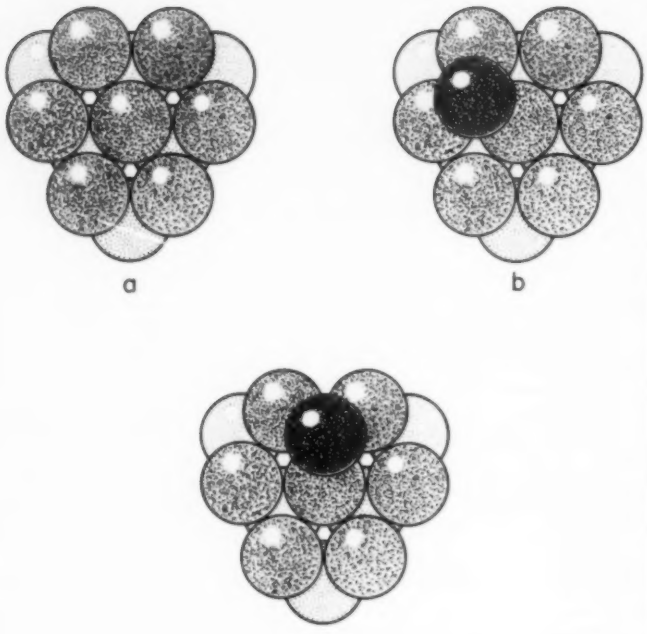

FIGURE 5. *Sketches of packed spheres depicting the atomic arrangements in the octahedral plane of copper.*

(a) The uppermost two layers in the octahedral plane, (b) the deposition of an atom of copper (dark sphere) in the first of two positions in which it might locate, and (c) the deposition of an atom of copper (dark sphere) in the second of two positions in which it might locate.

the deposition were such as to continue the atomic configuration of the basis metal, in kind. Figure 5,c shows the atom (dark sphere) located in the position that it would occupy if the deposition were such that the first layer deposited bore a twin relationship to the uppermost two layers of the base crystal.

Figure 6 shows by means of spheres the atomic arrangement at the interface of the base metal (bottom two layers) and electrodeposit (top layer) (a) if the atom were to locate as in figure 5,c, and (b) if the atom locates as in figure 5,b. The arrangement of spheres in figure 6,a represents the atoms positioned in the ABAB arrangement of the hexagonal system, in which case the atoms of each alternate close-packed layer are arranged directly above one another. In the face-centered cubic system (copper) the fourth layer of close-packed atoms is directly over the first layer, the fifth layer directly over the second layer, the sixth over the

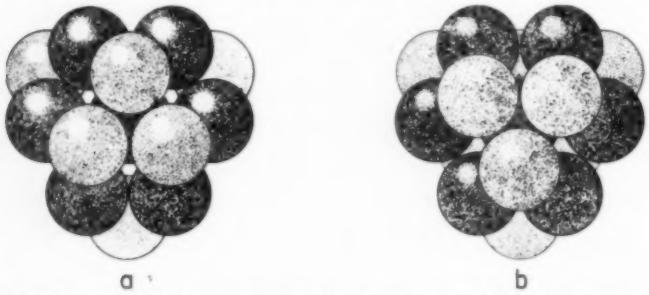

FIGURE 6. *Sketches of packed spheres depicting the atomic arrangements at the interface of base crystal and electrodeposit.*

(a) If copper atoms were to deposit at location shown in figure 5,c; (b) if copper atoms were to deposit at location shown in figure 5,b.

third, etc., in ABCABC fashion, as shown by the packing of spheres in figure 6,b.

Judging from the microstructure of the electrodeposit shown in figure 1,c, it is apparent that as copper atom deposits from solution on the surface of the base crystal in either of the two positions shown in figures 5,b and 5,c, since the electrodeposit is made up of many small crystals, some of which have the same orientation as the base crystal, and some of which are twinned with respect to it, as shown by the diffraction pattern obtained from the electrodeposit.

It is suggested that when the copper atom deposits from solution it locates randomly on the original surface, either twinned or untwinned with respect to the base crystal. The originally deposited atoms are then nucleation points around which subsequently depositing atoms locate. These atoms probably deposit in monolayers around the nucleation atoms, those locating around the originally deposited twinned atom forming a twinned area and the atoms surrounding the untwinned first-deposited atom forming an untwinned monolayer of atoms. The two monolayers then grow laterally into each other. The juncture of a monolayer of twinned atoms and one of untwinned atoms is a line of misfit of atoms which constitutes a twin boundary. These lines of atom misfit are probably the sides of the equilateral triangles seen in figure 1,c. As subsequent monolayers of atoms deposit, the areas in which misfitting of atoms occurs eventually become large enough to preclude subsequent deposition in an orderly fashion and an irregularly formed grain-boundary, such as may be observed in figure 1,c, results. As a consequence of this type of growth, the deposit is polycrystalline in character but with the individual crystals having a very high degree of preferred orientation. This structure is apparent both from the appearance of the microstructure, figure 1,c, and from the diffraction pattern of the electrodeposited crystal, figure 2,b.

3.2. Deposition on Surface Parallel to Dodecahedral Plane

Figure 7,a is a photograph of a Laue back-reflec-

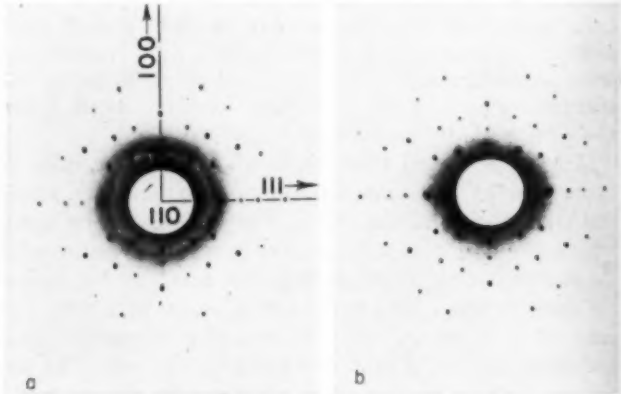

FIGURE 7. *Laue back-reflection diffraction patterns.*

(a) Before, and (b) after electrodeposition of copper on a copper monocrystal. The surface was parallel to a dodecahedral plane and the X-ray beam normal to the surface.

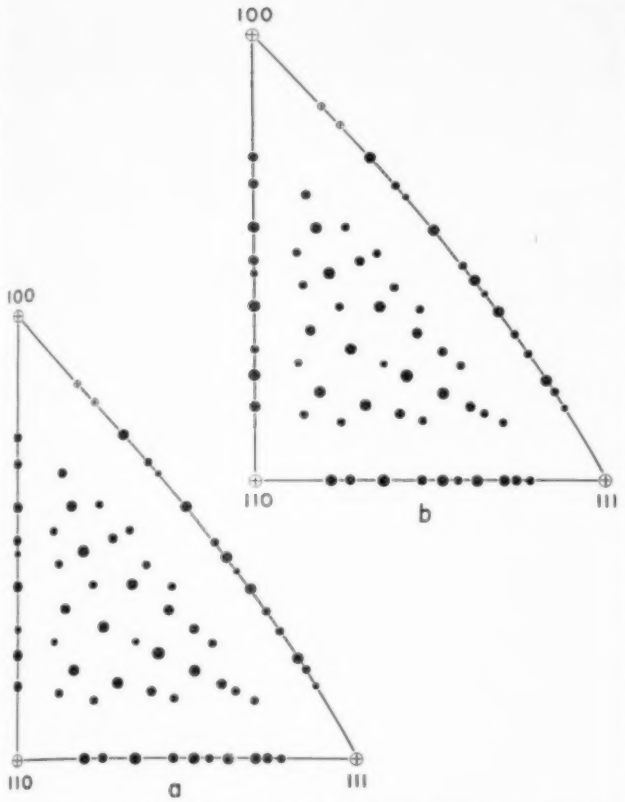

FIGURE 8. *Unit stereographic triangles showing orientation of poles that correspond to the reflection spots in figure 7.*

tion diffraction pattern of a monocrystalline copper specimen whose surface is parallel to the dodecahedral plane, the incident beam having been perpendicular to the specimen surface. Figure 7,b is a diffraction pattern of the same specimen after receiving a heavy deposit of copper.

Figures 8,a and 8,b are stereographic triangles representing the poles of reflecting planes from which Laue spots were obtained on the unplated and plated monocrystalline copper crystals shown in figure 7. The solid and crossed circles represent poles, as previosuly described for figure 3. It will be noted that there are no open circles in figure 8,b, as there were in figure 3,b, because reflections from planes other than those which caused reflections in the unplated specimen were not present on the diffraction pattern obtained from the electrodeposited specimen. Figure 9 is a stereographic triangle identifying the spots and zones shown in figure 8.

The appearance of the microstructure of the electrodeposited specimen whose surface is parallel to the dodecahedral plane, figure 1,b, would appear to indicate that the atomic arrangement in the electrodeposit is little, if any, different from that in the base metal. There is no indication in the diffraction patterns of the base metal and the electrodeposited specimen of any difference in their orientations.

Figure 10 illustrates (a) the configuration of the uppermost two layers of atoms in a monocrystalline copper specimen whose surface is parallel to the dodecahedral plane, and (b) the positions the first layer of deposited atoms takes with respect to the layers on which it deposits. An atom depositing from solution on the surface shown in 10,a may locate in any position on the surface and still preserve the atomic configuration of the substrate in so doing. Subsequently depositing atoms likewise do not alter the atomic configuration at the base crystal interface no matter where they deposit. Succeeding layers of atoms are deposited similarly, all in a very orderly fashion with respect to the underlying layers. Thus, when deposition is upon a surface parallel to a dodecahedral plane, the orientation of the atoms in the electrodeposit is exactly the same as that of the atoms in the base crystal. It is emphasized that such an electrodeposit was obtained at a specific current density. At other current densities it is conceivable that twinning might occur on this surface also.

3.3. Deposition on Surface Parallel to a Cubic Plane

Figure 11,a is a photograph of a Laue back-reflection diffraction pattern obtained at normal incidence on a monocrystalline copper specimen whose surface is parallel to a cubic plane. Figure 11,b is the same kind of pattern obtained after the specimen has received an electrodeposit of copper. The difference in the number of Laue spots on the two photographs is obvious.

Figures 12,a and 12,b are stereographic triangles whose poles correspond to the Laue spots shown in figure 11. The solid circles represent reflections obtained from both the unplated and plated specimens, and the open circles in figure 12,b, represent additional spots found only in the diffraction pattern from the electrodeposited specimen. Figure 13 is a stereographic triangle identifying the spots and zones shown in figure 12.

Comparing figures 12,a and 12,b, it is readily apparent that there are many more reflecting planes in the electrodeposit than there are in the base metal. Using figure 13 to identify the open-circle spots in figure 12,b it is obvious that the indices of reflections that were present only in the pattern from the electrodeposited copper were of a conspicuously higher order than the indices of reflections that were present in the pattern obtained from the base crystal.

Since the wavelengths, in accordance with Bragg's law, that correspond to the very high indices are smaller than the minimum wavelength used in making the patterns, it is obvious that the reflections are not from crystals having the same orientation as the base crystal. It is postulated that the apparently spurious reflections are from crystals that were formed by twinning on the octahedral planes of crystals that were deposited with an orientation corresponding to that of the base crystal. If this is true, then the twinning should result in the creation of certain low-index crystallographic planes in portions of the electrodeposit that are parallel to the high-index planes from which reflections have apparently been obtained. The high-index planes whose normals are shown in figure 13 were reindexed in accordance

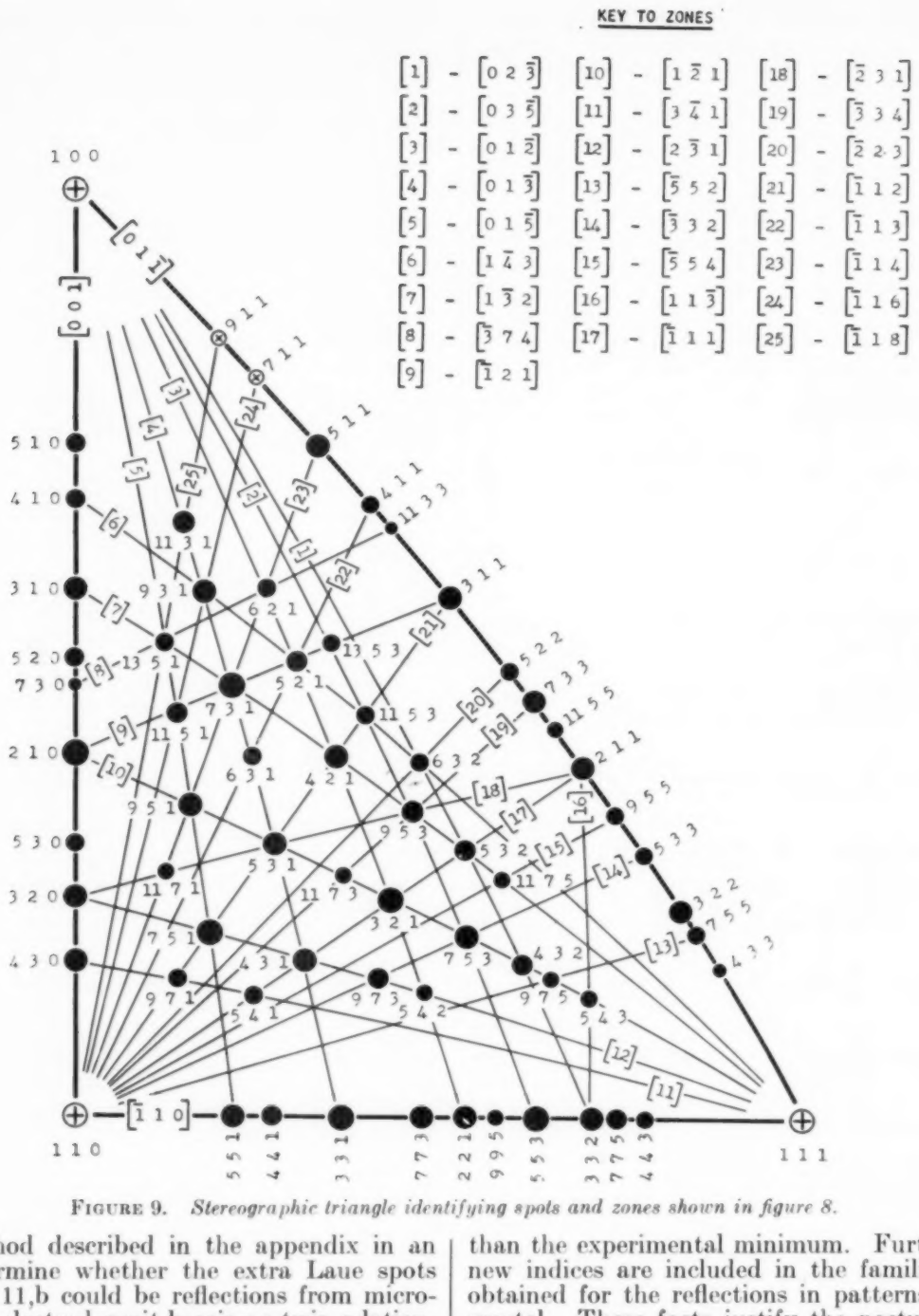

FIGURE 9. *Stereographic triangle identifying spots and zones shown in figure 8.*

with the method described in the appendix in an effort to determine whether the extra Laue spots seen in figure 11,b could be reflections from microcrystals in the electrodeposit bearing a twin relationship to the base crystal. Table 1 lists the reindexed planes as "true reflecting planes" opposite the planes as indexed in accordance with the orientation of the base crystal, which planes have been designated "apparent reflecting planes." The former are the low-index planes in the twinned portion of electrodeposit that are parallel to high-index planes in the base crystal and the untwinned portion of the electrodeposit. The apparently spurious reflections all now have indices with "*d*" spacings that, in accordance with Bragg's law, correspond to wavelengths greater than the experimental minimum. Furthermore, the new indices are included in the families of indices obtained for the reflections in patterns of the base crystal. These facts justify the postulate that the electrodeposited copper consisted of crystals having orientations of the base crystal and its four twins.

Figure 14 illustrates by means of the packing-of-spheres method the atomic arrangements present in the preferentially oriented microcrystals making up the electrodeposit whose microstructure is shown in figure 1,a.

Figure 14,a shows the atomic arrangement in the uppermost two layers when the surface is parallel to a cubic plane. Figure 14,b shows the position a depositing atom (dark sphere) will take with re-

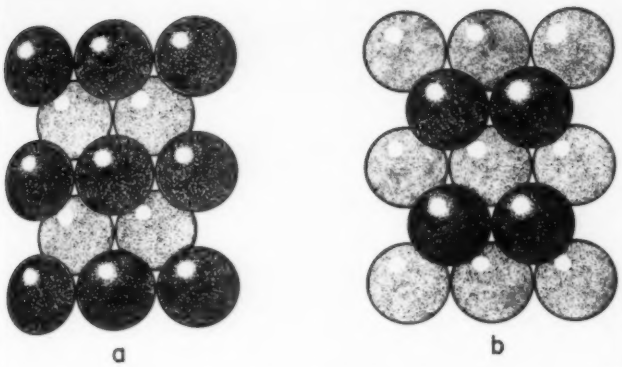

FIGURE 10. *Sketches of packed spheres depicting the atomic arrangement in the dodecahedral plane of copper.*

(a) The two top layers of atoms, and (b) the deposition of atoms of copper (dark spheres) in locations which perpetuate the orientation of the base metal, in kind.

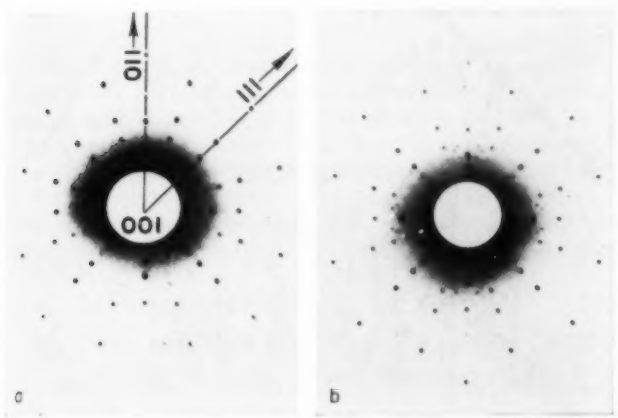

FIGURE 11. *Laue back-reflection diffraction patterns.*

(a) Before, and (b) after electrodeposition of copper on a copper monocrystal. The surface was parallel to a cubic plane and the X-ray beam normal to the surface.

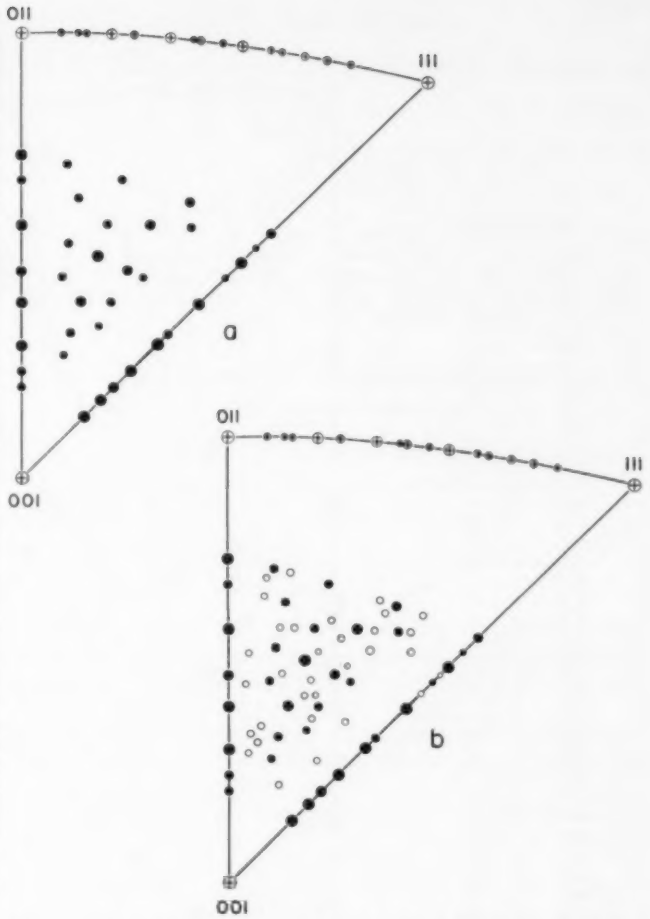

FIGURE 12. *Unit stereographic triangles showing orientation of poles that correspond to the reflection spots in figure 11.*

spect to the uppermost two layers in order for the orientation of the base crystal to be continued in the electrodeposit. There is no position in the cubic surface, as such, in which an atom can locate that would not continue the orientation of the base crystal. The microstructure of the electrodeposit, figure 1,a, and the diffraction pattern, figure 11,b, (with interpretation of extra spots as described herein), however, indicate that at some period during electrodeposition, situations are created whereby atoms are able to locate in a choice of positions, in one case where the atomic configuration of the base metal will be continued, in kind, and, in a second case, where the atomic arrangement is twinned with respect to the base metal.

It is postulated that the atoms at first all locate as shown in figure 14,b, building up as monolayers of atoms in accordance with the orientation of the base crystal as the atoms deposit laterally around the the atoms first depositing at random sites on the surface. In time, however, some of the layers of depositing atoms grow thicker than others as they grow laterally about nucleating atoms depositing at scattered points over the entire surface of the electrodeposit. This gives rise to the formation of octahedral planes as shown in figure 14,b, on which planes subsequently depositing atoms can locate in a choice of position, as in the sketches shown in figure 5. Atoms locating in twin positions on such surfaces, when viewed in a direction normal to the cubic plane, are depicted by the dark spheres in figure 14,c.

It is suggested that the atoms depositing from solution at low-current density have a great tendency to deposit such as to form monolayers whose orientation is the same as that of the base crystal. With increasing deposition time, twinning occurs on the octahedral planes, with a consequent formation of areas in which the atoms are in a state of misfit, these areas at first constituting twin boundaries. With additional deposition time the areas of misfit are aggravated and eventually become so large as to destroy the ability of depositing atoms to fit into the electrodeposit with any semblance of regularity, at which time a grain boundary is formed. Although there is considerable grain-boundary area in figure 1,a, the diffraction pattern, figure 11,b, indicates that the microcrystals in the electrodeposit which have grown in accordance with the orientation of the base

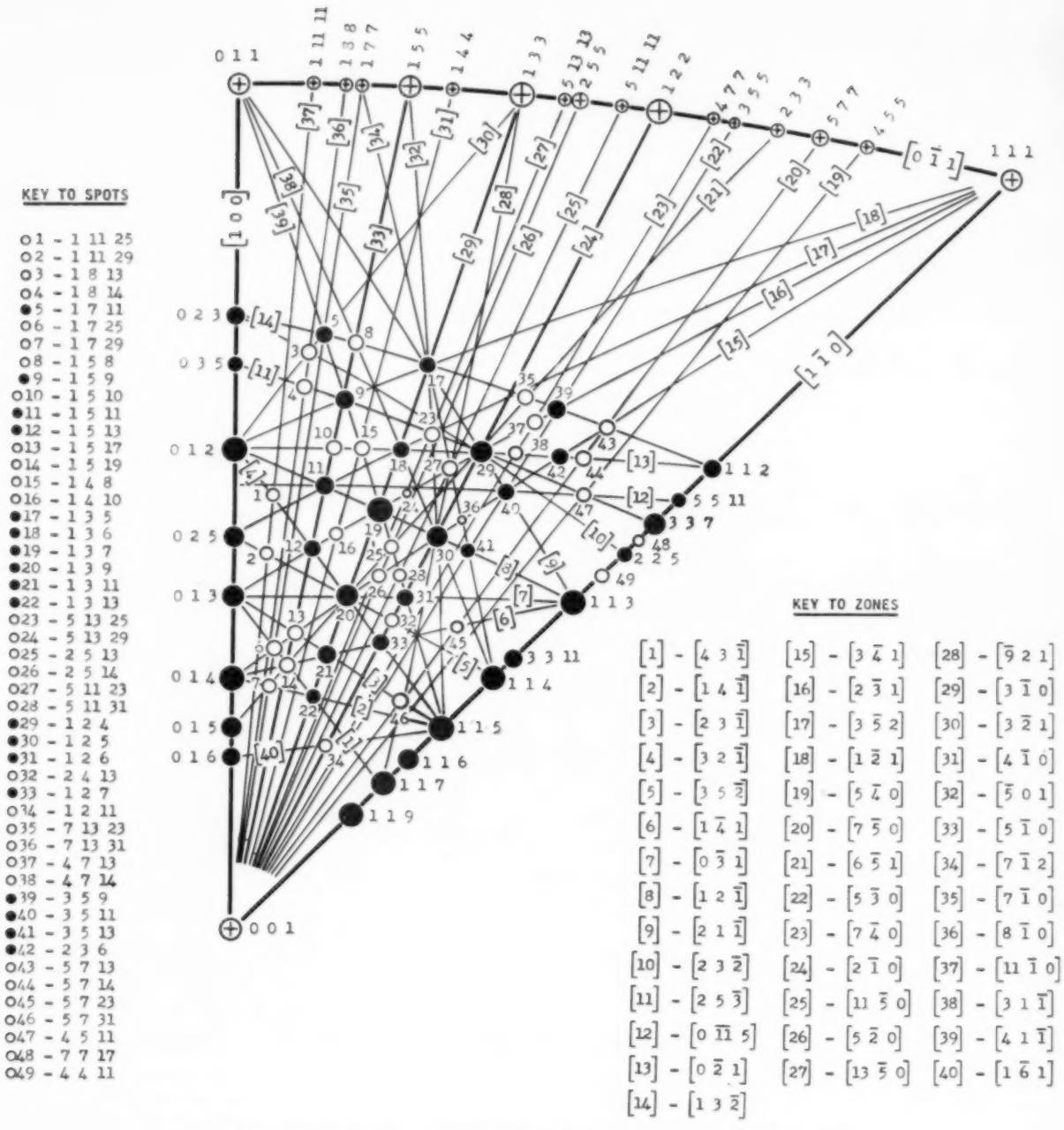

FIGURE 13. *Stereographic triangle identifying spots and zones shown in figure 12.*

crystal still predominate the structure. It is suggested that additional deposition would result in more and more areas becoming twinned and consequently the development of more areas of misfit as the preferentially oriented microcrystals grow into each other. Eventually, the areas of misfit evolve from twin boundaries to grain boundaries as the degree of misfit is further aggravated. The subsequent increase in the number of grain boundaries eventually diminishes the surfaces on which the atoms can preferentially locate and the entire surface then becomes a mass of microcrystals randomly oriented.

4. Conclusions

As a result of an analysis of Laue back-reflection diffraction patterns obtained from copper electrode deposits on monocrystalline copper base crystals of varying surface orientation at a current density of approximately 30 ma/cm^2, using an acid-sulfate electrolyte, the following conclusions can be drawn:

1. A copper electrodeposit on a surface parallel to the dodecahedral plane is monocrystalline in character and duplicates the orientation of the base crystal.

2. Copper electrodeposited on a surface parallel to the octahedral plane has a very preferentially ori-

TABLE 1. *Apparent reflecting planes shown in figure 13 and calculated true reflecting planes present in the twinned portions of the electrodeposit.*

Spot	Apparent reflecting plane	True reflecting plane	Spot	Apparent reflecting plane	True reflecting plane
1	1 11 25	$\bar{5}$ 3 7	27	5 11 23	5 1 7
2	1 11 29	1 9 5	28	5 11 31	7 7 5
3	1 8 13	3 $\bar{1}$ 4	32	2 4 13	1 4 2
4	1 8 14	0 5 2	34	1 2 11	1 3 2
6	1 7 25	5 $\bar{1}$ 7	35	7 13 23	5 7 3
7	1 7 29	7 5 5	36	7 13 31	7 1 9
8	1 5 8	0 3 1	37	4 7 13	3 1 4
10	1 5 10	2 $\bar{1}$ 3	38	4 7 14	3 4 2
13	1 5 17	1 5 3	43	5 7 13	1 5 1
14	1 5 19	3 3 5	44	5 7 14	2 $\bar{1}$ 5
15	1 4 8	$\bar{2}$ 2 1	45	5 7 23	3 $\bar{3}$ 7
16	1 4 10	2 0 3	46	5 7 31	3 9 5
23	5 13 25	1 9 3	47	4 5 11	1 4 1
24	5 13 29	5 $\bar{3}$ 9	48	7 7 17	3 5 3
25	2 5 13	3 3 2	49	4 4 11	2 3 2
26	2 5 14	3 0 4			

ented polycrystalline character, some of the individual crystals having the same orientation as the base crystal and some being twinned with respect to it.

3. The copper electrodeposit on a surface parallel to a cubic plane is polycrystalline in character, the individual crystals being very preferentially oriented with respect to the base crystal, some continuing the base-crystal orientation and others being twinned with respect to it.

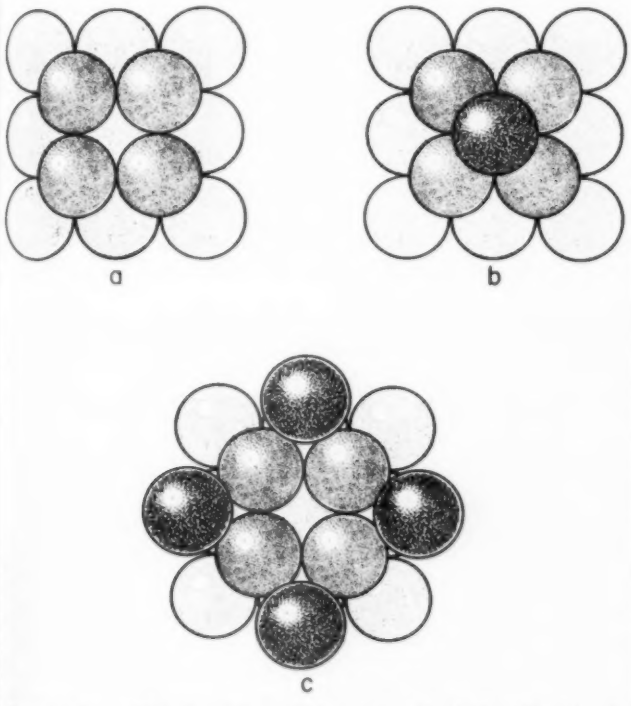

FIGURE 14. *Sketches of packed spheres depicting the atomic arrangements in the cubic plane of copper.*

(a) The two top layers of atoms, (b) the deposition of an atom of copper (dark sphere) in location which will perpetuate orientation of base metal in electrodeposit, in kind, and (c) the deposition of atoms of copper (dark spheres) in locations corresponding to the twin positions on the octahedral planes of the base metal.

5. References

[1] W. Blum and H. S. Rawdon, Trans. Am. Electrochem. Soc. **44,** 305 (1923).
[2] H. Hirata and Y. Tanaka, Mem. Coll. Sci. Kyoto Imp. Univ. [A] **15,** 9 (1932).
[3] W. A. Wood, Proc. Phys. Soc. (London) **43,** 138 (1931).
[4] H. E. Farnsworth, Phys. Rev. **35,** 1131 (1930).
[5] H. Leidheiser and A. T. Gwathmey, Trans. Electrochem. Soc. **91,** 95 (1947).
[6] C. S. Barrett, Structure of metals, 2d ed., p. 513 (1952).
[7] L. E. Samuels, J. Inst. of Metals **85,** 177 (1956–57).
[8] A. W. Hothersall, Trans. Faraday Soc. **31,** 1242 (1935).
[9] W. Cochrane, Proc. Phys. Soc. (London) **48,** 723 (1936).
[10] N. Takahasi, J. chim. phys. **50,** 624 (1953).

6. Appendix. Interpretation of Diffraction Patterns

The procedures for indexing the open-circle spots shown in figures 3,a and 12,b are outlined in the following sections.

6.1. Electrodeposit on Surface Parallel to Octahedral Plane

Figure 15 is a pole figure showing the relationship between principal poles in a stereographic projection when the octahedral pole is at the center of the pole figure. The darkly outlined triangle, 1 1 1, 1 1 0, 1 0 0, is the stereographic triangle shown in figure 4. It is one of six stereographic triangles bounded by the three cubic zones shown in the pole figure. The six stereographic triangles bounded by the short dashed lines are the above-mentioned six triangles rotated 60° clockwise about the normal to (1 1 1). The poles shown as open circles and identified with italicized indices in the rotated triangles are thus in twin positions with respect to the basic orientation. Only that part of the basic projection bounded by the cubic zones is shown in the rotated position in order to minimize confusion. Also shown in the basic projection are several principal zones, [$\bar{1}$ 0 1], [$\bar{1}$ 1 0], [0 $\bar{1}$ 1], [$\bar{2}$ 1 1], [1 $\bar{2}$ 1], [$\bar{3}$ 2 1] and [1 $\bar{3}$ 2]. The latter two zones contain 5 7 1 and 4 2 1, respectively, which are shown as solid circles as it is known that reflections from the planes normal to these two poles were present in the diffraction pattern from the electrodeposit on the surface parallel to the octahedral plane.

After rotating the basic projection 60° clockwise about the normal to (1 1 1), zones [*$\bar{1}$ 0 1*] and [*$\bar{1}$ 1 0*] in the rotated projection will coincide with zones [$\bar{1}$ 1 0] and [0 $\bar{1}$ 1], respectively, in the basic projection. The indices of the rotated zones are shown in italics. By rotating one zone so that it coincides with another, all poles on the two zones will lie on one zone. Poles on different zones, which before rotation have equivalent distances from the axis of rotation, will, of course, coincide when the pertinent zones coincide after rotation. Thus, in figure 15 and in figure 4, all poles shown as solid circles in zone [$\bar{1}$ 1 0] will lie on zone [0 $\bar{1}$ 1], where they are shown as open circles, after 60° clockwise rotation about the normal to (1 1 1). There is no open-circle spot corresponding to 7 7 1

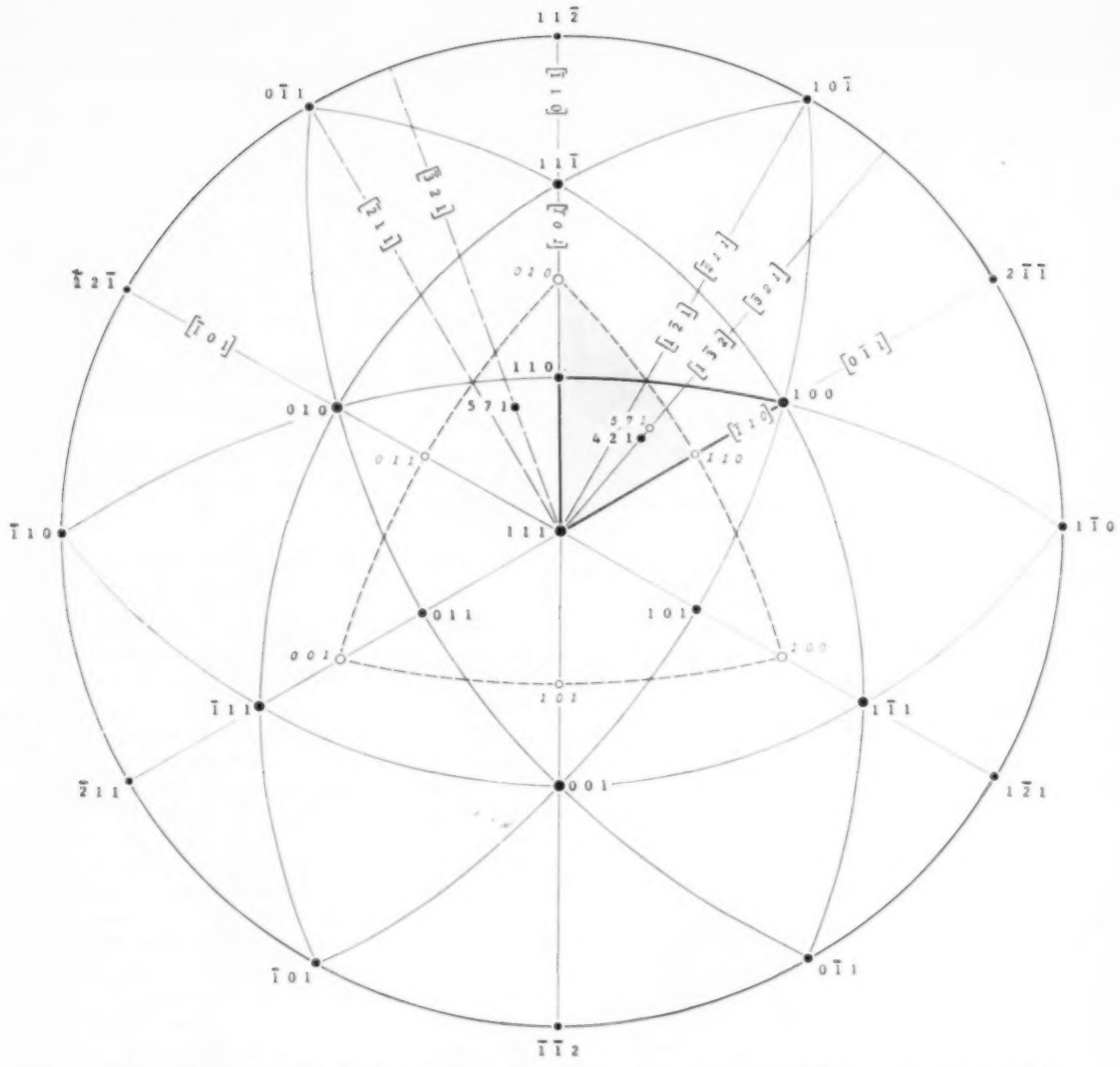

FIGURE 15. *Stereographic projection showing orientation of base crystal and the 1 1 1 twin orientation.*
Indices of planes and zones of the twin orientation are in italics and portions of the twin cubic zonal circles are dashed.

on zone [0 $\bar{1}$ 1] in this case because 7 7 1 and 3 1 1 both make equivalent angles, in their respective zones, with the axis of rotation, and, therefore, 7 7 1 is superimposed on 3 1 1 after rotation.

Similarly, in figure 15, all poles on zone [$\bar{1}$ 0 1] will fall on zone [$\bar{1}$ 1 0] after rotation. This is shown in figure 4. Here again, we have the case of a pole on one zone superimposing on a pole in a second zone after rotation. 1 3 1 in zone [$\bar{1}$ 0 1] (not shown in figure 15) coincides, after rotation, with 7 7 1 in zone [$\bar{1}$ 1 0] (shown in figure 4) and is not, therefore, shown as an open-circle spot in figure 4.

In rotating the basic projection 60° clockwise about the normal to (1 1 1), zone [$\bar{2}$ *1 1*] will coincide with zone [1 $\bar{2}$ 1] and, therefore, all poles in zone [$\bar{2}$ *1 1*] will superimpose on the poles in zone [1 $\bar{2}$ 1]. It will be noted that all poles on zone [1 $\bar{2}$ 1] in figure 4 are shown as closed circle spots. All zones of the type [$\bar{2}$ 1 1] and, consequently, all poles on those zones are common both to the basi projection and to the basic projection rotated 60 clockwise about the normal to (1 1 1).

The indexing of all of the open-circle spots show within the stereographic triangle, figure 4, is accom plished in the same manner described above for index ing the open circle spots on the sides of the triangle by the superimposition of zones of rotated triangle on zones of the basic projection. In figure 15 th normal to (5 7 1) in the basic projection is show within triangle 1 1 1, 1 1 0, 0 1 0, in zone [$\bar{3}$ 2 1 When this particular triangle is rotated 60° clockwis about the normal to (1 1 1), it is reoriented wit respect to the basic projection as shown by th shaded triangle. In the rotated position, zon [$\bar{3}$ *2 1*] now coincides with zone [1 $\bar{3}$ 2] of th basic projection and the normal to (5 7 1), whic lies on [$\bar{3}$ 2 1] of the basic projection, can be seen in relation to the normal to (4 2 1) of the basi projection. Compare with same spots in figure 4

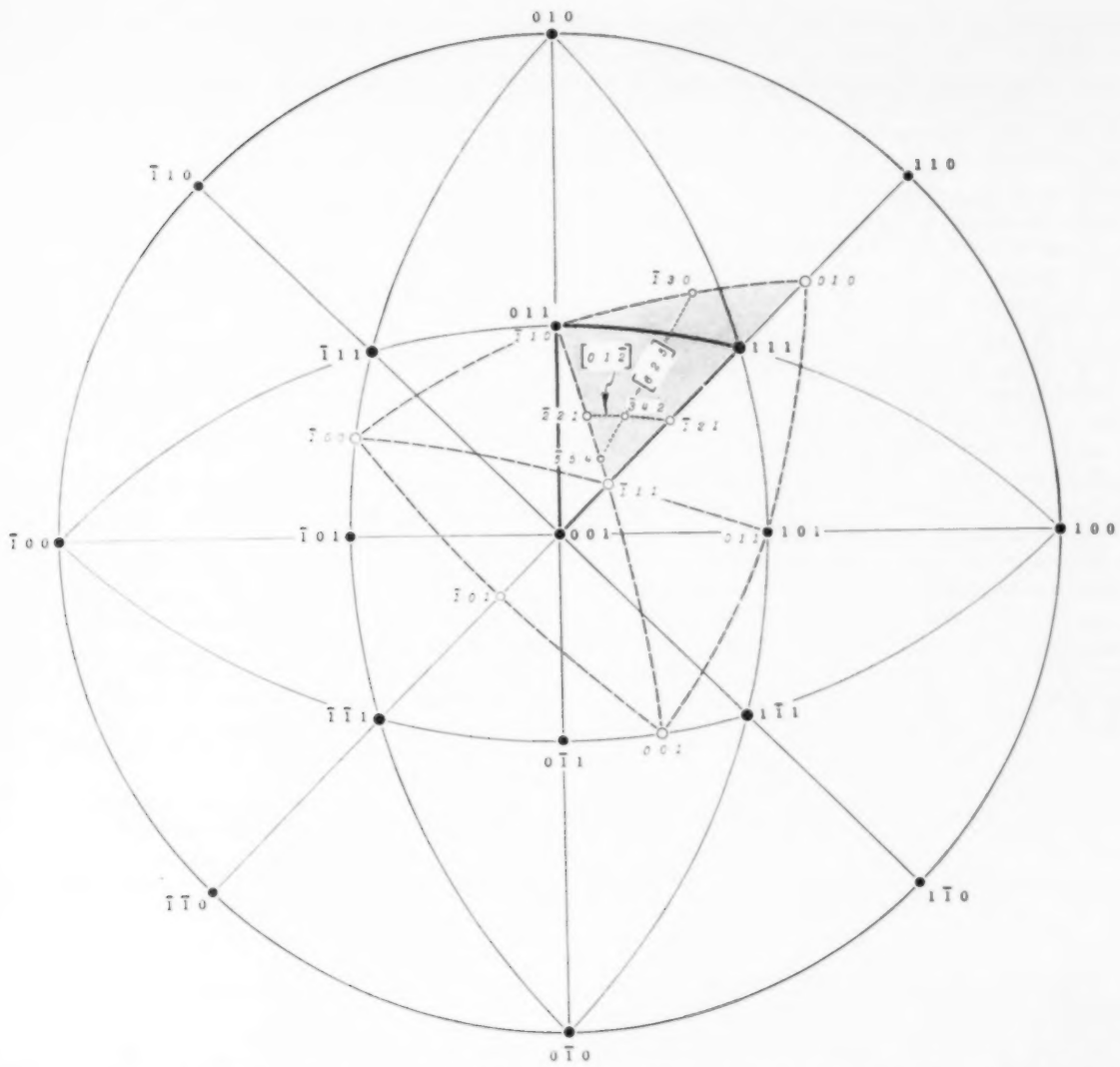

FIGURE 16. *Stereographic projection showing method of reindexing reflections on basis of a twin orientation of the base crystal.*
Indices of the $\bar{1}\,\bar{1}$ 1 twin orientation are shown in italics and parts of zonal circles are dashed.

All other open-circle spots within the stereographic triangle shown in figure 4 can be indexed in a similar manner.

The difference between the diffraction pattern in figure 2,a and that in figure 2,b is the result of simple rotation about the surface normal, the rotational angle being 60°. This indicates that some of the microcrystals making up the electrodeposit on the surface parallel to the octahedral plane are twinned with respect to the base crystal.

6.2. Electrodeposit on Surface Parallel to Cubic Plane

The determination of the indices of the open-circle spots shown in figure 12,b, which, when indexed with respect to the basic orientation, have the high indices shown in figure 13, can be accomplished by the following method:

Figure 16 is a pole figure showing the relationship between principal poles in a stereographic projection when the cubic pole is at the center of the pole figure. The darkly outlined triangle 1 1 1, 0 1 1, 0 0 1, in the vicinity of the center of the pole figure is the stereographic triangle shown in figure 13.

An example of this method is illustrated by means of figure 16. In figure 13, spot number 38 is indexed 4 7 14. It is the spot (pole) common to zones [0 $\bar{2}$ 1] and [7 $\bar{4}$ 0] (see fig. 13) of the base crystal, the basic orientation of figure 16. The dashed lines in figure 16 show the orientation of the octant $\bar{1}$ 0 0, 0 1 0, 0 0 1 after a clockwise rotation of 60° about the normal to the ($\bar{1}$ $\bar{1}$ 1). The rotated orientation of the $\bar{1}$ 1 1, $\bar{1}$ 1 0, 0 1 0 unit triangle is shown by shading. All poles and zones in the rotated orientations are shown in italics to differentiate them from the corresponding poles and zones shown in the basic orientation. The two zones [0 $\bar{2}$ 1] and [7 $\bar{4}$ 0], re-

indexed with respect to the system of indices of the rotated orientation should then define the indices of a spot that coincides with spot number 38, 4 7 14. The zone in the rotated orientation parallel to zone [7 $\bar{4}$ 0] in the basic orientation, projected to intersect a zone in the former containing *0 1 0* and $\bar{1}$ *1 0* intersects this zone at a point 26°34′ from $\bar{1}$ *1 0*. This is the angle between $\bar{1}$ 3 0 and $\bar{1}$ 1 0. The zone corresponding to [7 $\bar{4}$ 0] also intersects a zone containing $\bar{1}$ *1 0* and $\bar{1}$ *1 1* in the rotated orientation at a distance 29°30′ from $\bar{1}$ *1 0*. This is the angle between $\bar{5}$ 5 4 and $\bar{1}$ 1 0. The normals to ($\bar{1}$ *3 0*) and ($\bar{5}$ *5 4*) then lie in a zone in the rotated orientation, which is parallel to zone [7 $\bar{4}$ 0] in the basic orientation. This zone is thus indexed [*6 2 5*]. The second zone in the rotated orientation, which is parallel to zone [0 $\bar{2}$ 1] of the basic orientation, intersects a zone containing *0 1 0* and $\bar{1}$ *1 1* in the rotated orientation at a point 19°28′ from $\bar{1}$ *1 1*. This is the angle between $\bar{1}$ 2 1 and $\bar{1}$ 1 1. The zone corresponding to [0 $\bar{2}$ 1] also intersects a zone containing $\bar{1}$ *1 1* and $\bar{1}$ *1 0* in the rotated orientation at a point 15°48′ from $\bar{1}$ *1 1*. This is the angle between $\bar{2}$ 2 1 and $\bar{1}$ 1 1. The normals to ($\bar{1}$ *2 1*) and ($\bar{2}$ *2 1*) then lie in a zone of the rotated orientation, which is parallel to zone [0 $\bar{2}$ 1] of the basic orientation. This zone is thus indexed [*0 1* $\bar{2}$]. Zones [*6 2 5*] and [*0 1* $\bar{2}$] in the rotated orientation are then parallel to zones [7 $\bar{4}$ 0] and [0 $\bar{2}$ 1], respectively, of the basic orientation. The former two zones intersect to locate the normal to ($\bar{3}$ *4 2*), which plane is thus parallel to high-index plane (4 7 14).

The above example was selected to illustrate the case where a clockwise rotation of 60° about one of the four [1 1 1] axes resulted in low indices for the too high indices of the "apparent reflecting planes." A similar reindexing on the basis of rotations about the other three [1 1 1] axes resulted in high indices too high to be accountable by the limitation imposed by the minimum wave length used in obtaining the diffraction patterns. By following the procedure used in the foregoing illustration, all of the apparent reflecting planes were reindexed and are listed in table 1 under the heading "True reflecting planes."

The author expresses his appreciation to G. A. Ellinger and H. C. Vacher for critical review of the manuscript and for suggestions regarding presentation of data; to Mr. Vacher for furnishing the copper monocrystal used in the investigation, and to R. J. Fallon, a summer staff member currently doing graduate work at Catholic University, for his industrious experimentation which, in addition to corroborating the results obtained by the author, furnished information that added materially to the author's concept of the growth of the electrodeposits, as described herein.

WASHINGTON, January 15, 1958.

Journal of Research of the National Bureau of Standards Vol. 60, No. 6, June 1958 Research Paper 2874

Dielectric Constant of Deuterium Oxide

Cyrus G. Malmberg

An equal ratio-arm, capacitance-conductance bridge operated at frequencies below 100 kilocycles per second was used to measure the dielectric constant of deuterium oxide with an accuracy of 0.1 percent or better in the range 4° to 100° C. A value of 77.94 was found for the dielectric constant at 25° C. The data fit the relation

$$\epsilon = 87.48_2 - (0.40509)t + (9.638 \times 10^{-4})t^2 - (1.333 \times 10^{-6})t^3,$$

with a maximum deviation of less than 0.01 unit in dielectric constant. These values were obtained by using a sample having a deuterium oxide content of 99.38 mole percent. Deviation of these values from those for pure deuterium oxide, as a result of isotopic contamination, is estimated to be less than 0.005 unit. Some aspects of the temperature dependence of the dielectric constant and of that of a macroscopic polarization are discussed.

1. Introduction

Only a few determinations of the dielectric constant of deuterium oxide have been reported in the literature, and of these only Wyman and Ingalls [1] [1] report static values obtained over an extended range of temperature. Their work included a direct comparison with water from 0° to 100° C, and the values obtained were dependent on Wyman's [2] value for water at 25° C.

The present investigation was designed to redetermine the dielectric constant of deuterium oxide from 4° to 100° C with an accuracy of 0.1 percent or better. The measurements were made with a low-frequency bridge, equipped with a Wagner ground, and a three-terminal test cell. They were essentially absolute in that no standard medium other than air was required for calibrating the cell.

2. Materials

The deuterium oxide was a sample originally stated to be 99.5 mole percent deuterium oxide. Mass spectrographic analysis indicated that the oxygen content was 0.9 mole percent O^{18}. After distillation of the sample in a closed system and measurement of its dielectric constant, the density of the sample was found to be 1.1045_5 g/cm at 25° C. When corrected for the excess O^{18}, this density corresponds to a deuterium oxide content of 99.38 mole percent.

3. Experimental Techniques

The a-c bridge was of the equal ratio-arm, capacitance-conductance type employing a Wagner ground to permit proper use of the guarded test cell. With minor exceptions, this apparatus and the techniques employed in the present measurements were the same as previously described [3, 4]. All measurements were made at frequencies in the range 3 to 96 kc in a cell that was used for a previous determination on ordinary water [4] (cell A). To control its temperature more simply, this cell was fitted with a leakproof cover to allow its total immersion in the bath media, with control to better than 0.01° C.

Determinations of the air capacity of the cell were made both before and during the measurements on D_2O as part of stepwise recalibrations of the fundamental interval of the standard capacitor. These measurements and check measurements with ordinary water as the dielectric media indicate a very slight change of 0.01 percent in the replaceable capacity of the cell from that previously found. The long-term stability indicated by these checks also serves for purposes of comparison to relate more closely the present measurements on deuterium oxide with those previously made on water.

Because excessive conductance of the sample can be a major source of error, it is particularly desirable to eliminate ionizable impurity in the material under study. The apparatus shown in figure 1 was de-

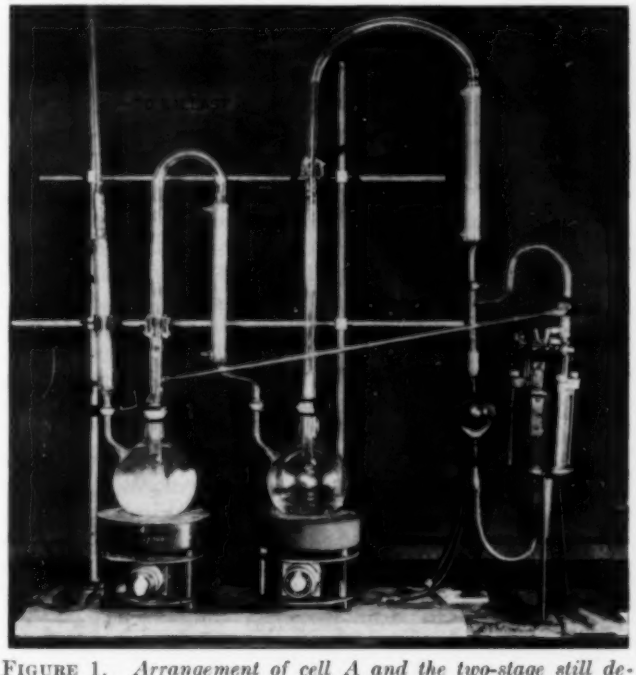

FIGURE 1. *Arrangement of cell A and the two-stage still designed for separation of ionizable impurity from the sample of* D_2O.

Figures in brackets indicate the literature references at the end of this paper.

signed for this purpose, in view of the limited sample available. It consists of the two simple Pyrex-glass evaporators and condensers connected in tandem with the cell. The output of the second stage is fed to the reservoir of the cell, and after passing through the cell is returned to the evaporator of the first stage. Isolation of the system is accomplished by connection to a 20-liter atmospheric ballast, through a reflux condenser from the first stage.

The two stages were required to free the distillate of volatile acidic and basic impurities, such as carbon dioxide and deutero-ammonia (ND_3). This was accomplished by placing 1 g of calcium oxide formed from the carbonate in the first evaporator and 2 g of phosphoric anhydride in the second evaporator. Approximately 600 ml of sample was then added to stage 1, and half of this was distilled into stage 2 to produce alkaline and acid solutions for respective conversion of volatile acidic and basic impurities to nonvolatile compounds. As the system was effectively closed, redistillation and recirculation through the cell could continue until minimum conductivity or that of a degree desired had been achieved. Through use of a temporary heating coil surrounding the cell, the contents could be maintained at the boiling point to aid in leaching out the cell and to permit adjustment of the final level as desired in its reservoir. Boiling the sample in the cell also eliminated the tendency for bubbles to form between the electrodes.

Contamination by water vapor and carbon dioxide was avoided by maintaining an atmosphere of nitrogen over the sample in the cell during the course of the measurements of dielectric constant. Following a set of measurements the cell was reinserted in the distillation train and refilled for companion measurements. During the various stages of "processing" the cell, the minimum conductivity observed at 25° C was 0.050μmho/cm.

Determinations of the dielectric constant of the deuterium oxide were made at 5-degree intervals. For each temperature the cell was refilled at least once and the measurements repeated.

Conditions of corresponding conductivity at a given temperature were avoided as a further check on the validity of the procedures used to correct for the influence of conductivity and related phenonema [4]. At any temperature the values of dielectric constant obtained agreed to better than 0.01 unit with respect to their mean.

In all, 60 determinations were made at 21 temperatures. Except for error resulting from isotopic contamination of the sample, which is estimated to be less than 0.005 unit, the known sources of error are similar, and their effects are comparable to those previously reported for water. (The residual uncertainty in dielectric constant as a result of any recognized source of error appears to be limited to 0.01 unit or less.)

4. Results

The values of the dielectric constant of the sample as measured over the range 4° to 100° C fit the equation

$$\epsilon = 87.48_2 - (0.40509)t + (9.638\times10^{-4})t^2 - (1.333\times10^{-6})t^3, \quad (1)$$

where t is the temperature in degrees Celsius. The values obtained from this equation, along with the difference between these values and those measured at specific temperatures, are listed in table 1. The maximum deviation is below 0.01 unit. Values of $d\epsilon/dt$ and the temperature coefficient $(1/\epsilon)(d\epsilon/dt)$ are listed in the remaining columns.

The data may also be represented by the relation

$$\mathrm{Log}_{10}\epsilon = 1.94167 - 0.0019940t, \quad (2)$$

with a maximum deviation of 0.03 unit and an average deviation of ±0.02 unit in dielectric constant. However, these deviations are not random with temperature. The over-all accuracy of the values of dielectric constant listed in table 1 is considered to be ±0.05 unit or better and that of the temperature coefficient 1 percent or better at all temperatures. Deviation of these values from those for pure deuterium oxide as a result of isotopic contamination is estimated to be less than 0.005 unit.

TABLE 1. *Dielectric constant of deuterium oxide and related data*

t	ϵ eq (1)	ϵ eq (1) − ϵ obs.	$-d\epsilon/dt$	$\frac{1}{\epsilon}\frac{d\epsilon}{dt}$
°C				
4	85.877	+0.007	0.3974	4.627×10^{-3}
5	85.480	−.001	.3956	4.628
10	83.526	+.002	.3862	4.624
15	81.618	−.001	.3771	4.620
20	79.755	+.001	.3681	4.615
25	77.936	−.001	.3594	4.611
30	76.161	+.002	.3509	4.607
35	74.427	−.001	.3425	4.602
40	72.735	+.002	.3344	4.597
45	71.083	.000	.3265	4.593
50	69.470	−.003	.3187	4.587
55	67.896	−.005	.3112	4.583
60	66.358	−.001	.3038	4.578
65	64.857	+.005	.2967	4.575
70	63.391	−.001	.2898	4.571
75	61.959	+.002	.2830	4.567
80	60.561	−.002	.2765	4.565
85	59.194	−.003	.2701	4.563
90	57.859	.000	.2640	4.563
95	56.554	.000	.2581	4.564
100	55.278	+.006	.2523	4.564

5. Discussion

A direct comparison of the present data with those of Wyman and Ingalls is not too significant due to the difference in absolute reference. A comparison by means of the companion measurements on ordinary water is possible and also advantageous because the similarity of D_2O and H_2O makes their difference in dielectric constant of some interest. These differences, as determined by Wyman and Ingalls, and by Malmberg and Maryott and the present data, are shown, respectively, by curves A and B of figure 2. The shape of these curves seems significant in that both show distinct maxima

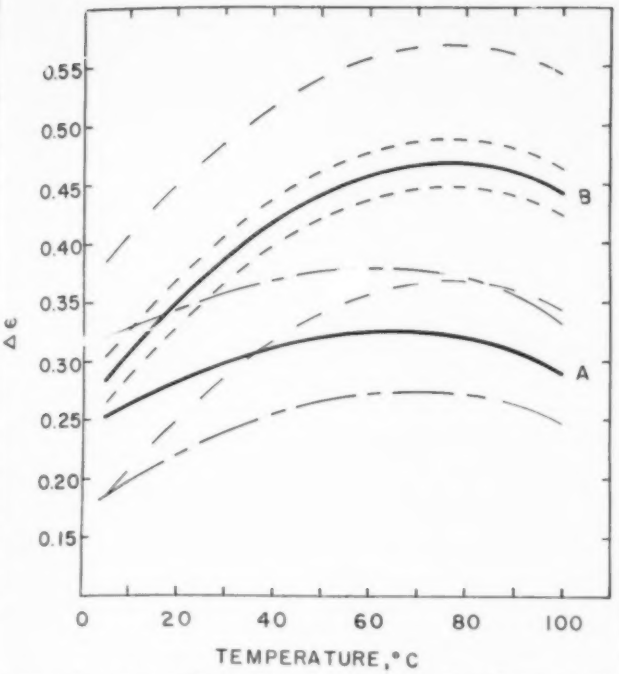

FIGURE 2. *Comparison of the temperature-dependence of the difference in dielectric constant between* H_2O *and* D_2O *as determined by Wyman and Ingalls (A) and by Malmberg and Maryott and the present work (B).*

in the same temperature range. At the same time, their lack of identity indicates that significant error exists for which correction has not been made. The differences involved are small but not negligible in view of the precision of measurement achieved. No positive explanation for the difference in $\Delta\epsilon$ is available and, as the limits of accuracy of $\Delta\epsilon$ are set by those of the parent data, it is difficult to assess its actual significance in any case. These limits are indicated in figure 2, where the bands centered about curve B respectively represent the experimental reproducibility obtained and the limits of accuracy in terms of the basic data. The band centered on curve A represents the sum of the mean deviations reported for the data supporting this curve (0.078%). A comparable band for curve B would be less than ± 0.01 unit wide, about one-sixth or less than that for curve A. If unrecognized sources of error involved in the measurements supporting curve B are constant, then the probable accuracy of this curve is closely related to the reproducibility of the data. It is believed that a near approach to these conditions was achieved experimentally and that the values of $\Delta\epsilon$ for curve B are probably accurate to ± 0.03 unit or better.

In figure 3, values of the temperature coefficient, $(1/\epsilon)(d\epsilon/dt)$, obtained by Wyman and Ingalls are compared with those listed in table 1. The values from the present data are considerably more constant with temperature, and consequently the data are more nearly represented by a logarithmic relation, such as eq (2), than are the data of Wyman and Ingalls. The agreement in temperature coefficient obtained is in general satisfactory, even though a knowledge of this

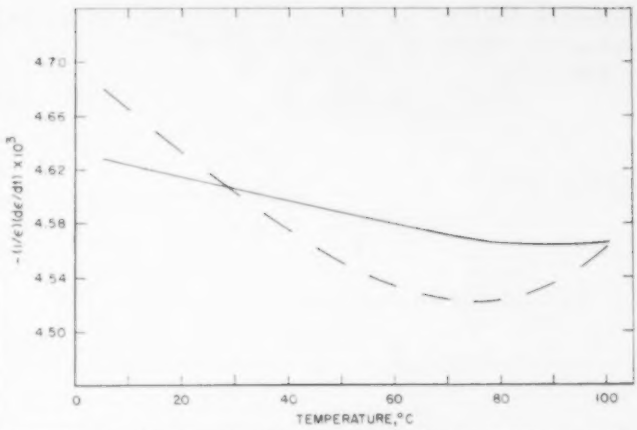

FIGURE 3. *Temperature-dependence of the temperature coefficient of* ϵ *for* D_2O.
----------, Reported by Wyman and Ingalls.
——————, Present work.

parameter to better than 1 percent is desirable in certain thermodynamic applications. It should be noted that the temperature dependence of $(1/\epsilon)(d\epsilon/dt)$ for the companion data on water exhibits a distinct parallelism with those on D_2O, indicating that the values obtained are significantly influenced by the procedures employed.

A comparison of dielectric properties can be made in terms of a "macroscopic polarization", P, defined by

$$P=(\epsilon-1)V, \tag{3}$$

where V is the molar volume. The temperature dependence of P frequently follows the relation

$$P_T \approx a+b/T, \tag{4}$$

where a and b are empirical constants and T the absolute temperature. Applied to existing data on nonpolar, polar, and on "associated" polar liquids, the approximation is in many cases quite good, 1 percent or better, over wide ranges of temperature.

Values of P calculated for deuterium oxide and water in accordance with eq 3 are listed in table 2. They are based on the present values for deuterium oxide and those for water obtained previously [4]. The molar volumes used were calculated by means of the table of densities due to T. L. Chang and L. H. Tung [5]. The respective values of 18.021_1 and 20.033_9 were used for the molecular weights of normal water and of 100-percent deuterium oxide having 0.21 mole percent O^{18}. The present sample of deuterium oxide does not exactly fit this description, but this is not significant for the present purpose because the effects of concentration errors are estimated to be less than 0.005 unit on the value of ϵ at any temperature. The difference in polarization, ΔP, for these two compounds is always relatively less than their difference in dielectric constant. Values of ΔP are always rather small, amounting to at most about 0.6 percent around 100° C, and the value changes sign between 15° and 20° C.

Because a graphical analysis was not sufficiently sensitive, mean values of the constants a and b

corresponding to eq (4) were calculated from the values of P listed in table 2.

For D_2O,

$$P=\frac{553{,}825}{T}-461.58, \tag{5}$$

and for H_2O,

$$P=\frac{544{,}265}{T}-428.14. \tag{6}$$

TABLE 2. *Macroscopic polarization of* H_2O *and* D_2O

$P=(\epsilon-1)V$

t	V_{cm^3}		P_{cm^3}		ΔP_{cm^3}
	H_2O	D_2O	H_2O	D_2O	
°C					
0	18.0235	.....	1,563.36	.....	.....
3.8	.0211$_4$	18.1240	.....	1,539.74	.....
5.0	.0213	.1212	1,527.54	1,530.88	−3.34
10.0	.0260	.1146	1,493.13	1,494.93	−1.80
15.0	.0368	.1166	1,460.01	1,460.52	−0.51
20.0	.0530	.1253	1,428.05	1,427.46	+0.59
25.0	.0741	.1400	1,397.20	1,395.62	1.56
30.0	.0993	.1599	1,367.33	1,364.92	2.41
35.0	.1288	.1847	1,338.41	1,335.25	3.14
40.0	.1619	.2139	1,310.40	1,306.57	3.83
45.0	.1988	.2474	1,283.23	1,278.83	4.42
50.0	.2387	.2849	1,256.83	1,251.97	4.88
55.0	.2820	.3261	1,231.20	1,225.95	5.29
60.0	.3283	.3706	1,206.28	1,200.67	5.65
65.0	.3779	.4184	1,182.05	1,176.15	5.96
70.0	.4301	.4693	1,158.46	1,152.32	6.20
75.0	.4853	.5235	1,135.50	1,129.18	6.36
80.0	.5435	.5807	1,113.11	1,106.69	6.48
85.0	.6044	.6410	1,091.32	1,084.80	6.54
90.0	.6682	.7042	1,070.04	1,063.50	6.56
95.0	.7346	.7703	1,049.27	1,042.76	6.49
100.0	.8038	.8391	1,028.94	1,022.55	6.33
101.4	.8238	.8591	.....	.....	.....

The agreement of the values of P calculated by these equations with those listed in table 2 is shown in figure 4. In only one instance is the deviation greater than 0.1 percent, and the mean deviations are 0.03 and 0.06 percent, respectively. The error associated with these calculations is controlled by the accuracy of the values of dielectric constant. This agreement is therefore very satisfactory as a support for the validity of eq 4. If this relation can be sufficiently well substantiated for a broad range of pure liquids, it will be useful for the interpolation and prediction of polarization with temperature as well as for possible identification of anomolous behavior in liquids.

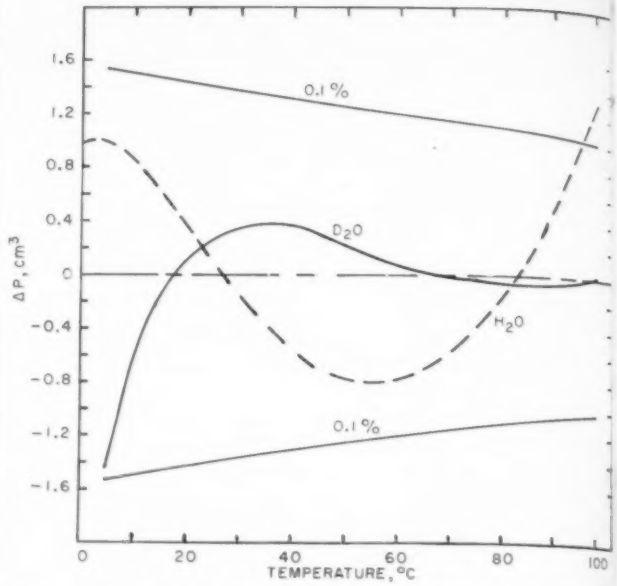

FIGURE 4. *The difference between calculated values of* P [*eq (5) or eq (6)*] *and measured values* $((\epsilon-1)V)$ *plotted as a function of temperature.*

6. References

[1] J. Wyman and E. N. Ingalls, J. Am. Chem. Soc. **60,** 1182 (1938).

[2] J. Wyman, Phys. Rev. **35,** 623 (1930).

[3] C. G. Malmberg and A. A. Maryott, J. Research NBS **45,** 299 (1950) RP2137.

[4] C. G. Malmberg and A. A. Maryott, J. Research NBS **56,** 1 (1956) RP2641.

[5] T. L. Chang and L. H. Tung, Chinese J. Phys. **7,** 230 (1949).

WASHINGTON, November 12, 1957.

Journal of Research of the National Bureau of Standards Vol. 60, No. 6, June 1958 Research Paper 2875

Additional Abscissas and Weights for Gaussian Quadratures of High Order: Values for n=64, 80, and 96

Philip Davis and Philip Rabinowitz [1]

Abscissas and weights for Gaussian quadratures of orders n=64, 80, and 96 are given to twenty decimal places.

In a previous paper,[2] tables of zeros of the Legendre polynomials $P_n(x)$ were published for various values of n up to n=48. It was also stated there that values were available for n=64, 80, and 96. Despite a brisk demand for these values, they were not published with the others because doubt was cast on their accuracy. It was feared that the round-off error accumulated in using the recursion formula for Legendre polynomials

$$P_n(x)=\left(2-\frac{1}{n}\right)xP_{n-1}(x)-\left(\frac{n-1}{n}\right)P_{n-2}(x) \qquad (1)$$

$$P_0(x)=1, \quad 1\ P_1(x)=x$$

would propagate to such an extent that for high values of n a significant loss of accuracy would result.

These values are now published since we have been able to show that these fears were unfounded. The way this was accomplished was as follows:

$P_n(x_{kn}+5.10^{-22})$ $(k=1, \ldots, \frac{n}{2})$ was evaluated on the WEIZAC (Weizmann Automatic Computer), using triple-precision operations, with the thought that if $P_n(x_{kn}+5.10^{-22})$ would be of different sign than $P_n(x_{kn}-5.10^{-22})$, then x_{kn} would be a correct 21-place zero of $P_n(x)$, The only triple-precision operations needed were addition, subtraction, and multiplication. In addition, the triple-precision quotient of two single-precision numbers was needed. An interpretive routine simplified the program for evaluating $P_n(x)$.

The results of this computation were that the SEAC (Standards Electronic Automatic Computer) values were all correct to 21 places with one exception; one value was in error by 1 in the 21st place and has been corrected in the present table.

Because the weights were computed by the formula

$$a_{kn}=\frac{2(1-x_{kn}^2)}{[nP_{n-1}(x_{kn})]^2}\ k=1, 2, \ldots, n/2, \qquad (2)$$

and because $P_n(x_{kn})$ was found to be correct to within 1 unit in the 21st place, it was felt that $P_{n-1}(x_{kn})$ was also correct to 21 places and hence a_{kn} can be considered correct to the 20 places given in the table.

In the tables, only the abscissas lying between 0 and 1 have been listed.

[1] Present address, Weizmann Institute, Rehovoth, Israel.
[2] P. Davis and P. Rabinowitz, Abscissas and weights for Gaussian quadratures of high order, J. Research NBS **56**, 35 (1956) RP2645.

Abscissas		Weights	
		n = 64	
0.9993050417	35772139457	0.0017832807	2169643294
0.9963401167	71955279347	0.0041470332	6056246763
0.9910133714	76744320739	0.0065044579	6897836285
0.9833362538	84625956931	0.0088467598	2636394772
0.9733268277	89910963742	0.0111681394	6013112881
0.9610087996	52053718919	0.0134630478	9671864259
0.9464113748	58402816062	0.0157260304	7602471932
0.9295691721	31939575821	0.0179517157	7569734308
0.9105221370	78502805756	0.0201348231	5353020937
0.8893154459	95114105853	0.0222701738	0838325415
0.8659993981	54092819761	0.0243527025	6871087333
0.8406292962	52580362752	0.0263774697	1505465867
0.8132653151	22797559742	0.0283396726	1425948322
0.7839723589	43341407610	0.0302346570	7240247886
0.7528199072	60531896612	0.0320579283	5485155358
0.7198818501	71610826849	0.0338051618	3714160939
0.6852363130	54233242564	0.0354722132	5688238381
0.6489654712	54657339858	0.0370551285	4024004604
0.6111553551	72393250249	0.0385501531	7861562912
0.5718956462	02634034284	0.0399537411	3272034138
0.5312794640	19894545658	0.0412625632	4262352861
0.4894031457	07052957479	0.0424735151	2365358900
0.4463660172	53464087985	0.0435837245	2932345337
0.4022701579	63991603696	0.0445905581	6375656306
0.3572201583	37668115950	0.0454916279	2741814448
0.3113228719	90210956158	0.0462847965	8131441729
0.2646871622	08767416374	0.0469681828	1621001732
0.2174236437	40007084150	0.0475401657	1483030866
0.1696444204	23992818037	0.0479993885	9645830772
0.1214628192	96120554470	0.0483447622	3480295717
0.0729931217	87799039450	0.0485754674	4150342693
0.0243502926	63424432509	0.0486909570	0913972038
		n = 80	
0.9995538226	51630629880	0.0011449500	0318694153
0.9976498643	98237688900	0.0026635335	8951268166
0.9942275409	65688277892	0.0041803131	2469489523
0.9892913024	99755531027	0.0056909224	5140319864
0.9828485727	38629070418	0.0071929047	6811731275
0.9749091405	85727793386	0.0086839452	6926085842
0.9654850890	43799251452	0.0101617660	4110306452
0.9545907663	43634905493	0.0116241141	2079782691
0.9422427613	09872674752	0.0130687615	9240133929
0.9284598771	72445795953	0.0144935080	4050907611
0.9132631025	71757654165	0.0158961835	8372568804
0.8966755794	38770683194	0.0172746520	5626930635
0.8787225676	78213828704	0.0186268142	0829903142
0.8594314066	63111096977	0.0199506108	7814199892
0.8388314735	80255275617	0.0212440261	1578200638
0.8169541386	81463470371	0.0225050902	4633246192
0.7938327175	04605449949	0.0237318828	6593010129
0.7695024201	35041373866	0.0249225357	6411549110
0.7440002975	83597272317	0.0260752357	6756511790
0.7173651853	62099880254	0.0271882275	0048638067
0.6896376443	42027600771	0.0282598160	5727686239
0.6608598989	86119801736	0.0292883695	8326784769
0.6310757730	46871966248	0.0302723217	5955798066
0.6003306228	29751743155	0.0312101741	8811470164
0.5686712681	22709784725	0.0321004986	7348777314
0.5361459208	97131932020	0.0329419393	9764540138
0.5028041118	88784987594	0.0337332149	8461152281
0.4686966151	70544477036	0.0344731204	5175392879

Abscissas		Weights	
		n = 80, Continued	
0.4338753708	31756093062	0.0351605290	4474759349
0.3983934058	81969227024	0.0357943939	5341605460
0.3623047534	99487315619	0.0363737499	0583597804
0.3256643707	47701914619	0.0368977146	3827600883
0.2885280548	84511853109	0.0373654902	3873049002
0.2509523583	92272120493	0.0377763643	6200139749
0.2129945028	57666132572	0.0381297113	1447763834
0.1747122918	32646812559	0.0384249930	0695942318
0.1361640228	09143886559	0.0386617597	7407646332
0.0974083984	41584599063	0.0388396510	5905196893
0.0585044371	52420668629	0.0389583959	6276953119
0.0195113832	56793997654	0.0390178136	5630665481
		n = 96	
0.9996895038	83230766828	0.0007967920	6555201242
0.9983643758	63181677724	0.0018539607	8894692173
0.9959818429	87209290650	0.0029107318	1793496400
0.9925439003	23762624572	0.0039645543	3844468667
0.9880541263	29623799481	0.0050142027	4292751769
0.9825172635	63014677447	0.0060585455	0423596168
0.9759391745	85136466453	0.0070964707	9115386526
0.9683268284	63264212174	0.0081268769	2569875921
0.9596882914	48742539300	0.0091486712	3078338663
0.9500327177	84437635756	0.0101607705	3500841575
0.9393703397	52755216932	0.0111621020	9983849859
0.9277124567	22308690965	0.0121516046	7108831963
0.9150714231	20898074206	0.0131282295	6696157263
0.9014606353	15852341319	0.0140909417	7231486091
0.8868945174	02420416057	0.0150387210	2699493800
0.8713885059	09296502874	0.0159705629	0256229138
0.8549590334	34601455463	0.0168854798	6424517245
0.8376235112	28187121494	0.0177825023	1604526083
0.8194003107	37931675539	0.0186606796	2741146738
0.8003087441	39140817229	0.0195190811	4014502241
0.7803690438	67433217604	0.0203567971	5433332459
0.7596023411	76647498703	0.0211729398	9219129898
0.7380306437	44400132851	0.0219666444	3874434919
0.7156768123	48967626225	0.0227370696	5832937400
0.6925645366	42171561344	0.0234833990	8592621984
0.6687183100	43916153953	0.0242048417	9236469128
0.6441634037	84967106798	0.0249006332	2248361028
0.6189258401	25468570386	0.0255700360	0534936149
0.5930323647	77572080684	0.0262123407	3567241391
0.5665104185	61397168404	0.0268268667	2559176219
0.5393881083	24357436227	0.0274129627	2602924282
0.5116941771	54667673586	0.0279700076	1684833444
0.4834579739	20596359768	0.0284974110	6508538564
0.4547094221	67743008636	0.0289946141	5055523654
0.4254789884	07300545365	0.0294610899	5816790597
0.3957976498	28908603285	0.0298963441	3632838598
0.3656968614	72313635031	0.0302999154	2082759379
0.3352085228	92625422616	0.0306713761	2366914901
0.3043649443	54496353024	0.0310103325	8631383742
0.2731988125	91049141487	0.0313164255	9686135581
0.2417431561	63840012328	0.0315893307	7072716855
0.2100313104	60567203603	0.0318287588	9441100653
0.1780968823	67618602759	0.0320344562	3199266321
0.1459737146	54896941989	0.0322062047	9403025066
0.1136958501	10665920911	0.0323438225	6857592842
0.0812974954	64425558994	0.0324471637	1406426936
0.0488129851	36049731112	0.0325161187	1386883598
0.0162767448	49602969579	0.0325506144	9236316624

WASHINGTON, January 27, 1958.

Journal of Research of the National Bureau of Standards Vol. 60, No. 6, June 1958 Research Paper 2876

Mass Spectra of Aromatic Hydrocarbons Filtered from Smoky Air [1]

Fred L. Mohler, Paul Bradt, and Vernon H. Dibeler

Public health service chemists collected particulate matter from smoky air and separated aliphatic and aromatic hydrocarbons from this material. These samples have been analyzed by two methods. In one method the sample is slowly evaporated from a tube furnace directly into the mass spectrometer and spectra recorded as the temperature is increased step by step. In the other method the sample is completely vaporized in a heated reservoir and the vapor passed through a leak into the mass spectrometer. Mass spectra of the aliphatic compounds are not reported in detail. Mass spectra of the aromatic fractions evaporated from the tube furnace show sharply defined fractionation with molecule ions of fused-ring aromatics predominant. Compounds containing three to seven fused rings are tentatively identified. The mass spectrum from the reservoir mass spectrometer was recorded at ionizing voltages of 70 v and at a low voltage, which gives predominantly molecule ions. The fused-ring aromatics include compounds that are carcinogenic.

1. Introduction

The Sanitary Engineering Center of the Public Health Service in Cincinnati, Ohio, has collected particulate matter from smoky air by drawing air through a glass filter. Hydrocarbons are dissolved out of the filter by an appropriate solvent, and aromatic compounds are separated from aliphatic and alicyclic compounds in a silica gel column. The solvent is then evaporated away at a temperature of 60° C. These samples have been submitted to the Bureau's Mass Spectrometry Section for study. The prolonged drying at 60° C evaporates away the lighter hydrocarbons, and the residues are mixtures of heavy hydrocarbons with molecular weight in excess of about 160. The smoky air samples were collected in London, England, and in St. Bernard, which is an industrial area near Cincinnati, Ohio. Coal smoke is probably predominant in both localities.

The following generalizations can be made about analysis of heavy hydrocarbon mixtures. In heavy aliphatic compounds the molecule ion peaks are always very small (of the order of 1 percent in *n*-paraffins and much smaller in branched compounds), and radical ions $C_4H_9^+$, $C_3H_7^+$, and $C_5H_{11}^+$ are usually the most abundant ions. In monocyclics the radical ions, $C_nH_{2n-1}^+$ are more abundant, in dicyclics $C_2H_{2n-3}^+$, etc. Thus the mass spectra are indicative of the type of compounds in a mixture, but the molecular weights are not definitely determined.

In aromatic compounds the molecule ions are more abundant, and in polycyclic aromatics the molecule ion is by far the most abundant ion. Thus in a mixture of heavy aromatics the polycyclic aromatic compounds can be identified by their molecule ions. The mass spectra of isomeric polycyclics are quite similar, and it is not feasible to distinguish individual compounds where there are several isomers [1].[2]

The mass spectrum at the customary ionizing voltages of 50 to 70 v is a mixture of fragment ions and molecule ions. In the case of aromatic compounds the appearance potentials of fragment ions are 4 v or more above the molecule ionization potentials. As the appearance potentials of molecule ions fall in a narrow range of less than a volt, it is possible to record a spectrum of the molecule ions alone at a low voltage of about 12 v [2]. In the case of aliphatic mixtures this is not feasible because the appearance potentials of the more abundant fragment ions are often within a volt of the molecule ion appearance potentials.

2. Experimental Procedure

Two different techniques have been used to obtain the mass spectra of the aromatic fractions. In one method the sample is evaporated directly from a tube furnace into the ionization chamber of a mass spectrometer [3]. The sample of a few milligrams of material is in a small tube in direct contact with a thermocouple that measures the temperature of evaporation. The temperature is increased step by step, and at each step the mass spectrum is recorded. The observations on a sample extend over a period of 5 or 6 days. This gradual evaporation fractionates the sample, and this is an advantage in dealing with a complicated mixture. The method is not quantitative, however, as the ion currents depend on the magnitude of the step-by-step changes in temperature. Steps are graduated to keep ion currents of a convenient magnitude and fairly constant over the time required to record the spectrum. The mass spectrometer was a 60° sector field instrument of 6-in. radius of curvature, and the spectra were recorded by varying the magnetic field at a constant ion-accelerating voltage.

In the second method used the sample was in a reservoir held at a temperature that completely vaporized it and the vapor passed through a pinhole

[1] This project was sponsored by the Department of Health, Education and Welfare.

[2] Figures in brackets indicate the literature references at the end of this paper.

leak into the mass spectrometer. The sample was introduced through a gallium-sealed valve into a 2-liter reservoir held at 300° C. A 180° Consolidated gas analysis mass spectrometer recorded the spectrum by varying the ion-accelerating voltage. This is a standard method of analysis developed by O'Neal [4], and it could be made quantitative if pure compounds were available for calibration.

3. Experimental Results

3.1. Aliphatic Fractions

Samples from St. Bernard and from London were run in the tube-furnace mass spectrometer. The spectra show a long sequence of mass peaks with ions containing from 1 to 40 carbon atoms, and in general the intensity decreases progressively from the C_4 group to the upper limit. The upper limit increases as the temperature is increased. Thus in the St. Bernard sample with the furnace at 83° C the spectrum extended to mass 404, $C_{29}H_{54}$. At 125° C, the limit was mass 500, $C_{36}H_{68}$; and at 163° C, the limit was mass 540, $C_{39}H_{72}$. In the lower and intermediate mass range, ions of formulas C_nH_{2n+1}, C_nH_{2n-1}, and C_nH_{2n-3} are the more abundant ions. In the London sample alkyl radical ions, C_nH_{2n+1}, are more abundant than in the St. Bernard sample. These mass spectra are not reported in detail, as they give no specific evidence as to the chemical composition.

3.2. Aromatic Fractions

The aromatic fractions were run both in the tube-furnace mass spectrometer and in the mass spectrometer with a heated reservoir. In contrast to the aliphatic samples, when the aromatic samples are slowly evaporated from the tube furnace there are striking changes in the mass spectrum as the temperature is increased step by step.

Table 1 lists the larger mass peaks in the mass spectra of the aromatic fraction from London smoke.

TABLE 1. *Selected peaks in the mass spectra of the London aromatic fraction*

m/e	Spectrum numbers and sample temperatures					
	No. 2 (62° C)	No. 5 (80° C)	No. 10 (110° C)	No. 12 (160° C)	No. 13 (199° C)	Reservoir (300° C)
105	.....	49	68	37	45	44.5
119	.....	71	95	58	72	48.6
145	.....	50	75	66	48	32.0
178	53	.....	.....	.....	.....	72.0
202	**407**	59	31	.....	20	**100.0**
216	102	42	.....	.....	18	26.1
228	45	**254**	29	.....	15	23.0
252	.....	149	**434**	48	16	27.7
276	.....	27	266	**575**	25	16.8
278	.....	.....	253	202	15	7.2
300	.....	.....	63	117	92	4.3
302	.....	.....	57	162	117	5.8
326	.....	.....	.....	50	**176**	1.6
328	.....	.....	.....	44	71	1.3
Max m/e	330	380	500	512	600	342

In the tube-furnace experiment, 25 mass spectra were recorded over a period of 6 days. In columns 2 to 6 of table 1 the larger peaks in five of these spectra are listed. The sample reached a temperature of 62° C without external heating, and the temperature was increased stepwise to 488° C, but there were no significant changes above 326° C. There were small peaks at almost every mass number, and the upper mass limit ranged from 330 at 62° C to over 600 at the higher temperatures. The upper mass limits of the spectra are given in the last row of the table. Columns 2 to 6 give ion currents in units of scale divisions on the most sensitive scale used. The last column gives the mass spectrum of the vapor in a reservoir at about 300° C, and ion currents are relative to mass 202 taken as 100.

Table 2 gives mass spectra obtained with the St. Bernard aromatic fraction. The arrangement of data is the same as in table 1, and the same mass peaks are reported. In this experiment, 19 spectra were recorded over a period of 5 days. Spectra 2, 6, 9, and 12 were obtained on successive days, and 13 was recorded on the same day as 12. In the St. Bernard sample the ions of mass 105, 119, and 145 are more abundant than in the London sample. In other respects the spectra are similar.

TABLE 2. *Selected peaks in the mass spectra of the St. Bernard aromatic fraction*

m/e	Spectrum numbers and sample temperatures					
	No. 2 (57° C)	No. 6 (74° C)	No. 9 (118° C)	No. 12 (143° C)	No. 13 (211° C)	Reservoir (300° C)
105	148	154	182	34	.....	25.6
119	151	190	370	63	.....	48.6
145	129	**230**	**520**	90	53	67.3
178	75	30	57	15	.....	40.0
202	**354**	73	78	15	.....	**100.0**
216	64	85	42	14	.....	28.9
228	37	**158**	42	12	.....	34.6
252	19	57	**170**	17	.....	20.2
276	4	23	156	28	38	14.0
278	4	25	78	15	.....	7.9
300	8	60	36	86	101	8.9
302	5	32	52	**115**	103	10.7
326	1	27	31	37	**192**	4.0
328	3	46	31	27	96	4.7
Max m/e	330	399	460	549	574	436.0

An experiment was tried with the London aromatic sample, using an ionizing voltage near the threshold for molecular ionization. The heated-reservoir mass spectrometer was used, and the results are presented in table 3. The ionizing voltage was set at 10 v, but the corrected voltage is probably about 12 v. The sensitivity was low but usable, as the most abundant ion of mass 202 gave a current of 60 scale divisions. All ions lighter than 167 were absent, and the only ions of odd mass number apart from C^{13} isotope peaks are 167, 181, 195, and 209. This indicates that fragment ions have been largely eliminated from the spectrum, and the remaining ions of even mass number are probably molecule ions.

TABLE 3. *Mass spectrum of London aromatic fraction at 10-v ionizing voltage*

Heated-reservoir mass spectrometer

m/e	Relative abundance	Possible identification	m/e	Relative abundance	Possible identification
167	15.0	.....	222	16.2	$C_{17}H_{18}$
170	11.1	.....	224	22.6	$C_{17}H_{20}$
178	**64.6**	$C_{14}H_{10}$			
180	7.8	$C_{14}H_{12}$	226	17.5	$C_{17}H_{22}$
181	16.6	.....	**228**	**21.4**	$C_{18}H_{12}$
			230	19.6	$C_{18}H_{14}$
182	14.2	$C_{14}H_{14}$	232	27.1	$C_{18}H_{16}$
184	18.6	$C_{14}H_{16}$	234	21.7	$C_{18}H_{18}$
190	9.9	.....			
192	61.5	$C_{15}H_{12}$	236	13.5	$C_{18}H_{20}$
194	14.4	$C_{15}H_{14}$	238	17.4	$C_{18}H_{22}$
			240	10.9	$C_{18}H_{24}$
195	18.1	.....	242	11.2	$C_{19}H_{14}$
196	28.0	$C_{15}H_{16}$	244	10.8	$C_{19}H_{16}$
198	19.8	$C_{15}H_{18}$			
202	**100.0**	$C_{16}H_{10}$	246	17.4	$C_{19}H_{18}$
204	17.8	$C_{16}H_{12}$	248	10.6	$C_{19}H_{20}$
			250	9.0	$C_{19}H_{22}$
206	54.4	$C_{16}H_{14}$	**252**	**17.5**	$C_{20}H_{12}$
208	19.5	$C_{16}H_{16}$	254	9.3	$C_{20}H_{14}$
209	13.2	.....			
210	31.0	$C_{16}H_{18}$			
212	26.2	$C_{16}H_{20}$	256	8.9	$C_{20}H_{16}$
			258	7.7	$C_{20}H_{18}$
216	37.0	$C_{17}H_{12}$	260	9.3	$C_{20}H_{20}$
218	32.2	$C_{17}H_{14}$	266	6.6	$C_{21}H_{14}$
220	32.7	$C_{17}H_{16}$	**276**	**7.8**	$C_{22}H_{12}$

4. Discussion

In table 1 the most abundant ions in spectra 2, 5, 10, 12, and 13 are at masses 202, 228, 252, 276, and 326, respectively. These could be fused-ring aromatics pyrene, $C_{16}H_{10}$; naphthacene, $C_{18}H_{12}$; benzpyrenes, $C_{20}H_{12}$; anthanthrene, $C_{22}H_{12}$; and benzanthanthrene, $C_{26}H_{14}$; or isomers of these compounds. In each case doubly-charged molecule ions are conspicuous, and spectra are consistent with the mass spectra of fused-ring aromatics published in the American Petroleum Institute tables of Mass Spectral Data [1]. Table 4 lists possible identifications of most of the peaks listed in tables 1 and 2. This table repeats from tables 1 and 2 the relative intensities as recorded by the heated-reservoir mass spectrometer. There are alternative explanations of many of these peaks, and results do not prove that all these peaks are fused-ring polycyclic aromatics. The list includes compounds with 3 to 7 fused six-membered rings, and in most instances there are several isomeric compounds of each mass number. Mass spectra of isomeric aromatics are in general quite similar, and it is not feasible to distinguish between isomers. Mass peaks 105, 119, and 145 are fragment ions from alkyl benzenes. These peaks, in contrast to the others in table 1, remain of comparable intensity as the temperature changes. This indicates that the fragment ions come from compounds with a wide range of molecular weights.

The mass spectra of the St. Bernard aromatic sample in table 2 are qualitatively like the London sample in table 1. The most conspicious difference is that the alkylbenzene fragment ions 105, 119, and 145 are much more abundant in the St. Bernard fraction. Also the ion of mass 302 is more abundant and is the most abundant ion in spectrum number 12

A comparison of the two samples can be made by comparing mass spectra obtained with the reservoir mass spectrometer in table 4.

TABLE 4. *Possible identifications of polycyclic aromatics*

m/e	Formulas	Abundance		Compounds
		London	St. Bernard	
178	$C_{14}H_{10}$	72.0	40.0	Anthracene.
202	$C_{16}H_{10}$	**100.0**	**100.0**	Pyrene.
216	$C_{17}H_{12}$	26.1	28.9	Benzanthrene.
228	$C_{18}H_{12}$	23.0	34.6	Naphthacene, etc.
252	$C_{20}H_{12}$	27.0	20.2	Benzpyrenes, etc.
276	$C_{22}H_{12}$	16.8	14.0	Anthanthrene, etc.
278	$C_{22}H_{14}$	7.2	7.9	Dibenzanthracenes, etc.
300	$C_{24}H_{12}$	4.3	8.9	Coronene.
302	$C_{24}H_{14}$	5.8	10.7	Dibenzpyrenes, etc.
326	$C_{26}H_{14}$	1.6	4.0	Benzanthanthrenes.
328	$C_{26}H_{16}$	1.3	4.7	Anthraceno anthracene.

In comparing spectra obtained with the tube-furnace mass spectrometer and the reservoir mass spectrometer it is to be noted that sensitivity of the former instrument operated at constant voltage increases as the molecular weight increases. The sensitivity of the other instrument operated at constant magnetic field tends to decrease. A recent paper reports a quantitative measurement of a known mixture of polyphenyls made with the tube-furnace spectrometer [3].

The low-voltage mass spectrum of table 3 presumably records molecule ions (except for the four peaks of odd mass number). The boldfaced mass peaks are peaks listed in tables 1 and 2 and are ascribed to fused-ring aromatics. The other peaks are interpreted as molecules derived by adding hydrogen or methyl radicals to these aromatics. The empirical formulas in the last column are derived on this assumption, but there are in most cases alternative possibilities. Because of the low sensitivity at low voltage, ions heavier than 276 were not detected in this experiment.

5. Conclusions

Results of table 3 indicate that there are at least 39 molecule ions in the limited mass range from 178 to 276 that is covered. The aromatic residues recovered from air are very complicated mixtures, and it is of interest that when these mixtures are slowly evaporated from the tube furnace, a few of the fused-ring compounds stand out conspicuously and can be identified. This is because the slow evaporation affords an effective fractionation of the mixture and because the mass spectrometer has exceptionally high sensitivity for fused-ring aromatic molecule ions.

The occurence of these fused-ring aromatics in smoky air is a matter of significance because some compounds of this class are carcinogenic. 3,4-Benzpyrene and 1,2-5,6-dibenzanthracene are known to be strongly carcinogenic [5], and it was recently found [6] that 3,4-9,10-dibenzpyrene is one of the most potent of the carcinogenic agents. Several other fused-ring aromatics are considered to be carcinogenic, and some alkyl derivatives are strongly carcinogenic.

Benzpyrenes of molecular weight 252 give the most abundant molecule ion in spectrum 10 of table 1 and spectrum 9 of table 2. Dibenzpyrenes and other somers of molecular weight 302 become most abundant in spectrum 12 of table 2, and dibenzanthracenes of molecular weight 278 are of comparable abundance. Although the mass spectra cannot distinguish between isomers, results indicate that carcinogenic compounds are probably present in appreciable quantities in smoky air. The formation of fused-ring aromatics seems to be associated with the formation of smoke when either solid or liquid fuels are burned [7].

6. References

[1] Am. Petrol. Inst. Catalog of Mass Spectral Data, Serial numbers 958, 959, 1017, 1018, 1019, 1020, 1022, and 1237.

[2] F. H. Field and S. H. Hastings, Anal. Chem. **28** 1248 (1956).

[3] Paul Bradt and Fred L. Mohler, J. Research NBS **60,** 143 (1958) RP2831.

[4] M. J. O'Neal and T. P. Weir, Anal. Chem. **23** 830 (1951).

[5] Erich Clar, Aromatische Kohlenwasserstoffe, (Polycyclische systeme) (Berlin, Springer Verlag, 1941).

[6] Lacassagne, Zajdela, Buu-Hoi and Chalvet. Compt. rend. **244** 273 (1957).

[7] J. F. Thomas and M. Mukai, Arch. Ind. Health **13** 567 (1956).

Washington, January 20, 1958.

INDEX TO VOLUME 60

January to June 1958—Research Papers 2815 to 2876

A

Page

Abscissas and weights for Gaussian quadratures of high order, additional: values for $n=64$, 80, and 96, RP2875 ... 613
Absorption spectra and the chemical constitution of dyes, relation between, RP2823 ... 65
Achhammer, B. G., M. R. Harvey, C. F. Bersch, Heat and ultraviolet aging of poly(vinyl chloride), RP2863 ... 481
—, *R. R. Stromberg, S. Straus,* Infrared spectra of thermally degraded poly(vinyl chloride), RP2832 ... 147
Acids, aromatic carboxylic, in benzene, relative strengths, RP2871 ... 569
Adiabatic calorimeter for the range 30° to 500° C, RP2848 ... 309
Aging, heat, and ultraviolet, of poly(vinyl chloride), RP2863 ... 481
Aircraft, delta-wing, effect of rib flexibility on the vibration modes of, RP2852 ... 335
Air shock, fragmentation of waterdrops in the zone behind an, RP2843 ... 245
Alkali silicate binary glasses, role of vitrons in, RP2854 ... 351
Alloys, enthalpy and heat capacity from 0° to 900° C of three nickel-chromium-iron of different carbon contents, RP2870 ... 563
Alloy, nickel, copper, and nickel-copper, annealed, creep of, RP2836 ... 173
Aluminum oxide, heat capacity, RP2848 ... 309
Aluminum single crystals, growth of, RP2868 ... 547
Annealed nickel, copper, and two nickel-copper alloys, creep of, RP2836 ... 173
Annular-slot antenna, low frequency, RP2822 ... 59
Antenna, annular-slot, low frequency, RP2822 ... 59
Attix, F. H., L. De La Vergne, V. H. Ritz, Cavity ionization as a function of wall material, RP2842 ... 235
Aromatic carboxylic acids in benzene at 25° C, relative strengths, RP2871 ... 569
Aromatic hydrocarbons filtered from smoky air, mass spectra of, RP2876 ... 615
Asphalt, changes in the properties, during the blowing operation, RP2835 ... 169
Average energy of sulfur-35 beta decay, RP2859 ... 447
Azo dyes, direct, interaction in aqueous solution, RP2823 ... 65

B

Barium hydrogen orthophosphate, crystal structure of, RP2817 ... 23
Bars, rectangular, shear modulus and torsional resonance frequencies, RP2861 ... 459
Belcher, H. V., H. S. White, Effects of capillary shape on flow characteristics and degradation of polymer solutions, RP2839 ... 215
Benzene, relative strengths of forty aromatic carboxylic acids in, at 25° C, RP2871 ... 569
Berger, M. J., J. C. Lamkin, Sample calculations of gamma-ray penetration into shelters: contributions of sky shine and roof contamination, RP2827 ... 109
Bersch, C. F., M. R. Harvey, B. G. Achhammer, Heat and ultraviolet aging of poly(vinyl chloride), RP2863 ... 481
Beta decay, average energy of sulfur-35, RP2859 ... 447
Blaine, R. L., C. M. Hunt, V. Dantzler, L. A. Tomes, Reaction of portland cement with carbon dioxide, RP2858 ... 441
—, *E. K. Plyler,* Infrared measurements with a small grating from 100 to 300 microns, RP2821 ... 55
Borohydrides, sodium and potassium, heat content of, from 0° to 400° C, RP2828 ... 117
Bradt, P., F. L. Mohler, Mass spectra and relative sensitivities of some polyphenyls, RP2831 ... 143
—, —, *V. H. Dibeler,* Mass spectra of aromatic hydrocarbons filtered from smoky air, RP2876 ... 615
Breckenridge, F. C., An evaluation of the luminous-transmittance requirements for railroad-signal glassware in terms of standard source A of the International Commission on Illumination, RP2849 ... 317
Brode, W. R., M. N. Inscoe, J. H. Gould, M. E. Corning, Relation between the absorption spectra and the chemical constitution of dyes: 29. Interaction of direct azo dyes in aqueous solution, RP2823 ... 65
Brown, E. H., J. W. Dean, Joule-Thomson process in the liquefaction of helium, RP2834 ... 161
Burgers, J. M., A. Ghaffari, On the application of steam-driven water jets for propulsion purposes, RP2830 ... 137
Burley, G., Crystal structure of barium hydrogen orthophosphate, RP2817 ... 23

C

Calorimeter, adiabatic, for the range 30° to 500° C, RP2848 ... 309
Capillary shape, effects on flow characteristics and degradation of polymer solutions, RP2839 ... 215
Carbon dioxide, reaction of portland cement with, RP2858 ... 441
Carpenter, L. H., G. H. Keulegan, Forces on cylinders and plates in an oscillating fluid, RP2857 ... 423
Cascade electrons and photons, energy spectra, RP2824 ... 85
Cathodic protection of steel in salt water, current and potential relations, RP2833 ... 153
Carallo, L. M., H. H. Seliger, W. B. Mann, Average energy of sulfur-35 beta decay, RP2859 ... 447
Cavity ionization as a function of wall material, RP2842 ... 235
Cellulose, degradation in a vacuum with ultraviolet light, RP2841 ... 229
Cellulosic materials, thermal degradation of, RP2853 ... 343
Cement, portland, reaction with carbon dioxide, RP2858 ... 441
Cleek, G. W., E. H. Hamilton, Shape of the liquidus surface as a criterion of stable glass formation, RP2872 ... 593
Coleman, C. D., R. E. Trees, Tables for diagonalizing second-order matrices, RP2838 ... 201
Color-mixture functions studied by means of a pair of metameric grays, observer differences, RP2825 ... 97
Cooter, I. L., W. P. Harris, Improved bridge method for the measurement of core losses in ferromagnetic materials at high flux densities, RP2865 ... 509
Copper, nickel, and nickel-copper alloy, annealed, creep of, RP2836 ... 173
Copper on copper, twinned epitaxy of, RP2873 ... 597
Core losses in ferromagnetic materials, RP2865 ... 509
Corning, M. E., M. N. Inscoe, J. H. Gould, W. R. Brode, Relation between the absorption spectra and the chemical constitution of dyes: 29. Interaction of direct azo dyes in aqueous solution, RP2823 ... 65
Counter sources, 4π, self-absorption in, RP2859 ... 447
Creep of annealed nickel, copper, and two nickel-copper alloys, RP2836 ... 173
Crystalline polyphenyls, infrared spectra of, RP2829 ... 125
Crystals, single aluminum, growth of, RP2868 ... 547
Crystal structure of barium hydrogen orthophosphate, RP2817 ... 23
Current and potential relations for the cathodic protection of steel in salt water, RP2833 ... 153
Current balance, NBS, current measured with RP2846 ... 297
Current measured with a Pellat-type electrodynamometer, RP2845 ... 287
Current, measurement with the National Bureau of Standards current balance, RP2846 ... 297
Cutkosky, R. D., R. L. Driscoll, Measurement of current with the National Bureau of Standards current balance, RP2846 ... 297
Cylinders and plates, forces on, in an oscillating fluid, RP2857 ... 423

D

Dantzler, V., C. M. Hunt, L. A. Tomes, R. L. Blaine, Reaction of portland cement with carbon dioxide, RP2858 ... 441
Darling, W. R., F. E. Washer, Marginal performance of corrected ophthalmic lenses, RP2869 ... 551
Davis, M. M., H. B. Hetzer, Relative strengths of forty aromatic carboxylic acids in benzene, RP2871 ... 569
Davis, P., P. Rabinowitz, Additional abscissas and weights for Gaussian quadratures of high order: values for $n=64$, 80, and 96, RP2875 ... 613
Dead space, indirectly calculated, RP2826 ... 105
Dean, J. W., E. H. Brown, Joule-Thomson process in the liquefaction of helium, RP2834 ... 161
Degradation and flow characterstics of polymer solutions, effect of capillary shape on, RP2839 ... 215
Degradation of cellulose in a vacuum with ultraviolet light, RP2841 ... 229
Degradation, thermal, of cellulosic materials, RP2853 ... 343
De La Vergne, L., F. H. Attix, V. H. Ritz, Cavity ionization as a function of wall material, RP2842 ... 235
Delta-wing aircraft, effect of rib flexibility on the vibration modes of, RP2852 ... 335
Deuterium oxide, dielectric constant of, RP2874 ... 609
Diagonalizing second-order matrices, tables for, RP2838 ... 201
Dibeler, V. H., P. Bradt, F. L. Mohler, Mass spectra of aromatic hydrocarbons filtered from smoky air, RP2876 ... 615
Dielectric constant of deuterium oxide, RP2874 ... 609
Diniak, A. W., E. R. Weaver, E. E. Hughes, Determination of water vapor from the change in electrical resistance of a hygroscopic film, RP2864 ... 489
Douglas, T. B., A. W. Harman, Enthalpy and heat capacity from 0° to 900° C of three nickel-chromium-iron alloys of different carbon contents, RP2870 ... 563
—, —, Heat content of sodium borohydride and of potassium borohydride from 0° to 400° C, RP2828 ... 117
Draper, J. W., D. H. Weitzel, W. V. Loebenstein, O. E. Park, Ortho-para catalysis in liquid-hydrogen production, RP2840 ... 221
Driscoll, R. L., R. D. Cutkosky, Measurement of current with the National Bureau of Standards current balance, RP2846 ... 297
—, Measurement of current with a Pellat-type electrodynamometer, RP2845 ... 287
Dyes, direct azo, interaction in aqueous solution, RP2823 ... 65

E

Elastic problem for a ring of uniform force in an infinite body, RP2855 ... 365
Electrodynamometer, Pellat-type, measurement of current with, RP2845 ... 287
Electrons, cascade, and photons, energy spectra, RP2824 ... 85
Energy spectra of cascade electrons and photons, RP2824 ... 85
Engel, O. G., Fragmentation of waterdrops in the zone behind an air shock, RP2843 ... 245
Epitaxy, twinned, of copper on copper, RP2873 ... 597

F

Ferromagnetic materials, measurement of core losses, RP2865 ... 509
Fibers, properties and behavior of, when impacted at high velocities, RP2866 ... 517
Flame gases, sampling, RP2818 ... 29
Flame speeds, measurement of by a nozzle burner method, RP2867 ... 535
Florin, R. E., L. A. Wall, Effect of structure on the thermal decomposition of polymers, RP2860 ... 451
Flow characteristics and degradation of polymer solutions, effects of capillary shape on, RP2839 ... 215
Flynn, J. H., W. K. Wilson, W. L. Morrow, Degradation of cellulose in a vacuum with ultraviolet light, RP2841 ... 229
Forces on cylinders and plates in an oscillating fluid, RP2857 ... 423
Fragmentation of waterdrops in the zone behind an air shock, RP2843 ... 245

G

Gamma-ray penetration into shelters, RP2827 ... 109
Gases, flame, sampling, RP2818 ... 29
Gases in water, measurement, RR2864 ... 489
Gaussian quadratures of high order, abscissas and weights for: values for $n=64$, 80, and 96, RP2875 ... 613
Ghaffari, A., J. M. Burgers, On the application of steam-driven water jets for propulsion purposes, RP2830 ... 137
Ginnings, D. C., E. D. West, An adiabatic calorimeter for the range 30° to 500° C, RP2848 ... 309
Glasses, structure of alkali silicate binary, RP2854 ... 351
Glass formation, stable, shape of the liquidus surface as a criterion of, RP2872 ... 593

Page

Glassware, railroad-signal, an evaluation of the luminous-transmittance requirements, RP2849 ... 317
Goldberg, K., Random notes on matrices, RP2850 ... 321
Gould, J. H., M. N. Inscoe, M. E. Corning, W. R. Brode, Relation between the absorption spectra and the chemical constitution of dyes: 29. Interaction of direct azo dyes in aqueous solution, RP2823 ... 65
Ground waves, transient radiofrequency, over the surface of a finitely conducting plane earth, RP2844 ... 281
Growth of preferentially oriented aluminum single crystals, RP2868 ... 547

H

Halpern, C., Measurement of flame speeds by a nozzle burner method, RP2867 ... 535
—, *F. W. Ruegg*, A study of sampling of flame gases, RP2818 ... 29
Hamilton, E. H., G. W. Cleek, Shape of the liquidus surface as a criterion of stable glass formation, RP2872 ... 593
Harman, A. W., T. B. Douglas, Enthalpy and heat capacity from 0° to 900° C of three nickel-chromium-iron alloys of different carbon contents, RP2870 ... 563
—, —, Heat content of sodium borohydride and of potassium borohydride from 0° to 400° C, RP2828 ... 117
Harris, W. P., I. L. Cooter, Improved bridge method for the measurement of core losses in ferromagnetic materials at high flux densities, RP2865 ... 509
Hart, V. E., S. L. Madorsky, S. Straus, Thermal degradation of cellulosic materials, RP2853 ... 343
Harvey, M. R., C. F. Persch, B. G. Achhammer, Heat and ultraviolet aging of poly(vinyl chloride), RP2863 ... 481
Heat and ultraviolet aging of poly(vinyl chloride), RP2863 ... 481
Heat capacity and enthalpy from 0° to 900° C of three nickel-chromium-iron alloys of different carbon contents, RP2870 ... 563
Heat capacity of aluminum oxide, RP2848 ... 309
Heat content of potassium borohydride, RP2828 ... 117
Heat content of sodium borohydride and of potassium borohydride from 0° to 400° C, RP2828 ... 117
Helium, Joule-Thomson process in the liquefaction of, RP2834 ... 161
Hellmann, M., J. E. Stewart, Infrared spectra of crystalline polyphenyls, RP2829 ... 125
Hetzer, H. B., M. M. Davis, Relative strengths of forty aromatic carboxylic acids in benzene, RP2871 ... 569
Hoffman, J. D., J. J. Weeks, Specific volume and degree of crystallinity of semicrystalline poly(chlorotrifluoroethylene), and estimated specific volumes of the pure amorphous and crystalline phases, RP2862 ... 465
Hughes, E. E., E. R. Weaver, A. W. Diniak, Determination of water vapor from the change in electrical resistance of a hygroscopic film, RP2864 ... 489
Hunt, C. M., V. Dantzler, L. A. Tomes, R. L. Blaine, Reaction of portland cement with carbon dioxide, RP2858 ... 441
Hydrocarbons, aromatic, filtered from smoky air, mass spectra, RP2876 ... 615
Hydrogen, liquid, ortho-para catalysis in production, RP2840 ... 221

I

Impact tests of textile yarns, RP2866 ... 517
Infrared measurements with a small grating from 100 to 300 microns, RP2821 ... 55
Infrared spectra of crystalline polyphenyls, RP2829 ... 125
Infrared spectra of thermally degraded poly(vinyl chloride), RP2832 ... 147
Infrared study of some structural changes in natural rubber during vulcanization, RP2816 ... 9
Inscoe, M. N., J. H. Gould, M. E. Corning, W. R. Brode, Relation between the absorption spectra and the chemical constitution of dyes: 29. Interaction of direct azo dyes in aqueous solution, RP2823 ... 65
Ionization, cavity, as a function of wall materials, RP2842 ... 235

J

Jenkins, W. D., C. R. Johnson, Creep of annealed nickel, copper, and two nickel-copper alloys, RP2836 ... 173
Jessup, R. S., Some thermodynamic properties of the systems polybutadiene-benzene and polyisobutene-benzene, RP2820 ... 47
Johler, J. R., Transient radiofrequency ground waves over the surface of a finitely conducting plane earth, RP2844 ... 281
Johnson, C. R., W. D. Jenkins, Creep of annealed nickel, copper, and two nickel-copper alloys, RP2836 ... 173
Joule-Thomson process in the liquefaction of helium, RP2834 ... 161

K

Kelly, K. L., Observer differences in color-mixture functions studied by means of a pair of metameric grays, RP2825 ... 97
Keulegan, G. B., L. H. Carpenter, Forces on cylinders and plates in an oscillating fluid, RP2857 ... 423
Kiess, C. C., Description and analysis of the second spectrum of molybdenum, Mo II, RP2856 ... 375
Kleinschmidt, L. R., H. R. Snoke, Changes in the properties of an asphalt during the blowing operation, RP2835 ... 169
Kroll, W. D., Effect of rib flexibility on the vibration modes of a delta-wing aircraft, RP2852 ... 335

L

Lamkin, J. C., M. J. Berger, Sample calculations of gamma-ray penetration into shelters: contributions of sky shine and roof contamination, RP2827 ... 109
Lenses, corrected ophthalmic, marginal performance of, RP2869 ... 551
Liquefaction of helium, RP2834 ... 161
Linnig, F. J., J. E. Stewart, Infrared study of some structural changes in natural rubber during vulcanization, RP2816 ... 9
Liquid-hydrogen production, ortho-para catalysis in, RP2840 ... 221
Liquidus surface, shape of, as a criterion of stable glass formation, RP2872 ... 593
Loebenstein, W. V., Precise evaluation of surface area with indirectly calculated dead space, RP2826 ... 105
—, *D. H. Weitzel, J. W. Draper, O. E. Park*, Ortho-para catalysis in liquid-hydrogen production, RP2840 ... 221

Page

Luminous-transmittance requirements for railroad-signal glassware in terms of standard source A of the International Commission on Illumination, an evaluation of, RP2849 ... 317

M

Madorsky, S. L., V. E. Hart, S. Straus, Thermal degradation of cellulosic materials, RP2853 ... 343
Magnetic measurements, core losses in ferromagnetic materials at high flux densities, RP2865 ... 509
Malmberg, C. G., Dielectric constant of deuterium oxide, RP2874 ... 699
Mann, W. B., H. H. Seliger, L. M. Cavallo, Average energy of sulfur-35 beta decay, RP2859 ... 447
Marginal performance of corrected ophthalmic lenses, RP2869 ... 551
Mass spectra and relative sensitivities of some polyphenyls, RP2831 ... 143
Mass spectra of aromatic hydrocarbons filtered from smoky air, RP2876 ... 615
Matrices, condition of, RP2815 ... 1
Matrices, random notes on, RP2850 ... 321
Matrices, second-order, tables for diagonalizing, RP2838 ... 291
McCrackin F. L., J. C. Smith, H. F. Schiefer, Stress-strain relationships in yarns subjected to rapid impact loading: 5. Wave propagation in long textile yarns impacted transversely, RP2866 ... 517
Measurement of flame speeds by a nozzle burner method, RP2867 ... 535
Mohler, F. L., P. Bradt, Mass spectra and relative sensitivities of some polyphenyls, RP2831 ... 143
—, —, *V. H. Dibeler*, Mass spectra of aromatic hydrocarbons filtered from smoky air, RP2876 ... 615
Molybdenum, second spectrum, description and analysis, RP2856 ... 375
Morrow, W. L., J. H. Flynn, W. K. Wilson, Degradation of cellulose in a vacuum with ultraviolet light, RP2841 ... 229

N

Nickel-chromium-iron alloys, heat capacity and enthalpy, RP2870 ... 563
Nickel, copper, and two nickel-copper alloys, annealed, creep of, RP2836 ... 173
Nozzle burner method, measurement of flame speeds by, RP2867 ... 535
Numerical analysis, matrices, RP2815 ... 1

O

Observer differences in color-mixture functions studied by means of a pair of metameric grays, RP2825 ... 97
Olson, C. A., L. V. Spencer, Energy spectra of cascade electrons and photons, RP2824 ... 85
Orem, T. H., Growth of preferentially oriented aluminum single crystals, RP2868 ... 547
—, Twinned epitaxy of copper on copper, RP2873 ... 597
Ortho-para catalysis in liquid-hydrogen production, RP2840 ... 221

P

Park, O. E., D. H. Weitzel, W. V. Loebenstein, J. W. Draper, Ortho-para catalysis in liquid-hydrogen production, RP2840 ... 221
Pellat-type electrodynamometer, measurement of current, RP2845 ... 287
Pell, W. H., The elastic problem for a ring of uniform force in an infinitie body, RP2855 ... 366
Photons, cascade, and electrons, energy spectra, RP2824 ... 85
Plyler, E. K., L. R. Blaine, Infrared measurements with a small grating from 100 to 300 microns, RP2821 ... 55
Polyamides, pyrolysis of, RP2819 ... 39
Polybutadiene-benzene, some thermodynamic properties of the system, RP2820 ... 47
Poly(chlorotrifluoroethylene), semicrystalline, specific volume and degree of crystallinity, RP2862 ... 465
Polyisobutene-benzene, some thermodynamic properties of the system, RP2820 ... 47
Polymers, effect of structure on the thermal decomposition of, RP2860 ... 451
Polymer solutions, effects of capillary shape on flow characteristics and degradation, RP2839 ... 215
Polyphenyls, crystalline, infrared spectra, RP2829 ... 125
Polyphenyls, mass spectra and relative sensitivities of some, RP2831 ... 143
Poly(vinyl chloride), heat and ultraviolet aging, RP2863 ... 481
Poly(vinyl chloride), infrared spectra of thermally degraded, RP2832 ... 147
Portland cement, reaction with carbon dioxide, RP2858 ... 441
Potassium borohydride, heat content of, from 0° to 400° C., RP2828 ... 117
Precise evaluation of surface area with indirectly calculated dead space, RP2826 ... 105
Projected images used with range finders, RP2851 ... 327
Pyrolysis of polyamides, RP2819 ... 39

R

Rabinowitz, P., P. Davis, Additional abscissas and weights for Gaussian quadratures of high order: values for $n = 64$, 80, and 96, RP2875 ... 613
Radial distribution of the center of gravity of random points on a unit circle, RP2847 ... 307
Radiofrequency ground waves, transient, over the surface of a finitely conducting plane earth, RP2844 ... 281
Railroad-signal glassware in terms of standard source A of the International Commission on Illumination, an evaluation of the luminous transmittance requirements for, RP2849 ... 317
Random notes on matrices, RP2850 ... 321
Range finders using projected images, RP2851 ... 327
Rib flexibility, effect on the vibration modes of a delta wing aircraft, RP2852 ... 335
Ritz, V. H., L. DeLaVergne, F. H. Attix, Cavity ionization as a function of wall material, RP2842 ... 235
Rubber, natural, infrared study of some structural changes in during vulcanization, RP2816 ... 9
Rubber vulcanizates, pure-gum, stress-strain relation in compression and tension, RP2837 ... 193
Ruegg, F. W., C. Halpern, A study of sampling of flame gases, RP2818 ... 29

S

Page

Sampling of flame gases, RP2818 29
Scheid, F., Radial distribution of the center of gravity of random points on a unit circle, RP2847 307
Schiefer, H. F., J. C. Smith, F. L. McCrackin, Stress-strain relationships in yarns subjected to rapid impact loading: 5. Wave propagation in long textile yarns impacted transversely, RP2866 517
Schwerdtfeger, W. J., Current and potential relations for the cathodic protection of steel in salt water, RP2833 153
Self-absorption in 4π-counter sources, RP2859 447
Seliger, H. H., W. B. Mann, L. M. Carallo, Average energy of sulfur-35 beta decay, RP2859 447
Semicrystalline poly(chlorotrifluoroethylene), specific volume and degree of crystallinity of, and estimated specific volumes of the pure amorphous and crystalline phases, RP2862 465
Shape of the liquidus surface as a criterion of stable glass formation, RP2872 593
Shear modulus and torsional resonance frequencies of bars of rectangular cross section, RP2861 459
Shelters, gamma-ray penetration, RP2827 109
Signal glassware, railroad, an evaluation of the luminous-transmittance requirements, RP2849 317
Silicate glasses, role of vitrons in alkali, RP2854 351
Smith, J. C., F. L. McCrackin, H. F. Schiefer, Stress-strain relationships in yarns subjected to rapid impact loading: 5. Wave propagation in long textile yarns impacted transversely, RP2866 517
Snoke, H. R., L. P. Kleinschmidt, Changes in the properties of an asphalt during the blowing operation, RP2835 169
Sodium borohydride, heat content of, from 0° to 400° C, RP2828 117
Specific volume and degree of crystallinity of semicrystalline poly(chlorotrifluoroethylene), and estimated specific volumes of the pure amorphous and crystalline phases, RP2862 465
Spectra, absorption, and chemical constitution of dyes, relation between, RP2823 65
Spectra, energy, of cascade electrons and photons, RP2824 85
Spectra, infrared, of crystalline polyphenyls, RP2829 125
Spectra, infrared, of thermally degraded poly(vinyl chloride), RP2832 147
Spectra, mass, and relative sensitivities of some polyphenyls, RP2831 143
Spectra, mass, of aromatic hydrocarbons filtered from smoky air, RP2876 615
Spectrum, second, of molybdenum, description and analysis, RP2856 375
Spencer, L. V., C. A. Olson, Energy spectra of cascade electrons and photons, RP2824 85
Spinner, S., R. C. Valore, Comparison of theoretical and empirical relations between the shear modulus and torsional resonance frequencies for bars of rectangular cross section, RP2861 459
Standardization of sulfur-35 by 4π counting, RP2859 447
Steam-driven water jets for propulsion purposes, on the application of, RP2830 137
Steel, cathodic protection in salt water, RP2833 153
Stephens, Robert D., Range finders, using projected images, RP2851 327
Stewart, J. E., F. J. Linnig, Infrared study of some structural changes in natural rubber during vulcanization, RP2816 9
Stewart, J. E., M. Hellmann, Infrared spectra of crystalline polyphenyls, RP2829 125
—, *S. L. Madorsky, V. E. Hart*, Thermal degradation of cellulosic materials, RP2853 343
Straus, S., L. A. Wall, Pyrolysis of polyamides, RP2819 39
—, *R. R. Stromberg, B. G. Achhammer*, Infrared spectra of thermally degraded poly(vinyl chloride), RP2832 147
Stress-strain relation of pure-gum rubber vulcanizates in compression and tension, RP2837 193
Stress-strain relationships in yarns subjected to rapid impact loading, RP2866 517
Stromberg, R. R., S. Straus, B. G. Achhammer, Infrared spectra of thermally degraded poly(vinyl chloride), RP2832 147
Structural changes in natural rubber during vulcanization, infrared study of, RP2816 9
Structure in alkali silicate binary glasses, RP2854 351
Sulfur-35 beta decay, average energy of, RP2859 447
Surface area, precise evaluation of, with indirectly calculated dead space, RP2826 105

T

Page

Tables for diagonalizing second-order matrices, RP2838 201
Textile yarns, rapid impact testing of, RP2866 517
Thermal decomposition of polymers, effect of structure on, RP2860 451
Thermal degradation of cellulosic materials, RP2853 343
Thermally degraded poly(vinyl chloride) infrared spectra, RP2832 147
Thermodynamic properties of polybutadiene-benzene, RP2820 47
Tilton, L. W., Role of vitrons in alkali silicate binary glasses, RP2854 351
Todd, J., The condition of certain matrices, III, RP2815 1
Tomes, L. A., C. M. Hunt, V. Dantzler, R. L. Blaine, Reaction of portland cement with carbon dioxide, RP2858 441
Transient radio waves, RP2844 281
Trees, R. E., C. D. Coleman, Tables for diagonalizing second-order matrices, RP2838 201
Twinned epitaxy of copper on copper, RP2873 597

U

Ultraviolet and heat aging of poly(vinyl chloride), RP2863 481

V

Valore, R. C., S. Spinner, Comparison of theoretical and empirical relations between the shear modulus and torsional resonance frequencies for bars of rectangular cross section, RP2861 459
Vitrons in alkali silicate binary glasses, role of, RP2854 351
Vulcanization of natural rubber, infrared study of structural changes during, RP2816 9

W

Wait, J. R., A low-frequency annular-slot antenna, RP2822 59
Wall, L. A., R. E. Florin, Effect of structure on the thermal decomposition of polymers, RP2860 451
—, *S. Straus*, Pyrolysis of polyamides, RP2819 39
Wall material, cavity ionization as a function of, RP2842 235
Washer, F. E., W. R. Darling, Marginal performance of corrected ophthalmic lenses, RP2869 551
Waterdrops, fragmentation in the zone behind an air shock, RP2843 245
Water jets, stream driven, for propulsion purposes, RP2830 137
Water vapor, determination from the change in electrical resistance of a hygroscopic film, RP2864 489
Wave propagation in long textile yarns impacted transversely, RP2866 517
Weaver, E. R., E. E. Hughes, A. W. Diniak, Determination of water vapor from the change in electrical resistance of a hygroscopic film, RP2864 489
Weeks, J. J., J. D. Hoffman, Specific volume and degree of crystallinity of semicrystalline poly(chlorotrifluoroethylene), and estimated specific volumes of the pure amorphous and crystalline phases, RP2862 465
Weitzel, D. H., W. V. Loebenstein, J. W. Draper, O. E. Park, Ortho-para catalysis in liquid-hydrogen production, RP2840 221
West, E. D., D. C. Ginnings, An adiabatic calorimeter for the range 30° to 500° C, RP2848 309
White, H. S., H. V. Belcher, Effects of capillary shape on flow characteristics and degradation of polymer solutions, RP2839 215
Wilson, W. K., J. H. Flynn, W. L. Morrow, Degradation of cellulose in a vacuum with ultraviolet light, RP2841 229
Wood, L. A., Stress-strain relation of pure-gum rubber vulcanizates in compression and tension, RP2837 193

Y

Yarns, stress-strain relationships in, RP2866 517

THE NATIONAL BUREAU OF STANDARDS

The scope of activities of the National Bureau of Standards at its headquarters in Washington, D. C., and its major laboratories in Boulder, Colo., is suggested in the following listing of the divisions and sections engaged in technical work. In general, each section carries out specialized research, development, and engineering in the field indicated by its title. A brief description of the activities, and of the resultant publications, appears on the inside front cover.

WASHINGTON, D. C.

Electricity and Electronics. Resistance and Reactance. Electron Devices. Electrical Instruments. Magnetic Measurements. Dielectrics. Engineering Electronics. Electronic Instrumentation. Electrochemistry.

Optics and Metrology. Photometry and Colorimetry. Optical Instruments. Photographic Technology. Length. Engineering Metrology.

Heat. Temperature Physics. Thermodynamics. Cryogenic Physics. Rheology. Engine Fuels. Free Radicals Research.

Atomic and Radiation Physics. Spectroscopy. Radiometry. Mass Spectrometry. Solid State Physics. Electron Physics. Atomic Physics. Neutron Physics. Nuclear Physics. Radioactivity. X-rays. Betatron. Nucleonic Instrumentation. Radiological Equipment.

Chemistry. Organic Coatings. Surface Chemistry. Organic Chemistry. Analytical Chemistry. Inorganic Chemistry. Electrodeposition. Molecular Structure and Properties of Gases. Physical Chemistry. Thermochemistry. Spectrochemistry. Pure Substances.

Mechanics. Sound. Mechanical Instruments. Fluid Mechanics. Engineering Mechanics. Mass and Scale. Capacity, Density, and Fluid Meters. Combustion Controls.

Organic and Fibrous Materials. Rubber. Textiles. Paper. Leather. Testing and Specifications. Polymer Structure. Plastics. Dental Research.

Metallurgy. Thermal Metallurgy. Chemical Metallurgy. Mechanical Metallurgy. Corrosion. Metal Physics.

Mineral Products. Engineering Ceramics. Glass. Refractories. Enameled Metals. Concreting Materials. Constitution and Microstructure.

Building Technology. Structural Engineering. Fire Protection. Air Conditioning, Heating, and Refrigeration. Floor, Roof, and Wall Coverings. Codes and Safety Standards. Heat Transfer.

Applied Mathematics. Numerical Analysis. Computation. Statistical Engineering. Mathematical Physics.

Data Processing Systems. SEAC Engineering Group. Components and Techniques. Digital Circuitry. Digital Systems. Analog Systems. Application Engineering.

• Office of Basic Instrumentation.

• Office of Weights and Measures.

BOULDER, COLORADO

Cryogenic Engineering. Cryogenic Equipment. Cryogenic Processes. Properties of Materials. Gas Liquefaction.

Radio Propagation Physics. Upper Atmosphere Research. Ionospheric Research. Regular Propagation Services. Sun-Earth Relationships. VHF Research.

Radio Propagation Engineering. Data Reduction Instrumentation. Modulation Systems. Navigation Systems. Radio Noise. Tropospheric Measurements. Tropospheric Analysis. Radio Systems Application Engineering. Radio Meteorology.

Radio Standards. High Frequency Electrical Standards. Radio Broadcast Service. High Frequency Impedance Standards. Electronic Calibration Center. Microwave Physics. Microwave Circuit Standards.

Recent Publications of the National Bureau of Standards

Periodicals

Journal of Research of the National Bureau of Standards, Volume 60, No. 4, April 1958 (RP2844 to RP2856 incl.). 60 cents. Annual subscription $4.00, $1.25 additional for foreign mailing.

Technical News Bulletin, Volume 42, No. 4, April 1958. 10 cents. Annual subscription $1.00, 35 cents additional for foreign mailing.

Basic Radio Propagation Predictions for July 1958. Three months in advance. CRPL–D 164. Issued April 1958. 10 cents. Annual subscription $1.00, 25 cents additional for foreign mailing.

Available from the Superintendent of Documents, U. S. Government Printing Office, Washington 25, D. C. The three NBS periodicals are available on a 1-, 2-, or 3-year subscription basis, although no reduction in rates can be made.

UNIVERSITY OF MICHIGAN
GENERAL LIBRARY
DOCUMENTS DIVISION
1276 ANN ARBOR MICH

U
GOVERNMI ... OFFICE
DIVISION OF PUBLIC DOCUMENTS
WASHINGTON 25, D. C.

OFFICIAL BUSINESS

PENALTY FOR PRIVATE USE TO AVO
PAYMENT OF POSTAGE, $300
(GPO)

Journal of Research of the National Bureau of Standards Vol. 60, No. 6 June 19

Contents

		Page
Measurement of flame speeds by a nozzle burner method. Carl Halpern.	RP2867	535
Growth of preferentially oriented aluminum single crystals. Theodore H. Orem.	RP2868	547
Marginal performance of corrected ophthalmic lenses. Francis E. Washer and Walter R. Darling.	RP2869	551
Enthalpy and heat capacity from 0° to 900° C of three nickel-chromium-iron alloys of different carbon contents. Thomas B. Douglas and Ann W. Harman.	RP2870	563
Relative strengths of forty aromatic carboxylic acids in benzene at 25° C. Marion Maclean Davis and Hannah B. Hetzer.	RP2871	569
Shape of the liquidus surface as a criterion of stable glass formation. Edgar H. Hamilton and Given W. Cleek.	RP2872	593
Twinned epitaxy of copper on copper. Theodore H. Orem.	RP2873	597
Dielectric constant of deuterium oxide. Cyrus G. Malmberg.	RP2874	609
Additional abscissas and weights for Gaussian quadratures of high order: values for $n=64$, 80, and 96. Philip Davis and Philip Rabinowitz.	RP2875	613
Mass spectra of aromatic hydrocarbons filtered from smoky air. Fred L. Mohler, Paul Bradt, and Vernon H. Dibeler.	RP2876	615
Index to volume 60 (January to June 1958, Research Papers RP2815 to RP2876).		619

[A list of recent NBS publications is given on page 3 of the cover.]

For sale by the Superintendent of Documents, U. S. Government Printing Office, Washington 25, D. C. Price 60 cents (single copy). Subscription price: $4.00 a year; $1.25 additional for foreign mailing.
UNITED STATES GOVERNMENT PRINTING OFFICE, WASHINGTON : 1958